

DISCRETE ELEMENT METHOD  
MODELLING OF FORCES AND WEAR ON  
MILL LIFTERS IN DRY BALL MILLING

Johnny Tshibangu Kalala

A thesis submitted to the Faculty of Engineering and the Built Environment,  
University of the Witwatersrand, Johannesburg, in fulfilment of the requirements  
for the degree of Doctor of Philosophy in Engineering.

September 2008

# Declaration

I declare that this thesis is my own, unaided work. It is being submitted for the Degree of Doctor of Philosophy in Engineering in the University of the Witwatersrand, Johannesburg. It has not been submitted before for any degree or examination in any other University.

.....

Johnny Tshibangu Kalala

.....day of .....

# Abstract

Since the beginning of the last century, many studies have been performed in order to improve our understanding on the milling process. Recently, Mishra and Rajamani (1992) applied the Discrete Element Method (DEM) to solve the milling problem. Since then, this method gained considerable success due to its ability to predict load motion and power draw by tumbling mills as affected by operating conditions. The application of this method at an industrial stage requires a more rigorous validation in order to produce realistic output.

Lifter profiles play a key role in the performance of tumbling mills since they influence the motion of mill charge. Since lifters change profiles during their useful life due to wear, the performance of tumbling mills will correspondingly vary as a function of time. There is therefore a need to predict forces and wear on mill lifters in order not only to chose or design an initial lifter profile which optimizes tumbling mills performance over the lifters' useful life but also to evaluate lifter replacement time and type and also modifications which can be performed on lifters and/or operating mill conditions in order to extend the lifters' useful life. Despite the importance related to this subject, few works has been done in this field.

In this thesis, we firstly assess the ability of the Discrete Element Method to model the tangential and normal forces exerted by the mill charge on lifters. Data from an experimental two-dimensional mill designed in order to record the normal and tangential forces exerted on an instrumented lifter were available. The measured results obtained at different speeds and percentages of filling have been compared to the Discrete Element Method simulated results in the same conditions. A good agreement has been found between the experimental and the simulated results in terms of toe, shoulder positions and amplitude of forces.

After this validation of the DEM, we secondly assess the ability of this method to predict the wear of lifters in dry milling conditions. We derived a mathematical wear equation describing the removal of materials from lifters which takes into account all types of wear occurring in dry milling environment. We introduce a new approach to implement this equation in the DEM code in order to produce realistic simulated profiles. Our new method developed has been tested against laboratory and industrial data of evolving lifter profiles due to wear. Good agreement has been found between the simulated and the measured profiles.

The variation of the load behaviour as a function of lifter wear in industrial tumbling mills studied was also investigated in this thesis. The objectives were to improve the understanding of the grinding process and quantify the variation of load behaviour as a function of lifter wear. Lifter modifications were also explored in order to extend lifters useful life.

An attempt was also made in this thesis to derive, from the description of the load behaviour, equations in order to predict the wear of lifters without using the Discrete Element Method. Equations derived show the difficulty to use this approach. Success in this case was achieved only in a particular case where no significant changes occur in the load behaviour as a function of lifters wear. This finding confirms the DEM as the adequate tool to model forces and wear of tumbling mill lifters.

The results obtained are of great economical significance since they can improve the profitability of mineral processing plants. A step forward in the use of the DEM not only to design milling equipments but also to improve the understanding, optimise and quantify the change occurring as a function of lifters wear was achieved.

## Related publications

1. Johnny T. Kalala, Michael H. Moys, 2004, DEM modelling of liner wear in dry ball milling, Journal of The South African Institute of Mining and Metallurgy (SAIMM), Vol. 104, No10, 597 – 602
2. Johnny T. Kalala, Murray Bwalya, Michael H. Moys, 2005, DEM modelling of evolving mill liner profiles due to wear. Part I: DEM validation. Minerals Engineering, 18, 1386 - 1391
3. Johnny T. Kalala, Murray Bwalya, Michael H. Moys, 2005, DEM modelling of evolving mill liner profiles due to wear. Part II: Industrial case study. Minerals Engineering, 18, 1392 – 1397
4. Johnny T. Kalala, Mark Breetzke and Michael H. Moys, 2008, Study of the influence of liner wear on the load behaviour of an industrial dry tumbling mill using the Discrete Element Method (DEM), International Journal of Mineral Processing, Vol. 86, Issues 1-4, 33-39



This work is dedicated to my wife Natacha

# Acknowledgments

I would like to acknowledge the following people for their contribution to this dissertation.

- Professor Michael H. Moys, my supervisor for his guidance and support during my researches.
- Murray Bwalya for the development of the Wits DEM mill model.
- Professor Waldo Valderrama for providing experimental data of evolving lifter profiles due to wear.
- Dr Martin van Nierop, for providing experimental signals of measured forces on liners.
- ESKOM for their permission to publish work done on their tumbling mills.
- The Wits “comminution group” for creating an appropriate environment for research.
- All the COMPS researchers and staff members for their friendship.
- My parents and family for always being there for me. No words can express what you have done for me.
- To the following families for their support: Patrick Kamembo and Jean-Pierre Tshilunga.

Last, by no means least, I would like to thank God.



## TABLE OF CONTENTS

DECLARATION.....	i
ABSTRACT.....	ii
RELATED PUBLICATIONS.....	iv
DEDICATION.....	v
ACKNOWLEDGEMENTS.....	vi
TABLE OF CONTENTS.....	vii
LIST OF FIGURES.....	xiii
LIST OF TABLES.....	xxiii
<b>Chapter 1 Introduction.....</b>	<b>1</b>
1.1 Importance of grinding.....	2
1.2 Reasons of modelling forces and wear on mill lifters.....	2
1.3 Objectives.....	3
1.4 Thesis overview.....	3
<b>Chapter 2 Review of literature.....</b>	<b>6</b>
2.1 Introduction.....	8
2.2 Mill load behaviour and power draw.....	8
2.3 Wear.....	11
2.3.1 Introduction.....	11
2.3.2 Types of wear.....	11
2.3.2.1 Adhesive wear.....	11
2.3.2.2 Abrasive wear.....	11
2.3.2.3 Erosive wear.....	12
2.3.2.4 Corrosive wear.....	12
2.3.2.5 Surface fatigue wear.....	12
2.3.3 Measurement of wear.....	12
2.3.3.1 Weighing method.....	12
2.3.3.2 Distribution of wear over the lifter surface.....	13
2.3.4 Mathematical models of wear.....	13
2.3.4.1 Adhesive model: Archard wear equation.....	13
2.3.4.2 Abrasive model: Rabinowicz equation.....	15
2.3.4.3 Erosion by impact of solid particles: Finnie equation.....	16
2.3.4.4 Impact wear model: Wellinger and Breckel wear equation.....	18
2.4 Review of modelling the wear of mill lifters.....	18
2.4.1 Bond.....	18
2.4.2 Radziszewski and Tarasiewicz.....	19
2.4.3 Glover and de Beer.....	20
2.4.4 Cleary.....	20
2.4.5 Xiangjun Qiu, Alexander Potapov, Ming Song and Lawrence Nordell.....	21
2.5 Conclusions.....	22

<b>Chapter 3 Discrete Element Method.....</b>	<b>23</b>
3.1 Introduction.....	24
3.2 Calculations.....	24
3.3 Contacts models.....	25
3.4 Parameters used in the Discrete Element Method simulations.....	27
3.4.1 Time step.....	27
3.4.2 Material stiffness.....	28
3.4.3 Coefficient of restitution.....	28
3.4.4 Coefficient of friction.....	29
3.5 Simulation Outputs.....	29
3.5.1 Mill power draw.....	29
3.5.2 Impact energy spectra.....	30
3.5.3 Plot file (plt file), trace path and the position density plot (PDP).....	30
3.5.4 Forces on lifters, frictional and impact energies dissipated in the mill.....	30
3.6 DEM validations in milling.....	32
3.7 Conclusions.....	34
<b>Chapter 4 Modelling of evolving mill lifter profiles due to wear.....</b>	<b>35</b>
4.1 Introduction.....	37
4.2 Parameters affecting the wear of mill lifters.....	39
4.2.1 Lifter characteristics.....	39
4.2.1.1 <i>Lifter design</i> .....	39
4.2.1.2 <i>Lifter material</i> .....	39
4.2.2 Type of grinding: Dry or wet.....	39
4.2.3 Mill operating parameters.....	40
4.2.3.1 <i>Mill speed</i> .....	40
4.2.3.2 <i>Mill filling</i> .....	40
4.2.3.3 <i>Mill feed rate</i> .....	40
4.2.3.4 <i>Mill temperature</i> .....	40
4.2.4 Media properties.....	40
4.2.4.1 <i>Shape</i> .....	40
4.2.4.2 <i>Abrasiveness</i> .....	41
4.2.4.3 <i>Size distribution</i> .....	41
4.2.4.4 <i>Material</i> .....	41
4.3 Types of wear in milling environment.....	42
4.4 Choice of a wear mathematical model.....	43
4.5 Implementation of the wear mathematical model in the DEM code .....	45
4.5.1 Introduction.....	45
4.5.2 Lifter discretisation.....	47
4.5.2.1 <i>Vertical discretisation</i> .....	48
4.5.2.2 <i>Radial discretisation</i> .....	49
4.5.3 Objective function.....	50
4.5.3.1 <i>Definition</i> .....	50
4.5.3.2 <i>Two – dimensional (2D) model</i> .....	51
4.5.3.3 <i>Three – dimensional (3D) model</i> .....	55
4.5.3.4 <i>Influence of weight factors of the objective function</i> .....	60
4.5.3.4.1 <i>Introduction</i> .....	60

4.5.3.4.2	<i>Influence of beta</i> .....	61
4.5.3.4.3	<i>Influence of lambda</i> .....	61
4.5.3.4.4	<i>Influence of alpha</i> .....	62
4.6	Conclusions.....	63

## **Chapter 5 Comparison between experimental and DEM simulated forces on mill lifters.....64**

5.1	Introduction.....	65
5.2	Moys et al(2001) laboratory mill used for measurements of forces on a lifter.....	65
5.3	Experimental results of measurement of forces.....	67
5.3.1	Tests procedure.....	67
5.3.2	No-load signals at different speeds.....	67
5.3.3	Measured signals at different speeds.....	70
5.3.4	Net tangential and normal forces at different speeds.....	72
5.4	DEM Simulated results.....	76
5.5	Comparison between measured and DEM simulated forces.....	81
5.5.1	Introduction.....	81
5.5.2	Comparison between measured and simulated forces.....	81
5.6	Conclusions.....	84

## **Chapter 6 Comparison between experimental and DEM simulated evolving lifter profiles due to wear.....86**

6.1	Introduction.....	88
6.2	Valderrama et al (1996) laboratory experimental mill used to measure the wear of mill lifters.....	88
6.3	Laboratory experimental results.....	89
6.4	DEM simulations.....	94
6.4.1	Parameters used in the DEM simulations.....	94
6.4.2	Lifter discretisation.....	95
6.4.3	Calculations of the simulated wear rate.....	95
6.4.4	Calculation of weight factors.....	96
6.4.5	Simulated load behaviour at 75 % of critical speed with and without the deflector.....	98
6.4.6	Energies dissipated on the unworn lifter divisions.....	98
6.4.6.1	<i>Energies dissipated on the unworn lifter divisions at 75 % of critical speed with the deflector</i> .....	98
6.4.6.2	<i>Energies dissipated on the unworn lifter divisions at 75% of critical speed without the deflector</i> .....	100
6.5	Comparison between experimental and DEM simulated predictions.....	101
6.5.1	Comparison between experimental and DEM simulated results at 75% of critical speed in the presence of the deflector plate in the experimental mill.....	101
6.5.1.1	<i>Lifter profiles</i> .....	101
6.5.1.2	<i>Energies on lifter divisions</i> .....	102
6.5.1.3	<i>Model accuracy</i> .....	103
6.5.1.4	<i>Contribution of impact wear</i> .....	104

6.5.2	Comparison between experimental and DEM simulated results at 75% of critical speed without deflector.....	105
6.6	Influence of starting values .....	106
6.7	Conclusions.....	107

## **Chapter 7 DEM Modelling of the wear of industrial tumbling mills lifters.108**

7.1	Introduction.....	110
7.2	Industrial tumbling mills.....	110
7.2.1	Introduction.....	110
7.2.2	Lifter used in tumbling mills at LETHABO power station.....	111
7.2.3	Lifter used in tumbling mills at KENDAL power station.....	111
7.2.4	Lifter used in tumbling mills at MATIMBA power station.....	112
7.3	Parameters used in the DEM simulations and wear model.....	112
7.4	Procedure to model the wear of lifters.....	114
7.5	Modelling of the wear of tumbling mill lifters used at Lethabo power station.....	115
7.5.1	Introduction.....	115
7.5.2	Simulated profiles.....	115
7.5.3	Impact and abrasion/adhesion energies as a function of time.....	115
7.5.4	Comparison between the volume removed predicted and effectively removed.....	118
7.6	Modelling of the wear of tumbling mill lifters used at Kendal power station.....	119
7.6.1	Simulated profiles.....	119
7.6.2	Impact and abrasion/adhesion energies as a function of time.....	119
7.7	Modelling of the wear of tumbling mill lifters used at Matimba power station.....	121
7.7.1	Simulated profiles.....	121
7.7.2	Impact and abrasion/adhesion energies as a function of time.....	122
7.8	Discussions.....	125
7.8.1	Simulating the wear of lifters using one ball slice length.....	125
7.8.2	Determination of weight parameters used in the objective function.....	126
7.8.3	Determination of weight parameters $a_{\text{impact}}$ and $a_{\text{ad/abr}}$ .....	127
7.8.4	Decoupling abrasion and impact energy in the prediction of wear.....	129
7.8.5	Detachment versus removal of particles in the wear process.....	129
7.9	Conclusions.....	130

## **Chapter 8 DEM studies of the influence of lifter wear on the load behaviour of industrial dry tumbling mills.....131**

8.1	Introduction.....	132
8.2	Variation of load behaviour in tumbling mills used at Lethabo power station.....	132
8.2.1	DEM simulated load behaviour.....	132
8.2.2	Tangential velocities of balls as a function of lifters wear.....	135
8.3	Variation of load behaviour in tumbling mills used at Kendal power station.....	136

8.3.1	Introduction.....	136
8.3.2	DEM simulated load behaviour.....	138
8.3.3	Impact energy spectra.....	141
8.4	Variation of load behaviour in tumbling mills used at Matimba power station.....	145
8.5	Applications.....	147
8.5.1	DEM contribution to the prediction of ball wear.....	147
8.5.2	Design of lifter profiles.....	147
8.5.3	Determination of lifter replacement time .....	148
8.5.4	Determination of lifter replacement type.....	148
8.6	Conclusions.....	149
<b>Chapter 9 Development of lifters wear model in dry tumbling mills.....</b>		<b>151</b>
9.1	Introduction.....	152
9.2	Development of lifter wear model.....	152
9.2.1	Introduction.....	152
9.2.2	Impactive wear.....	153
9.2.3	Adhesive – abrasive wear.....	155
9.3	Derivation of semi-empirical equations predicting the wear of lifters.....	157
9.3.1	Introduction.....	157
9.3.2	Impact energies.....	158
9.3.3	Adhesive – abrasive energies.....	160
9.4	Conclusions.....	161
<b>Chapter 10 Conclusions and recommendations.....</b>		<b>164</b>
10.1	Introduction.....	165
10.2	DEM modelling of forces exerted by mill charge lifters.....	166
10.3	DEM modelling of evolving lifter profiles due to wear in dry milling.....	166
10.4	Recommendations.....	168
<b>Appendices.....</b>		<b>170</b>
Appendix A: Measurements of lifter profiles.....		171
Appendix B: Modelling of liner wear.....		174
Appendix C: Calculation of volume effectively removed in 3D lifter discretisation.....		176
Appendix D: Two dimensional mill.....		179
Appendix E: Comparison between experimental and DEM simulated forces....		182
Appendix F: Matlab program minimizing the objective function.....		184
Appendix G: ESKOM tumbling mills design.....		186
Appendix H: Measured lifters worn out profiles in tumbling mills used at Kendal power station.....		188
Appendix I: DEM simulated worn profiles of lifters used in tumbling mills at Lethabo, Kendal and Matimba power stations.....		190
Appendix J: Comparison between volume removed predicted and effectively removed.....		193
Appendix K: DEM simulated worn profiles beyond tilting the worn lifter by 50 mm in tumbling mills at ESKOM Kendal power station.....		197
Appendix L: DEM contribution to the prediction of ball wear.....		199

Appendix M: Development of abrasive wear model in dry tumbling mills.....205

**REFERENCES.....217**

## LIST OF FIGURES

Figure		Page
2.1	Active load charge in a mill and coordinate used in the development of the model of power consumption after Morrel (1993).....	9
2.2	Schematic diagram showing the evolution of a single contact patch as two asperities move over each other after Archard 1953).....	14
2.3	Simplified abrasive wear model after Rabinowicz (1965).....	15
2.4	Incident erosive particle cutting into a ductile surface at an angle of Attack $\alpha$ after Finnie (1972).....	16
2.5	DEM simulated profiles after Glover and de Beer (1997).....	20
2.6	DEM simulated profile at a) $N_c=60\%$ ; b) $N_c=80\%$ after Cleary (1998).....	21
3.1	The linear spring – dashpot contact model.....	26
3.2	Comparison between measured and simulated load behaviour at 60 and 80% of critical speed at 20 and 35% of mill filling after Van Nierop et al (2001).....	32
3.3	Comparison between measured and simulated power draw for ball Mills of different diameters after Datta et al (1999).....	33
4.1.a	Lifter profiles after Wills (1992).....	38
4.1.b	Lifter profiles after Kelly and Spottiswood (1982).....	38
4.1.c	Noranda and Ical lifter profiles respectively after Cleary et al (2001).....	38
4.2	Ball charge motion in a mill.....	42
4.3	Three Dimensional (3D) discretisation of a trapezoidal lifter.....	47
4.4	Vertical discretisation of a trapezoidal lifter.....	48
4.5	Vertical discretisation of a rectangular lifter.....	49
4.6	Radial discretisation of a rectangular lifter.....	50

<b>Figure</b>		<b>Page</b>
<b>4.7</b>	Vertical discretisation of a trapezoidal lifter and worn profile .....	<b>51</b>
<b>4.8</b>	Radial discretisation of a trapezoidal lifter and worn profile.....	<b>51</b>
<b>4.9</b>	Non-uniform lifter wear profile observed in an industrial mill (after Banisi, S. and Hadizadeh, M., 2006).....	<b>55</b>
<b>4.10</b>	Three dimensional (3D) discretisation of a portion of a lifter.....	<b>56</b>
<b>4.11</b>	Influence of the weight factor $b$ (beta) used in the objective Function for the prediction of the simulated worn profile.....	<b>60</b>
<b>4.12</b>	Influence of the weight factor $l$ (lambda) used in the objective Function for the prediction of the simulated worn profile.....	<b>61</b>
<b>4.13</b>	Influence of the weight factor $a$ (alpha) used in the objective Function for the prediction of the simulated worn profile.....	<b>62</b>
<b>5.1</b>	Two-dimensional mill used for measurements of forces on an instrumented lifter (Moys et al, 2001).....	<b>66</b>
<b>5.2</b>	Instrumented lifter bar (Moys et al, 2001).....	<b>66</b>
<b>5.3</b>	Measured and modelled zero load instrumented lifter bar signal at 60% of critical speed as a function of cumulated angle where 0 degree correspond to 12 o'clock position. Each vertical line represents one revolution.....	<b>68</b>
<b>5.4</b>	Measured and modelled zero load instrumented lifter bar signal at 50% of critical speed as a function of cumulated angle where 0 degree correspond to 12 o'clock position. Each vertical line represents one revolution.....	<b>68</b>
<b>5.5</b>	Measured and zero load instrumented lifter bar signal at 60% of critical speed plotted as a function of cumulated angle where 0 degree correspond to 12 o'clock position. Each vertical line represents one revolution. $J=20\%$ , $d=6.7$ mm.....	<b>70</b>
<b>5.6</b>	Measured and zero load instrumented lifter bar signal at 50% of critical speed plotted as a function of cumulated angle where 0 degree correspond to 12 o'clock position. Each vertical line represents one revolution. $J=20\%$ , $d=6.7$ mm.....	<b>70</b>



<b>Figure</b>	<b>Page</b>
<b>5.7</b>	Measured and zero load instrumented lifter bar signal at 30% of critical speed plotted as a function of cumulated angle where 0 degree correspond to 12 o'clock position. Each vertical line represents one revolution. $J=20\%$ , $d=22.2$ mm..... <b>71</b>
<b>5.8</b>	Measured instrumented lifter bar tangential forces per revolution as a function of angle where 0 degree correspond to 12 o'clock position (mill rotation: anticlockwise). Percentage of critical speed $N_c=60\%$ . Balls diameter $d=6.7$ mm. The trends are separated from each other by 3N to increase legibility..... <b>72</b>
<b>5.9</b>	Measured instrumented lifter bar normal forces per revolution as a function of angle where 0 degree correspond to 12 o'clock position(mill rotation: anticlockwise): Percentage of critical speed $N_c=60\%$ . Balls diameter $d=6.7$ mm. The trends are separated from each other by 3N to increase legibility..... <b>73</b>
<b>5.10</b>	Measured instrumented lifter bar tangential forces per revolution as a function of angle where 0 degree correspond to 12 o'clock position (mill rotation: anticlockwise). Percentage of critical speed $N_c=50\%$ . Balls diameter $d=6.7$ mm. The trends are separated from each other by 3N to increase legibility..... <b>73</b>
<b>5.11</b>	Measured instrumented lifter bar normal forces per revolution as a function of angle where 0 degree correspond to 12 o'clock position (mill rotation: anticlockwise): Percentage of critical speed $N_c=50\%$ . Balls diameter $d=6.7$ mm. The trends are separated from each other by 3N to increase legibility..... <b>74</b>
<b>5.12</b>	Measured instrumented lifter bar tangential forces per revolution as a function of angle where 0 degree correspond to 12 o'clock position (mill rotation: anticlockwise): Percentage of critical speed $N_c=30\%$ . Balls diameter $d=22.2$ mm. The trends are separated from each other by 10N to increase legibility..... <b>74</b>
<b>5.13</b>	Measured instrumented lifter bar normal forces per revolution as a function of angle where 0 degree correspond to 12 o'clock position (mill rotation: anticlockwise): Percentage of critical speed $N_c=30\%$ . Balls diameter $d=22.2$ mm. The trends are separated from each other by 10N to increase legibility..... <b>75</b>

<b>Figure</b>	<b>Page</b>
<b>5.14</b> Simulated tangential forces exerted on 12 lifters for one revolution. Critical speed $N_c=60\%$ , percentage of filling $J=20\%$ , ball diameter $d=6.7\text{mm}$ . The trends are separated from each other by 3N to increase legibility. (0 degree=12 O'clock position, mill rotation: anticlockwise).....	77
<b>5.15</b> Simulated normal forces exerted on 12 lifters for one revolution. Critical speed $N_c=60\%$ , percentage of filling $J=20\%$ , ball diameter $d=6.7\text{mm}$ . The trends are separated from each other by 2N to increase legibility. (0 degree=12 O'clock position, mill rotation: anticlockwise).....	78
<b>5.16</b> Simulated tangential forces exerted on 12 lifters for one revolution, critical speed $N_c=50\%$ , percentage of filling $J=20\%$ , ball diameter $d=6.7\text{mm}$ . The trends are separated from each other by 2N to increase legibility. (0 degree=12 O'clock position, mill rotation: anticlockwise).....	78
<b>5.17</b> Simulated normal forces exerted on 12 lifters for one revolution, critical speed $N_c=50\%$ , percentage of filling $J=20\%$ , ball diameter $d=6.7\text{mm}$ . The trends are separated from each other by 2N to increase legibility. (0 degree=12 O'clock position, mill rotation: anticlockwise).....	79
<b>5.18</b> Simulated tangential forces exerted on 12 lifters for one revolution, critical speed $N_c=30\%$ , percentage of filling $J=20\%$ , ball diameter $d=22.4\text{mm}$ . The trends are separated from each other by 7N to increase legibility. (0 degree=12 O'clock position, mill rotation: anticlockwise).....	79
<b>5.19</b> Simulated normal forces exerted on 12 lifters for one revolution, critical speed $N_c=30\%$ , percentage of filling $J=20\%$ , ball diameter $d=22.4\text{mm}$ . The trends are separated from each other by 7N to increase legibility. (0 degree=12 O'clock position, mill rotation: anticlockwise).....	80
<b>5.20</b> Comparison between average experimental (over 6 revolutions) and simulated (for 12 lifters) results and their respective standard deviation at 60% of critical speed.....	81
<b>5.21</b> Comparison between average experimental (over 5 revolutions) and simulated (for 12 lifters) results and their respective standard deviation at 50% of critical speed .....	82

<b>Figure</b>		<b>Page</b>
<b>5.22</b>	Comparison of between average experimental and simulated tangential and normal forces at 50% of critical speed. The trends are separated by 2N to increase legibility.....	<b>82</b>
<b>5.23</b>	Comparison between average tangential and normal forces simulated and measured at 30% of critical speed. The trends are separated by 2N to increase legibility.....	<b>83</b>
<b>5.24</b>	Comparison between average experimental (over 3 revolutions) and simulated + standard deviation (for 12 lifters) results at 30% of critical speed .....	<b>84</b>
<b>6.1</b>	Evolving lifter profile (Valderrama et al (1996)) in a mill of diameter $D=0.28\text{m}$ , length $L=0.11\text{m}$ , critical speed $N_c=75\%$ , percentage of filling $J=30\%$ , ball diameter $d=4.5\text{mm}$ , lifter front angle= $75$ degrees, with deflector.....	<b>89</b>
<b>6.2</b>	Evolving lifter profile (Valderrama et al (1996)) in a mill of diameter $D=0.28\text{m}$ , length $L=0.11\text{m}$ , critical speed $N_c=75\%$ , percentage of filling $J=30\%$ , ball diameter $d=4.5\text{mm}$ , lifter front angle= $75$ degrees, without deflector.....	<b>90</b>
<b>6.3</b>	Cumulative percentage of lifter volume lost function of time in a mill of diameter $D=0.28\text{m}$ , length $L=0.11\text{m}$ , percentage of filling $J=30\%$ , ball diameter $d=4.5\text{mm}$ , lifter front angle= $25$ degrees, percentage of critical speed $N_c=75\%$ with and without the deflector plate in the mill.....	<b>91</b>
<b>6.4</b>	DEM load behaviour position density plot (PDP) at 75% of critical speed in Valderrama's experimental mill without using a deflector.....	<b>92</b>
<b>6.5</b>	DEM load behaviour position density plot (PDP) at 75% of critical speed in Valderrama's experimental mill using a deflector.....	<b>92</b>
<b>6.6</b>	Lifter discretised.....	<b>95</b>
<b>6.7</b>	Simulated load behaviour in the presence of a deflector in a mill of diameter $D=0.28\text{m}$ , critical speed $N_c=75\%$ , percentage of filling $J=30\%$ , ball diameter $d=4.5\text{mm}$ , unworn new lifter with front angle= $75$ degrees.....	<b>97</b>

<b>Figure</b>		<b>Page</b>
<b>6.8</b>	Simulated load behaviour without a deflector in a mill of diameter $D=0.28\text{m}$ , critical speed $N_c=75\%$ , percentage of filling $J=30\%$ , ball diameter $d=4.5\text{mm}$ , unworn new lifter with front angle $=75$ degrees.....	<b>97</b>
<b>6.9</b>	Average adhesion/abrasion energies per $\text{m}^2$ of the unworn new lifter divisions at 75% of critical speed in the presence of the deflector.....	<b>98</b>
<b>6.10</b>	Average impact energies per $\text{m}^2$ of discretised lifter divisions of the unworn lifter at 75% of critical speed in the presence of the deflector.....	<b>99</b>
<b>6.11</b>	Average abrasion/adhesion energies per $\text{m}^2$ of discretised lifter divisions of the unworn lifter at 75% of critical speed without using the deflector plate in the experimental mill.....	<b>100</b>
<b>6.12</b>	Average impact energies per $\text{m}^2$ of discretised lifter divisions of the unworn lifter at 75% of critical without using the deflector plate speed in the experimental mill.....	<b>100</b>
<b>6.13</b>	Comparison between experimental (Valderrama et al,1996) and DEM simulated lifter profiles at different time in a mill of diameter $D=0.28\text{m}$ , critical speed $N_c=75\%$ , percentage of filling $J=30\%$ , ball diameter $d=4.5\text{mm}$ , with the deflector plate inside the mill.....	<b>101</b>
<b>6.14</b>	DEM Energies dissipated on the evolving lifter profile on each discretised lifter division. The trends are separated from each other by 0.0002 Joules to increase legibility.....	<b>102</b>
<b>6.15</b>	Simulated vs. Measured points.....	<b>103</b>
<b>6.16</b>	Influence of the contribution of impact energy on the wear of lifters.....	<b>104</b>
<b>6.17</b>	Comparison between experimental and DEM simulated lifter profiles at different time in a mill of diameter $D=0.28\text{m}$ , critical speed $N_c=75\%$ , percentage of filling $J=30\%$ , ball diameter $d=4.5\text{mm}$ , without the deflector inside the experimental mill.....	<b>105</b>
<b>7.1</b>	Unworn and worn out lifter profile used at LETHABO power station.....	<b>111</b>

<b>Figure</b>	<b>Page</b>
<b>7.2</b> Unworn and worn out lifter profile used at KENDAL power station.....	<b>112</b>
<b>7.3</b> Unworn and worn out lifter profile used at MATIMBA power station.....	<b>112</b>
<b>7.4</b> Procedure to model the wear of lifters.....	<b>114</b>
<b>7.5</b> DEM simulated evolving LETHABO double wave lifter profile.....	<b>115</b>
<b>7.6</b> Impact and abrasion energies dissipated on discretised lifter divisions of the double wave lifter used at Lethabo power station as a function of lifter wear.....	<b>116</b>
<b>7.7</b> Cumulative percentage of total energy as a function of impact energy on the discretised unworn lifter division at the front and back of lifter waves.....	<b>117</b>
<b>7.8</b> Volume removed predicted and effectively removed on discretised lifter divisions of the unworn double wave lifter used at Lethabo power station.....	<b>118</b>
<b>7.9</b> DEM simulated evolving lifter profile used at KENDAL power station.....	<b>119</b>
<b>7.10</b> Impact and abrasion energies dissipated on discretised lifter divisions of the lifter used at Kendal power station as a function of lifter wear.....	<b>120</b>
<b>7.11</b> Volume removed predicted and effectively removed on discretised lifter divisions of the unworn lifter used at Kendal power station.....	<b>121</b>
<b>7.12</b> DEM simulated evolving lifter profile used at Matimba power station.....	<b>122</b>
<b>7.13</b> Impact and abrasion energies dissipated on discretised lifter divisions of the lifter used at Matimba power station as a function of lifter wear.....	<b>123</b>

<b>Figure</b>	<b>Page</b>
<b>7.14</b> Comparison between volume removed predicted and effectively removed on discretised lifter divisions of the unworn lifter used at Matimba power station.....	<b>124</b>
<b>7.15</b> 3D vs One ball slice normalised impact energies dissipated on discretised unworn lifter used at Lethabo power station.....	<b>125</b>
<b>7.16</b> Top ball size in contact with lifter used at Matimba power station...	<b>126</b>
<b>7.17</b> Procedure to calculate the ratio ( $a_{\text{impact}}/a_{\text{abr/ad}}$ ).....	<b>128</b>
<b>8.1</b> Moving lifter waves as lifters wear in a mill used at Lethabo power station.....	<b>134</b>
<b>8.2</b> Tangential velocities of balls as a function of their respective radial position at different lifter age in the mill used at Lethabo power station.....	<b>135</b>
<b>8.3</b> Evolving lifter profile used at Kendal power station and modifications performed.....	<b>136</b>
<b>8.4</b> Relative mill capacity as a function of lifter age.....	<b>137</b>
<b>8.5</b> Lifters in the mill used at Kendal power station.....	<b>138</b>
<b>8.6</b> Tangential velocities of balls as a function of their respective radial position at different lifter age in the Kendal mill.....	<b>140</b>
<b>8.7</b> Impact energy spectra as a function of lifters wear and modifications in the Kendal Mill.....	<b>143</b>
<b>8.8</b> Lifter pattern replacement at Matimba power station.....	<b>148</b>
<b>9.1</b> Collision between a discretised lifter division $i$ and a mill charge layer $z$ .....	<b>153</b>
<b>9.2</b> Description of load behaviour and centrifugal and gravitational forces exerted on a discretised lifter division $i$ at the mill position $\theta_i$ (the size of the lifter relative to the mill has been exaggerated to increase legibility).....	<b>156</b>

<b>Figure</b>	<b>Page</b>
<b>9.3</b> Impact energies as a function of Lethabo double wave discretised lifter divisions angle and height.....	<b>159</b>
<b>9.4</b> Simulation of the wear of the double wave lifter used at Lethabo power station using an empirical model.....	<b>160</b>
<b>A.1</b> Measurement of lifters profiles in a Semiautogenous mill using a laser scanner developed by Conveyor Dynamics International and Svedala (after Nordell and Potapov, 2001).....	<b>171</b>
<b>A.2</b> Measurement of lifter profile using a profiling gauge.....	<b>172</b>
<b>A.3</b> Pin profiling gauge after Meekel et al (1996).....	<b>173</b>
<b>B.1</b> Wave lifter profile discretisation after Radziszewski and Tarasiewicz (1993).....	<b>174</b>
<b>B.2</b> Simulated wave liner profiles after Radziszewski and Tarasiewicz (1993).....	<b>174</b>
<b>B.3</b> Simulated bevelled lifter profiles after Radziszewski and Tarasiewicz (1993).....	<b>175</b>
<b>B.4</b> Comparison between experimental and simulated profiles after Qiu et al (2001).....	<b>175</b>
<b>C.1</b> 3D Discretised volume element.....	<b>176</b>
<b>C.2</b> Representation of a tetrahedron.....	<b>177</b>
<b>D.1</b> Two – dimensional mill.....	<b>179</b>
<b>D.2</b> Normal and tangential forces exerted on the instrumented lifter at zero load.....	<b>180</b>

<b>Figure</b>		<b>Page</b>
<b>G.1</b>	Air swept tumbling mill used at Eskom for the grinding of coal.....	<b>186</b>
<b>G.2</b>	Mill feed and removal design.....	<b>187</b>
<b>H.1</b>	Measured worn out lifter profiles used at Kendal power station.....	<b>188</b>
<b>J.1</b>	Difference of volume removed predicted and effectively removed at each step on different discretised lifter divisions (Lifter used at Lethabo power station).....	<b>194</b>
<b>J.2</b>	Difference of volume removed predicted and effectively removed at each step on different discretised lifter divisions (Lifter used at Kendal power station).....	<b>195</b>
<b>J.3</b>	Difference of volume removed predicted and effectively removed at each step on different discretised lifter divisions (Lifter used at Matimba power station).....	<b>196</b>
<b>K.1</b>	DEM simulated worn profiles beyond tilting the worn lifter by 50 mm in tumbling mills at ESKOM Kendal power station.....	<b>197</b>
<b>K.2</b>	Comparison of impact energy spectra beyond tilting worn out lifter used at Kendal power station by 50mm.....	<b>198</b>
<b>L.1</b>	Total frictional energy dissipated as a function of ball size at different mill speed in a mill of 600 mm of diameter filled at 30%....	<b>201</b>
<b>L.2</b>	Total impact energy dissipated as a function of ball size at different mill speed in a mill of 600 mm of diameter filled at 30%.....	<b>202</b>
<b>L.3</b>	Relative frictional energy per unit of ball surface.....	<b>203</b>
<b>L.4</b>	Relative impact energy per unit of ball volume.....	<b>203</b>
<b>M.1</b>	Description of load behaviour and centrifugal and gravitational forces exerted on a discretised lifter division $i$ at the mill position $\theta_i$ (the size of the lifter relative to the mill has been exaggerated to increase legibility).....	<b>205</b>
<b>M.2</b>	Gravitational force exerted on a discretised lifter division $i$ at the mill position $\theta_i$ .....	<b>209</b>



## LIST OF TABLES

<b>Table</b>		<b>Page</b>
<b>3.1</b>	Representation of the load behaviour using the position density plot (PDP).....	<b>31</b>
<b>5.1</b>	Average shoulder and toe positions at different speeds from experimental data.....	<b>76</b>
<b>5.2</b>	Parameters used in the DEM simulations to simulate forces on mill lifters.....	<b>76</b>
<b>5.3</b>	Shoulder and toe position from simulated data at different speed.....	<b>80</b>
<b>6.1</b>	Correlations between cumulative lifter volume lost (y) and time (x).....	<b>93</b>
<b>6.2</b>	Parameters used in the DEM simulations to simulate the load behaviour and wear of lifter profiles.....	<b>94</b>
<b>6.3</b>	Ratio between experimental and simulated time at 75% of critical speed.....	<b>96</b>
<b>6.4</b>	Model accuracy.....	<b>103</b>
<b>7.1</b>	Characteristics of tumbling mills used at LETHABO, KENDAL and MATIMBA power stations.....	<b>110</b>
<b>7.2</b>	Parameters used in the DEM simulation to simulate the wear of lifters used at ESKOM Lethabo, Kendal and Matimba power stations.....	<b>113</b>
<b>8.1</b>	DEM Variation of the load behaviour as a function of lifters wear in tumbling mills used at Lethabo power station.....	<b>133</b>
<b>8.2</b>	Variation of lifter angle and ratio spacing: height as a function of lifter wear for the double wave lifter used at Lethabo power station.....	<b>134</b>
<b>8.3</b>	DEM Variation of the load behaviour as a function of lifter wear in tumbling mills used at Kendal power station.....	<b>139</b>
<b>8.4</b>	Equations of tangential velocities of balls as a function of their respective radial position at different lifter age.....	<b>141</b>

<b>Table</b>	<b>Page</b>
<b>8.5</b> Variation of relative total cumulated impact and frictional energy dissipated by the ball charge as a function of lifter wear.....	<b>144</b>
<b>8.6</b> DEM Variation of the load behaviour as a function of lifter wear in tumbling mills used at Matimba power station.....	<b>146</b>
<b>9.1</b> Correlation results of impact energy as a function of discretised lifter divisions height and angle for the double wave lifter used at Lethabo power station mill.....	<b>159</b>
<b>E.1</b> Statistical comparison between measured and DEM simulated tangential forces at 30% of critical speed.....	<b>183</b>
<b>E.2</b> Statistical comparison between measured and DEM simulated normal forces at 30% of critical speed.....	<b>183</b>
<b>H.1</b> Location of measured lifter profiles inside a mill used at Kendal power station.....	<b>188</b>
<b>H.2</b> Measured data in mm of worn lifter profiles used in tumbling mill at Kendal power station .....	<b>189</b>
<b>I.1</b> Data of simulated profiles of lifters used in tumbling mills at Lethabo power station (the unworn lifter is used as reference and measurement are in cm).....	<b>190</b>
<b>I.2</b> Data of simulated profiles of lifters used in tumbling mills at Eskom Kendal power station (the unworn lifter is used as reference and measurement are in cm).....	<b>191</b>
<b>I.3</b> Data of simulated profiles of lifters used in tumbling mills at Eskom Matimba power station (the unworn lifter is used as reference and measurement are in cm).....	<b>192</b>
<b>J.1</b> Difference in percentage (%) between the total volume removed predicted and effectively removed at each step (double wave lifter used at Lethabo power station).....	<b>193</b>
<b>J.2</b> Difference in % between the total volume removed predicted and effectively removed at each step (Lifter used at Kendal power station).....	<b>194</b>
<b>J.3</b> Difference in percentage (%) between the total volume removed predicted and effectively removed at each step (Lifter used at Matimba power station).....	<b>195</b>

# Chapter 1

## Introduction

**1.1 Importance of grinding**

**1.2 Reasons for modelling forces and wear on mill lifters**

**1.3 Objectives**

**1.4 Thesis overview**

## **1.1 Importance of grinding**

Minerals extracted from mines are generally not ready to be used as final products. They require firstly physical treatments in a number of steps grouped in what is called mineral processing. The grinding of ore is an important operation in mineral processing plants. By this operation, the size of ore rocks are reduced in order to liberate “utile mineral” from gangue before separation or to reach a size distribution compatible with the requirement of the following operation or the usage.

The growth of metal and minerals demand in the world implies more grinding of ore since the average grade of minerals available is decreasing.

## **1.2 Reasons for modelling forces and wear on mill lifters**

The mineral processing industry is requested to optimise its process to remain competitive. A special attention must be paid on the grinding process since it is generally, the greatest single operating cost. Tumbling mills which include rod mills, ball mills, Semi and Autogenous mills are the most reliable grinding device used for the size reduction of particles in mineral processing plants. However, they consume inefficiently a large amount of energy and at the same time, they are expensive to run due to the wear of grinding media and lifters.

Lifter profiles influence the charge motion in tumbling mills and therefore the grinding performance. As lifters change profiles over their useful life due to wear, the mill performance will correspondingly vary. Simulating forces exerted by the charge on mill lifters and evolving lifter profiles due to wear will contribute to optimising the following objectives:

- Ø Choose for a particular operation the best initial lifter design which optimises mills performance over their useful life.
- Ø Determine the optimal replacement time for a worn lifter.
- Ø Determine the optimal type of lifter replacement.
- Ø Improve the understanding of grinding process as a function of lifter wear.

- Ø Evaluate modifications which can be performed on lifter or mill operating conditions in order to extend lifters useful life.

The success of modelling the forces exerted by the mill charge on tumbling mill lifters and the wear of mill lifters is therefore of great economic significance since it has the potential of increasing the profitability of mineral processing plants.

### **1.3 Objectives**

The objectives of this thesis are to assess the ability of the Discrete Element Method (DEM) applied to tumbling mills to:

- Model the normal and tangential forces exerted by the charge on lifters as affected by the mill speed, the mill filling and the charge composition.
- Model the evolving lifter profiles due to wear as affected by the mill speed, the charge composition and the lifter profiles.

### **1.4 Thesis overview**

This thesis is structured in ten (10) chapters.

Chapter 1 is this introduction

Chapter 2 reviews firstly the literature on efforts by some authors to accurately predict the load behaviour and power draw by tumbling mills. Secondly, this chapter reviews wear mathematical models predicting the volume of material removed due to wear as a function of operating conditions. Thirdly, published work on modelling of the wear of mill lifters are reviewed in order to present the current position of researches in this field.

Chapter 3 presents the Discrete Element Method approach to simulating the load behaviour in tumbling mills and justifies the choice of this method to model the forces exerted by the charge on mill lifters and their wear.

Chapter 4 explains firstly the object of mill lifters, the types of wear in milling environment and the parameters affecting the wear of tumbling mill lifters. Secondly, a wear mathematical model which takes into account all types of wear occurring in the milling environment is derived. Moreover, in order to produce realistic simulated profiles, we developed an objective function to be used when our wear mathematical model (or any mathematical model) is implemented in the Discrete Element Method code.

Chapter 5 describes firstly a modified laboratory tumbling mill (Moys et al, 2001) used to measure tangential and normal forces exerted by the mill charge on an instrumented lifter. The measured forces are compared to the Discrete Element Method simulated forces predicted in the same conditions.

Chapter 6 analyses laboratory data of evolving mill lifter profiles due to wear found in the literature (Valderrama et al, 1996). Discrete Element Method simulations are conducted in the same conditions of laboratory experiments in order to predict the wear of lifters. The measured and simulated profiles are compared.

Chapter 7 applies our Discrete Element Method approach to predict the wear of lifters developed in chapter 4 to industrial tumbling mills operating in dry conditions. Our simulated profiles are compared to measured industrial data.

Chapter 8 uses the results predicted in Chapter 7 to study the variation of the load behaviour of industrial tumbling mills as a function of lifter wear. The results found improve our understanding of the grinding process in these industrial tumbling mills as lifters wear. Moreover, modifications in order to extend the useful life of these lifters are explored.

Chapter 9 is an attempt to derive equations from the description of load behaviour in order to predict the wear of lifters without using the Discrete Element Method.

Chapter 10 summarises our thesis and makes recommendations for further research.

# Chapter 2

## Review of literature

### **2.1 Introduction**

### **2.2 Mill load behaviour and power draw**

### **2.3 Wear**

#### 2.3.1 Introduction

#### 2.3.2 Types of wear

##### *2.3.2.1 Adhesive wear*

##### *2.3.2.2 Abrasive wear*

##### *2.3.2.3 Erosive wear*

##### *2.3.2.4 Corrosive wear*

##### *2.3.2.5 Surface fatigue wear*

#### 2.3.3 Measurement of wear

##### *2.3.3.1 Weighing method*

##### *2.3.3.2 Distribution of wear over the lifter surface*

#### 2.3.4 Mathematical models of wear

##### *2.3.4.1 Adhesive model: Archard wear equation*

##### *2.3.4.2 Abrasive model: Rabinowicz equation*

##### *2.3.4.3 Erosion by impact of solid particles: Finnie equation*

##### *2.3.4.4 Impact wear model: Wellinger and Breckel wear equation*

### **2.4 Review of modelling the wear of mill lifters**

#### 2.4.1 Bond

#### 2.4.2 Radziszewski and Tarasiewicz

#### 2.4.3 Glover and de Beer

#### 2.4.4 Cleary

#### 2.4.5 Xiangjun Qiu, Alexander Potapov, Ming Song and Lawrence Nordell



## 2.5 Conclusions

## 2.1 Introduction

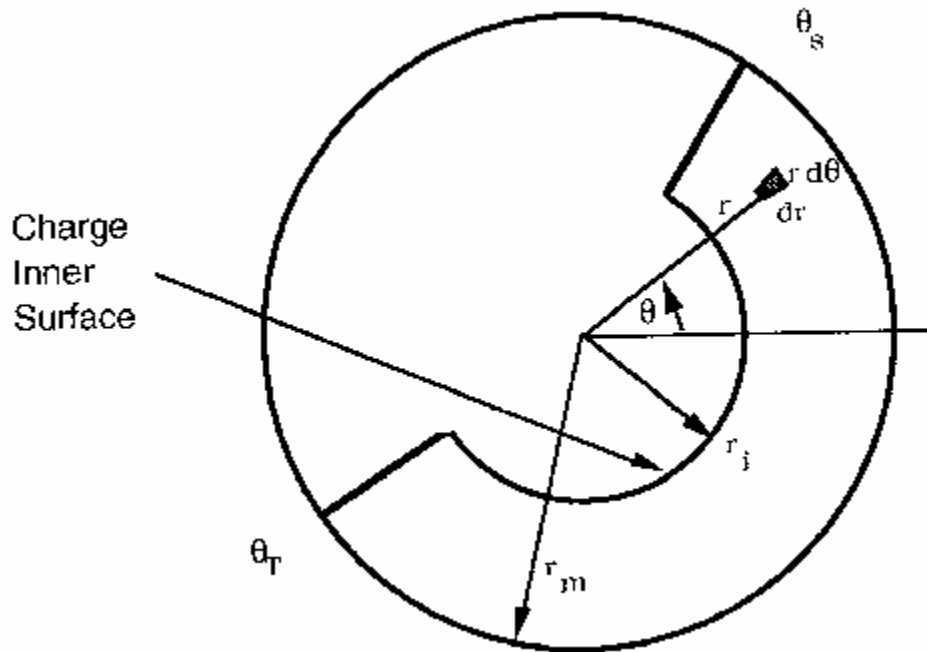
In order to simulate the forces and the wear on mill lifters, it is important to accurately predict the mill load behaviour and its associate characteristics such as the power draw, the toe and the shoulder positions as affected by mill operating conditions. A review of literature containing the evolution of major models published to describe the load behaviour and calculate the power draw by tumbling mills from the beginning of the last century till recently with the application of the Discrete Element Method was performed by Morrel (1993). This Chapter reviews firstly Morrel's description of load behaviour and power draw which will be used later to derive equations predicting the wear of lifters. Secondly, models and equations of wear developed in order to predict the volumes of material removed on a surface due to wear are described in order to provide a background of the wear phenomenon. This will guide us in the choice of appropriate equations predicting the wear of lifters as it occurs in dry tumbling mills. Although this section is not exhaustive due to the immensity and the complexity of the wear subject, we explored nevertheless important mathematical models and their applicability. Thirdly, the actual position of researches in terms of modelling the wear of mill lifters is reviewed by analysing published work.

## 2.2 Mill load behaviour and power draw

Since the beginning of the last century, many studies have been performed in order to improve our understanding on the milling process and its efficiency. As quoted by H. A. White (1905), in the early 19<sup>th</sup>, Herman Fischer (1904) paper devoted to the use of tumbling mills for dry grinding was regarded at that time as the most significant contribution of knowledge on the milling subject. White confirmed Fischer's conclusions in his paper: *The Theory of Tumbling Mill*.

Morrell (1993) reviewed the contribution of the following authors in the description of load behaviour and prediction of tumbling mills power draw: White (1905), Davis (1919), Rose and Evans (1956), Rose and Sullivan (1958), Bond (1961), Hogg and Fuerstenau (1972), Harris et al (1985), Moys (1990) and Kapur et al (1992).

Morrel (1993) describing the load behaviour assumes that the active charge of the load can be represented by Figure 2.1.



**Figure 2.1** Active load charge in a mill and coordinate used in the development of the model of power consumption after Morrel (1993)

The mass  $dm$  of an element of cross sectional area  $dr * rdq$  having a length of  $L$  is given by:

$$dm = dr * rdq * L * r \quad (2.1)$$

Where  $r$  is the charge density

The torque  $T$  required for that element is given by:

$$T = r * r^2 * g * L * \cos q * dr * dq \quad (2.2)$$

where  $g$  is the acceleration due to gravity.

The net power can be calculated from the torque using the following equation:

$$P = 2pNT \quad (2.3)$$

Where N is the mill speed

Replacing equation (2.2) in (2.3) and integrating between the limits  $r_i$  and  $r_m$  and between  $q_T$  and  $q_S$ , the net power is given by:

$$P_{net} = \frac{p \cdot g \cdot L \cdot r \cdot N_m \cdot r_m}{3(r_m - zr_i)} [2r_m^3 - 3zr_m^2r_i + r_i^3(3z - 2)] [\sin q_S - \sin q_T] \quad (2.4)$$

where:

$$z = (1 - J)^{0.4532} \quad (2.5)$$

$N_m$  is the rotational rate at the mill shell

$r_i$  is the radius of the charge inner surface

$r_m$  is the radius of the charge at the mill shell

$q_S$  is the shoulder angle

$q_T$  is the toe angle

$J$  is the percentage of mill filling

The gross power draw by the mill is given by:

$$\text{Gross power, kW} = \text{No-load power} + K (\text{Net power}) \quad (2.6)$$

where K is a correction factor

K=1.22 for grate discharge mills.

K=1.03 for overflows mills

Mishra and Rajamani (1992) choose from previous researchers in the field, a different approach to model the load behaviour in the mill and to predict the mill power draw. They used the Discrete Element Method to solve the milling problem. Since then, this method gained considerable success due to its ability to accurately predict the power draw and load behaviour in the mill as affected by operating parameters. This method is described in detail in chapter 3.

## 2.3 Wear

### 2.3.1 Introduction

Wear can be defined as the progressive removal or displacement of a volume of material from a body which is repeatedly stressed in mechanical contact with another body or bodies (Hutchings, 1992). It is a very complex phenomenon involving chemical and physical interactions. The complexity of wear makes difficult: i) the classification of different types of wear and ii) the determination of a mathematical equation linking all variables and parameters of the system subjected to wear to the volume of material removed or displaced. Despite efforts made in understanding the wear process, it is difficult to predict with confidence the wear of materials. There is no model or equation valid for all situations.

### 2.3.2 Types of wear

Most situations of wear can be classified into the five following categories.

#### 2.3.2.1 *Adhesive wear*

Adhesive wear occurs when there is relative motion between two smooth contacting surfaces.

#### 2.3.2.2 *Abrasive wear*

It is characterised by the penetration of a surface by rough hard particles resulting in material displacement.

#### 2.3.2.3 *Erosive wear*

Erosion wear occurs when particles carried in a fluid hit a solid surface and remove materials from it.

#### 2.3.2.4 *Corrosive wear*

This refers to surface damage caused by the impingement of corrosive gas or liquid streams which may or not contain solid particles.

#### 2.3.2.5 *Surface fatigue wear*

This form of wear is observed during repeated sliding or rolling over a surface. The repeated loading and unloading cycles to which the materials are exposed may induce the formation of surface or subsurface cracks and the removal of loosened particles over time.

### 2.3.3 Measurement of wear

The wear is measured by examination of the material subject to wear before and after the test. Any difference (loss) in the material is attributed to wear (Hutchings, 1992).

The following techniques are used to measure the wear of tumbling mill lifters:

#### 2.3.3.1 *Weighing method*

It consists of measuring the lifter weight before and after a number of operating hours. The mass (or volume) lost per unit of specific power draw or ton of ore ground of a continuous operation is of great importance as it provides a quantitative comparison of the severity of wear for different operations. Once the mill is running, the weight of selected lifters can only be measured when the lifter is taken out from the mill shell. This method is therefore not used frequently since removing lifters from tumbling mill shell in order to measure their weight decreases mill availability.

### 2.3.3.2 *Distribution of wear over the liner surfaces*

This is the most important method as the change of the mill lifter profiles due to wear affects the mill performance. Efforts by different researchers are made in order to monitor accurately the profiles and weight of lifters in industrial tumbling mills as a function time. Figures A1 and A2 in Appendix A show profiling gauge used to measure lifters profiles. The profiling gauge can be used when lifters are removed from the mill or in situ as long as the reference point can be detected to compare the initial profile to the actual. Figure A3 in Appendix A shows a laser scanner developed by Conveyor Dynamics International and Svedala (Nordell, L. K. and Potapov A. V. (2001)) to measure lifter profiles in situ. To increase the accuracy of measurements, Banisa, S. and Hadizedh, M. (2006) developed a 3D method of lifter profile measurement which takes into account the non-uniform wear observed through the mill length. Chandramohan, R. and Powell, M.S. (2006) developed a mechanical gauge to monitor the wear of lifters and Radziszewski et al. (2006) developed a sensor also to monitor the wear of lifters.

The limit of resolution depends on the method used.

### 2.3.4 Mathematical models of wear

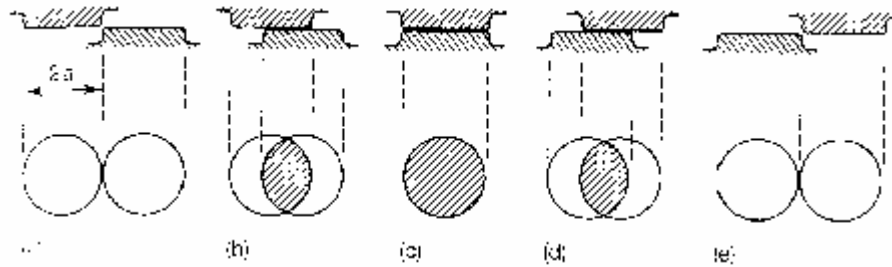
#### 2.3.4.1 *Adhesive model: Archard wear equation.*

Archard (1953) developed a simple equation of adhesive wear. He assumes that the contacts between two surfaces occur where asperities touch, and that the total area of contact is the sum of individual asperity contact areas. Figure 2.2 shows a schematic diagram of the evolution of a single contact patch as two asperities move over each other.

The normal load  $dW$  supported by one asperity of radius  $a$  is given by:

$$dW = Ppa^2 \quad (2.7)$$

where  $P$  is the yield pressure for plastically deforming asperity.



**Figure 2.2** Schematic diagram showing the evolution of a single contact patch as two asperities move over each other after Archard (1953)

He assumed that the volume of material removed by wear  $dV$  is proportional to the cube of the contact dimension  $a$ , which implies that the shape of the wear particle should be independent of its size. Assuming that it is a hemisphere:

$$dV = \frac{2pa^3}{3} \quad (2.8)$$

It is also assumed that only a proportion  $k$  of all asperities undergo the wear. The average volume  $dV$  of material worn due to sliding of the one pair of asperities through a distance  $S = 2a$  is given by:

$$dV = \frac{kSpa^2}{3} \quad (2.9)$$



The total wear is the sum of all the contributions over the entire area of contact. Thus:

$$V = \frac{kSW}{3P} \quad (2.10)$$

The yield pressure  $P$  can be approximated to the hardness  $H$  of the material worn. Equation (2.10) can therefore be rewritten into the following form:

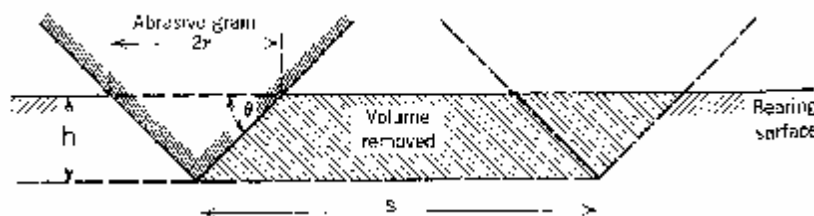
$$V = \frac{KSW}{H} \quad (2.11)$$

The dimensionless constant  $K$  called the wear coefficient can be used to compare the severity of wear process in different systems.

The ratio  $\frac{K}{H}$  is called the wear rate.

#### 2.3.4.2 Abrasive model: Rabinowicz wear equation

Rabinowicz (1965) derived a quantitative expression of abrasive wear assuming that asperities on the hard surface are conical. Figure 2.3 shows a simplified model of a conical asperity removing materials.



**Figure 2.3** Simplified abrasive wear model after Rabinowicz (1965)

One asperity carrying a load of  $dW$  will penetrate the softer surface to an extent given by:

$$dW = Hpr^2 \quad (2.12)$$

Where  $H$  is the hardness of the softer surface

$r$  is the radius of the cone base

When the cone moves through a distance  $S$ , it will remove a volume  $dV$  given by:

$$dV = \frac{dW * \tan q * S}{pH} \quad (2.13)$$

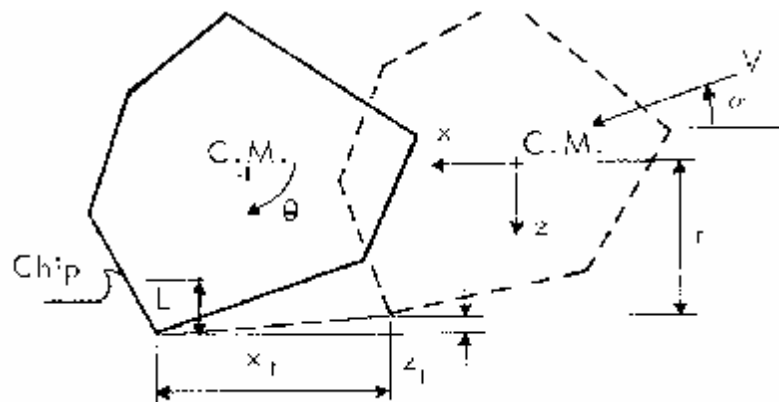
Taking into account all asperities, we have:

$$V = \frac{\tan q * SW}{pH} \quad (2.14)$$

Rabinowicz equation predicts the volume of material removed due to abrasion as a function of the hardness of the soft material, the sliding distance, the normal load and the angle of attack.

#### 2.3.4.3 Erosion by solid particles impact: Finnie wear equation

Finnie (1972) developed an equation predicting the volume of material eroded by solid particles in a fluid stream. Figure 2.4 described, represents the idealised picture of the erosion caused by one particle in a fluid stream on a surface of a ductile material.



**Figure 2.4** Incident erosive particle cutting into a ductile surface at an angle of attack  $\alpha$  after Finnie (1972)

Based on the equation of the particle motion in the fluid stream and assuming that the volume displaced is the volume removed by the particle, the following equation was derived:

$$V = \frac{cMv^2}{4p\left(1 + \frac{mr^2}{I}\right)} \left[ \cos^2 a - \left(\frac{\dot{x}_t'}{v}\right)^2 \right] \quad (2.15)$$

where

$V$  is the volume removed from the surface

$c$  is the fraction of particles cutting in this idealised manner

$M$  is the mass of eroding particle

$v$  is the particle velocity

$p$  is the horizontal component of flow pressure

$I$  is the moment of inertia of particle about its center of gravity

$m$  is the mass of one particle

$a$  is the angle of impact

$\dot{x}_t'$  is the horizontal velocity of the particle when the cutting ceases. It is given by:

$$\dot{x}_t' = v \cos a - \frac{2v}{P} \sin a \quad (2.16)$$

where

$$P = \left( \frac{K}{1 + \frac{mr^2}{I}} \right) \quad (2.17)$$

with  $K$  equal to the ratio of the vertical force to the horizontal force on the particle.

#### 2.3.4.4 Impact wear model: Wellinger and Breckel wear equation

Wellinger and Breckel (1969) conducted several repetitive impact wear tests with different materials. They found a good agreement between the volume of material removed  $V$  and the impact velocity  $v$  at a fixed number of cycles. They found that:

$$V \propto v^n \quad (2.18)$$

where the exponent  $n$  varied between 1.5 and 2.2 depending on material properties. Theoretical equations give an exponent value of 2.

## 2.4 Review of modelling the wear of mill lifters

Energy consumption and metal wear are the principal cost factors in milling plants. Over the past years, much emphasises have been given to accurately predict and optimise the energy consumption in tumbling mills. If that objective is satisfactorily achieved, much works still remains to be done in terms of metal wear prediction and particularly, the prediction of evolving lifter profiles due to wear. The literature contains few publications related to the modelling of the wear of lifters. Important papers by different authors are discussed below.

### 2.4.1 Bond

Bond (1964) developed, from laboratory experiments and available plant data, the following equations which relate the liner mass lost per kilowatt-hour of mill energy consumed:

o Wet rod mills:

$$\frac{lb}{Kwh} = 0.035 * (A_i - 0.015)^{0.30} \quad (2.19)$$

- Wet ball mills, overflow and grate discharge:

$$\frac{lb}{Kwh} = 0.026 * (A_i - 0.015)^{0.30} \quad (2.20)$$

- Dry ball mills, grate discharge:

$$\frac{lb}{Kwh} = 0.005 * A_i^{0.5} \quad (2.21)$$

where  $A_i$  is the abrasion index.

Although the prediction of the liner mass lost is important, we are more interested in the prediction of evolving liner profiles, as it affects the performance of the mill.

#### 2.4.2 Radziszewski and Tarasiewicz

Radziszewski and Tarasiewicz (1993) used a static charge profile to predict the wear of lifters. They assumed that the lifters wear due to gravitational and centrifugal forces exerted by the ball charge. They assumed also that the wear rate is a function of the position and the intensity of the total force. These authors combined an adhesive and abrasive mathematical model to predict the volume of material removed on lifters.

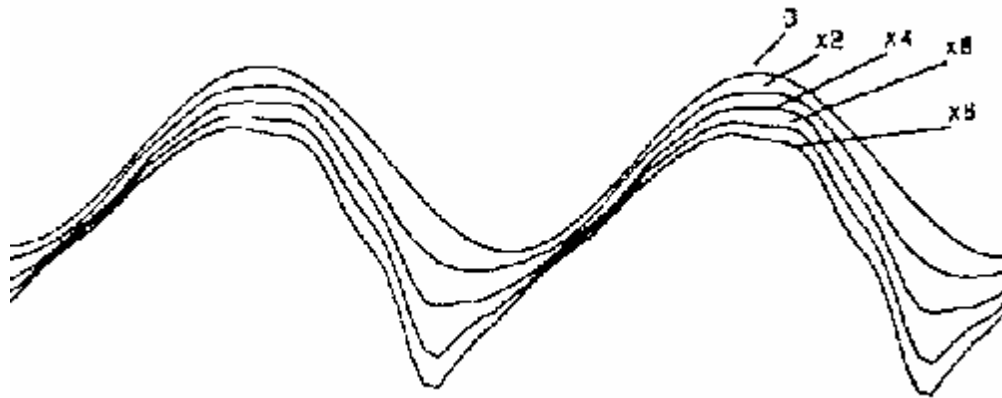
Lifters are discretised in order to apply the wear equation on each division. Appendix B shows the discretisation method they used on a wave liner profile. Their simulated results for a wave and a bevelled liner profile are also shown in Appendix B.

Although their simulated profiles are realistic, these authors did not compare their prediction to experimental data. On the other hand, their static model can not accurately predict the load behaviour in the mill as affected by operating parameters.

### 2.4.3 Glover and de Beer

Glover and de Beer (1997) applied the Discrete Element Method to simulate the charge motion in ball mills and predict the wear of lifters. After discretisation of lifters into a number of straight line elements, they assume that material is removed from the lifter according to the Archard wear equation.

The resulting worn profile is generated after a simulation by subtracting the volume lost and smoothing the profile using a three point moving average process. Figure 2.5 shows their simulated results of a double wave liner profile.



**Figure 2.5** DEM simulated profiles after Glover and de Beer (1997)

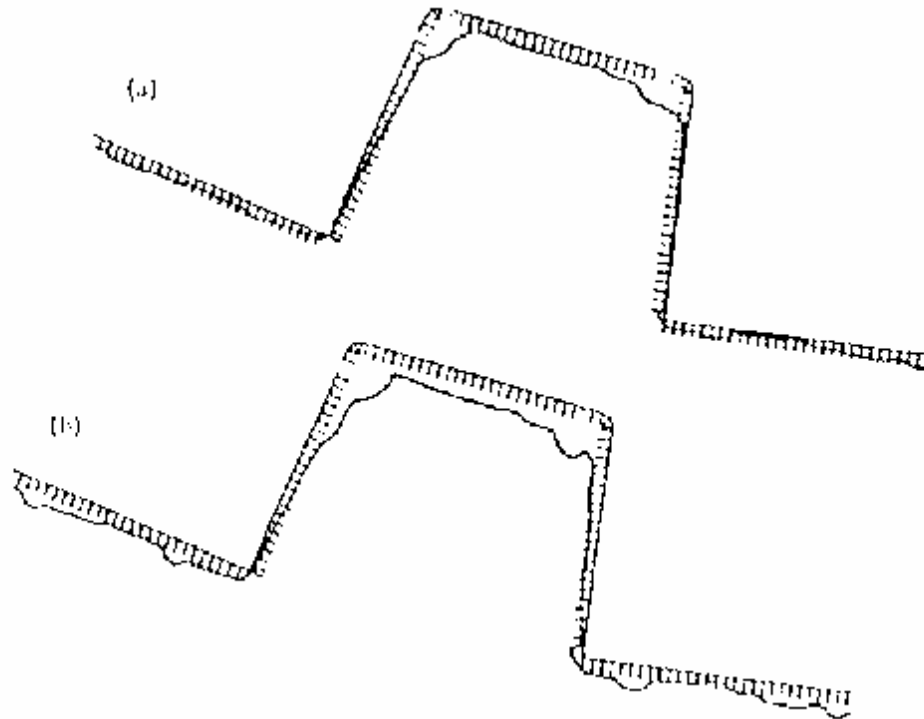
It can be deduced from Figure 2.5 that the worn profiles predicted are not realistic comparatively to those observed practically. In practice, worn profiles become smooth whereas these become more pronounced.

On the other hand, using the Archard equation implies that impact collisions without sliding do not produce wear. In reality, both, impact and abrasion contribute to the wear of lifters.

### 2.4.4 Cleary

Cleary (1998) predicted the wear of lifters using also the Discrete Element Method. He used Finnie's wear model to predict the volume of material removed on lifters due

to particle – lifter collisions. The results of his prediction at 60 and 80% of critical speed are represented in Figure 2.6.



**Figure 2.6** DEM simulated profile at a)  $N_c=60\%$ ; b)  $N_c=80\%$  after Cleary (1998)

Again, it can be seen from Figure 2.6 that the simulated worn profiles are unrealistic comparatively to those observed practically where worn profiles are smooth.

#### 2.4.5 Xiangjun Qiu, Alexander Potapov, Ming Song and Lawrence Nordell

Qiu et al (2001) applied the Discrete Element Method to predict the wear of lifters. Like Glover and de Beer, they used also the Archard equation to predict the volume of lifters lost in the wear process. Figure B4 in Appendix B shows the comparison between their simulated and the measured lifter profiles used in a semi autogenous mill. A good agreement is found between the simulated and the measured profiles. Despite the good results presented, the authors did not report or show the way to solve the problem faced by Glover, de Beer and Cleary to obtain a simulated smooth profile. On the other hand, the use of the Archard equation to predict the material

removal does not take into account other type of wear which occur in the semiautogenous mill.

## 2.5 Conclusions

Our literature review focused firstly on the effort by different authors to accurately predict the load behaviour and power draw in the mill since the beginning of the last century. From the proposed models, only the discrete element method applied to milling is able to accurately predict the power draw and the load behaviour as affected by the mill dimensions, the mill speed, the mill filling, the charge composition and the liner design. Moreover, using the Discrete Element Method offers the advantage of recording energies or forces involve in particle – liner collisions which is the starting point to model the wear of lifters. Secondly, we introduced different models and equations of wear predicting the volume displaced or removed from a material surface due to wear. We show that due to the complexity of the wear phenomenon, there is no mathematical model which can predict the volume of material worn in all cases. Thirdly, we reviewed published work modelling the wear of lifters in the mill. Despite the importance of modelling the wear of lifters, only four (4) important papers have been found in the literature related to the topic.

Two problems emerge from this review: firstly, mathematical models used to predict the wear of lifters do not take into account all mechanisms of wear which occur in the milling environment. Secondly, simulated profiles must be smooth as observed practically.

There is therefore no doubt from this review of literature that there is a need to develop a new approach predicting accurate and realistic simulated profiles.



# Chapter 3

## Discrete Element Method

### **3.1 Introduction**

### **3.2 Calculations**

### **3.3 Contact models**

### **3.4 Parameters used in the Discrete Element Method simulations**

#### 3.4.1 Time step

#### 3.4.2 Material stiffness

#### 3.4.3 Coefficient of restitution

#### 3.4.4 Coefficient of friction

### **3.5 Simulation Outputs**

#### 3.5.1 Mill power draw

#### 3.5.2 Impact energy spectra

#### 3.5.3 Plot file (plt file), trace path and the position density plot (PDP)

#### 3.5.4 Forces on lifters, frictional and impact energies dissipated in the mill

### **3.6 DEM validations in milling**

### **3.7 Conclusions**

### 3.1 Introduction

The Discrete Element Method (DEM) is a numerical tool capable of simulating the motions and interactions of individual particles in a dynamic environment such as tumbling-mills, chutes and fluidised bed. This technique was originated by Cundall (1971) for the analysis of rocks mechanics problems. In 1979, Cundall and Strack applied the tool to model the behaviour of assemblies of discs. The comparison between the vector forces simulated by the Discrete Element Method and calculated shows a good correspondence. Since that validation, the method gained popularity in many fields where discrete particles are involved in dynamic motion.

The discrete or discontinuous numerical modelling offers more flexibility compared to continuum analytical modelling. This flexibility includes taking into account: the design configurations, the particle sizes, the size distribution and properties of particles. The major disadvantage of this method, so far, despite the development of computer hardware, is the time of simulation which is high when the number of particles involved is more than ten thousand.

### 3.2 Calculations

In the Discrete Element Method simulation, every particle and object is identified separately. The motion of particles resulting from forces acting on them is calculated using Newton's second law. Newton's second law applied to a particle is given by:

$$m \ddot{x}_i = \sum F_i + mg_i \quad (3.1)$$

$$I \ddot{\theta}_i = \sum M_i \quad (3.2)$$

where

$i$  represents the coordinate X, Y and Z

$m$  is the mass of the particle

$\ddot{\mathbf{r}}_i$  is the acceleration of the particle

$F_i$  is the force acting on the particle

$g_i$  is the acceleration due to gravity

$I$  is the moment of inertia of the particle

$q_i$  is the angular position

$M_i$  is the moment of the particle

Equations (3.1) and (3.2) are integrated over a time step  $\Delta t$  to find the new position, velocity, and angular velocity of each particle.

For tumbling mills, all particles are contained in the liner – lifter configuration as boundary. The liner wall positions are updated each time step as a function of the rotational speed of the mill.

In the DEM simulations, particles are modelled as disks (usually in 2D simulations), spheres or super-quadratics (Cleary, 2001) using different size distributions. Super-quadratics are defined by the following equation:

$$x^n + \left(\frac{y}{A}\right)^n = s^n \quad (3.3)$$

where  $n$  determines the blockiness of the resulting particle.

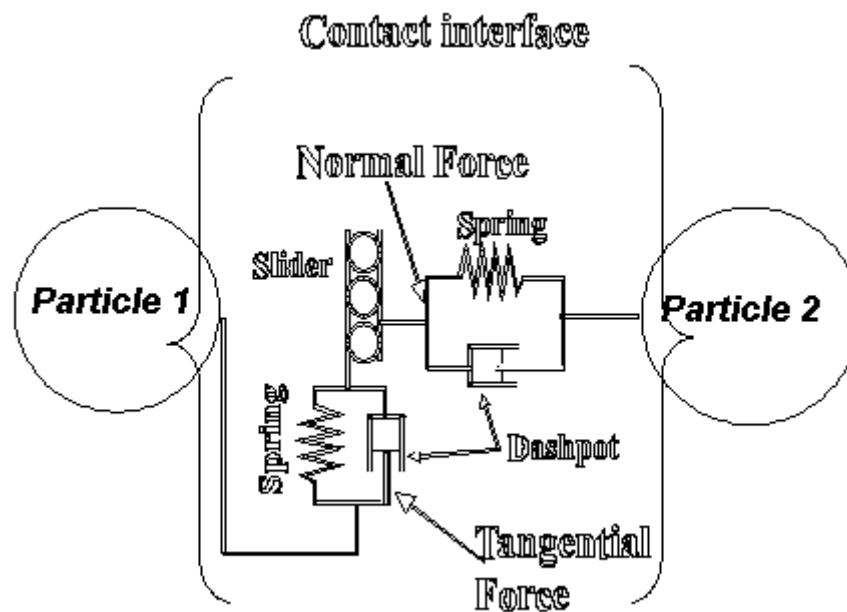
$A$  is the aspect ratio

### 3.3 Contact models

Interactions between particles or between particles and mill walls are modelled assuming that there is a spring, a dashpot and a slider between them. The spring accounts for the repulsive force which depends on the material stiffnesses  $K_n$  and  $K_t$  in the normal and tangential direction respectively. The dashpot dissipates a proportion of the relative kinetic energy in each collision. The dissipation of energy is represented by the coefficient of restitution  $e$  which is the ratio of the velocity of a particle in the normal direction after and before a collision event. The slider accounts for surface interactions represented by the coefficient of friction  $m$ . Function of the

disposition of the spring and the dashpot, we have a linear spring- dashpot model or a non linear spring – dashpot model.

The linear spring – dashpot model is represented by Figure (3.1).



**Figure 3.1** The linear spring – dashpot contact model

Particles are allowed to overlap by an amount  $\Delta x$ . Using the linear spring – dashpot model, the normal  $F_n$  and tangential  $F_t$  forces acting between two particles in contact are given by:

$$F_n = K_n \Delta x + C_n v_n \quad (3.4)$$

$$F_t = \min \left\{ m F_n, K_t \int v_t dt + C_t v_t \right\} \quad (3.5)$$

Where

$v_n$  and  $v_t$  are the relative velocities of the particles in the normal and tangential directions respectively.

$dt$  is the time step used in the simulation

$C_n$  and  $C_t$  are the normal and tangential damping coefficients respectively.

The normal damping coefficient  $C_n$  is related to the coefficient of restitution  $e$  by:

$$C_n = -\frac{2 \ln e \sqrt{m_{ij} K_n}}{\sqrt{\ln^2(e) + p^2}} \quad (3.6)$$

$$m_{ij} = \frac{m_i m_j}{m_i + m_j} \quad (3.7)$$

Where  $m_{ij}$  is the reduced mass of two particles  $i$  and  $j$  of masses  $m_i$  and  $m_j$  respectively.

Based on extensive validation work of the Discrete Element Method (Mishra and Rajamani, 1993; van Nierop et al, 2001; Moys and Dong, 2002) in our simulations, the tangential stiffness  $K_t$  and damping coefficient  $C_t$  are respectively chosen equal to  $3/4$  of the value in the normal direction.

Nonlinear contact models described by Mishra and Murty (2001) can also be used to model the behaviour of particles.

### 3.4 Parameters used in the Discrete Element Method simulations

#### 3.4.1 Time step $dt$

The stability and accuracy of this numerical method depends on the choice of the time step. This value must be equal or less than the critical time step which depends on the contact model. If the time step is chosen higher than the critical time step, the energy balance is violated. An estimation by Mishra (1991) of the critical time step of a mass  $m$  connected to a spring of stiffness  $K$  having one degree of freedom is given by:

$$dt \leq 2\sqrt{\frac{m}{K}} \quad (3.8)$$

In our simulations,  $m$  represents the mass of the particle having the smallest mass.  $K$  is the normal stiffness. A reduced time step is typically used to account for multi-particle collision by dividing the critical time step with a suitable number between 5 and 20 (Mishra, 2003). A large value of  $K$  require a prodigious number of calculations and time of simulation particularly when the simulation involves a large number of particles.

#### 3.4.2 Material stiffness

The material stiffness is determined experimentally by video studies of balls bouncing off other balls or off targets of specified liner material. The experimental results are generally too high and must be adjusted in order to allow an overlapping of particles of 0.1 to 1 % of their dimension and to have a reasonable critical time step without loosing the accuracy and stability of simulations. Mishra (1991) and van Nierop et al (2001) show that, the power draw in tumbling mills is more sensitive to the coefficient of restitution and coefficient of friction than the material stiffness. In our simulations, the values used for the normal and tangential stiffness are 400,000 N/m and 300,000 N/m respectively.

#### 3.4.3 Coefficient of restitution

The coefficient of restitution is an important parameter in the DEM simulation as its affects the power draw by tumbling mills and the energy spectra (Mishra, 2003). Johnson (1985) shows that the coefficient of restitution is not a material property but it is function of the impact velocity, the geometry, and the hardness of the material. Dong and Moys (2001, 2003) confirmed these results by calculating the velocity of a ball moving in an experimental tumbling mill at different speeds and in an idealized situation. In our simulations, we assume that the coefficient of restitution is constant and its correct value (0.4 to 0.7) is deduced after validation of simulated results (power draw by tumbling mills, load behaviour and forces on liners) in comparison to experimental results.

### 3.4.4 Coefficient of friction

The power draw by tumbling mills is sensitive to the variation of the coefficient of friction depending on the lifter design, and the mill percentage of critical speed (Moys et al, 2001). Values comprise between 0.2 and 0.4 found after validation of simulated results are used in our DEM simulations.

## 3.5 Simulation outputs

### 3.5.1 Mill power draw

The power required to maintain the mill moving at a constant speed is given by the product of the total torque by the angular mill speed. The total torque  $T$  is determined by the following equation:

$$T = \sum_{i=1}^n r_i * F_{t,i} \quad (3.9)$$

Where

$r_i$  is the distance from the mill centre to the point of contact of particle  $i$  in contact with the mill liner - lifter.

$F_{t,i}$  is the force normal to the mill radius exerted by a particle  $i$  at the contact point with the mill liner – lifter.

The torque is calculated for each time step  $dt$ . The total torque is the average torque during the simulation.

The power consumption can also be found by dividing the sums of energies dissipated in every particle collision during each time step and the time of simulation.

### 3.5.2 Impact energy spectra

The impact energy spectra are the collision frequency plotted as a function of the collision intensity of ball media in the mill. It gives an indication of the mill energy available in order to reduce the size of particles.

### 3.5.3 Plot file (plt file) , trace path and the position density plot (PDP)

The plot file (Plt) gives for each frame the coordinate (X, Y and Z), the speed and the characteristic (density and radius) of each particle in the mill. It is therefore possible to select a specific ball or balls and study their behaviour in the load.

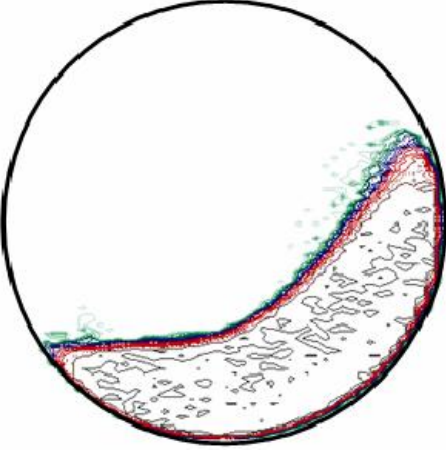

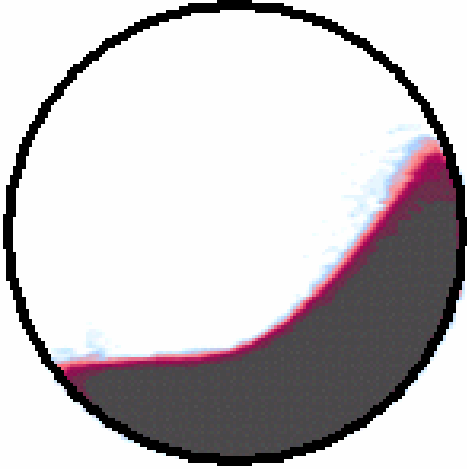
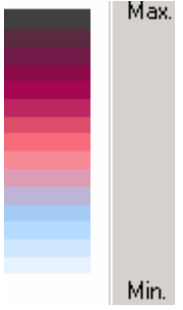
The trace path plots trajectories of selected balls in the mill.

The position density plot (PDP) represents the average of the load position in a mill. The mill is divided into grids and the number of times a ball centre occurs in a grid is displayed graphically in the grid with an area proportional to the number of occurrences. Colours can also be used to differentiate the number of occurrence. Table 3.1 shows an example of representation of the load behaviour using the position density plot. A logarithmic grading was used to differentiate the frequency of appearance of particles in grids. The maximum appearance is represented by the black colour and the lack of appearance in white colour. The same grading will be used in this thesis.

### 3.5.4 Forces on lifters, frictional and impact energies dissipated in the mill

The normal and tangential forces exerted by the ball charge on liners/ lifters (Equations 3.4 and 3.5) can be recorded at any mill angular position  $\theta_i$  during a mill revolution. The frictional and impact energies dissipated during collisions between balls and between balls and liners/lifters can also be quantified and recorded as a function of time during a mill revolution.



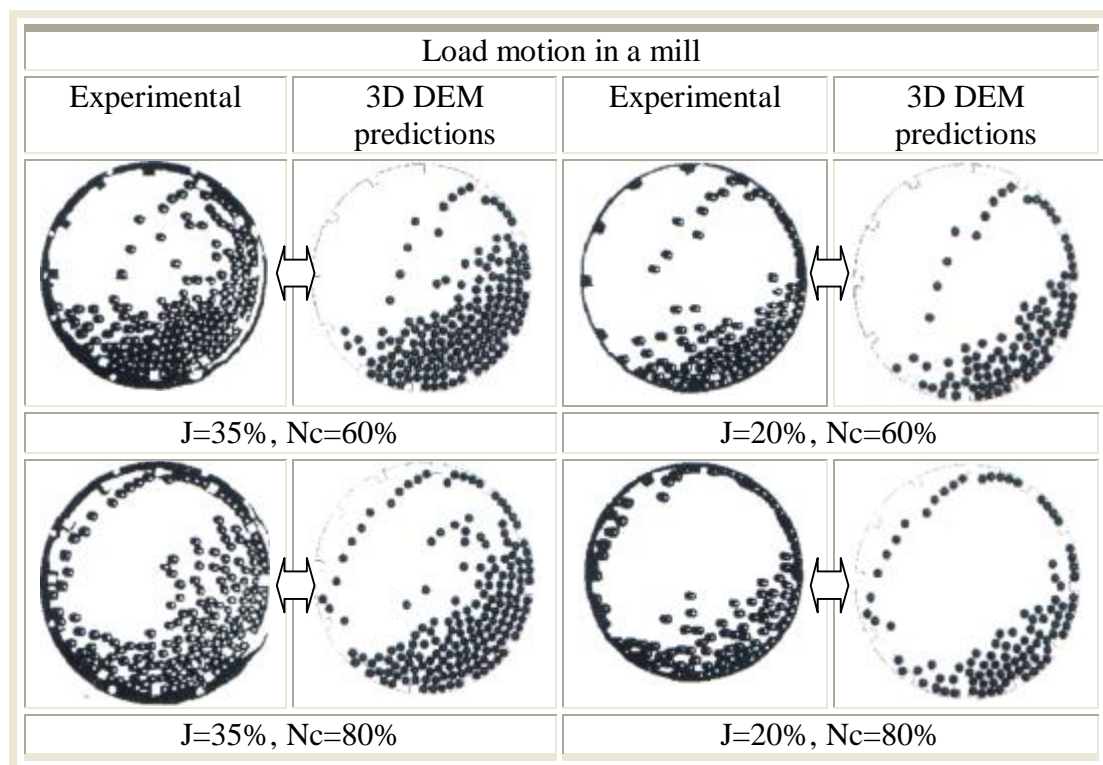
	
<p>Contour plot of the position density plot (PDP) using colour lines</p>	<p>Frequency</p>
	
<p>Contour plot of the position density plot (PDP) using gradation solid colours</p>	<p>Frequency</p>

**Table 3.1** Representation of the load behaviour using the position density plot (PDP)

A logarithmic grading is used to differentiate the frequency of appearance of particles in grids. The maximum appearance is represented by the black colour and the lack of appearance in white colour.

### 3.6 DEM validations in milling

Since the DEM allows simulating the motion of particles in a dynamic environment, many initial studies have been performed to analyse the motion of charge in a wide range of tumbling mills. Van Nierop et al (2001) compared the simulated and experimental load behaviour observed in a laboratory mill at different speeds and percentage of filling. Figure 3.2 shows the results at 60 and 80% of critical for the percentage filling of 20 and 35%.



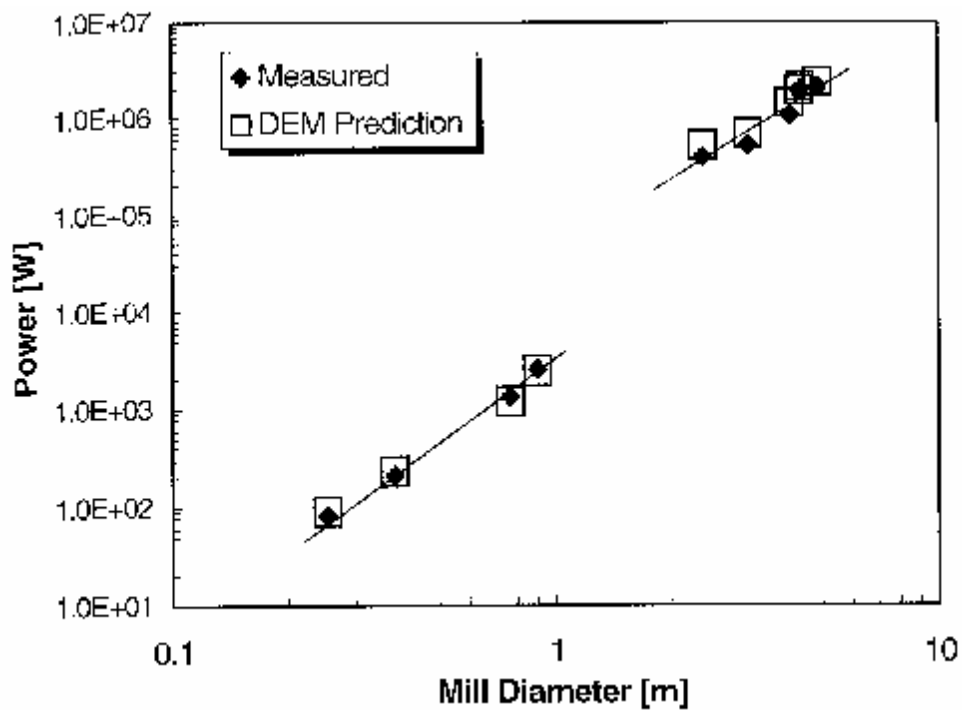
**Figure 3.2** Comparison between measured and simulated load behaviour at 60 and 80% of critical speed at 20 and 35% of mill filling after Van Nierop et al (2001)

It can be seen from Figure 3.2 that there is a good agreement between the measured and simulated load behaviour. The DEM predicts accurately the load motion in tumbling mills as affected by the mill speed, the mill filling, the liner design and the charge composition.

The accurate prediction of mill power draw has been the preoccupation of many researchers since the first attempt by Davis (1919). Despite the progress made by

many authors, it is difficult to predict the load behaviour and power draw as affected by the lifter profiles. The DEM offers that advantage.

Figure 3.3 compares the measured results to the DEM prediction for a wide range of mill diameter. It can be seen from Figure 3.3 that there is a good agreement between the measured and simulated powers.



**Figure 3.3** Comparison between measured and simulated power draw for ball mills of different diameters after Datta et al (1999)

### **3.7 Conclusions**

The Discrete Element Method can successfully be used to predict the charge motion and power draw by tumbling mills as affected by the mill speed, the mill filling, the charge composition and the lifters profiles. From contact model equations, it is also possible to quantify interactions between particles and between particles and liners in terms of forces and energy involved in collisions. This method has therefore the potential to model the forces exerted by the charge on mill lifters and predict the evolving lifter profiles due to wear. In this thesis we assess the ability of this method to perform these predictions. The Itasca's PFC code originated by Cundall was used in this thesis.

# Chapter 4

## Modelling of evolving mill lifter profiles due to wear

### **4.1 Introduction**

### **4.2 Parameters affecting the wear of mill lifters**

#### 4.2.1 Lifter characteristics

##### *4.2.1.1 Lifter design*

##### *4.2.1.2 Lifter material*

#### 4.2.2 Type of grinding: Dry or wet

#### 4.2.3 Mill operating parameters

##### *4.2.3.1 Mill speed*

##### *4.2.3.2 Mill filling*

##### *4.2.3.3 Mill feed rate*

##### *4.2.3.4 Mill temperature*

#### 4.2.4 Media properties

##### *4.2.4.1 Shape*

##### *4.2.4.2 Abrasiveness*

##### *4.2.4.3 Size distribution*

##### *4.2.4.4 Material*

Conclusion

### **4.3 Types of wear in milling environment**

### **4.4 Choice of a wear mathematical model**

## **4.5 Implementation of the wear mathematical model in the DEM code**

### 4.5.1 Introduction

### 4.5.2 Lifter discretisation

#### *4.5.2.1 Vertical discretisation*

#### *4.5.2.2 Radial discretisation*

### 4.5.3 Objective function

#### *4.5.3.1 Definition*

#### *4.5.3.2 Two Dimensional (2D) model*

#### *4.5.3.3 Three Dimensional (3D) model*

#### *4.5.3.4 Influence of weight factors of the objective function*

##### *4.5.3.4.1 Introduction*

##### *4.5.3.4.2 Influence of beta*

##### *4.5.3.4.3 Influence of lambda*

##### *4.5.3.4.4 Influence of alpha*

## **4.6 Conclusions**

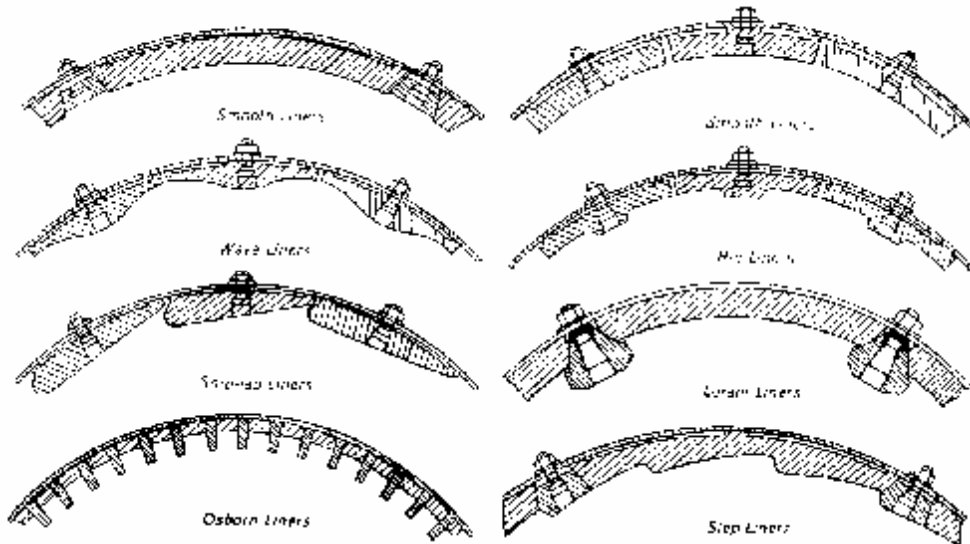
## 4.1 Introduction

The wear of mill lifters reduces the performance and efficiency of tumbling mills. Lifters are therefore replaced in the mill when the cost associated to the loss of production due to the wear is higher than the cost of relining (Meekel et al, 1996) or when they reach a critical thickness susceptible to breakage if used further. The cost associated with the lifters wear includes not only the cost of the lost of production due to the wear and the cost of replacement, but also the cost due to the lack of production during the downtime of replacement.

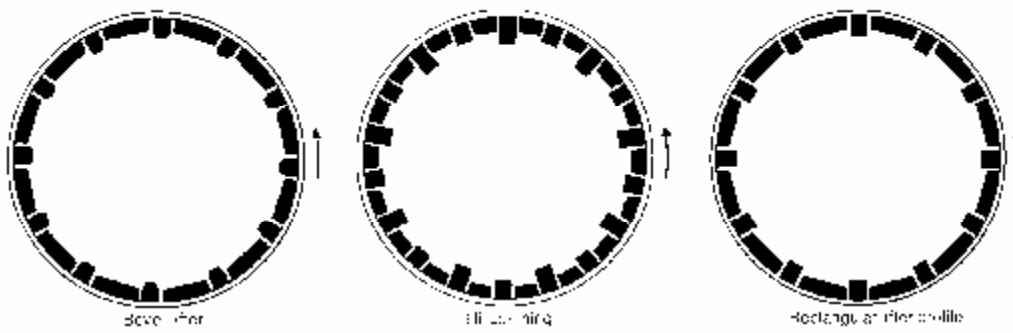
Mill lifters have different profiles. Figure 4.1.a, 4.1.b and 4.1.c show lifter profiles reported by Wills (1992), Kelly and Spottiswood (1982) and Cleary et al (2001) respectively. Lifters have the following functions:

- To protect the mill shell against forces exerted by the mill charge.
- To transfer energy to the mill charge allowing cascading and cataracting motions.
- To classify the media (in some cases).
- To promote the most favourable motion of the charge for a particular operation.

In early work, the driving force behind the change of the lifter design was the reduction of the downtime of lifter replacement and its associated costs (Parks, 1996). Later work is oriented toward the design of lifters which optimise tumbling mills performance over their useful life. The Discrete Element Method being able to predict accurately the load behaviour and power draw by tumbling mills as affected by lifter design is the appropriate tool to conduct these researches. After the validation of the Discrete Element Method to predict the mill power draw and load behaviour, an important step which can increase the profitability of milling plant is the assessment of this method to accurately predict the wear of tumbling mill lifters.



**Figure 4.1.a** Lifter profiles after Wills (1992)



**Figure 4.1.b** Lifter profiles after Kelly and Spottiswood (1982)



**Figure 4.1.c** Noranda and Ical lifter profiles respectively after Cleary et al (2001)



## 4.2 Parameters affecting the wear of tumbling mill lifters

The following factors influence the wear of lifters in tumbling mills:

### 4.2.1 Lifter characteristics

#### 4.2.1.1 *Lifter design*

Experience (Parks, J.L., 1996) and analysis of energies involved in ball collisions with liners, which affect the wear of lifters (see Chapter 6) show that the lifter design is a critical factor in the wear process. “Aggressive” lifters wear more quickly than non-aggressive for the same operating conditions.

#### 4.2.1.2 *Lifter material*

Materials respond differently to impact, abrasion and corrosion types of wear present in the milling environment. Different materials will therefore offer different resistance to the wear process. An optimal combination of toughness, resistance to abrasion and corrosion is required for all lifters. The selection of lifter material for a particular operation is based on economic considerations. The most cost-effective materials should have a high useful life for a low price.

### 4.2.2 Type of grinding: Dry or Wet

Bond (1964) conducted a comparative study between the dry and the wet grinding in terms of lifter wear. He noticed that the lifter wear in wet conditions is higher than in the dry conditions. This is caused by the contribution of the corrosive wear which is high in wet conditions.

### 4.2.3 Mill operating conditions

#### 4.2.3.1 Mill speed

Energies involved in collisions between balls, ore particles and lifters, which affect the wear of lifters depend on the mill speed. Consequently, the mill speed is an important factor of the wear of mill lifters.

#### 4.2.3.2 Mill filling

The amount of charge in the mill affects the frequency and the amplitude of energy involved during charge - lifters contact during each mill revolution and therefore the wear of lifters.

#### 4.2.3.3 Mill feed rate

The lifter wear rate is high in a mill running without ore due to direct impact and abrasion of balls and lifters. The presence of ore prevents the lifter exposure and reduces the wear rate. This reduction depends on the mill feed rate or the percentage of the maximum capacity feed. Increasing the feed rate leads generally to a decrease of the lifter wear rate.

#### 4.2.3.4 Mill temperature

Material properties being function of temperature, lifters resistance to wear will be affected by operating temperature in the mill.

### 4.2.4 Media properties

#### 4.2.4.1 Shape

The shape of grinding media and particles influences the lifter wear rate. For instance, cylpebs and spherical balls used as grinding media in the same conditions produce different lifter wear rate.

#### *4.2.4.2 Abrasiveness*

The more the ore is abrasive, the more the contribution of abrasion wear is important and therefore, the lifter wear rate is higher. Standard tests giving the Abrasive Index (AI) have been designed in order to characterise the abrasiveness of coal or ore.

#### *4.2.4.3 Size distribution*

For the same mass of grinding media in the mill, the energy consumed in ball – lifter interactions, and therefore the wear of lifters, will be function of the size distribution of the grinding media.

#### *4.2.4.4 Material*

Balls and ores properties such as hardness influence the wear rate of lifters due to interactions occurring between them.

### Conclusions

It can be seen that most of the factors influencing the wear of lifters influence also the performance of tumbling mills. Reducing the wear of lifters by changing these parameters will have an influence on mill performance. The optimal mill operating conditions are chosen in order to maximise the mill performance and minimise the wear of lifters.

### 4.3 Types of wear in milling environment

In order to choose an appropriate wear model predicting the volume or mass of material removed on lifters, it is important to identify the types of wear occurring in milling environment. It is also important to understand that despite the classification of wear as described in Chapter 2, none of the types of wear occurs alone. In reality, there is always a combination of different mechanisms with one of them being the main factor. It is the main factor, which determines the type of wear and is used to derive the wear equation.

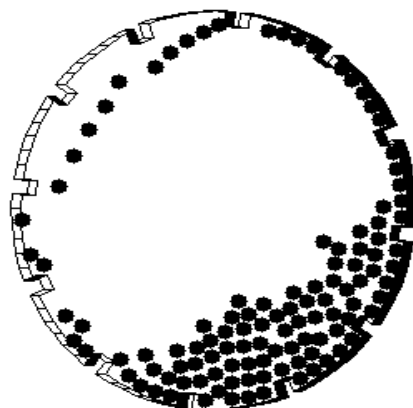
Figure 4.2 represents a simulated typical ball charge motion in a mill.

It can be seen from Figure 4.2 that there are:

- A layer of the charge in contact with the liners. By the contact between that layer and liners, liners can be subjected to the corrosive wear, particularly in wet conditions.

It is recognised that the charge layer in contact with liners is generally not moving at the same speed as the liners. There is therefore a relative motion between that layer and the liners. That relative motion is mainly responsible of adhesion and abrasion wear on liners.

- Balls and particles in free flight impact the liners at the toe. Those cataracting balls are mainly responsible of impact wear on liners. Major impact wear occurs also when lifters enter underneath the mill charge at the toe.



**Figure 4.2** Ball charge motion in a mill

We have therefore identified the following types of wear in milling environment:

- Adhesion wear
- Abrasion wear
- Corrosion wear and
- Impact wear.

In dry conditions, the corrosive wear can be neglected due to the absence of aqueous media allowing chemical reactions to take place.

#### **4.4 Choice of a wear mathematical model**

Since our Discrete Element Method code predicts the load behaviour and power draw in dry conditions, our model must also be valid in dry conditions. Adhesion, abrasion and impact are the main types of wear occurring in dry tumbling mills. The mathematical model predicting the wear of lifters must consequently take into account these three types in order to accurately predict the volume removed on lifters due to wear.

There is no mathematical model predicting the volume of material removed in all cases. Existing models have been developed for particular type of wear such as adhesion, abrasion, corrosion or impact. To take into account all types of wear, we assume, like Radziszewski (2002) exploring the total media wear, that the total volume removed is the sum of the contribution of each mechanism.

Adhesion mathematical equation is represented by the Archard wear equation described in Chapter 2.

Abrasion mathematical equation predicted by Rabinowicz (1965) has the same form as Archard equation where the coefficient of wear  $K$  is function of the attack angle of the abrasive particle. Thus, both abrasion wear and adhesion wear can be predicted using the single Archard wear equation. The Archard equation can be transformed into the following form:

$$V = W * E_{ad-abr} \quad (4.1)$$

Where

$$W = \frac{K}{H} \quad (4.2)$$

$$E_{ad-abr} = F_n * S \quad (4.3)$$

$V$  is the volume of material removed,  $m^3$

$W$  is the wear rate,  $Pa^{-1}$

$K$  is the wear coefficient, -

$H$  is the hardness of the material subjected to wear, Pa

$E_{ad-abr}$  is the adhesion or abrasion energy, J

$F_n$  is the normal load, N

$S$  is the sliding distance, m

From the transformed equation, we can deduce that when there is no relative motion between media and liner ( $S = 0$ ) there is no wear. This is not true as we showed in our literature that the wear can occur when there is only impact without sliding.

This situation shows the limitation of the Archard equation to predict alone with accuracy the wear occurring in milling environment since it is not taking into account the impact wear.

Studies of repetitive impact wear by Wellinger and Breckel (1969) and Hutchings (1992) show that the volume of material removed  $V$  is proportional to the impact velocity  $v$  according to the following equation:

$$V \propto Kv^n \quad (4.4)$$

They found experimentally that the velocity exponent  $n$  varies from 1.5 to 2.4 depending on the material tested. We use the theoretical value 2.

As energy and velocity are related ( $E = \frac{mv^2}{2}$ ), equation (4.4) can be by rewritten into the following form:

$$V = KE_{impact} \quad (4.5)$$

Assuming that the total wear occurring on a surface  $i$  is the sum of adhesion/abrasion and impact wear, we deduce the following equation:

$$V_i = W(a_{ad-abr} * E_{ad-abr,i} + a_{impact} * E_{impact,i}) \quad (4.6)$$

where

$V_i$  is the volume of material removed on a surface  $i$

$W$  is the wear rate

$a_{ad-abr}$  and  $a_{impact}$  are weight factors given to adhesion/abrasion and impact energies respectively depending on material (lifters and balls) and ore properties.

$E_{ad-abr,i}$  and  $E_{impact,i}$  are adhesion/abrasion and impact energies dissipated on a surface  $i$

## 4.5 Implementation of the wear mathematical model in the DEM code

### 4.5.1 Introduction

Lifter useful life varies depending on material properties, type of grinding (wet or dry) and operating conditions. In order to simulate the wear of lifters within a reasonable time, there is a need to reduce the actual time observed industrially. In simulating the wear of lifters using the Discrete Element Method, the reduction of industrial or experimental time must be achieved while the following conditions are respected:

- The mechanism and type of wear in the mill must be the same in the experiment and in the simulation. In our milling case, the load behaviour and particles interactions must be the same. This condition eliminates for instance the possibility of increasing the mill speed or the charge mass in order to have the same worn profiles in less time.
- The lifter profile predicted must be a function of operating conditions in the mill and the initial profile.

To obey these rules, we use in our simulation a very high wear rate in comparison to the experimental allowing a high volume of material removed in less time as predicted by equation 4.6.

Qiu et al (2001) suggested that:

- Increasing the simulated wear rate by a factor of  $n$  must correspond to decreasing the simulation time by the same factor (this not always possible)
- The simulation time must be sufficiently long so that the statistical variance associated with discrete events is small in the DEM output data.

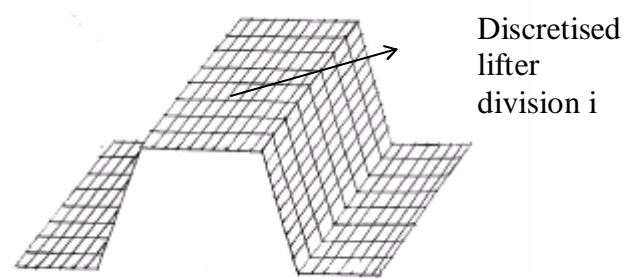
The wear is a continuous process where materials are removed or displaced due to direct interactions. Theoretically, in order to predict the evolving lifter profiles using the DEM, it is sensible to calculate the new profile each time step  $\Delta t$  and for every lifter in the mill. This approach will require a prodigious amount of simulation time. To avoid this situation, in our simulations, the new profile is calculated after one revolution. The new lifter is found by subtracting from the initial lifter profile a volume of material predicted by equation 4.6. Based on observation and tests in industrial tumbling mills, we assume that the wear on all the lifters at any mill axial position around the mill shell is similar.



#### 4.5.2 Lifter discretisation

In order to apply the wear mathematical model (equation 4.6), it is necessary to discretise lifter profiles into smaller surfaces. Impact, adhesion and abrasion energies consumed on those surfaces will be responsible of the removal of material on them according to the wear equation.

Figure 4.3 shows an example of a trapezoidal lifter discretised into different small surfaces  $i$ .



**Figure 4.3** Three Dimensional (3D) discretisation of a trapezoidal lifter

For simplification, we assume firstly that energies are distributed uniformly through the length  $L$  of the lifter and we adopt for this reason a two dimensional (2D) representation.

The object of the discretisation being to apply our wear mathematical model on smaller surfaces in order to remove a volume of material, it is recommended to discretise lifters in such a way that the volume removed on that surface is function on energies dissipated on it.

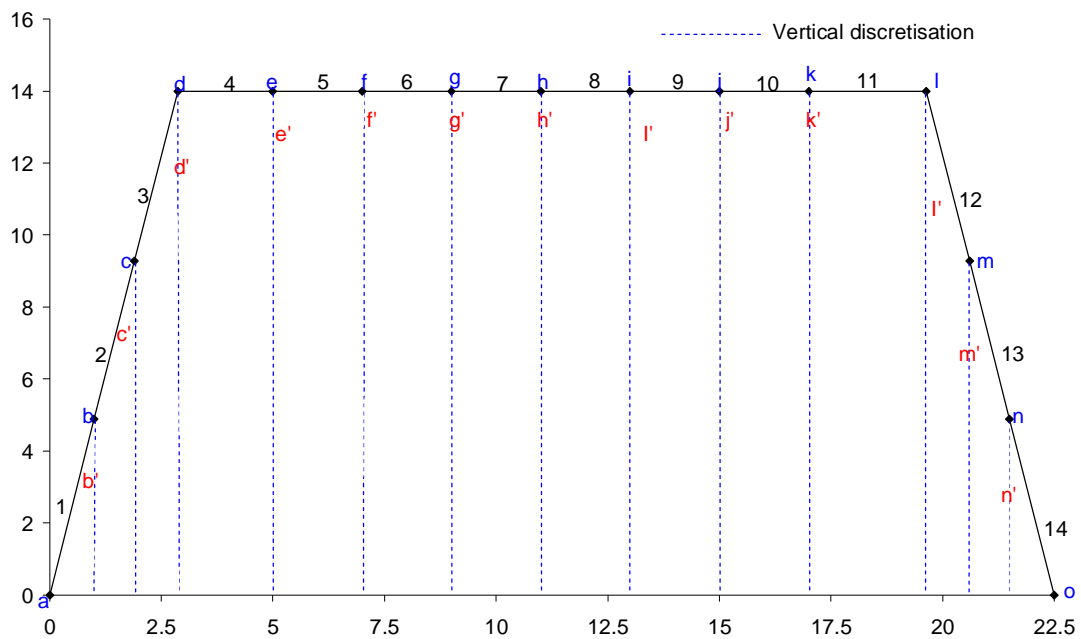
The more discretised lifter divisions we have, the slower is the DEM simulation due to the amount of data stored each time step. On the other hand, the more discretised lifter divisions we have, the better the prediction. A balance must therefore be found to simulate the wear of lifters within a reasonable time without sacrificing the accuracy of predictions. In discretising lifters: i) it is not necessary to use a uniform discretisation. ii) more divisions should be applied in area where most events occurs or where it is expected a dramatic change in the lifter profile such as corners.

Depending on lifter profiles, two types of lifter discretisation were identified.

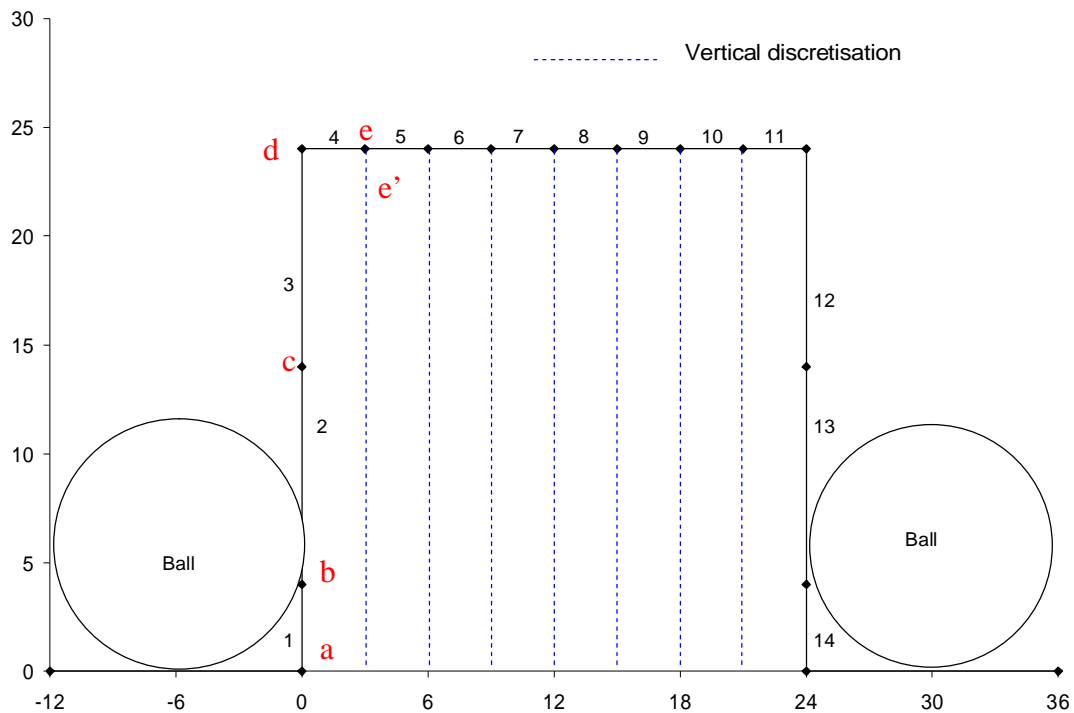
#### 4.5.2.1 Vertical discretisation

The lines used to discretise a lifter are vertical in this case. The points representing a lifter profile move from an initial profile to the simulated profile vertically through the vertical lines of discretisation. Figure 4.4 shows the vertical discretisation for a trapezoidal lifter and Figure 4.5 shows the vertical discretisation applied on a rectangular lifter. The coordinates  $(x, y)$  of points  $a$  to  $o$  in the Figure 4.4 represent the initial lifter profile. After a simulation, abrasion/ adhesion and impact energies will be dissipated on discretised lifter divisions 1 to 14. Applying our mathematical wear model on these divisions will remove materials on them resulting in a new simulated profile. The new simulated profile will be defined by points  $a'$  to  $o'$  belonging respectively to the vertical line of discretisation  $a$  to  $o$ . Initial points  $a$  and  $o$  defining the width of the lifter are usually keep at the same place as liners wear.

It can be seen from Figure 4.5 that lifter divisions 1 and 14 are not in contact with balls having a radius higher than their length. Therefore, no wear occurs on their surfaces. Lifter divisions 2, 3 and 12, 13 will lose material since they are in contact with balls. Since lifter divisions 1, 2, 3 (and 11, 12, 13) have the same vertical line of discretisation it is difficult to remove material from them. An alternative to solve this problem is found by using a radial discretisation.



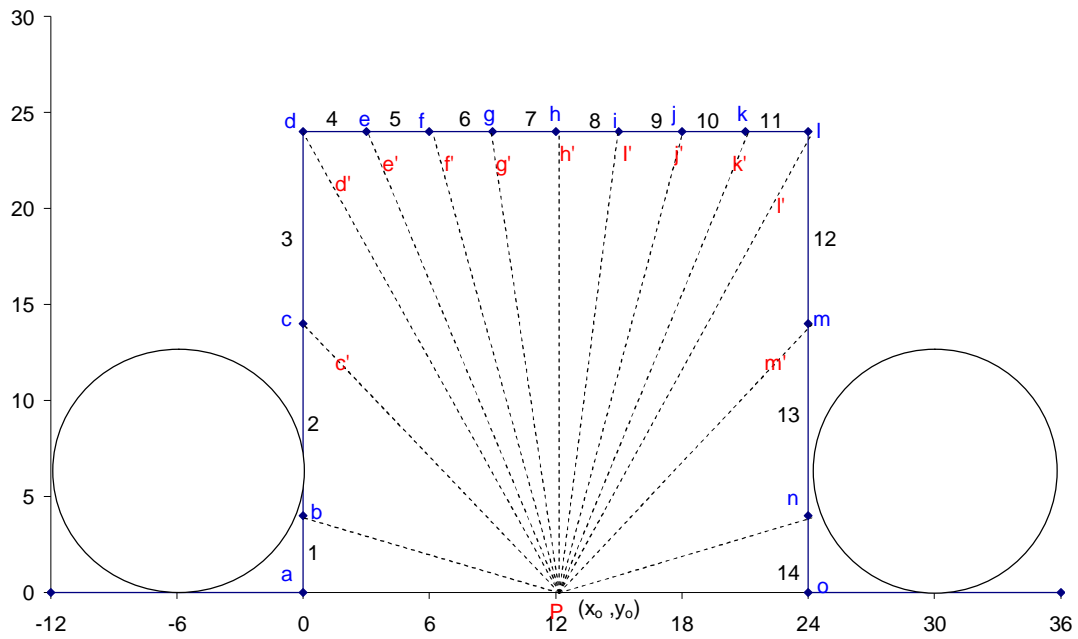
**Figure 4.4** Vertical discretisation of a trapezoidal lifter



**Figure 4.5** Vertical discretisation of a rectangular lifter

#### 4.5.2.2 Radial discretisation

Figure 4.6 shows the radial discretisation applied on a rectangular lifter. Using this discretisation offers the advantage of giving lifter divisions 1, 2, 3, and 4 (and also 11, 12, 13 and 14) their own lines of lifter discretisation in comparison to the vertical discretisation. As there is no contact between the lifter divisions 1 and 14 and balls, there is therefore no wear predicted on those lifter divisions. The points  $a$ ,  $b$  and  $n$ ,  $o$  will remain at the same position in this case while the points  $c$  to  $m$  will move down through their respective radial line of discretisation in order to define the new simulated profile. The coordinate  $(x_o, y_o)$  of the “pivot” point P is chosen in the middle for symmetrical reasons. It is also chosen at the bottom in order to have every time the ordinate of the simulated points ( $b'$  to  $n'$  since  $a$  and  $o$  are usually constant) lower than or equal to the initial ordinate ( $b$  to  $n$ ) respectively.



**Figure 4.6** Radial discretisation of a rectangular lifter

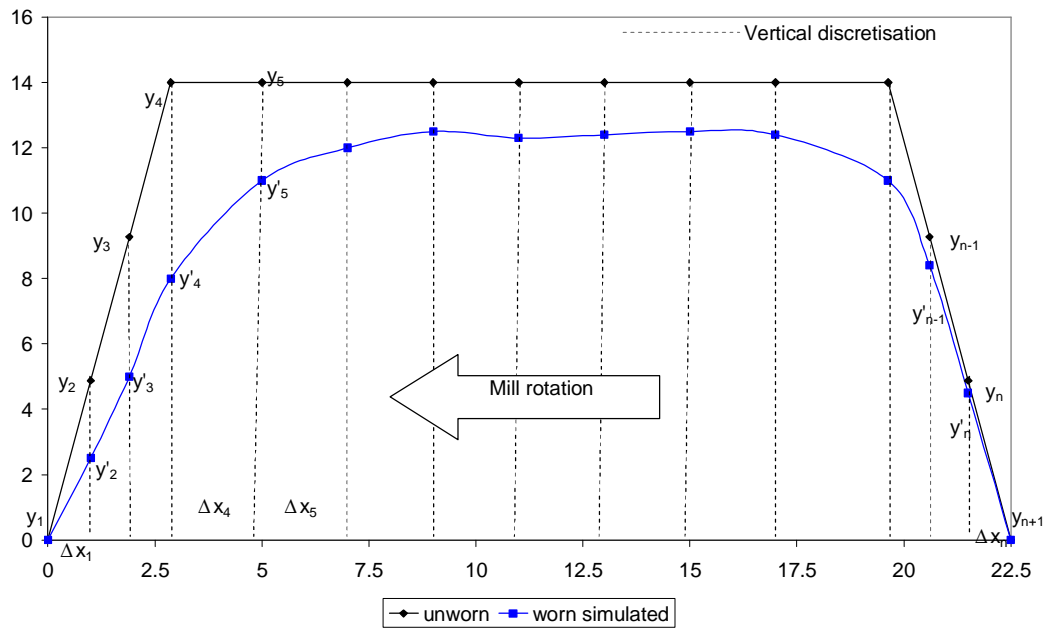
### 4.5.3 Objective function

#### 4.5.3.1 Definition

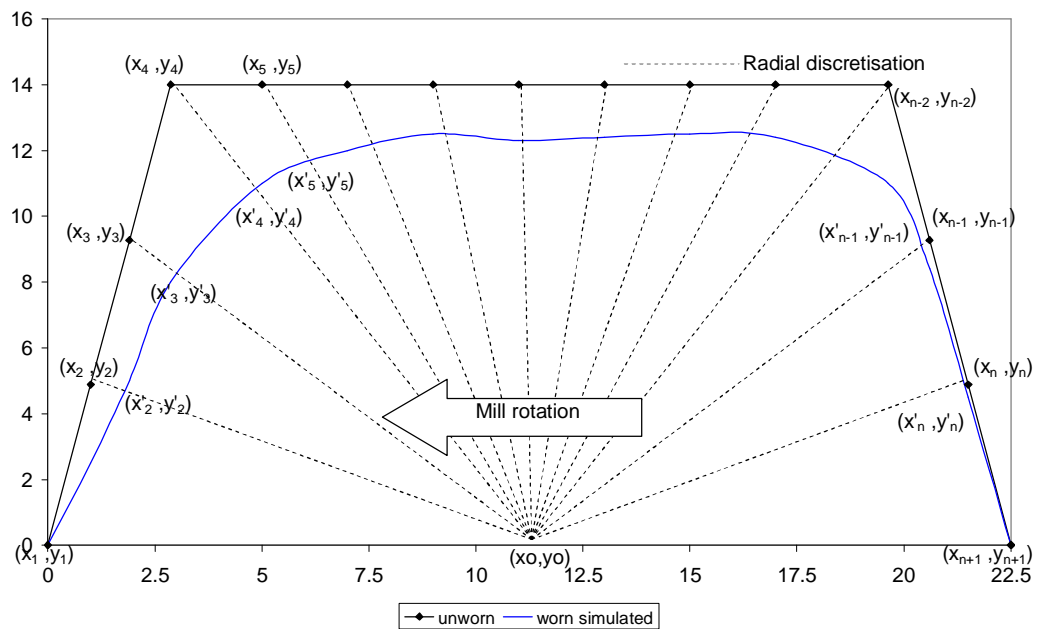
The new lifter profile is calculated from the initial profile by subtracting the volume removed on each discretised lifter surface according to the wear equation. As predicted by Cleary (1998) and Glover and de Beer (1997) such direct subtractions can lead to unrealistic simulated profiles as shown in Chapter 2, Figures 2.5 and 2.6.

In reality, worn profiles are smooth which means that the difference of two consecutive slopes is generally small.

## 4.5.3.2 Two-dimensional ( 2D) model



**Figure 4.7** Vertical discretisation of a trapezoidal lifter and worn profile



**Figure 4.8** Radial discretisation of a trapezoidal lifter and worn profile

Figure 4.7 and 4.8 show in two-dimension a trapezoidal lifter discretised into  $n$  elements vertically and radially respectively with their simulated worn profiles.

To produce realistic simulated profiles, we have defined an objective function  $S^2$  with components:  $S_1^2$ ,  $S_2^2$ ,  $S_3^2$  and  $S_4^2$  which have the following functions:

- $S_1^2$  minimises for each discretised lifter segment, the difference of volume removed predicted by our wear equation (equation 4.6) and the volume effectively removed.

For the vertical discretisation,  $S_1^2$  is given by:

$$S_1^2 = \sum_{i=1}^n \left[ \left( \frac{(y_i - y'_i) + (y_{i+1} - y'_{i+1})}{2} \Delta x_i * L \right) - V_i \right]^2 \quad (4.7)$$

For the radial discretisation,  $S_1^2$  is given by:

$$S_1^2 = \sum_{i=1}^n \left\{ \left[ \left( \left\| \begin{matrix} 1 & 1 & 1 \\ x_o & x_i & x_{i+1} \\ y_o & y_i & y_{i+1} \end{matrix} \right\| - \left\| \begin{matrix} 1 & 1 & 1 \\ x_o & x'_i & x'_{i+1} \\ y_o & y'_i & y'_{i+1} \end{matrix} \right\| \right) * \frac{L}{2} \right] - V_i \right\}^2 \quad (4.8)$$

Where:

$n$  is the number of segments of the discretised lifter

$x_i$  and  $y_i$  are the coordinate of the initial position of the lifter profile with  $i = 1$  to  $n + 1$

$x'_i$  and  $y'_i$  are the coordinate of the worn lifter profile with  $i = 1$  to  $n + 1$

$L$  is the mill length

$\Delta x_i$  is the width of the element  $i$  using the vertical discretisation of lifter with  $i = 1$  to  $n$

$V_i$  is the predicted volume removed by our wear equation (Equation 4.6) on the element  $i$  with  $i = 1$  to  $n$

$x_o$  and  $y_o$  are the coordinate of the “pivot” point in the radial discretisation

- $S_2^2$  minimises the difference of two neighbouring discretised slopes of the worn profile in order to get a smooth profile. We used the same notation as previously.

For the vertical discretisation  $S_2^2$  is given by:

$$S_2^2 = \sum_{i=1}^{n-1} \left( \frac{y'_{i+2} - y'_{i+1}}{\Delta x_{i+1}} - \frac{y'_{i+1} - y'_i}{\Delta x_i} \right)^2 \quad (4.9)$$

For the radial discretisation  $S_2^2$  is given by:

$$S_2^2 = \sum_{i=1}^{n-1} \left( \frac{y'_{i+2} - y'_{i+1}}{x'_{i+2} - x'_{i+1}} - \frac{y'_{i+1} - y'_i}{x'_{i+1} - x'_i} \right)^2 \quad (4.10)$$

- $S_3^2$  minimises the difference of discretised slopes between the  $j^{\text{th}}$  profile and the  $(j+1)^{\text{th}}$  simulated profile. This criterion prevents a dramatic change of the simulated profile from the initial.

For the vertical discretisation  $S_3^2$  is given by:

$$S_3^2 = \sum_{i=1}^n \left( \frac{y_{i+1} - y_i}{\Delta x_i} - \frac{y'_{i+1} - y'_i}{\Delta x_i} \right)^2 \quad (4.11)$$

For the radial discretisation  $S_3^2$  is given by:

$$S_3^2 = \sum_{i=1}^n \left( \frac{y_{i+1} - y_i}{x_{i+1} - x_i} - \frac{y'_{i+1} - y'_i}{x'_{i+1} - x'_i} \right)^2 \quad (4.12)$$

- $S_4^2$  maintains a steadily decreasing profile height at any longitudinal position by penalising heavily any tendency for the ordinate of the simulated worn profile to increase with time.

For the vertical and radial discretisation  $S_4^2$  is given by:

$$S_4^2 = \sum_{i=1}^{n+1} e^{b(y'_i - y_i)} \quad (4.13)$$

where  $b$  is a large number.

The objective function  $S^2$  is given by:

$$S^2 = S_1^2 + I * S_2^2 + a * S_3^2 + S_4^2 \quad (4.14)$$

where

$I$  and  $a$  are the weight factors which decide the importance to give to the component  $S_2^2$  and  $S_3^2$  respectively of the objective function.

Thus, for the vertical discretisation, the objective function is given by:

$$S^2 = \sum_{i=1}^n \left[ \left( \frac{(y_i - y'_i) + (y_{i+1} - y'_{i+1})}{2} \Delta x_i * L \right) - V_i \right]^2 + I \sum_{i=1}^{n-1} \left( \frac{y'_{i+2} - y'_{i+1}}{\Delta x_{i+1}} - \frac{y'_{i+1} - y'_i}{\Delta x_i} \right)^2 + a \sum_{i=1}^n \left( \frac{y_{i+1} - y_i}{\Delta x_i} - \frac{y'_{i+1} - y'_i}{\Delta x_i} \right)^2 + \sum_{i=1}^{n+1} e^{b(y'_i - y_i)} \quad (4.15)$$



For the radial discretisation, we have:

$$S^2 = \sum_{i=1}^n \left\{ \left[ \left( \left\| \begin{matrix} 1 & 1 & 1 \\ x_o & x_i & x_{i+1} \\ y_o & y_i & y_{i+1} \end{matrix} \right\| - \left\| \begin{matrix} 1 & 1 & 1 \\ x_o & x'_i & x'_{i+1} \\ y_o & y'_i & y'_{i+1} \end{matrix} \right\| \right) * \frac{L}{2} \right] - V_i \right\}^2 +$$

$$I \sum_{i=1}^{n-1} \left( \frac{y'_{i+2} - y'_{i+1}}{x'_{i+2} - x'_{i+1}} - \frac{y'_{i+1} - y'_i}{x'_{i+1} - x'_i} \right)^2 + a \sum_{i=1}^n \left( \frac{y_{i+1} - y_i}{x_{i+1} - x_i} - \frac{y'_{i+1} - y'_i}{x'_{i+1} - x'_i} \right)^2 + \sum_{i=1}^{n+1} e^{b(y'_i - y_i)}$$

(4.16)

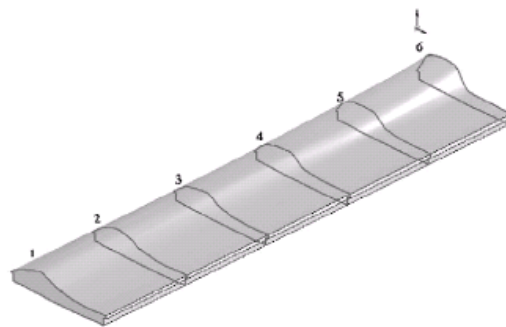
Using the radial discretisation of lifters, since  $(x'_i, y'_i)$  belong to the discretisation line passing via  $(x_o, y_o)$  and  $(x_i, y_i)$ ,  $x'_i$  can therefore be expressed in equation (4.16) as a function of  $y'_i$ . Thus,

$$x'_i = x_o + \frac{(y'_i - y_o)(x_o - x_i)}{(y_o - y_i)}$$

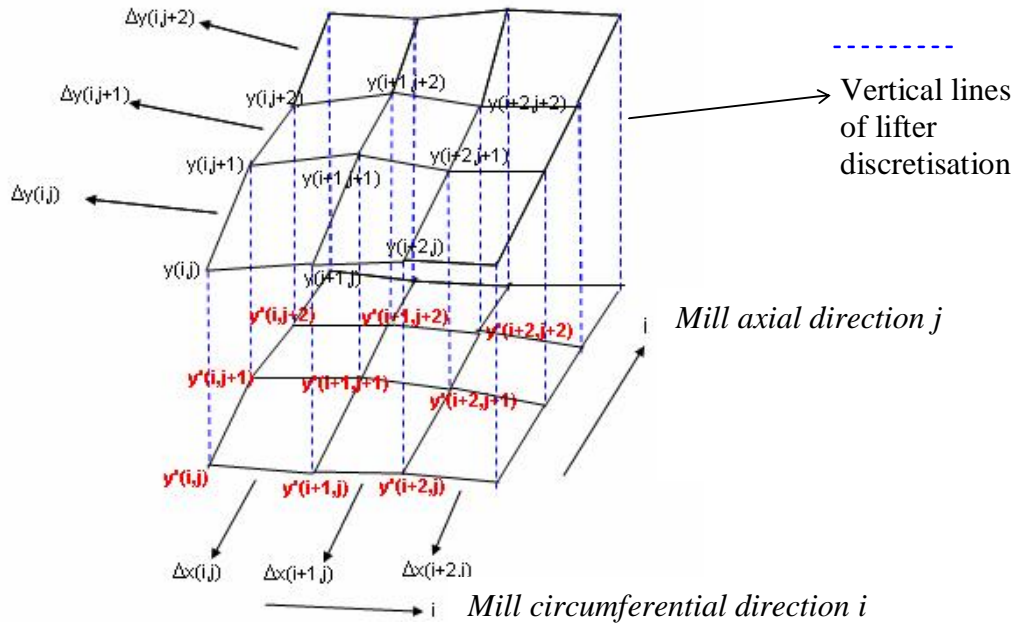
(4.17)

#### 4.5.3.3 Three dimensional (3D) model

Due to non uniform lifters wear process occurring through the length of tumbling mills as observed by Banisi, S. and Hadizadeh, M., 2006 (Figure 4. 9), it is important to develop a 3 D model predicting the wear of lifters.



**Figure 4.9** Non-uniform lifter wear profile observed in an industrial mill (after Banisi, S. and Hadizadeh, M., 2006)



**Figure 4.10** Three dimensional (3D) discretisation of a portion of a lifter

The 3D model will have the advantage of accurately predicting the wear of lifters and load behaviour in tumbling mills developing a non uniform wear of lifters as a function of mill length. Figure 4.10 shows a 3D discretisation of a portion of a lifter. The 3D model will be used only when a 3D DEM simulation is conducted.

Using the same approach for the 2D model, the following 3D objective function was developed:

$$\begin{aligned}
 S^2 = & \sum_{i=1}^n \sum_{j=1}^m (V'(i, j) - V(i, j))^2 \\
 & + I \sum_{i=1}^{n-1} \sum_{j=1}^{m+1} \left( \frac{y'(i+1, j) - y'(i, j)}{\Delta x(i, j)} - \frac{y'(i+2, j) - y'(i+1, j)}{\Delta x(i+1, j)} \right)^2 + d \sum_{j=1}^{m-1} \sum_{i=1}^{n+1} \left( \frac{y'(i, j+1) - y'(i, j)}{\Delta y(i, j)} - \frac{y'(i, j+2) - y'(i, j+1)}{\Delta y(i, j+1)} \right)^2 \\
 & + a \sum_{i=1}^n \sum_{j=1}^{m+1} \left( \frac{y(i+1, j) - y(i, j)}{\Delta x(i, j)} - \frac{y'(i+1, j) - y'(i, j)}{\Delta x(i, j)} \right)^2 + g \sum_{j=1}^m \sum_{i=1}^{n+1} \left( \frac{y(i, j+1) - y(i, j)}{\Delta y(i, j)} - \frac{y'(i, j+1) - y'(i, j)}{\Delta y(i, j)} \right)^2 \\
 & + \sum_{i=1}^{n+1} \sum_{j=1}^{m+1} \exp b(y'(i, j) - y(i, j))
 \end{aligned} \tag{4.18}$$

where

$n$  and  $m$  are respectively the number of discretised segment in the  $i$  (mill circumferential) and  $j$  (mill axial) direction respectively

$y(i,j)$  is the ordinate of the initial position of the lifter profile with  $i = 1$  to  $n + 1$  and  $j = 1$  to  $m + 1$

$y'(i,j)$  is the ordinate of the worn simulated lifter profile with  $i = 1$  to  $n + 1$  and  $j = 1$  to  $m + 1$

$\lambda$  and  $\delta$  are weight factors, used in the  $i$  ( mill circumferential) and  $j$  (mill axial) direction respectively, given to the difference of two neighbouring slopes of the worn profile in order to get a smooth profile

$\alpha$  and  $\gamma$  are weight factors, used in the  $i$  (mill circumferential) and  $j$  (mill axial) direction respectively, given to difference of slopes between the  $j^{th}$  profile and the  $(j + 1)^{th}$  simulated profile. This criterion prevents a dramatic change of the simulated profile from the initial.

$b$  is a large number. It allows maintaining a steadily decreasing profile height at any longitudinal position by penalising heavily any tendency for the ordinate of the simulated worn profile to increase with time.

$\Delta x(i, j)$  is the width of the element  $i$  in the mill circumferential direction with  $i = 1$  to  $n$

$\Delta y(i, j)$  is the width of the element  $j$  in the mill axial direction with  $j = 1$  to  $m$

$V(i, j)$  is the predicted volume of material removed on a discretised lifter division  $(i, j)$

$$V(i, j) = W \left( a_{impact} E_{impact}(i, j) + a_{ad-abr} E_{ad-abr}(i, j) \right) \quad (4.19)$$

with

$E_{impact}(i, j)$  the impact energy dissipated on a discretised lifter division (i, j) with  $i = 1$  to n and with  $j=1$  to  $m$

$E_{ad-abr}(i, j)$  the abrasion energy dissipated on a discretised lifter division (i, j) with  $i = 1$  to n and with  $j=1$  to  $m$

$W$  is the wear rate

$a_{ad-abr}$  and  $a_{impact}$  are weight factors given to adhesion/abrasion and impact energies respectively depending on material and ore properties.

$V'(i, j)$  is the volume of material effectively removed on a discretised lifter division (i, j)

The volume  $V'(i, j)$  of each element can be calculated by dividing it into 6 tetrahedron (see Appendix C for the calculation of  $V'(i, j)$ ).

All 4 predicted points ( $y'(i,j); y'(i+1,j); y'(i+1,j+1); y'(i,j+1)$ ) of a 3D discretised element must belong to the same plane. Consequently, the volume of the tetrahedron formed by these 4 points must be equal to zero. This implies that the following determinant must be equal to zero:

$$\begin{vmatrix} 0 & d_1 & d_2 & d_3 & 1 \\ d_1 & 0 & d_4 & d_5 & 1 \\ d_2 & d_4 & 0 & d_6 & 1 \\ d_3 & d_5 & d_6 & 0 & 1 \\ 1 & 1 & 1 & 1 & 0 \end{vmatrix} = 0 \quad (4.20)$$

Where

$d_i$  is the distance between the 4 points.

$$d_1 = \left( (\Delta x(i, j))^2 + (y'(i+1, j) - y(i, j))^2 \right)^{1/2} \quad (4.21)$$

$$d_2 = \left( (\Delta y(i, j))^2 + (y'(i, j+1) - y(i, j))^2 \right)^{1/2} \quad (4.22)$$

$$d_3 = \left( (\Delta x(i, j) + \Delta y(i, j))^2 + (y'(i+1, j+1) - y(i, j))^2 \right)^{1/2} \quad (4.23)$$

$$d_4 = \left( (\Delta x(i, j))^2 + (y'(i+1, j+1) - y(i, j+1))^2 \right)^{1/2} \quad (4.24)$$

$$d_5 = \left( (\Delta y(i, j))^2 + (y'(i+1, j+1) - y(i+1, j))^2 \right)^{1/2} \quad (4.25)$$

$$d_6 = \left( (\Delta x(i, j) + \Delta y(i, j))^2 + (y'(i+1, j) - y(i, j+1))^2 \right)^{1/2} \quad (4.26)$$

The values of the coordinate of the simulated worn profiles  $(x'_i, y'_i)$  are found by minimising the objective function. The procedure is equivalent to equalising the derivative of the objective function to 0.

$$\frac{\partial S^2}{\partial y'_i} = 0 \quad (4.27)$$

This gives an underdetermined system of  $n$  equations for  $n+1$  unknowns.

During the mill revolution, if there is no contact between balls or particles and any particular discretised lifter divisions, the volume of material removed on these particular discretised lifter divisions should be strictly equal to zero. We introduce therefore a constraint in our objective function.

Mathematically in 2D discretisation:

When  $V_i = 0$

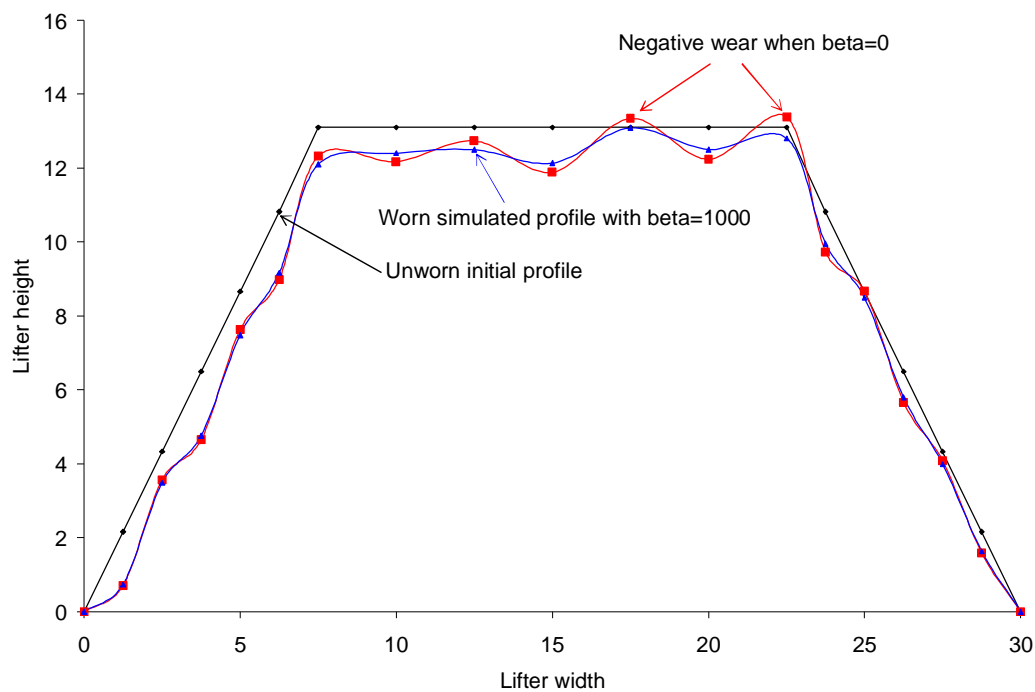
For the vertical discretisation:  $y_i = y'_i$  and  $y_{i+1} = y'_{i+1}$

For the radial discretisation:  $(x_i, y_i) = (x'_i, y'_i)$  and  $(x_{i+1}, y_{i+1}) = (x'_{i+1}, y'_{i+1})$

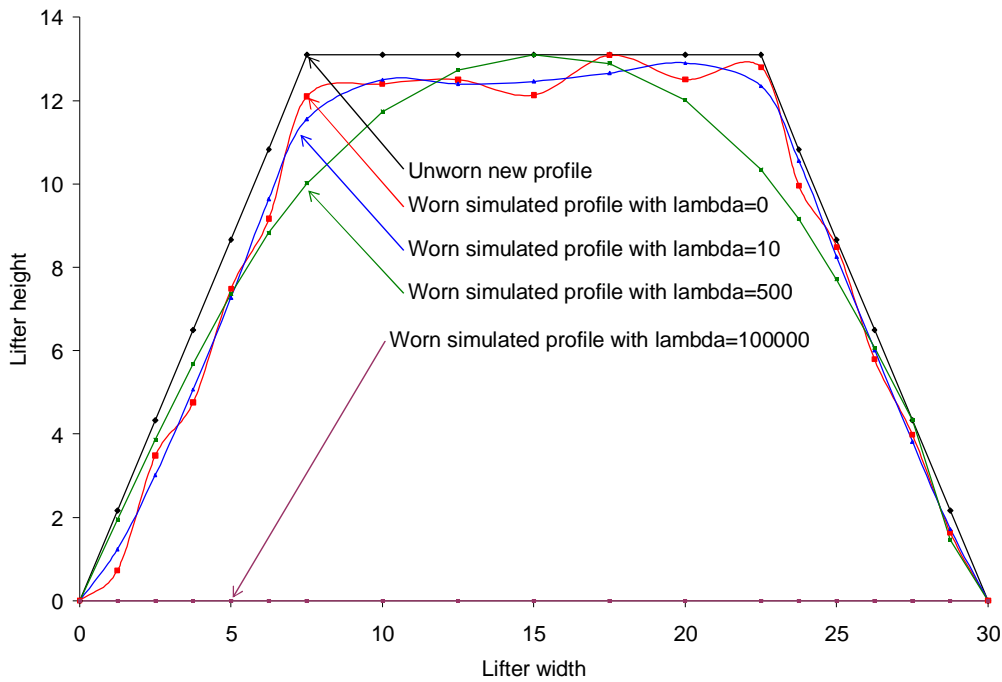
#### 4.5.3.4 Influence of weight factors in the objective function

##### 4.5.3.4.1 Introduction

Weight factors used in the objective function allow the prediction of realistic simulated profiles. The values used should not violate rules motivated in section 4.5.1. A simple way to check if there is violation is to compare the volume removed predicted (Equation 4.6) and the volume effectively removed on each discretised lifter division.



**Figure 4.11** Influence of the weight factor  $b$  (beta) used in the objective function for the prediction of the simulated worn profile.



**Figure 4.12** Influence of the weight factor  $I$  ( $\lambda$ ) used in the objective function for the prediction of the simulated worn profile.

#### 4.5.3.4.2 Influence of beta $b$

Figure 4.11 shows an example of the influence of the weight factor  $b$  (beta) in the prediction of a simulated worn profile ( $I$  and  $a$  are set equal to 0 in the objective function). A mathematical solution can be found predicting a value of the ordinate of the worn profile higher than the initial profile ( $y'_i > y_i$ ) as shown by Figure 4.11 when  $b = 0$ . To solve this “negative” wear, a higher value of  $b$  is required to penalise this tendency.

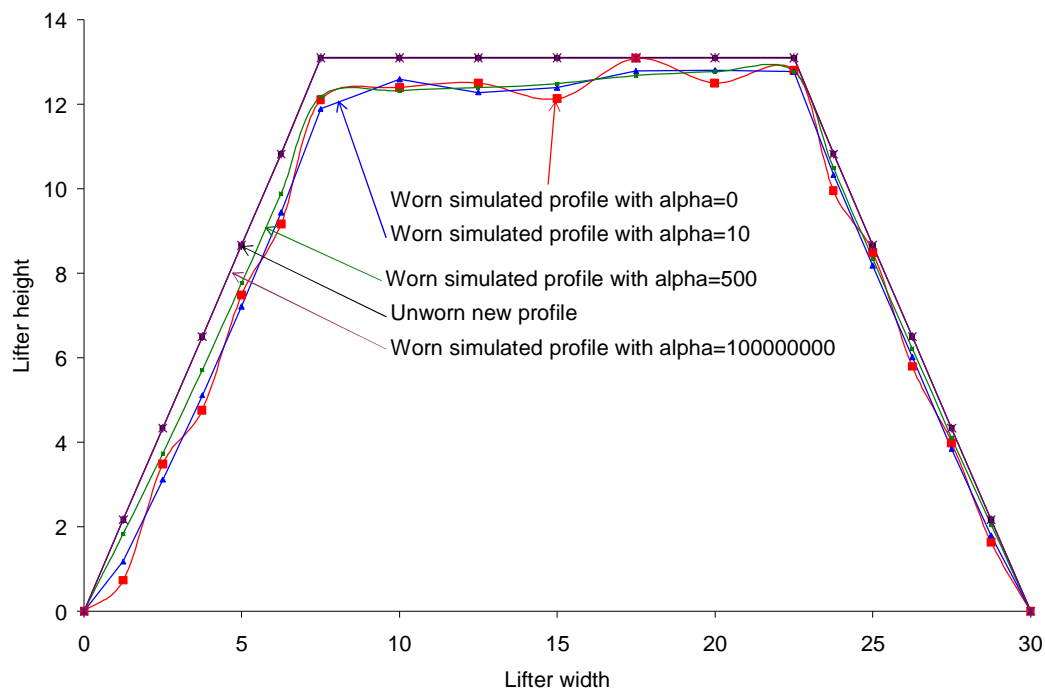
#### 4.5.3.4.3 Influence of lambda $I$

Figure 4.12 shows the influence of the weight factor  $I$  ( $\lambda$ ) in the prediction of a simulated worn profile ( $a = 0$  and  $b = 1000$ ). By subtracting the volume removed on each lifter division and using  $I = 0$ , the resultant profile predicted is unrealistic as oscillations (or waves) are formed in contradiction to observation. Using a value of  $I = 10$  solves this problem as “valleys” have been flattened. Using very high values

of  $I$  as shown by Figure 4.12 lead to simulated profiles which do not depend on operating conditions and initial profile. The utilisation of a very high value of  $I$  implies that the differences of two consecutive slopes of the worn profile is the main criterion instead of the volume removed due to energies dissipated on lifter divisions. For a value of  $I = 500$ , we have a parabola and for  $I = 10^6$ , we have a straight line. The value of  $I$  must therefore be chosen in order to produce realistic profiles without violating rules motivated in 4.5.1.

#### 4.5.3.4.4 Influence of alpha $a$

Figure 4.13 shows the influence of the weight factor  $a$  for the prediction of a simulated worn profile ( $I = 0$  and  $b = 1000$ ). The object of this component of the objective function is to prevent dramatic slope change for the worn simulated profile. It can be seen from Figure 4.13 that the higher  $a$  is, the more the simulated profile keeps the slope of the initial profile. For a high value of alpha, the initial profile and the simulated are the same. The exact value must be chosen without violating principles motivated in 4.5.1



**Figure 4.13** Influence of the weight factor  $a$  (alpha) used in the objective function for the prediction of the simulated worn profile



## 4.6 Conclusions

Based on adhesion, abrasion and impact wear which occur in dry milling environment, we derived a mathematical wear model predicting the volume of material removed on lifters due to wear. Our model assumes that the total volume removed on a lifter surface  $i$  is the sum of the volume removed due to abrasion/adhesion and impact energies dissipated on that surface. We demonstrated the necessity to take into account all types of wear as individual models such as Archard's, Finnie's, Rabinowicz's cannot be used directly. To take into account ore properties, the difference of material resistance to adhesion/abrasion and impact types of wear, we introduced in our model weight factors given to impact and adhesion/abrasion energy function of materials (lifters and balls) and ore properties.

To remove material on lifters using our wear mathematical model, there is a need to discretise lifters into small surfaces. We developed the vertical or radial discretisation which can be applied depending on lifter design. Developed 2D or 3D discretisation of lifters can be used. The 2D discretisation assumes that the wear of lifter is uniform through the length of the mill while the 3D discretisation allows exploring the non-uniform lifter wear.

In order to produce realistic simulated profiles, we implement our wear mathematical model in the Discrete Element Method code with an objective function having four components. The first component minimises the difference of volume predicted by our wear mathematical model and the volume effectively removed. The second component ensures that the simulated profile is smooth. The third component prevents a dramatic change for the simulated profile. The fourth component maintains the ordinates of the worn simulated profiles lower than the ordinate of the initial profiles to avoid a "negative" wear.

Our new approach to model the wear of lifters presented in this Chapter is tested in Chapter 6 by the comparison between laboratory experimental data of evolving lifter profiles due to wear and the Discrete Element Method simulated predictions. Our approach is also tested against industrial data in Chapter 7.

# Chapter 5

## Comparison between experimental and DEM simulated forces on mill lifters

### **5.1 Introduction**

### **5.2 Moys et al(2001) laboratory mill used for measurements of forces on a lifter**

### **5.3 Experimental results of measurement of forces**

#### 5.3.1 Tests procedure

#### 5.3.2 No-load signals at different speeds

#### 5.3.3 Measured signals at different speeds

#### 5.3.4 Net tangential and normal forces at different speeds

### **5.4 DEM Simulated results**

### **5.5 Comparison between measured and DEM simulated forces**

#### 5.5.1 Introduction

#### 5.5.2 Comparison between measured and simulated forces

### **5.6 Conclusions**

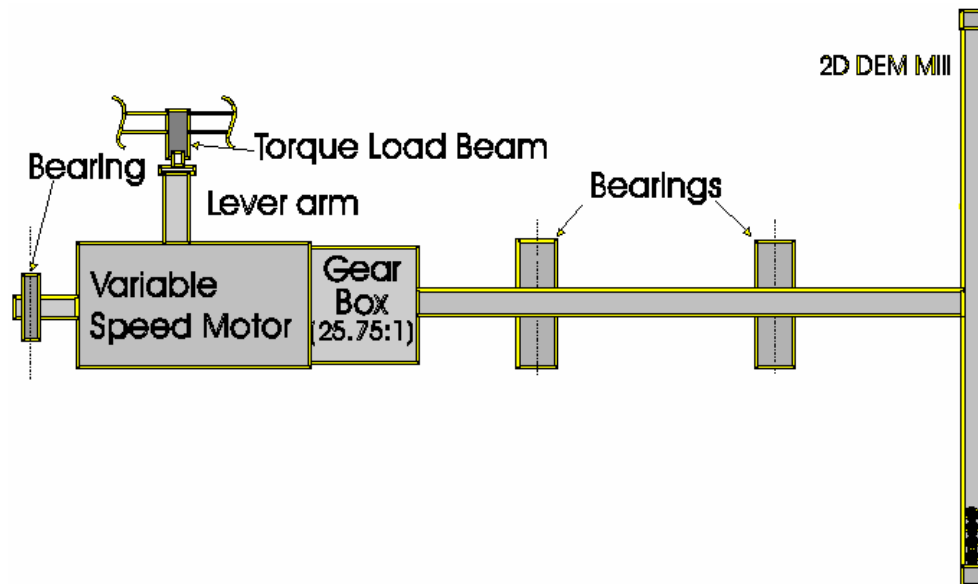
## 5.1 Introduction

The Discrete Element Method has been successfully used in the prediction of balls motion in tumbling mills and power draw as affected by the mill filling, the charge composition, the mill speed and the lifter design (Cleary, 2001; Moys et al, 2004). The application of this method at an industrial stage in order to produce realistic outputs requires a more rigorous assessment of this method to accurately predict secondary factors such as forces for collisions between balls and lifters.

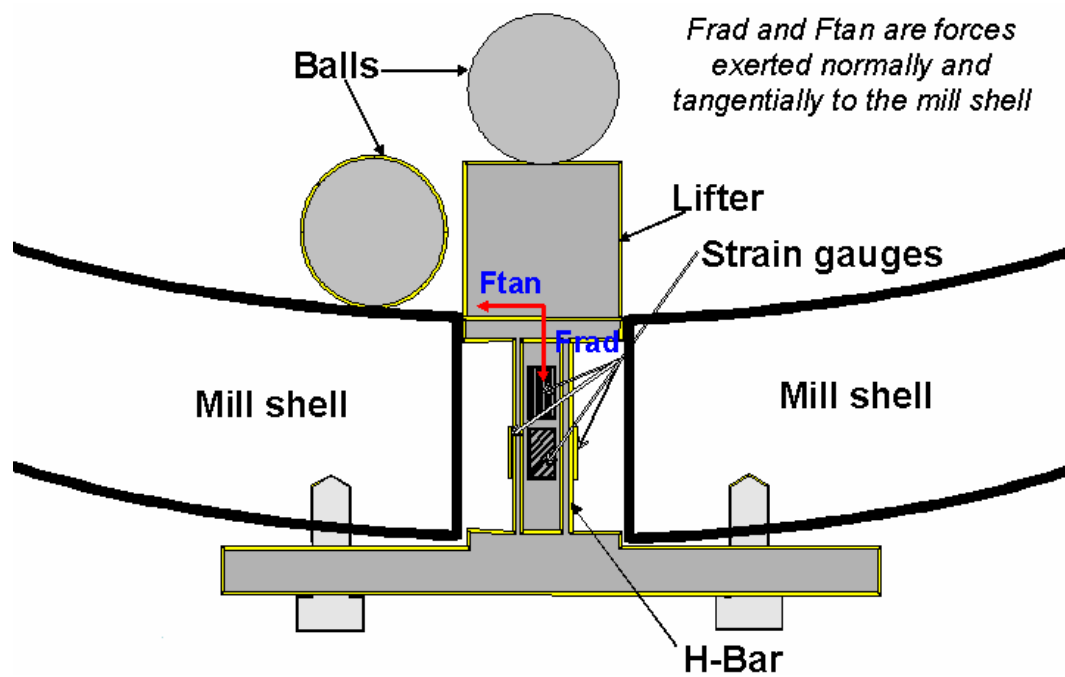
This chapter firstly describes an experimental laboratory mill used by Moys et al (2001) to measure the normal and tangential forces exerted by the charge on an instrumented lifter. Secondly, provided raw signals in millivolt recorded during tests are analysed and converted to forces via a calibrated model. Thirdly, simulations using the Discrete Element Method are conducted in the same conditions as experimental measurements in order to simulate the normal and tangential forces on lifters. Fourthly, experimental and simulated results in the same conditions are compared. Assessment of the accuracy of these predictions will provide a detailed check on the validity of the Discrete Element Method model.

## 5.2 Moys et al (2001) laboratory mill used for measurement of forces on a lifter

The experimental two-dimensional mill designed by Moys et al (2001) to measure the forces exerted by the charge on an instrumented lifter had an internal diameter of 0.55 m for a length of 0.023 m. The length of the mill was chosen to allow the motion of balls of 0.02225 m of diameter to move only in two dimensions. This controlled environment can be quickly and easily simulated using one slice ball. The mill was equipped with 12 equally spaced square lifters of 0.022 x 0.022 m. The schematic diagram of the mill is represented by Figure 5.1. One of the lifters was instrumented using strain gauges (Figure 5.2) in order to record the normal and tangential forces exerted on it. Strain gauges were mounted on an aluminium beam with an H cross section to allow measurements of radial compression and shear forces exerted on the beam.



**Figure 5.1** Two-dimensional mill used for measurements of forces on an instrumented lifter (Moys et al, 2001)



**Figure 5.2** Instrumented lifter bar (Moys et al, 2001)

The mill speed was varied from 0 to up to 200% of the critical speed. The mill was previously designed to run as a 2D with balls of 0.02225m of diameter. However, these balls damaged the instrumented lifter. Balls of 0.0067 m were used instead. The mill filling was varied from 20 to 45 % of the mill volume. Appendix D shows a photo of the modified laboratory mill.

### 5.3 Experimental results of measurements of forces

#### 5.3.1 Tests procedure

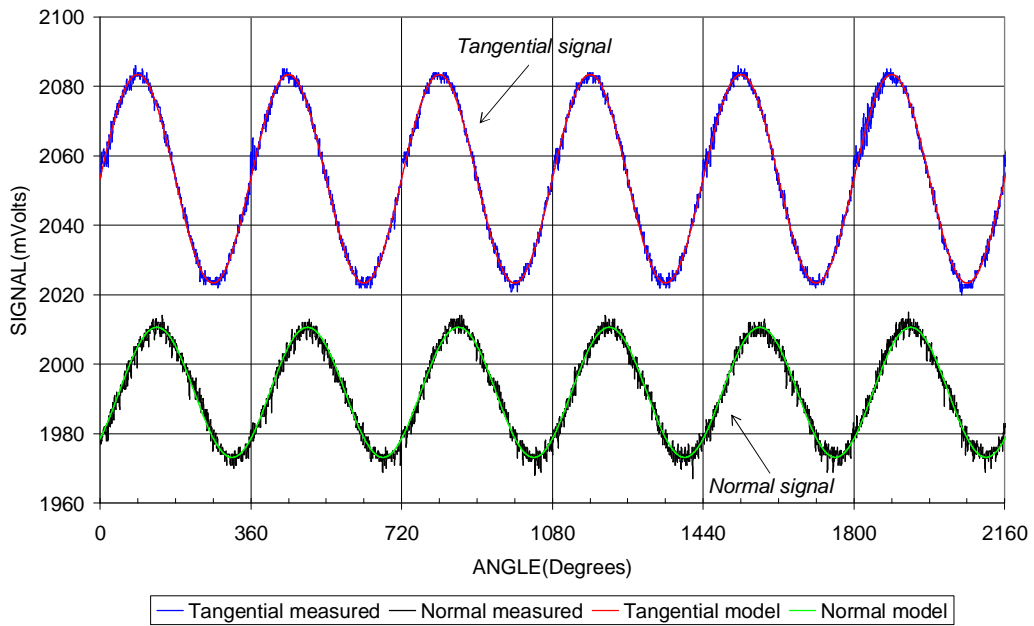
The forces on the instrumented lifter are recorded at any speed or percentage of filling once the mill reaches a load behaviour steady state. The instrumented lifter bar records the signal of normal and tangential forces exerted by the charge on it in Volts. The signals in Volts are converted to Newtons via a calibrated model. The instrumented lifter was set up to give 2500 readings during an interval time of 0.0048 second independent of the mill speed or 205 readings per second. Consequently, the lower the mill speed, the higher the data recorded per mill revolution.

At zero load when the mill is running without any charge, there are centrifugal and gravitational forces exerted on the instrumented lifter. For this reason, the real or net forces exerted on the instrumented lifter by the mill charge at any  $\theta$  position in the mill running at  $N$  revolution per minute and filled at  $J$  percent, are calculated by subtraction between measurements with and without charge in the mill at any speed. Thus,

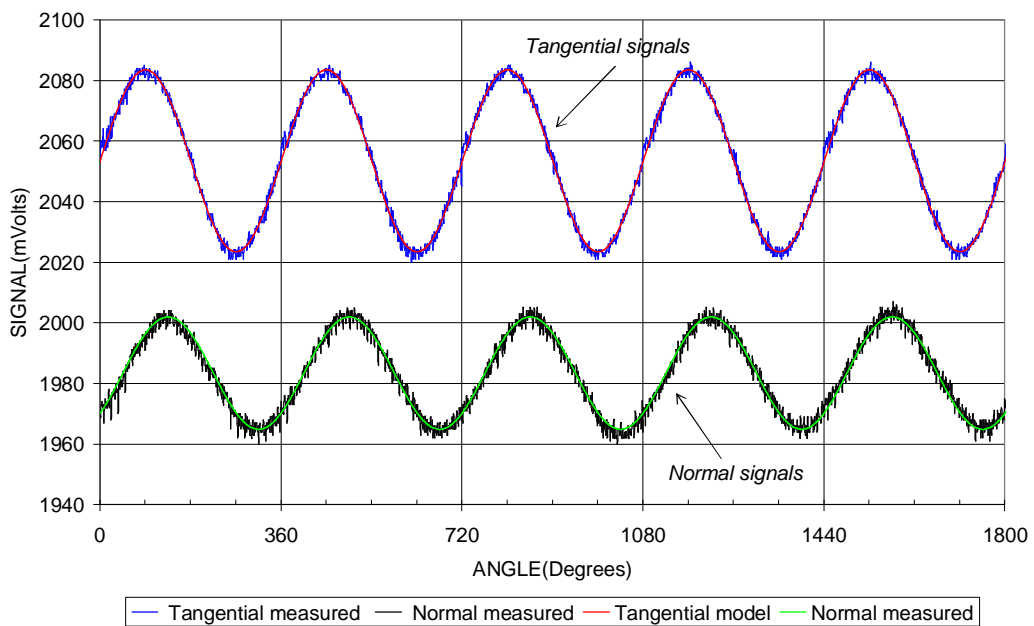
$$F_{net}(q, J, N) = F(q, J, N) - F(q, J = 0, N) \quad (5.1)$$

#### 5.3.2 No-load signals at different speeds

Figures 5.3 and 5.4 show the results of signals given by the instrumented lifter when the mill is running without charge ( $J = 0$ ) at 60 and 50 % of critical speed respectively. At 60% of critical speed, we have the results for 6 revolutions while at 50%, 5 revolutions.



**Figure 5.3** Measured and modelled zero load instrumented lifter bar signal at 60% of critical speed as a function of cumulated angle where 0 degree correspond to 12 o'clock position. Each vertical line represents one revolution.



**Figure 5.4** Measured and modelled zero load instrumented lifter bar signal at 50% of critical speed as a function of cumulated angle where 0 degree correspond to 12 o'clock position. Each vertical line represents one revolution.

It can be seen from these two figures that the no-load measured signals are slightly noisy. The measured no-load signals caused by centrifugal and gravitational forces exerted on the instrumented lifter were modelled by the following sinusoidal model:

$$Y = a + b\sin(q + c) \quad (5.2)$$

where

$Y$ : signal [mV];  $a$ : *Offset*;  $b$  and  $c$  are constant

$q$  is the angle with 0 degree corresponding to 12 O'clock position and the mill is rotating anticlockwise.

The replacement of the noisy signals measured by the modelled signal offers the advantage of not subtracting a noisy signal by another noisy signal which could have increased the fluctuations. It can be seen from Figures 5.3 and 5.4 that the modelled tangential and normal signals fit very well the measured.

The no-load tangential signals are very similar while the normal signals are different. In appendix D we demonstrate the dependence of the normal signals with the mill speed. The no-load tangential and normal forces as a function of the mill angular position are given respectively by:

$$F_t = m * g * \cos q \quad (5.3)$$

and,

$$F_n = m * \left( \frac{2pN}{60} \right)^2 * R - (m * g * \sin q) \quad (5.4)$$

where

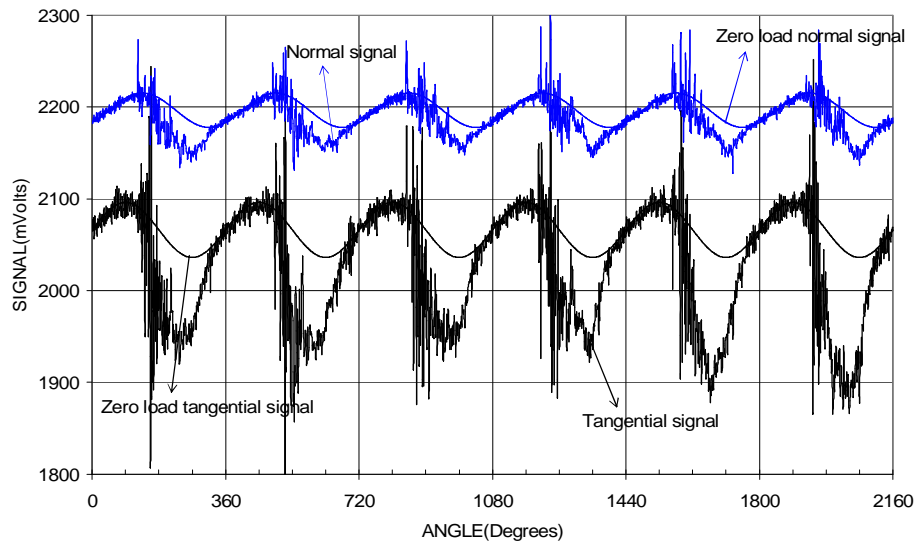
$m$  is the weight of the instrumented lifter

$N$  is the number of revolution per minute

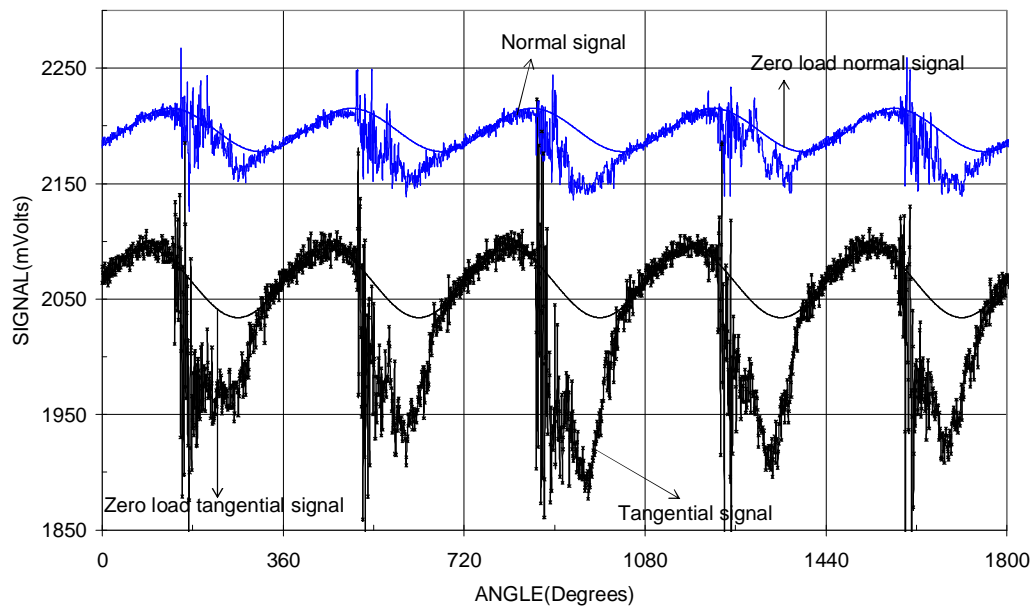
$R$  is the mill radius

$g$  is the acceleration due to gravity

### 5.3.3 Measured signals at different speeds

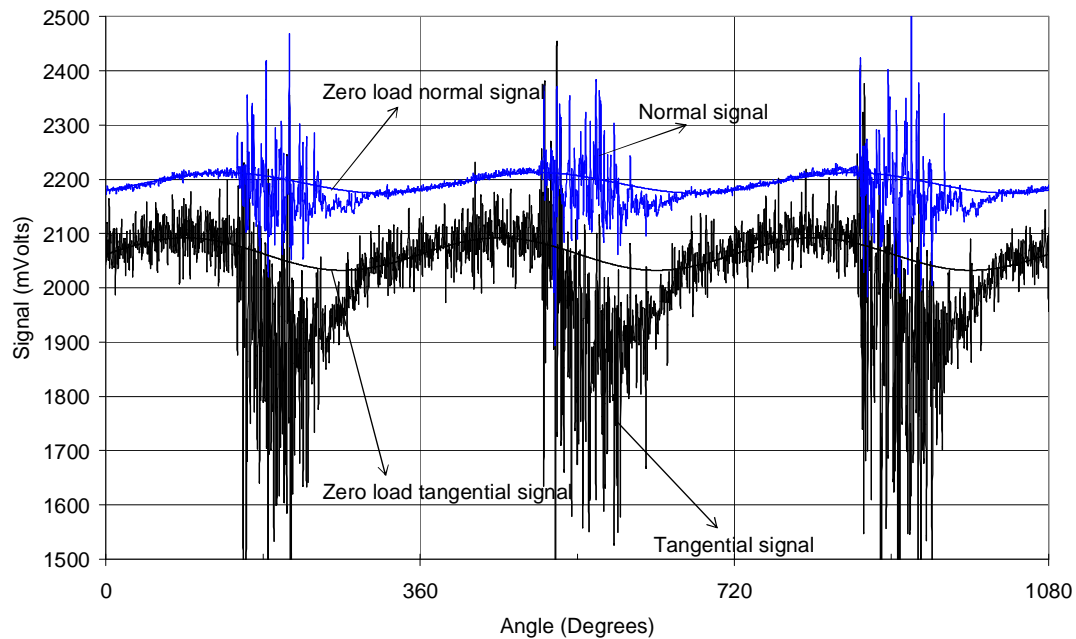


**Figure 5.5** Measured and zero load instrumented lifter bar signal at 60% of critical speed plotted as a function of cumulated angle where 0 degree correspond to 12 o'clock position. Each vertical line represents one revolution.  $J=20\%$ ,  $d=6.7$  mm



**Figure 5.6** Measured and zero load instrumented lifter bar signal at 50% of critical speed plotted as a function of cumulated angle where 0 degree correspond to 12 o'clock position. Each vertical line represents one revolution.  $J=20\%$ ,  $d=6.7$  mm





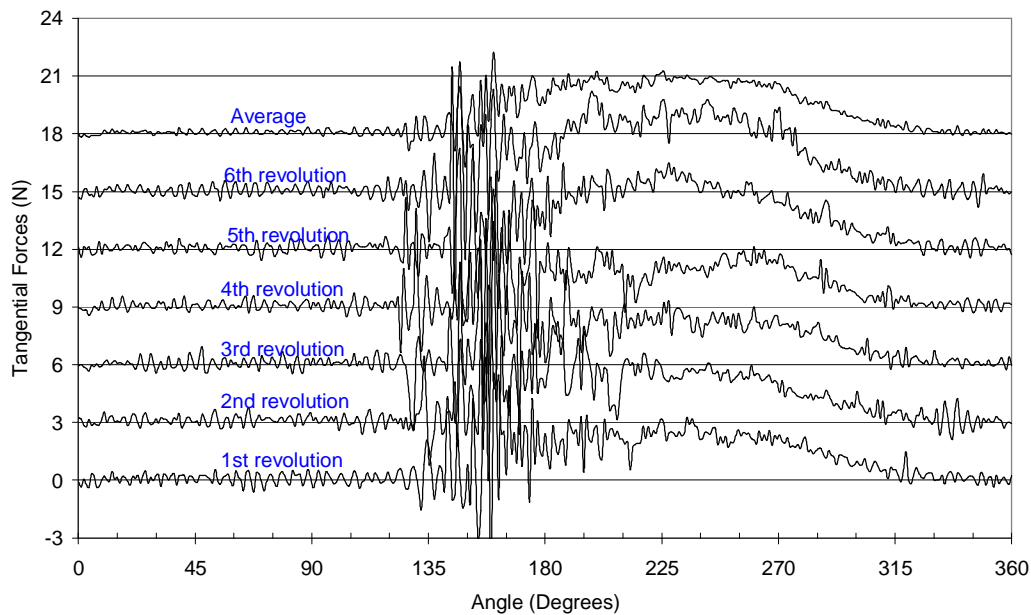
**Figure 5.7** Measured and zero load instrumented lifter bar signal at 30% of critical speed plotted as a function of cumulated angle where 0 degree correspond to 12 o'clock position. Each vertical line represents one revolution.  $J=20\%$ ,  $d=22.25$  mm

Figures 5.5 and 5.6 show the normal and tangential signals in Volts recorded when the mill is filled at 20% with balls of 6.7 mm of diameter respectively at 60 and 50 % of critical speed. Figure 5.7 shows the measured normal and tangential signals when the mill is filled at 20% with balls of 22.25 mm. The modelled no-load tangential and normal signals at the same speed are also superimposed respectively on the same figures to show the difference between no-load and load signals. In all 3 cases, the measured data diverges from the no-load line when the instrumented lifter is underneath the load. The net force exerted on the instrumented lifter during a mill revolution is therefore equal to 0 when the no-load and the load signals coincide. The toe and the shoulder positions can be accurately identified from these data. The toe position, detected when the instrumented lifter goes underneath the load, corresponds in the figures to the points where the measured signals diverge from the no-load signals. The shoulder position detected when the instrumented lifter is out of the active charge corresponds to the points where the measured signals rejoin the no-load signals.

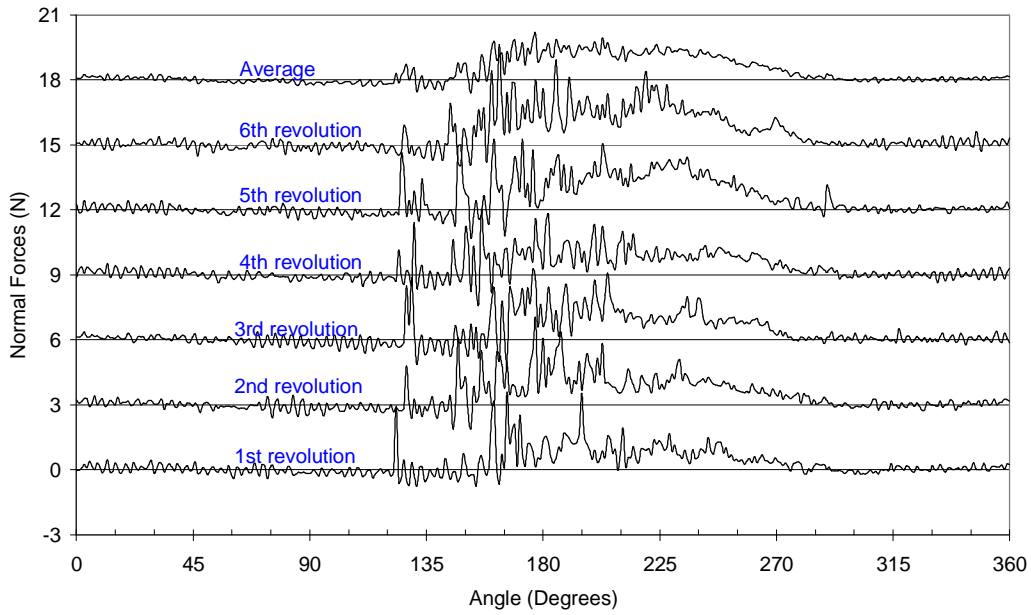
It can also be seen from these Figures (5.5, 5.6 and 5.7) that the profiles of signals in all 3 cases are slightly different from one revolution to another. We therefore expect to have slight differences in the net forces measured each revolution.

#### 5.3.4 Net tangential and normal forces at different speeds

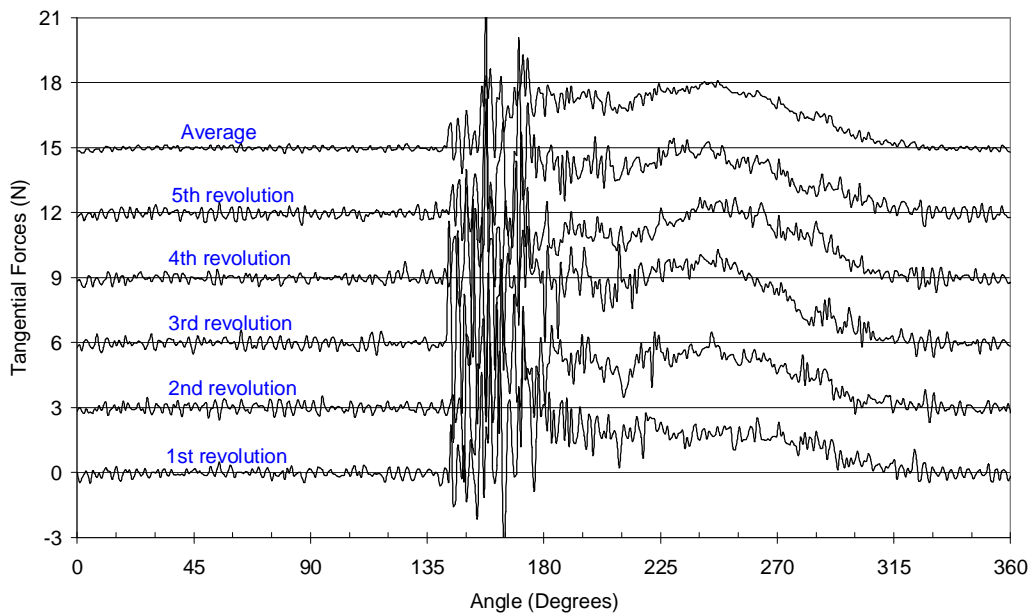
The net signal due to actual forces exerted by balls on the instrumented lifter is calculated by subtracting the load signals and the no-load signals. The net signal in mVolts is converted in Newton via a calibrated model. Figure 5.8 to 5.13 show the net tangential and normal forces exerted on the instrumented lifter for different mill revolutions at 60, 50 and 30% of critical speed.



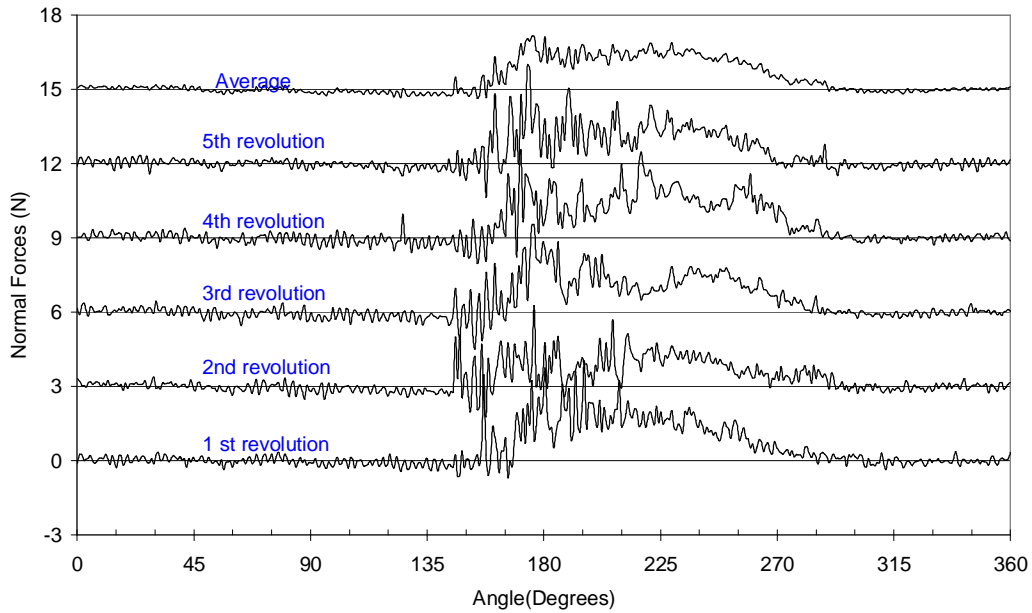
**Figure 5.8** Measured instrumented lifter bar tangential forces per revolution as a function of angle where 0 degree correspond to 12 o'clock position (mill rotation: anticlockwise). Percentage of critical speed  $N_c=60\%$ . Balls diameter  $d=6.7$  mm. The trends are separated from each other by 3N to increase legibility.



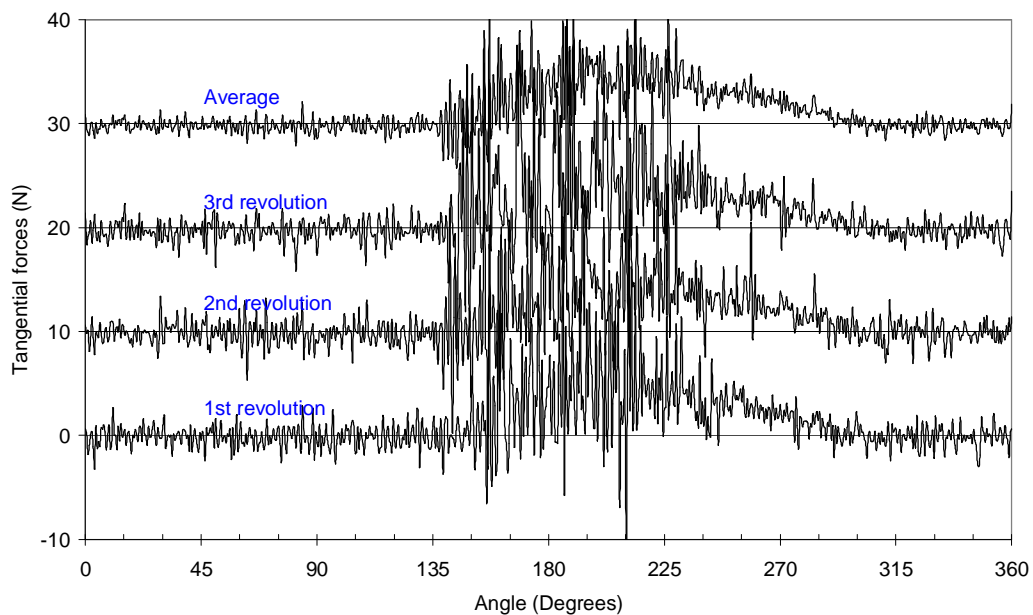
**Figure 5.9** Measured instrumented lifter bar normal forces per revolution as a function of angle where 0 degree correspond to 12 o'clock position (mill rotation: anticlockwise): Percentage of critical speed  $N_c=60\%$ . Balls diameter  $d=6.7$  mm. The trends are separated from each other by 3N to increase legibility.



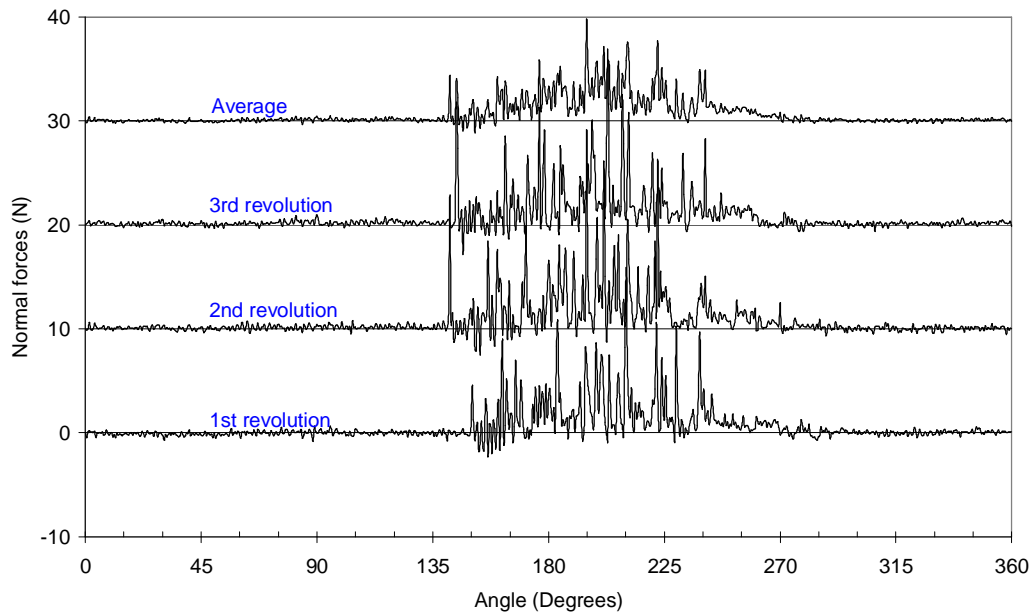
**Figure 5.10** Measured instrumented lifter bar tangential forces per revolution as a function of angle where 0 degree correspond to 12 o'clock position (mill rotation: anticlockwise). Percentage of critical speed  $N_c=50\%$ . Balls diameter  $d=6.7$  mm. The trends are separated from each other by 3N to increase legibility.



**Figure 5.11** Measured instrumented lifter bar normal forces per revolution as a function of angle where 0 degree correspond to 12 o'clock position (mill rotation: anticlockwise): Percentage of critical speed  $N_c=50\%$ . Balls diameter  $d=6.7$  mm. The trends are separated from each other by 3N to increase legibility.



**Figure 5.12** Measured instrumented lifter bar tangential forces per revolution as a function of angle where 0 degree correspond to 12 o'clock position (mill rotation: anticlockwise): Percentage of critical speed  $N_c=30\%$ . Balls diameter  $d=22.2$  mm. The trends are separated from each other by 10N to increase legibility.



**Figure 5.13** Measured instrumented lifter bar normal forces per revolution as a function of angle where 0 degree correspond to 12 o'clock position (mill rotation: anticlockwise): Percentage of critical speed  $N_c=30\%$ . Balls diameter  $d=22.2$  mm. The trends are separated from each other by 10N to increase legibility.

It can be seen from these figures that the respective forces (tangential or normal) at a particular speed vary slightly from one revolution to another. This was expected since balls do not follow the same path each revolution.

The net forces on the instrumented lifter while it is out of the active charge should strictly be equal to zero. In our cases, noisy signals with average amplitude of 0.05N around 0 have been found due to vibrations caused by balls impacting on the mill shell.

The toe and shoulder positions are easily found in all cases. The tangential forces give better prediction of the shoulder position as the normal forces are almost equal to zero at the shoulder. Table 5.1 gives the average angular positions of shoulder and toe at different speed. 12 O'clock represents 0 degree and the mill is rotating anticlockwise.

**Table 5.1** Average shoulder and toe positions at different speeds from experimental data

	Toe position (Degrees)	Shoulder position (Degrees)
60% of critical speed, J=20%, Balls d=6.7 mm	144	327
50% of critical speed, J=20%, Balls d=6.7mm	143	321
30% of critical speed, J=20%, Balls d=22.2 mm	140	297

It can be seen from these data that the shoulder position is more affected by the mill speed than the toe position. Increasing the mill speed increases the shoulder position.

#### 5.4 DEM simulated results

In the same conditions of experimental measurement: Mill diameter  $D=0.55\text{m}$ , mill length  $L=23\text{mm}$ , percentage of filling  $J=20\%$ , ball diameter  $d=6.7\text{mm}$  at 50 and 60% of critical speed and  $d=22.25\text{mm}$  at 50% of critical speed, 12 square lifters ( $22 \times 22\text{mm}$ ), simulations using the DEM were performed in order to predict the normal and tangential forces exerted on lifters. The parameters used for the simulation are represented in Table 5.2. These parameters have been chosen in order to match the mill power predicted and simulated.

**Table 5.2** Parameters used in the DEM simulations to simulate forces on mill lifters

	Ball	Wall
Coefficient of friction	0.14	0.39
Coefficient of restitution	0.66	0.36
	Ball	Wall
Normal stiffness ( $\text{Nm}^{-1}$ )	400,000	400,000
Tangential stiffness ( $\text{Nm}^{-1}$ )	300,000	300,000

The DEM provides directly for each mill revolution, the net normal and tangential forces exerted on all mill lifters in Newton. DEM simulated tangential and normal forces data are recorded per lifter each degree of mill revolution. Therefore 360 data are recorded per mill revolution for each lifter respectively for the tangential and normal forces. The recorded forces are not instantaneous forces, but average forces during a mill revolution of  $d\theta = 1$  degree.

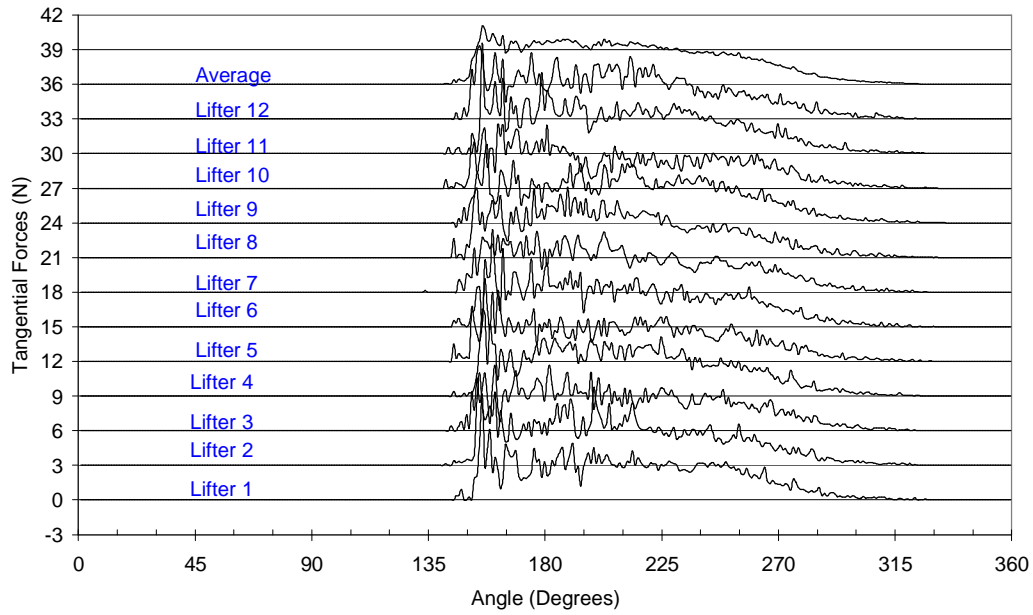
The formula to calculate normal and tangential forces in each collision was shown in Chapter 3 (Equations 3.4 and 3.5).

$$F_n = K_n \Delta x + C_n v_n; \quad F_t = \min \left\{ mF_n, K_t \int v_t dt + C_t v_t \right\}$$

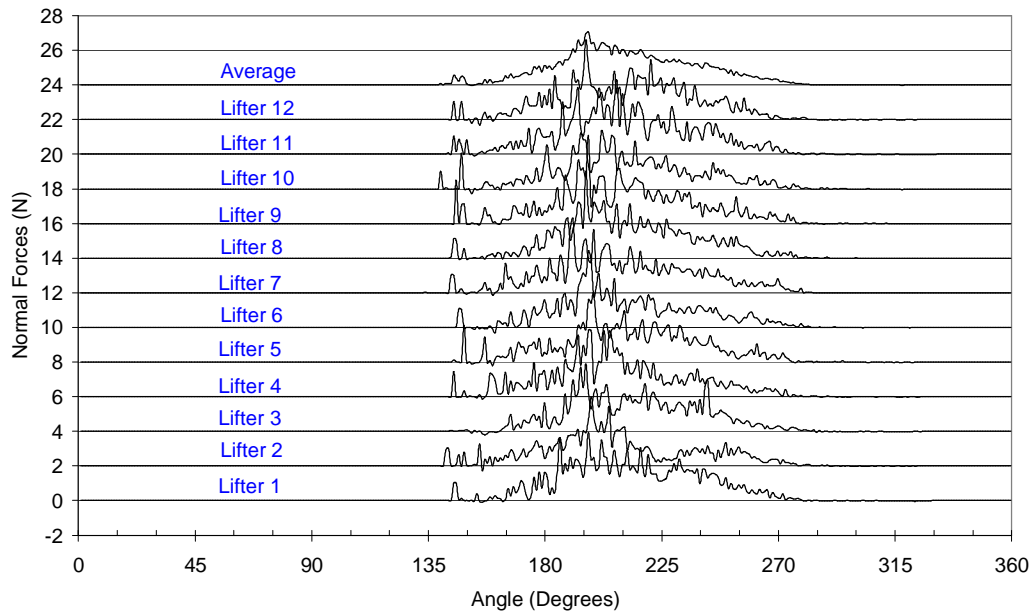
During an interval time  $t_i$  and  $t_{i+1}$  corresponding to 1 degree of mill revolution, The number of collisions between ball and lifter  $n$  and intensity of force  $F_i$  occurring on all lifters are recorded. The average force is given by the sum of forces divided by the number of collisions.

$$F_{qi} = \frac{\sum_{t=t_i}^{t_{i+1}} F_i}{n} \quad (5.5)$$

The forces are recorded once the mill is running under steady state conditions. The forces were recorded for one revolution. Since the mill is equipped with 12 lifters, we will have 12 different measurements of forces, which is equivalent to 12 revolutions using one instrumented lifter bar. Figures 5.14 and 5.15 show the results at 60% of critical speed of the tangential and normal forces respectively. Figures 5.16 and 5.17 show the results at 50% of critical speed while Figures 5.18 and 5.19 at 30% of critical speed.

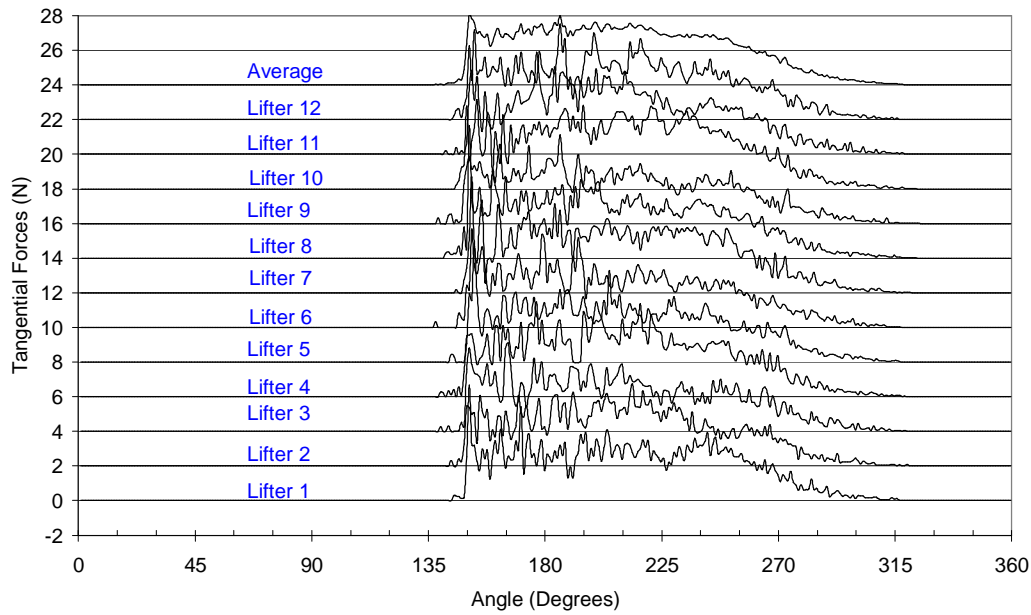


**Figure 5.14** Simulated tangential forces exerted on 12 lifters for one revolution. Critical speed  $N_c=60\%$ , percentage of filling  $J=20\%$ , ball diameter  $d=6.7\text{mm}$ . The trends are separated from each other by 3N to increase legibility. (0 degree=12 O'clock position, mill rotation: anticlockwise)

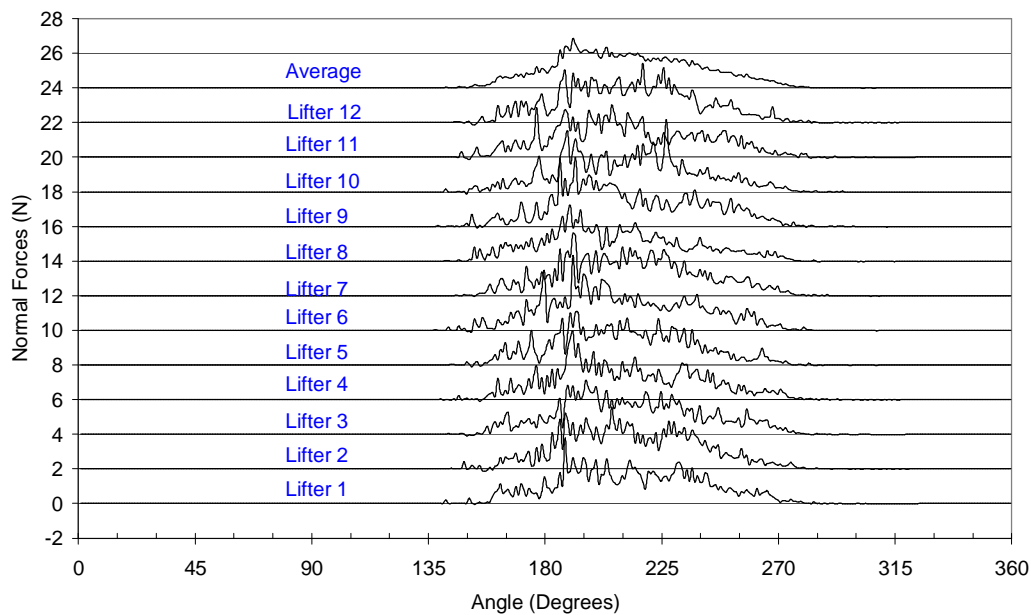


**Figure 5.15** Simulated normal forces exerted on 12 lifters for one revolution. Critical speed  $N_c=60\%$ , percentage of filling  $J=20\%$ , ball diameter  $d=6.7\text{mm}$ . The trends are separated from each other by 2N to increase legibility. (0 degree=12 O'clock position, mill rotation: anticlockwise)

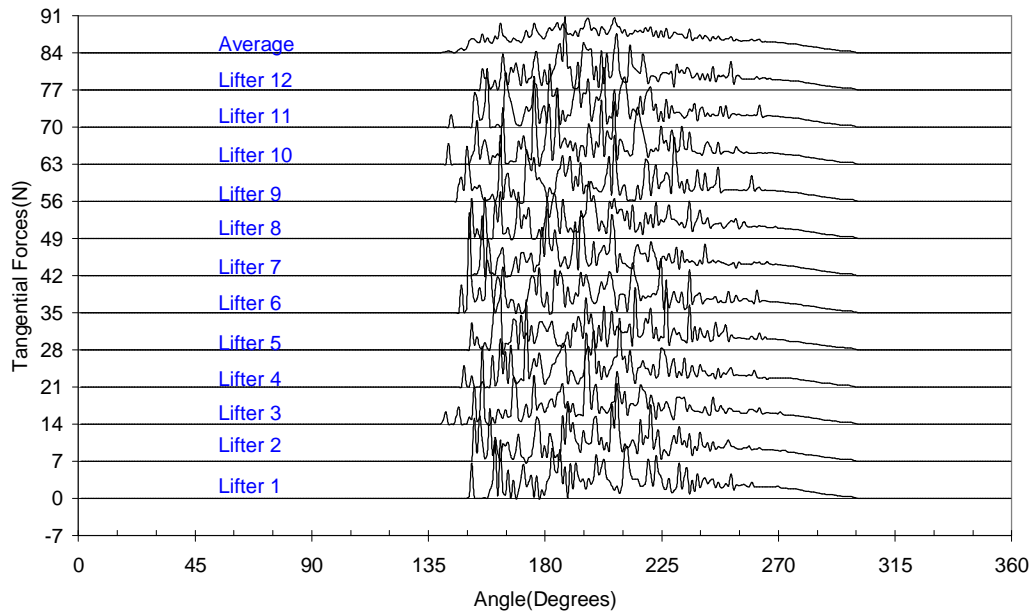




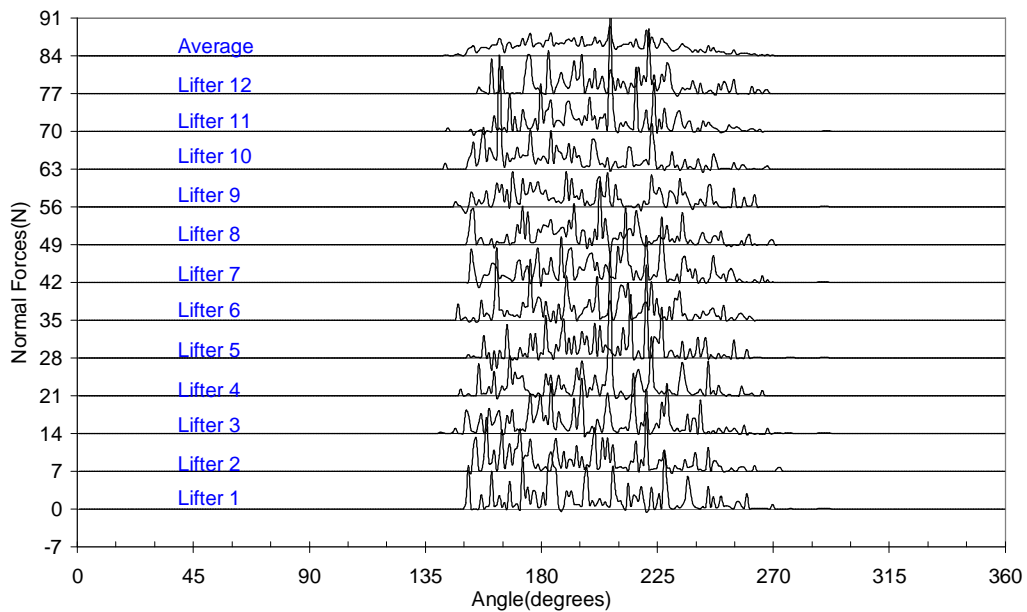
**Figure 5.16** Simulated tangential forces exerted on 12 lifters for one revolution, critical speed  $N_c=50\%$ , percentage of filling  $J=20\%$ , ball diameter  $d=6.7\text{mm}$ . The trends are separated from each other by 2N to increase legibility. (0 degree=12 O'clock position, mill rotation: anticlockwise)



**Figure 5.17** Simulated normal forces exerted on 12 lifters for one revolution, critical speed  $N_c=50\%$ , percentage of filling  $J=20\%$ , ball diameter  $d=6.7\text{mm}$ . The trends are separated from each other by 2N to increase legibility. (0 degree=12 O'clock position, mill rotation: anticlockwise)



**Figure 5.18** Simulated tangential forces exerted on 12 lifters for one revolution, critical speed  $N_c=30\%$ , percentage of filling  $J=20\%$ , ball diameter  $d=22.4\text{mm}$ . The trends are separated from each other by 7N to increase legibility. (0 degree=12 O'clock position, mill rotation: anticlockwise)



**Figure 5.19** Simulated normal forces exerted on 12 lifters for one revolution, critical speed  $N_c=30\%$ , percentage of filling  $J=20\%$ , ball diameter  $d=22.4\text{mm}$ . The trends are separated from each other by 7N to increase legibility. (0 degree=12 O'clock position, mill rotation: anticlockwise)

It can be seen from these Figures that the amplitude of forces are slightly different from one lifter to another in the same conditions. The shoulder and toe positions are similar for a particular mill speed as the data were recorded when the mill reached a steady state. Table 5.3 gives positions of shoulder and toe at different speed.

**Table 5.3** Shoulder and toe position from simulated data at different speed

% of critical speed	Toe			Shoulder		
	Earliest toe	Latest toe	Bulk toe	Earliest shoulder	Latest shoulder	Average of all lifters
60	138	143	140	318	330	322
50	136	142	140	312	321	315
30	141	155	144	300	300	300

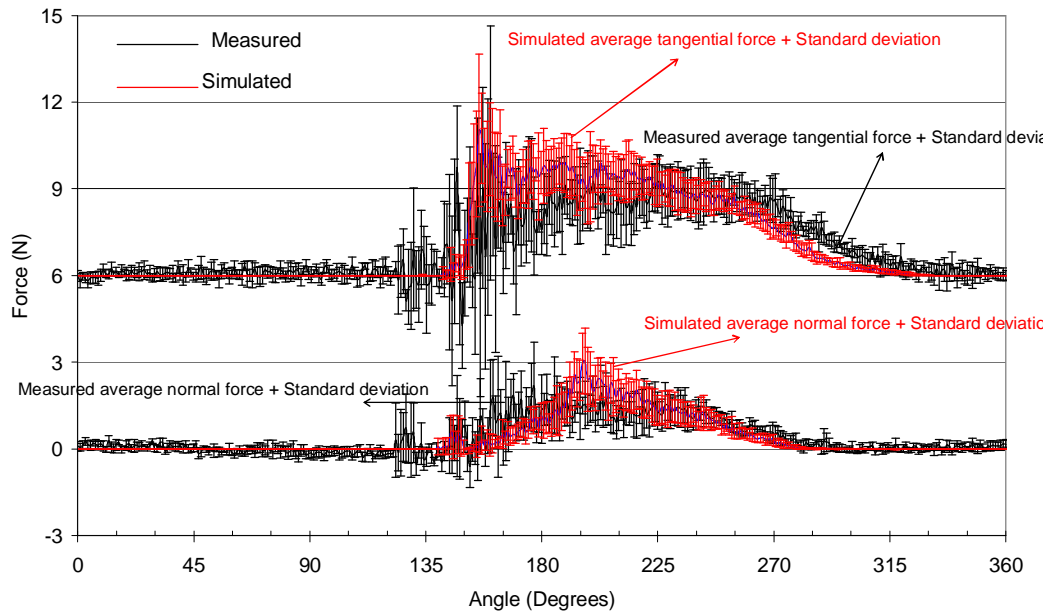
## 5.5 Comparison between measured and DEM simulated forces

### 5.5.1 Introduction

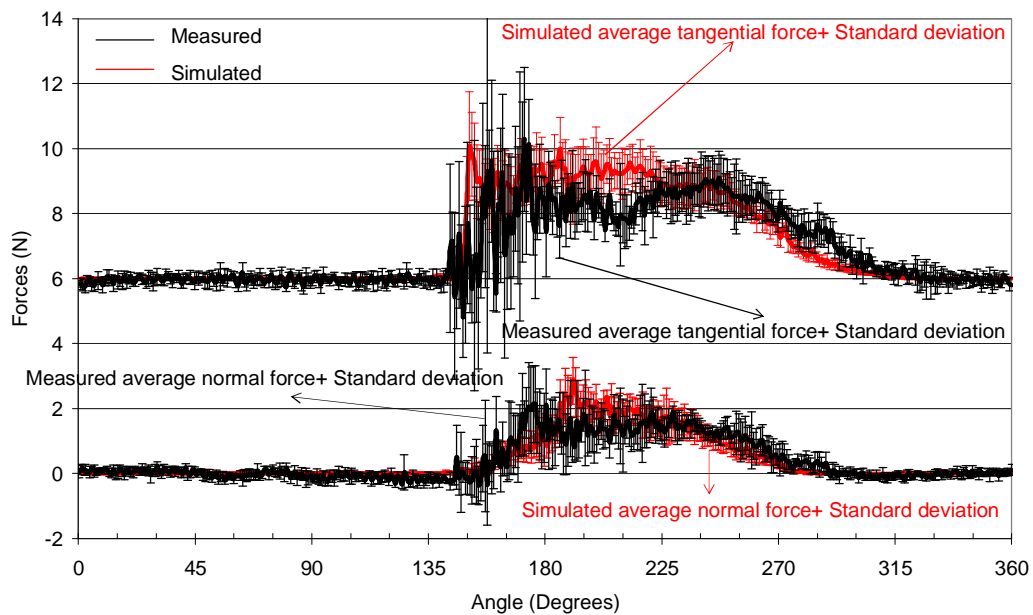
The comparison between the DEM simulated and measured tangential and normal forces at different speed will be performed in terms of positions of shoulder and toe and amplitude of forces at different mill angular positions.

### 5.5.2 Comparison between measured and simulated forces

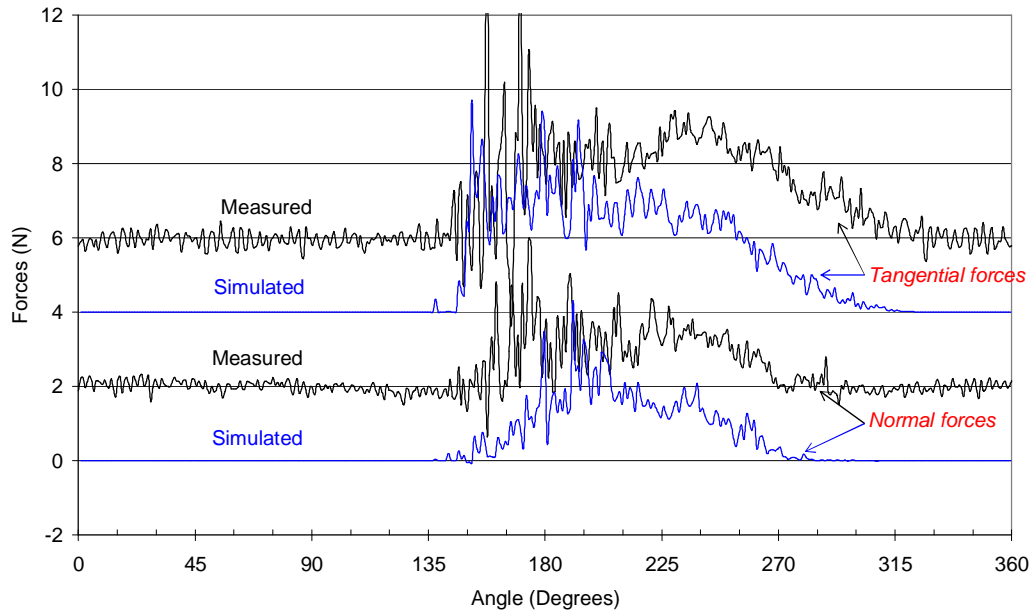
Figure 5.20 compares the results at 60% of critical speed of the average measured forces and average simulated forces and their respective standard deviation. It can be seen that signals are noisy in terms of amplitude of forces. There is nevertheless a good agreement in terms of toe and shoulder positions.



**Figure 5.20** Comparison between average experimental (over 6 revolutions) and simulated (for 12 lifters) results and their respective standard deviation at 60% of critical speed



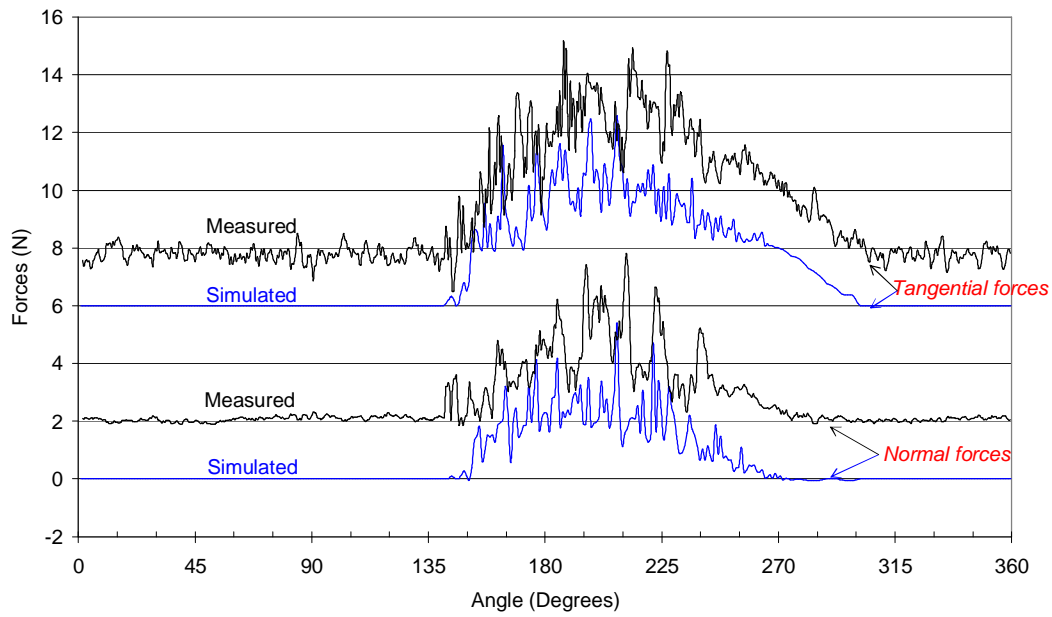
**Figure 5.21** Comparison between average experimental (over 5 revolutions) and simulated (for 12 lifters) results and their respective standard deviation at 50% of critical speed



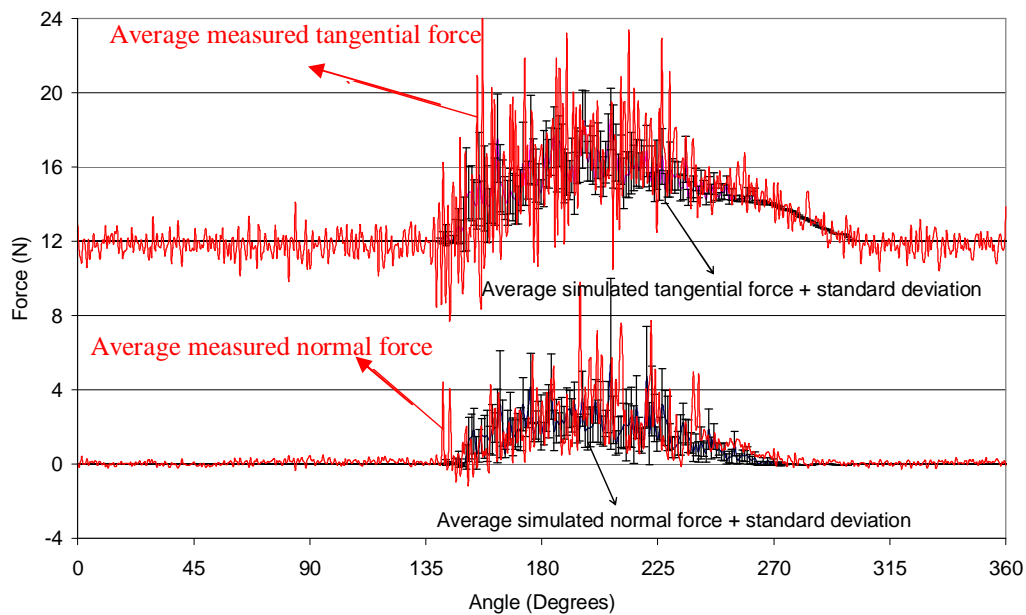
**Figure 5.22** Comparison between average experimental and DEM simulated tangential and normal forces at 50% of critical speed. The trends are separated by 2N to increase legibility.

Figure 5.21 shows the comparison between the average tangential and normal forces simulated and measured at 50% of critical speed. The respective standard deviations of these measurements are also plot on the same graph. It can be seen that there is a better agreement between the average tangential and normal forces simulated and measured in comparison to the data at 60% of critical speed. The slight difference observed in the comparison of the tangential forces between 180 and 195 degree is not significant. Figure 5.22 shows the comparison between average forces. There is a good correspondence between positions of toe and shoulder. The trends of amplitude of forces are similar.

Figure 5.23 compares the average tangential and normal forces at 30% of critical speed. A very good agreement is found between those measurements. The position of the toe and the shoulder and the amplitude of forces are very similar. Figure 5.24 confirms the results by including in the comparison the standard deviation of simulated forces. Appendix E shows a statistical comparison between measured and simulated forces at 30% of critical speed.



**Figure 5.23** Comparison between average tangential and normal forces simulated and measured at 30% of critical speed. The trends are separated by 2N to increase legibility.



**Figure 5.24** Comparison between average experimental (over 3 revolutions) and simulated + standard deviation (for 12 lifters) results at 30% of critical speed

## 5.6 Conclusions

A comprehensive study has been performed in order to validate the DEM simulations results. Different authors validated the DEM in terms of load behaviour and power draw by tumbling mills as a function of operating conditions. In our thesis, a more meticulous option has been taken to compare the experimental and DEM simulated forces exerted on lifters. Moys et al (2001) designed a two-dimensional mill recording the normal and tangential forces exerted on an instrumented lifter bar by the mill charge. Measured raw signals in Volts were provided. These signals were converted into forces in Newton via a calibrated model. Only data at 60, 50 and 30% of critical speed were analysed. The experimental results obtained were compared to DEM simulated results in the same conditions. It was found that the more the mill speed increases, the noisier signals become due to vibrations of the mill shell produce by ball impacting lifters. The accuracy of predictions depends therefore on the mill speed for two reasons: Firstly because at low speed we have less vibrations and consequently signals are less noisy, secondly because the rate of sampling data per second is constant giving more data per mill revolution at low speed.

A good correspondence between experimental and DEM simulated data has been found in the prediction of the toe and shoulder positions and the magnitude of forces at 30% of critical speed. At 50 and 60% of critical speed, rough similarities were achieved in terms of amplitude of forces but good similarities in terms of positions of shoulder and toe. The process of grinding being inherently noisy and random at high speed, a very good accuracy in terms of amplitude of force between the measured and simulated was not expected. Rough similarities achieved are good enough.

We showed that the Discrete Element Method is able to predict the forces or energies involved collisions between particle – ball and lifter as a function of mill speed and mill composition. The wear of lifters depends on energies dissipated in particles and lifters collisions. The DEM is consequently an appropriate tool to model the wear of lifters.

## Chapter 6

# Comparison between experimental and DEM simulated evolving lifter profiles due to wear

### 6.1 Introduction

### 6.2 Valderrama et al (1996) laboratory experimental mill used to measure the wear of mill lifters

### 6.3 Laboratory experimental results

### 6.4 DEM simulations

#### 6.4.1 Parameters used in the DEM simulations

#### 6.4.2 Lifter discretisation

#### 6.4.3 Calculations of the simulated wear rate

#### 6.4.4 Calculation of weight factors

#### 6.4.5 Simulated load behaviour at 75 % of critical speed with and without the deflector

#### 6.4.6 Energies dissipated on the unworn lifter divisions

##### 6.4.6.1 *Energies dissipated on the unworn lifter divisions at 75 % of critical speed with the deflector*

##### 6.4.6.2 *Energies dissipated on the unworn lifter divisions at 75% of critical speed without the deflector*

### 6.5 Comparison between experimental and DEM simulated predictions

#### 6.5.1 Comparison between experimental and DEM simulated results at 75% of critical speed in the presence of the deflector plate in the experimental mill

##### 6.5.1.1 *Lifter profiles*

##### 6.5.1.2 *Energies on lifter divisions*

##### 6.5.1.3 *Model accuracy*



6.5.1.4 *Contribution of impact wear*

6.5.2 Comparison between experimental and DEM simulated results at 75% of critical speed without deflector

**6.6 Influence of starting values**

**6.7 Conclusions**

## **6.1 Introduction**

Lifter profiles play a key role in the performance of tumbling mills. Due to the wear, lifter profiles evolve and tumbling mills performance varies correspondingly. The ability of simulating the change of lifter profile due to wear can therefore be used to design initial lifter profiles optimising tumbling mills performance over their useful life.

This chapter describes firstly a laboratory experimental mill used in order to measure evolving lifter profiles due to wear. Secondly, laboratory experimental results are analysed. Thirdly, Discrete Element Method simulations are conducted in the same conditions as experiments and both results are compared.

## **6.2 Valderrama et al (1996) laboratory experimental mill used to measure the wear of mill lifters**

Valderrama et al (1996) performed measurement of evolving lifter profiles due to wear in a laboratory ball mill. The object of their tests was to study the role of cascading and cataracting motion of balls on the wear of lifters. They used a mill having a diameter of 0.28 m and a length of 0.11 m. The mill was filled at 30% with balls of 0.0045m as diameter. The mill speeds used for the tests were 45, 55, 65, 75 and 85 % of the critical speed. The mill was equipped with 16 equally spaced lifters of five types: 30, 45, 60, 75 and 90° as front angle. Lifters were made in quick wearing ceramic quartz sand of size 60 – 80 Tyler mesh agglomerated with a catalytic resin. The quantity of resin used was enough to observe the same wear process as it occur for metal and to allow lifters to last at least one hour of mill test. Since fine powders were released from lifters during the tests due to the wear, a vacuum cleaner was connected to the mill in order to extract these particles. The presence of particles released could have prevented the direct contact ball – lifter and would have reduced the wear of lifters. Moreover, the motion of balls would have been also affected by the presence of fine powder.

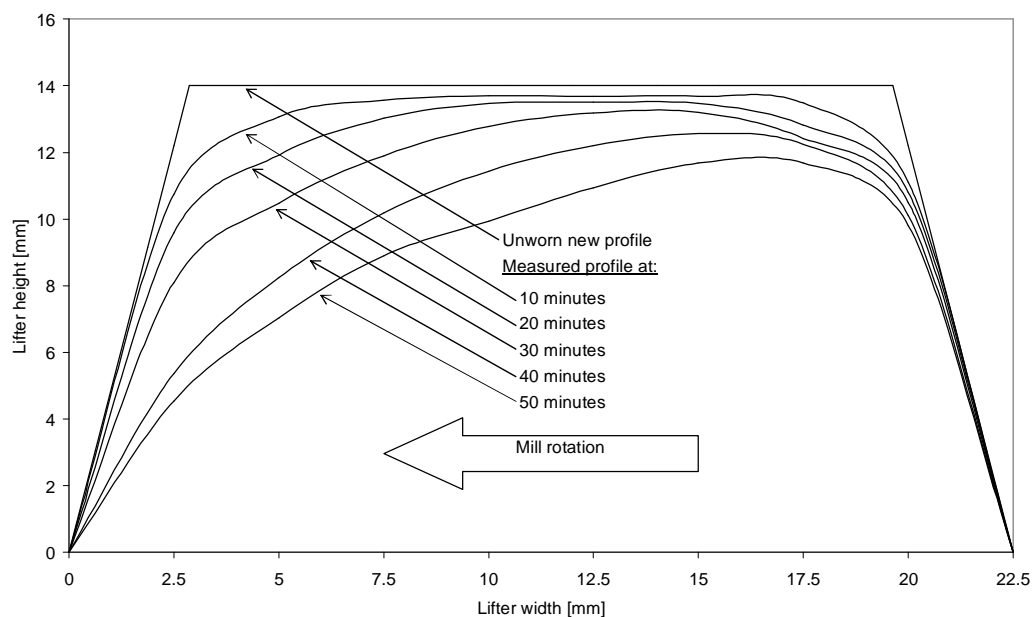
To distinguish the effect of cascading from the effect of cataracting, the laboratory mill was redesigned by inserting a deflector plate which prevents cataracting balls in the mill from falling on the lifters. Balls were therefore constrained to cascade in the mill.

All tests have been conducted in the presence and in absence of the deflector plate. The wear of lifters was monitored by recording the average lifter weight lost and by measuring the evolving lifter profile. Measurements were conducted on intervals of 10 minutes for 60 minutes of tests and each measurement presented is the average of 9 to 16 test probes. No standard deviation associated to measured lifter profiles was provided.

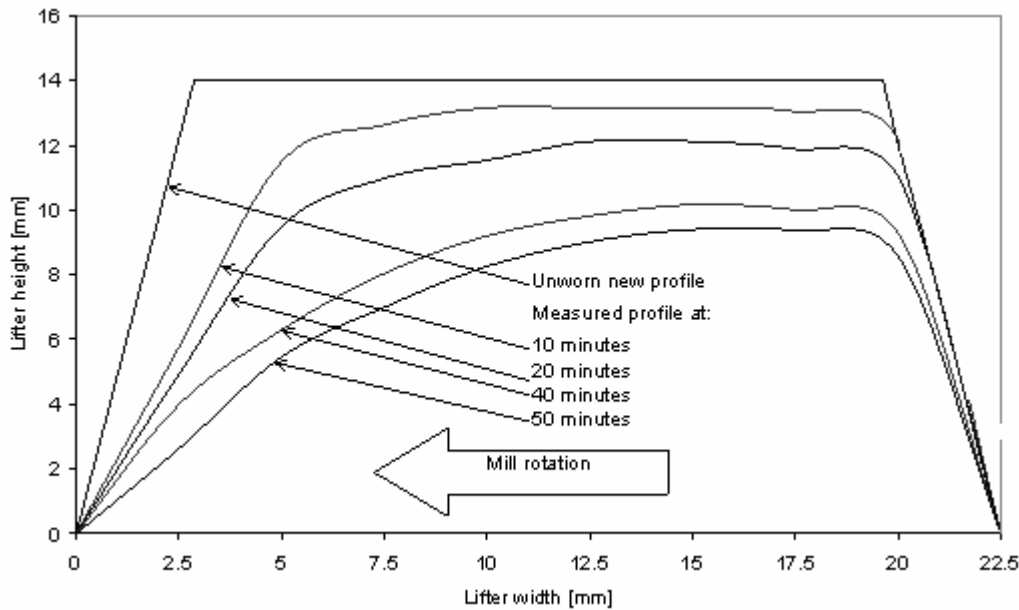
### 6.3 Laboratory experimental results

In the present dissertation, we have analysed only the results at 75% of critical speed for the trapezoidal lifter with a front angle of 75 degrees in the presence and in the absence of the deflector plate in the experimental mill.

Figure 6.1 shows the evolving lifter profiles measured at 75% of critical speed in the presence of the deflector while Figure 6.2 shows the results at the same speed without the deflector. The corners of unworn lifters were slightly rounded in both cases prior to tests.



**Figure 6.1** Evolving lifter profile (Valderrama et al (1996)) in a mill of diameter  $D=0.28\text{m}$ , length  $L=0.11\text{m}$ , critical speed  $N_c=75\%$ , percentage of filling  $J=30\%$ , ball diameter  $d=4.5\text{mm}$ , lifter front angle= $75$  degrees, with deflector.



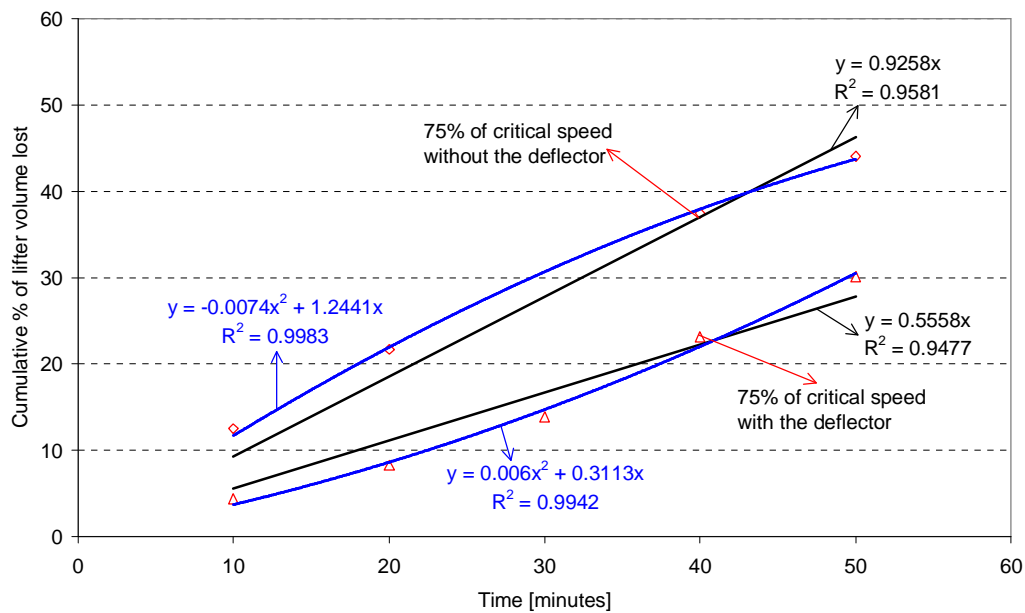
**Figure 6.2** Evolving lifter profile (Valderrama et al (1996)) in a mill of diameter  $D=0.28\text{m}$ , length  $L=0.11\text{m}$ , critical speed  $N_c=75\%$ , percentage of filling  $J=30\%$ , ball diameter  $d=4.5\text{mm}$ , lifter front angle  $=75$  degrees, without deflector

It can be seen from Figure 6.1 that at 75% of critical speed in the presence of the deflector, most wear occurs at the front of the lifter while from Figure 6.2 most of the wear occurs not only at the front of the lifter but also on the top due to cataracting balls. The lifter height decreases more rapidly in the absence of the deflector. The volume of material removed in the absence of the deflector is higher than in the presence of the deflector.

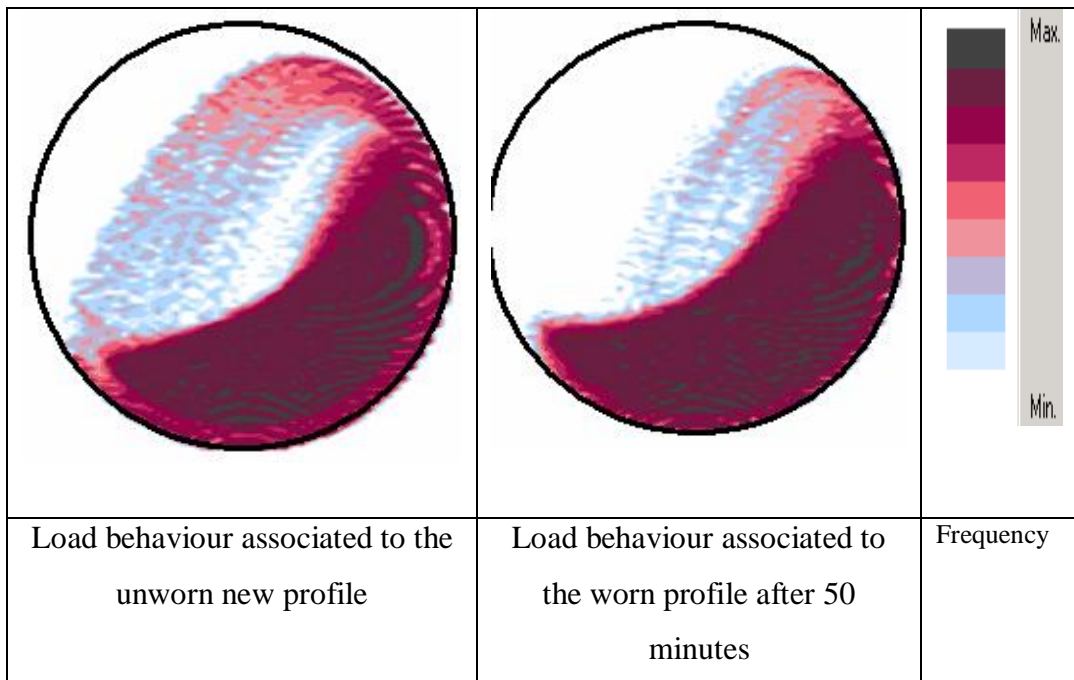
Figure 6.3 shows the cumulative percentage of lifter volume lost as a function of time in both cases. Valderrama et al (1996) reported a linear correlation between the cumulated lifter volumes lost and the time for all their data. The linear correlation factors  $R^2$  found in our cases are acceptable ( $R^2 > 0.94$ ) as indicated in Table 6.1. However, better correlations are found using a power (parabola) regression type ( $R^2 > 0.99$ ). This observation is justified by the change occurring in the mill load behaviour as lifters are wearing.

In the absence of the deflector plate, as lifters are wearing, the amount of cataracting balls impacting lifters decreases. This is shown by the DEM simulated position density plot (PDP) of balls in the mill for the unworn and worn lifter profiles as indicated in Figure 6.4. The lifter volume lost per unit of time is therefore high initially but decreases with time as lifters wear. For this reason, a better correlation

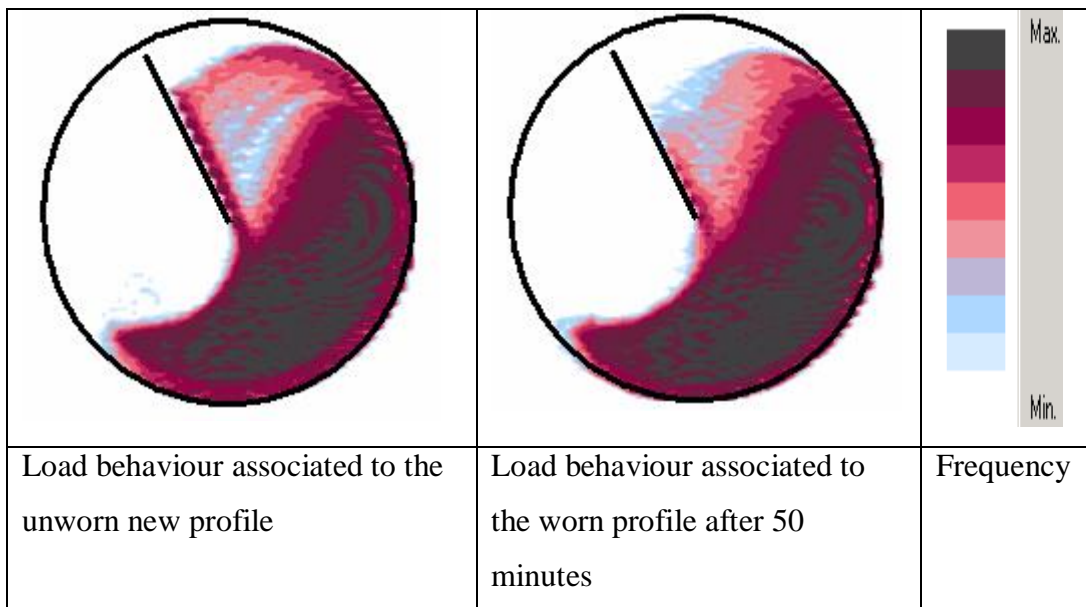
between the cumulative volume lost ( $y$ ) and the time ( $x$ ) was found using a parabola model as indicated in Table 6.1. The negative sign of  $x^2$  ( $y = -0.0074x^2 + 1.24x$ ) indicates the concave downwards trend of the parabola showing a decrease in the cumulative volume lost as a function of time in comparison to a constant loss predicted by a linear trend. After 50 minutes of tests, 44% of lifter volume is lost at 75% of critical speed in the absence of a deflector.



**Figure 6.3** Cumulative percentage of lifter volume lost function of time in a mill of diameter  $D=0.28\text{m}$ , length  $L=0.11\text{m}$ , percentage of filling  $J=30\%$ , ball diameter  $d=4.5\text{mm}$ , lifter front angle  $=75$  degrees, percentage of critical speed  $N_c=75\%$  with and without the deflector plate in the mill.



**Figure 6.4** DEM load behaviour position density plot (PDP) at 75% of critical speed in Valderrama's experimental mill without using a deflector



**Figure 6.5:** DEM load behaviour position density plot (PDP) at 75% of critical speed in Valderrama's experimental mill using a deflector

A logarithmic grading was used to differentiate the frequency of appearance (Frequency in Figure 6.4 and 6.5) of particles in grids. The maximum appearance (100%) is represented by the black colour and the lack of appearance (0%) in white colour. Ten (10) subdivisions were used from 0 to 100%.

**Table 6.1** Correlations between cumulative lifter volume lost (y) and time (x)

Regression type		Without the deflector	With the deflector
Linear	Equation	$y = 0.9258x$	$y = 0.5558x$
	R <sup>2</sup>	0.9581	0.9477
Power	Equation	$y = -0.0074x^2 + 1.24x$	$y = 0.006x^2 + 0.3113x$
	R <sup>2</sup>	0.9983	0.9942

In the presence of the deflector as indicated by Figure 6.5, although the amount of cataracting balls decreases as lifters wear, the deflector plate prevents them to fall directly on lifters. As lifters wear, the space between two consecutive lifters increases resulting in an augmentation of the intensity of balls impact on lifters. In this case therefore, as lifters are wearing, there is a slight increase in volume removed. For this reason a better correlation between the cumulative volume lost (y) and the time (x) was found using a parabola model as indicated in Table 6.1. The positive sign of  $x^2$  ( $y = 0.006x^2 + 0.3113x$ ) indicates the convex trend of the parabola showing an increase in the cumulative volume lost as a function of time in comparison to a constant lost predicted by a linear trend.

After 50 minutes of tests in the presence of the deflector plate, 30% of lifter volume is lost. The wear rate is consequently higher without the deflector plate.

## 6.4 DEM simulations

### 6.4.1 Parameters used in the DEM simulations

The laboratory experiments conducted by Valderrama et al (1996) involve around 22,300 balls of 4.5mm of diameter which correspond to a percentage of filling of 30%. The DEM simulations conducted in the same conditions will require several days in order to complete a full revolution. In order to reduce this prodigious amount of time of simulation, we chose to simulate one ball slice. The mill length was therefore reduced in our simulation from 0.11m to 5mm allowing the motions of 4.5 mm balls only in two-dimension. The coefficient of friction on the end wall was set to 0 in order to reduce their effect on the ball motion in the mill.

No measurements of power or load behaviour were recorded at the time of experiments. The only factor of comparison will therefore be the simulated evolving lifter profiles. Table 6.2 shows the parameters used in the DEM simulations

**Table 6.2** Parameters used in the DEM simulations to simulate the load behaviour and wear of lifter profiles

	Ball – Ball	Ball - Wall
Coefficient of friction	0.2	0.39
Coefficient of restitution	0.5	0.5
	Ball	Wall
Normal stiffness ( $\text{Nm}^{-1}$ )	400,000	400,000
Tangential stiffness ( $\text{Nm}^{-1}$ )	300,000	300,000

The steady state condition in the mill was reached after 2 revolutions and data were recorded from the third revolution.

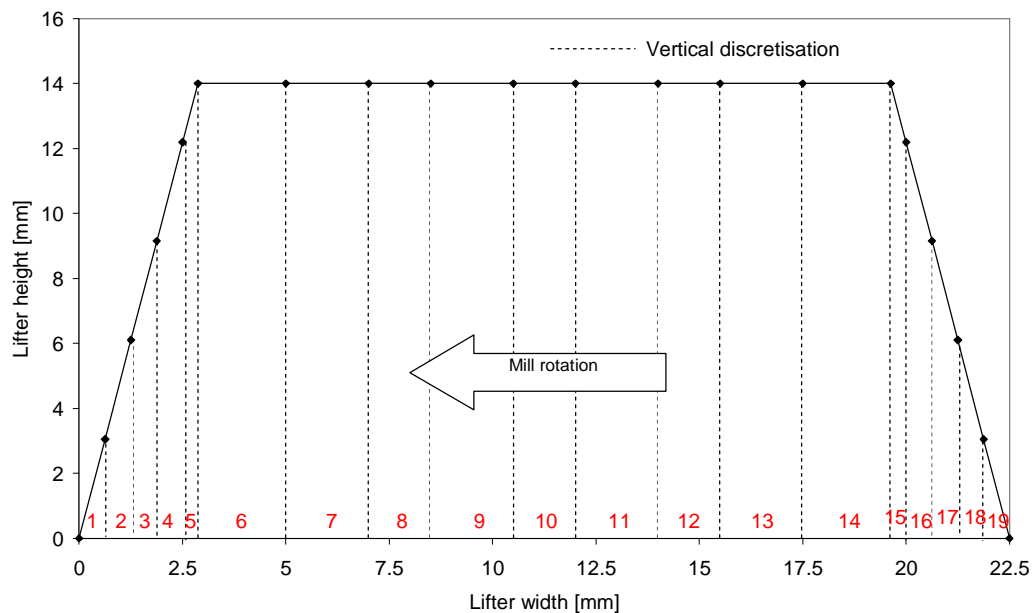


### 6.4.2 Lifter discretisation

The vertical discretisation described in Chapter 4 was used in this case since it is appropriate for trapezoidal lifters. The number of segments of discretised lifter was chosen in order:

- to keep a practical number of lifters divisions allowing the DEM simulation to be conducted within a reasonable time,
- to have discretised lifter divisions length less than the ball diameter, and
- to have more divisions on the front (and back) of the lifter where most events and change occur. Figure 6.6 shows the 2D discretised lifter.

The lifter was discretised in 19 segments and the DEM impact and abrasion/adhesion energies were recorded on these lifter divisions.



**Figure 6.6** Lifter discretised

### 6.4.3 Calculations of the simulated wear rate

In the experiments at 75% of critical speed in the presence and in absence of the deflector, lifters were lasting 50 minutes and the profiles measured at the interval of 10 minutes. Fifty minutes of experiments are equivalent to 3022 revolutions at 75 % of critical speed. It takes two days to simulate one revolution of one ball slice mill when the mill reaches the steady state condition.

In order to simulate the wear profiles within a reasonable time and achieve good predictions, we used a simulated wear rate higher than the experimental wear rate. We applied Qiu et al (2001) suggestions (described in Chapter 4) to calculate the simulated wear rate in order to produce the same wear characteristics. The simulation time was set equal to one revolution corresponding to 10 minutes of experiments. The entire simulation time is therefore sufficiently long so that the statistical variance associated with discrete events is small. By choosing one revolution, we have reduced the simulation time by a factor of  $n$  which must correspond to an increase of the simulated wear rate by the same factor. Table 6.3 shows the ratio between the experimental time and the simulated time at 75% of critical speed.

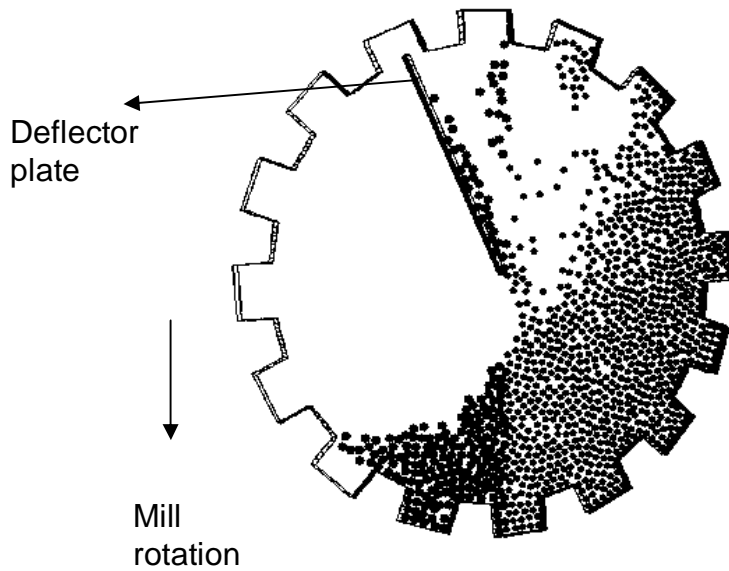
**Table 6.3** Ratio between experimental and simulated time at 75% of critical speed

Percentage of critical speed	Time		Ratio Experimental time/ Simulation time
	Experimental (Seconds)	Simulation (Seconds)	
75	600	0.9927	604.42

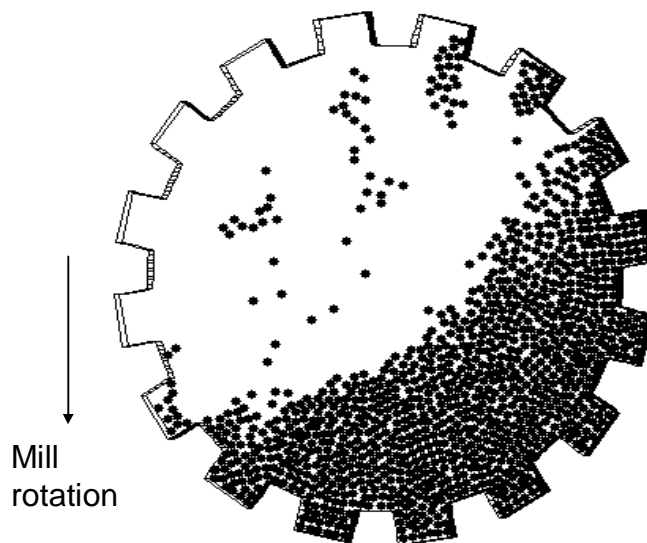
The experimental wear rate is proportional to the slope of the cumulative absolute lifter volume lost as a function of time. The simulated wear rate at 75 % of critical speed is found by multiplying the experimental wear rate by the ratio of experimental time and simulation time.

#### 6.4.4 Calculation of weight factors

In our approach of modelling the wear of lifters, the weight factors given to: impact energy  $a_{impact}$ , abrasion/adhesion energy  $a_{abr-ad}$ , the difference of slope between two consecutive worn profiles  $I$  and to the difference of slope in each discretised lifter division between the  $i^{th}$  and the  $(i+1)^{th}$  profile  $a$  used in order to predict evolving lifter profiles were in this case calculated recursively to match the simulated and measured profile. The calculated parameters found were constant for simulations in the presence and in the absence of the deflector plate.



**Figure 6.7** Simulated load behaviour in the presence of a deflector in a mill of diameter  $D=0.28\text{m}$ , critical speed  $N_c=75\%$ , percentage of filling  $J=30\%$ , ball diameter  $d=4.5\text{mm}$ , unworn new lifter with front angle  $=75$  degrees



**Figure 6.8** Simulated load behaviour without a deflector in a mill of diameter  $D=0.28\text{m}$ , critical speed  $N_c=75\%$ , percentage of filling  $J=30\%$ , ball diameter  $d=4.5\text{mm}$ , unworn new lifter with front angle  $=75$  degrees

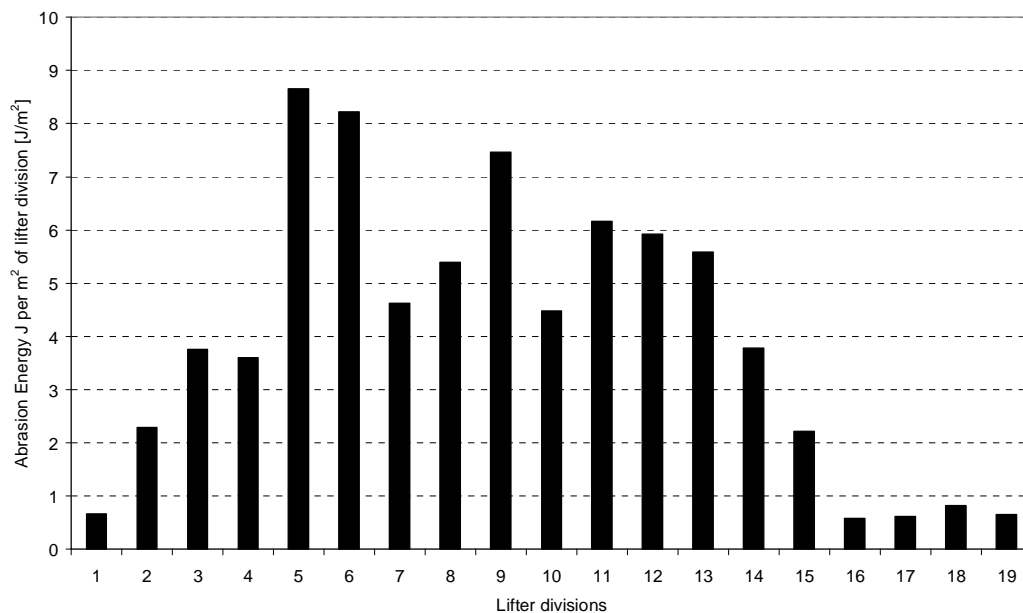
#### 6.4.5 Simulated load behaviour at 75 % of critical speed with and without the deflector respectively

Figure 6.7 and 6.8 show one frame of the DEM simulated load behaviour at 75 % of critical speed for the new unworn lifter respectively, in the presence of the deflector and in its absence. The deflector prevents cataracting balls from impacting on lifters while in its absence, balls impact directly on the lifters. As lifter profiles evolve due to wear, the load behaviour is changing (Figure 6.4 and 6.5). Energies on discretised lifter divisions will therefore vary as a function of time.

#### 6.4.6 Energies dissipated on the unworn lifter divisions

##### 6.4.6.1 Energies dissipated on lifter divisions at 75% of critical speed with the deflector

Figure 6.9 shows the average adhesion/abrasion energies dissipated per  $\text{m}^2$  of the discretised lifter divisions (Figure 6.6) for all 16 unworn lifters for the experimental mill in the presence of a deflector.

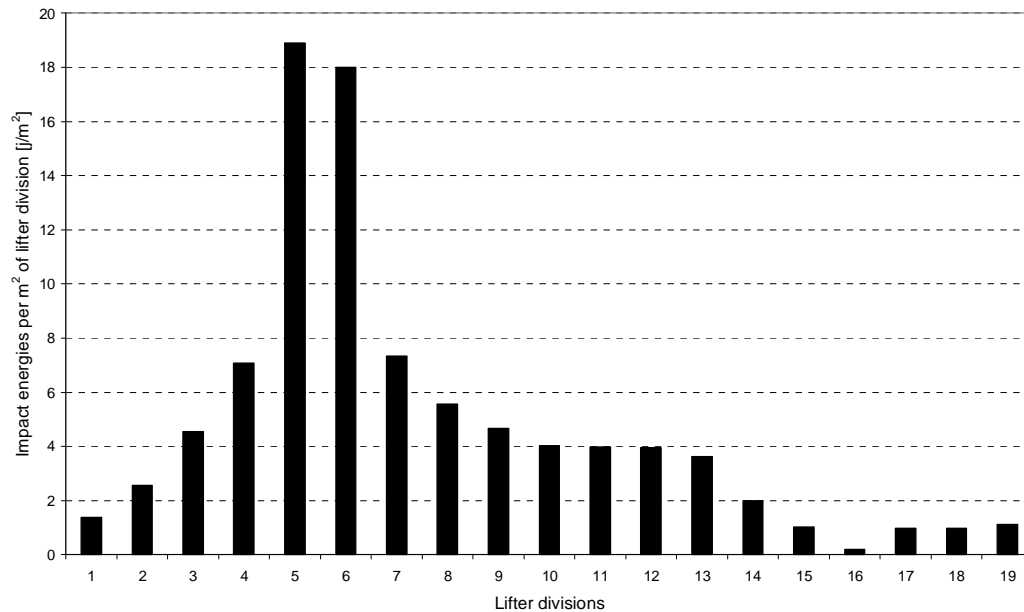


**Figure 6.9** Average adhesion/abrasion energies per  $\text{m}^2$  of the unworn new lifter divisions at 75% of critical speed in the presence of the deflector.

Most of adhesion/abrasion energies are dissipated on top of the lifter (divisions 6 to 14) and at the front of the lifter (divisions 1 to 5) with a maximum on lifter division 5.

Low energies are dissipated at the back (divisions 16 to 19) of the lifter as less contact occurs between balls and lifter. These results are in agreement with the observation from the simulated load behaviour.

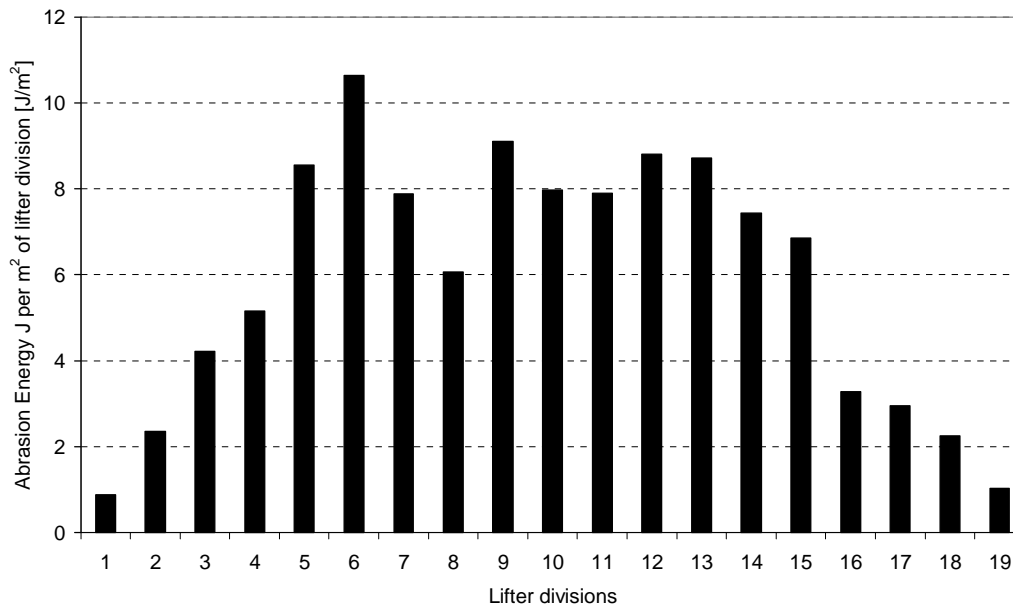
Figure 6.10 shows the average impact energies dissipated per  $\text{m}^2$  of the unworn lifter division for all 16 lifters.



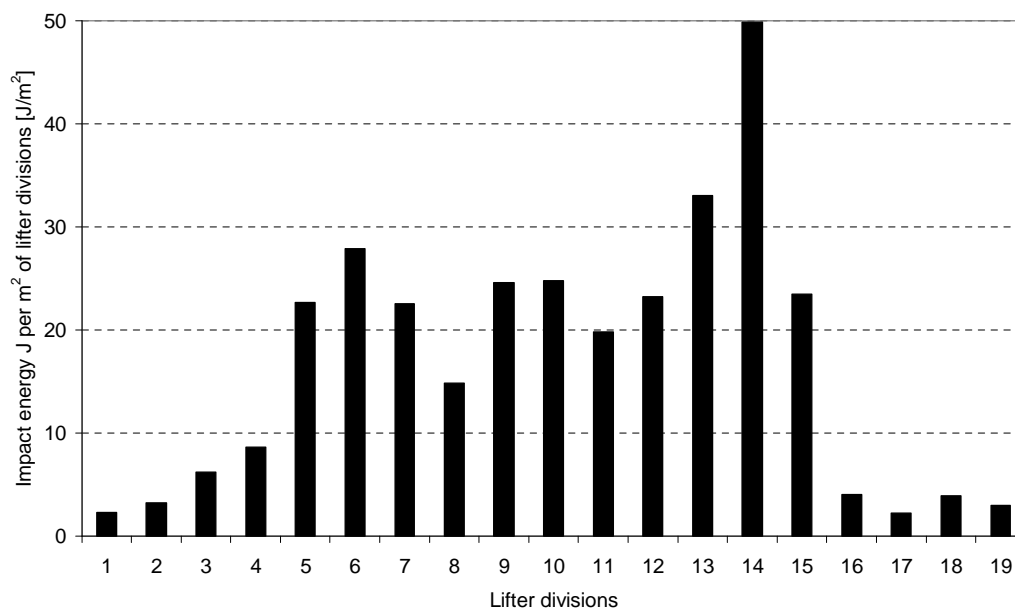
**Figure 6.10** Average impact energies per  $\text{m}^2$  of discretised lifter divisions of the unworn lifter at 75% of critical speed in the presence of the deflector

High impact energies occur on lifter divisions 5 and 6 as shown by Figure 6.10. These results were expected from the analysis of the simulated load behaviour in the mill. Lifters division 1 and 19 have the same average impact energy due to the packing of balls between consecutive lifters as indicated by the load behaviour (Figure 6.7). These packed balls impact at the front and at the back on lifters.

#### 6.4.6.2 Energies dissipated on lifter divisions at 75% of critical speed without the deflector



**Figure 6.11** Average abrasion/adhesion energies per  $\text{m}^2$  of discretised lifter divisions of the unworn lifter at 75% of critical speed without using the deflector plate in the experimental mill.



**Figure 6.12** Average impact energies per  $\text{m}^2$  of discretised lifter divisions of the unworn lifter at 75% of critical without using the deflector plate speed in the experimental mill.

Figure 6.11 shows the average abrasion energies per  $\text{m}^2$  of discretised lifter division at 75% of critical speed without the deflector in the mill. It can be seen that high

abrasion/adhesion occur at the top of the lifter. Figure 6.12 showing the average impact energies per  $m^2$  of discretised lifter division illustrates the same trend where high impact energies occur at the top of lifter.

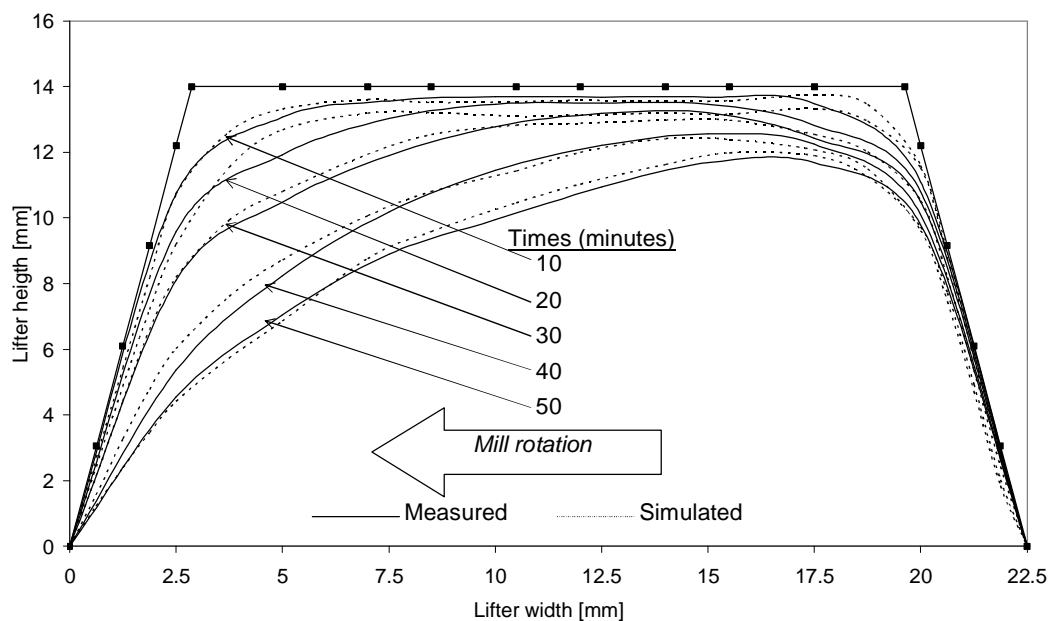
## 6.5 Comparison between experimental and DEM simulated predictions

6.5.1 Comparison between experimental and DEM simulated results at 75% of critical speed in the presence of the deflector plate in the experimental mill

### 6.5.1.1 Lifter profiles

The first simulated profile at 10 minutes was predicted from the unworn profile. The remaining 2<sup>nd</sup>, 3<sup>rd</sup>, 4<sup>th</sup> and 5<sup>th</sup> simulated profiles were derived from the 1<sup>st</sup>, 2<sup>nd</sup>, 3<sup>rd</sup> and 4<sup>th</sup> simulated profiles respectively.

Figure 6.13 compares our Discrete Element Method simulated results to the experimental measured profiles. A good agreement is found between these results.



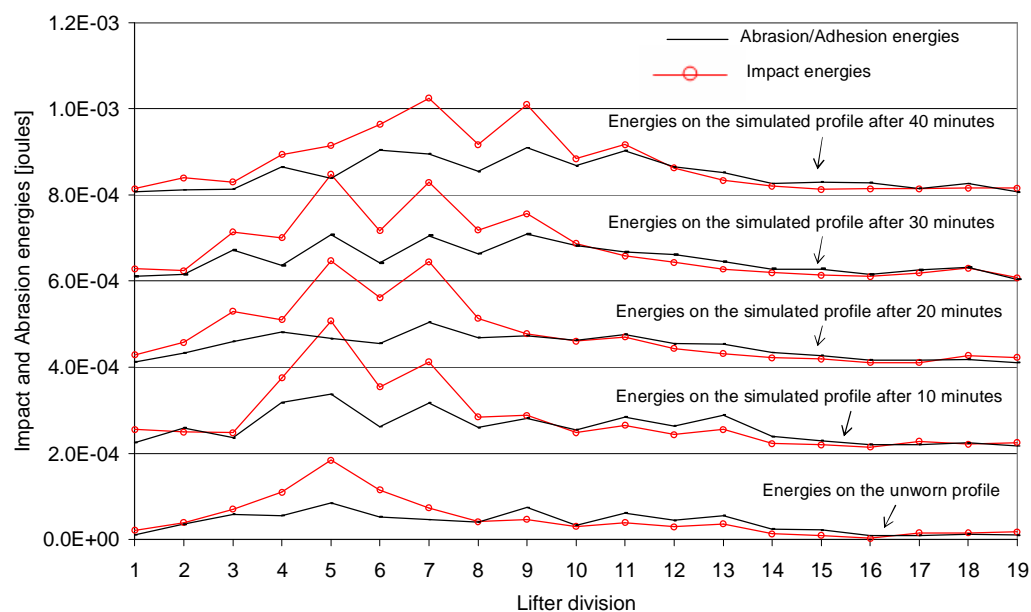
**Figure 6.13** Comparison between experimental (Valderrama et al,1996) and DEM simulated lifter profiles at different time in a mill of diameter  $D=0.28m$ , critical speed  $N_c=75\%$ , percentage of filling  $J=30\%$ , ball diameter  $d=4.5mm$ , with the deflector plate inside the mill.

Parameters in the objective function and weight factors given to impact and abrasion energies were back calculated by predicting the 2<sup>nd</sup>, 3<sup>rd</sup>, 4<sup>th</sup> and 5<sup>th</sup> measured profile from respectively the 1<sup>st</sup>, 2<sup>nd</sup>, 3<sup>rd</sup> and 4<sup>th</sup> measured profiles.

### 6.5.1.2 Energies on lifter divisions

Figure 6.14 shows the simulated energies dissipated on the evolving lifter profile on each discretised lifter division. These energies predicted by the DEM were used to predict the simulated profiles.

It can be seen that energies dissipated on discretised lifter divisions 1 to 19 (Figure 6.6) vary as the lifter profile evolves. Most changes in the amplitude of energies occur at the front of the lifter while little changes are observed at the back. Impact energies are always higher in comparison to abrasion/ adhesion at the front of the lifter where most impact occurs. The opposite observation is valid at the back of the lifter where balls slide on the lifter.

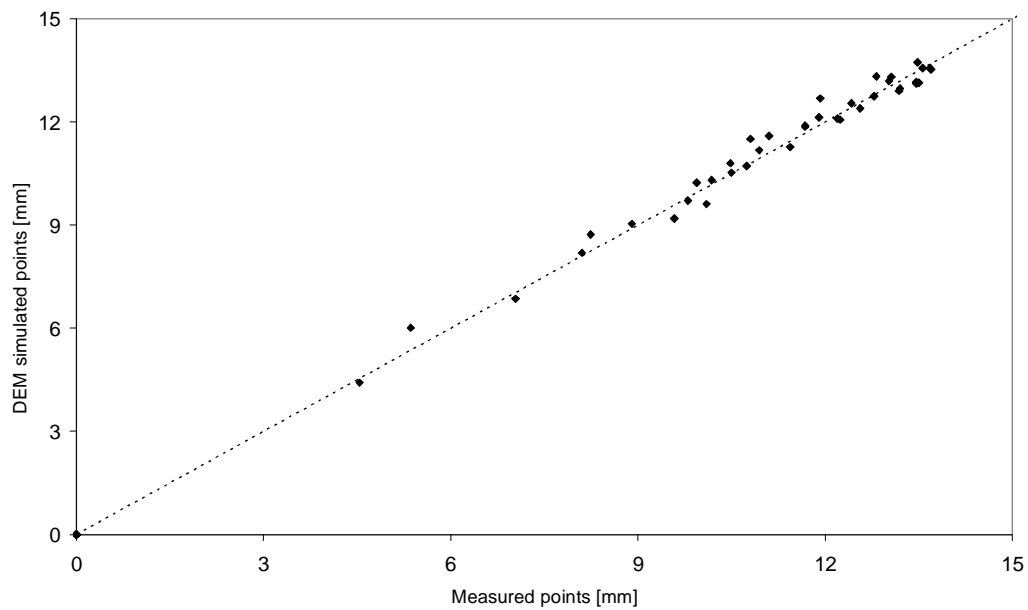


**Figure 6.14** DEM average energies dissipated on the evolving lifter profile on each discretised lifter division. The trends are separated from each other by 0.0002 Joules to increase legibility.



### 6.5.1.3 Model accuracy

A good correspondence has been found between the DEM simulated and the experimental results. The model accuracy is illustrated in the Figure 6.15 and Table 6.4 comparing the position in mm of measured points to simulated points.



**Figure 6.15** Simulated vs. Measured points.

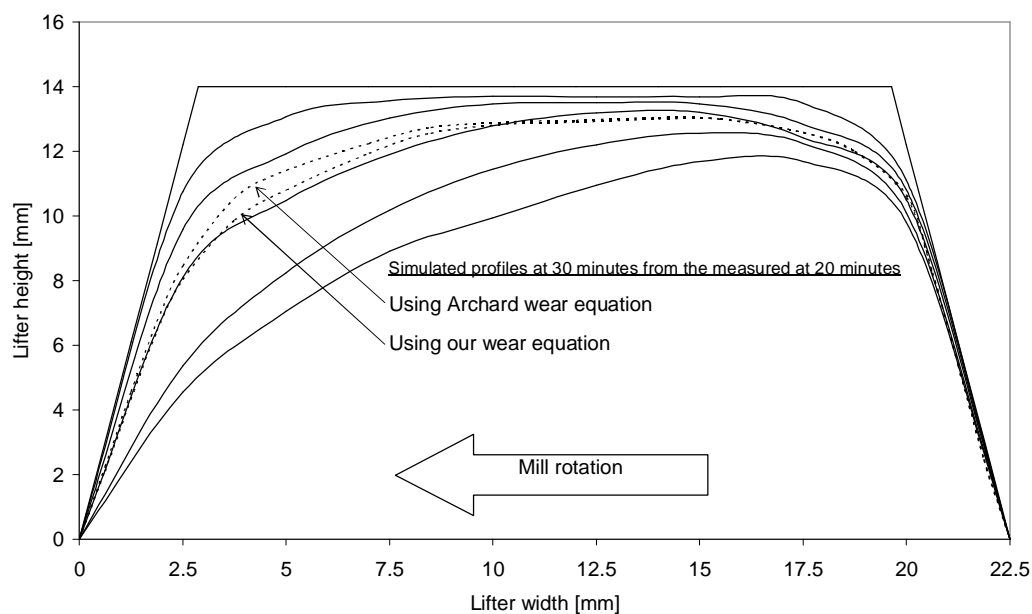
**Table 6.4** Model accuracy

Number of points	50
Value of “a” at 95% confidence interval in the model $Y = aX$	$1.00427 \pm 0.0077$
Coefficient of correlation $R^2$	0.9969
Variance $s^2$	0.0779
Standard deviation $s$	0.279

The ability of our model to predict the experimental data is due to the use of a wear mathematical model which takes into account all mechanism of wear in the mill and the implementation of the mathematical model in the DEM code using an objective function producing realistic profiles.

#### 6.5.1.4 Contribution of impact wear

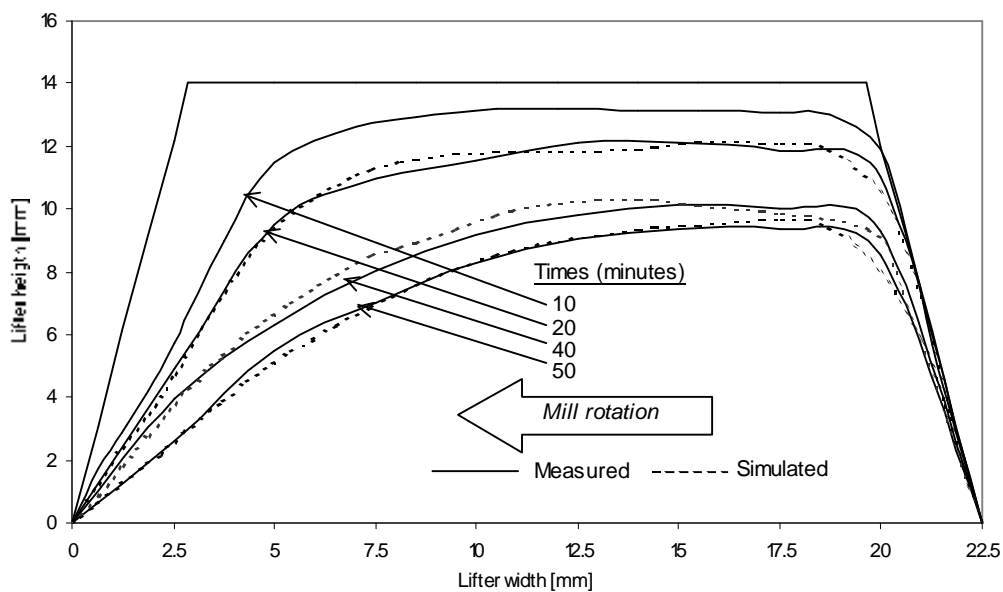
In the Equation 4.6 (Chapter 4) predicting the volume of material removed on a discretised lifter division  $i$  ( $V_i = W(a_{impact} E_{impact,i} + a_{ad-abr} E_{ad-abr,i})$ ), the calculated constant weight factor given to impact energy was 0.64 while the weight factor given to abrasion/adhesion was 1. The impact energy was responsible for 48% of material removal and the abrasion/adhesion energy 52%. It was expected that the contribution of the impact energy in the simulations performed in the presence of the deflector will not be significant as the deflector prevent cataracting balls to impact directly on lifters. In order to assess the contribution of the impact energy in the wear of lifters, the impact energy weight factor,  $a_{impact}$  was set to zero in the above mentioned equation and the results compared to the measured profiles. Fixing the value of  $a_{impact}$  at zero is equivalent to use only the Archard's wear equation in the prediction of the wear of lifters.



**Figure 6.16** Influence of the contribution of impact energy on the wear of lifters.

Figure 6.16 shows the results of the influence of impact energies on the prediction of the simulated wear profile. It can be seen from the figure that the simulated profiles predict using our wear equation is in better agreement with the measured profile than the profile found using only the Archard equation. It was expected, in this case where the deflector prevents cataracting balls from impacting lifters that the impact energy will have less effect on the accuracy of the prediction but it can be seen that it is playing an important role in the accuracy of the prediction.

### 6.5.2 Comparison between experimental and simulated results at 75% of critical speed without the deflector plate in the experimental mill



**Figure 6.17** Comparison between experimental and DEM simulated lifter profiles at different time in a mill of diameter  $D=0.28\text{m}$ , critical speed  $N_c=75\%$ , percentage of filling  $J=30\%$ , ball diameter  $d=4.5\text{mm}$ , without the deflector inside the experimental mill.

Energies dissipated on the unworn discretised lifter divisions as shown by Figure 6.11 and 6.12 indicates that lifter division 16 to 18 at the back of the lifter will lose a volume of material. An observation of the measured profile (Figure 6.2) shows that there is no wear occurring at the back of the lifter. We started therefore our simulations from the measured profile at 10 minutes to predict the simulated profile at 20 minutes. The simulated profile at 40 and 50 minutes were predicted respectively from the simulated profiles at 30 and 40 minutes. The results found are represented in the Figure 6.17. A good agreement is found between the measured and the simulated profile.

## 6.6 Influence of starting values

Optimisation algorithms require first parameter estimates or interval to locate a minimum or a maximum. There is no guarantee that the values found correspond to the global minimum unless the problem is continuous and has only one minimum (Kreyszig, 1983).

To ensure that the minimisation of our objective function  $S^2$  leads to a global and not a local minimum, we have studied the influence of starting values. We found that a good starting guess improve the efficiency and help to reach the global minimum in less iterations. We advice therefore that the ordinates of the starting values of the simulated profiles at a position  $i$  must be less than the initial ordinate at  $i$  or  $y'_i < y_i$ . The amplitude of difference between both ordinate must be function on the wear rate used. Furthermore we wrote a program in Matlab (Appendix F) which can be used together with the Excel solver function to find the global minimum.

## 6.7 Conclusions

Our approach described in Chapter 4 to model the wear of lifters has been tested against Valderrama et al (1996) published laboratory experimental data. These authors performed tests of measurement of evolving lifter profiles due to wear in a laboratory ball mill. The tests were conducted in the presence and absence of a deflector preventing balls from impacting directly on lifters. These authors used quick ceramic wearing lifters in order to record the wear of lifter in a reasonable time. The wear of lifter observed experimentally was similar to the wear of metallic lifters observed industrially.

In the same conditions of experiments, Discrete Element Method simulations have been performed in order to simulate the wear of lifters. The simulated and experimental results at 75 % of critical speed in the presence and in the absence of the deflector have been compared in this chapter. A good correspondence has been found between the measured and simulated profiles.

We found that it was possible to reduce the simulation time by using a simulated wear rate higher than the experimental.

We established also that it was important to use our mathematical wear equation taking into account all types of wear occurring in the mill environment in order to improve the accuracy of predictions.

We attribute the success of modelling the wear of lifters to firstly, the use of a mathematical equation removing material on lifters which takes into account all mechanism of wear occurring in the milling environment. Secondly, the implementation of that equation using an objective function producing realistic profiles.

We conclude that the DEM can be used successfully to predict the wear of lifters.

# Chapter 7

## DEM Modelling of the wear of industrial tumbling mills lifters

### **7.1 Introduction**

### **7.2 Industrial tumbling mills**

#### 7.2.1 Introduction

#### 7.2.2 Lifter used in tumbling mills at LETHABO power station

#### 7.2.3 Lifter used in tumbling mills at KENDAL power station

#### 7.2.4 Lifter used in tumbling mills at MATIMBA power station

### **7.3 Parameters used in the DEM simulations and wear model**

### **7.4 Procedure to model the wear of lifters**

### **7.5 Modelling of the wear of tumbling mill lifters used at Lethabo power station**

#### 7.5.1 Introduction

#### 7.5.2 Simulated profiles

#### 7.5.3 Impact and abrasion/adhesion energies dissipated on discretised lifter divisions as a function of time

#### 7.5.4 Comparison between the volume removed predicted and effectively removed

### **7.6 Modelling of the wear of tumbling mill lifters used at Kendal power station**

#### 7.6.1 Simulated profiles

#### 7.6.2 Impact and abrasion/adhesion energies dissipated on discretised lifter divisions as a function of time

### **7.7 Modelling of the wear of tumbling mill lifters used at Matimba power station**

#### 7.7.1 Simulated profiles

#### 7.7.2 Impact and abrasion/adhesion energies dissipated on discretised lifter divisions as a function of time

### **7.8 Discussions**

#### 7.8.1 Simulating the wear of lifters using one ball slice length

- 7.8.2 Determination of weight parameters( $\alpha, \lambda$ ) in the objective function
- 7.8.3 Determination of weight parameters  $a_{\text{impact}}$  and  $a_{\text{ad/abr}}$
- 7.8.4 Decoupling abrasion and impact energy in the prediction of wear
- 7.8.5 Detachment versus removal of particles in the wear process

## **7.9 Conclusions**

## 7.1 Introduction

To ensure that the approach developed in this thesis to simulate the wear of lifters has the ability to accurately predict the evolving lifter profiles in all cases, our model was also tested to predict the wear of three different lifter profiles used in industrial tumbling mills operating in dry conditions.

In this Chapter we analyse, the results obtained from tumbling mills used in South Africa at ESKOM LETHABO, KENDAL and MATIMBA power stations for the grinding of coal.

## 7.2 Industrial tumbling mills

### 7.2.1 Introduction

LETHABO, KENDAL and MATIMBA power stations are ESKOM South Africa coal fired stations. LETHABO power station is located between Vereeniging and Sasolburg in the Free State province. KENDAL power station is situated 40Km Southwest of Witbank in the Mpumalanga province and MATIMBA power station is located in the Northern Province near Ellisras. These power stations produce electricity by using coal ground in tumbling mills. The characteristics of tumbling mills used at these power stations in order to grind and dry coal are indicated in Table 7.1.

**Table 7.1** Characteristics of tumbling mills used at LETHABO, KENDAL and MATIMBA power stations

	LETHABO	KENDAL	MATIMBA
Mill diameter to the shell [mm]	4267	4692	4740
Mill Length [mm]	5790	6557	7400
Mill speed [rpm]	15.7	14.9	15.5
Mill % of critical speed	76.67	76.30	79.78
Percentage of filling [%]	24.2	22.9	19
Make-up top ball size dimension [mm]	50	50	50
Number of circumferential lifter	30	30	40

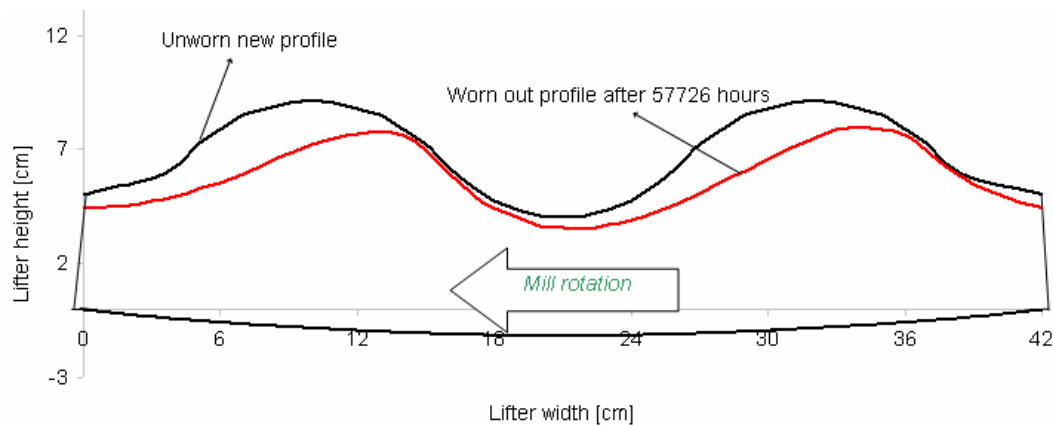


Air is swept in these tumbling mills in order to remove coal particles ground. Appendix G shows the difference between these mills in terms of coal removal from the mill.

### 7.2.2 Lifters used in tumbling mills at LETHABO power station

Tumbling mills used at ESKOM LETHABO power station are equipped with double wave lifters. Figure 7.1 represents one lifter. Both the new lifter (0 hour of service) and the worn lifter after 57726 hours are represented in the same figure. The direction of mill rotation is also indicated.

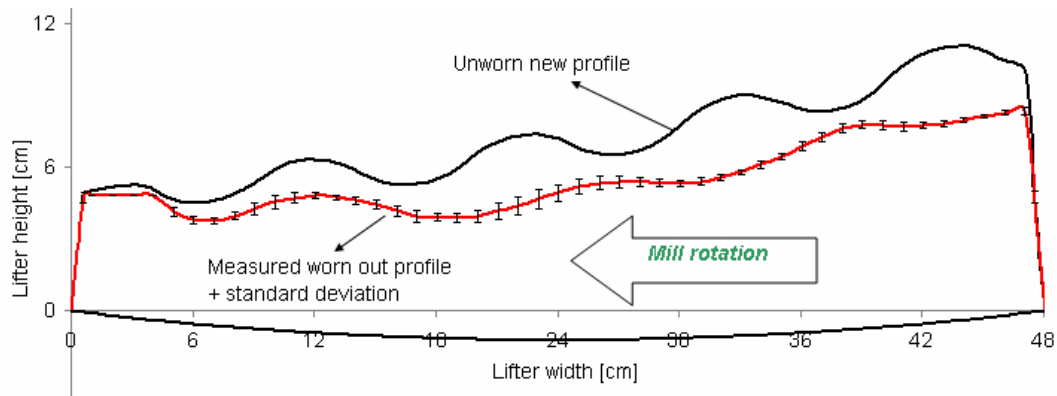
It can be seen from Figure 7.1 that most of the wear occurs at the front of the lifter waves while the back of the two waves are less affected.



**Figure 7.1** Unworn and worn out lifter profile used at LETHABO power station

### 7.2.3 Lifters used in tumbling mills at KENDAL power station

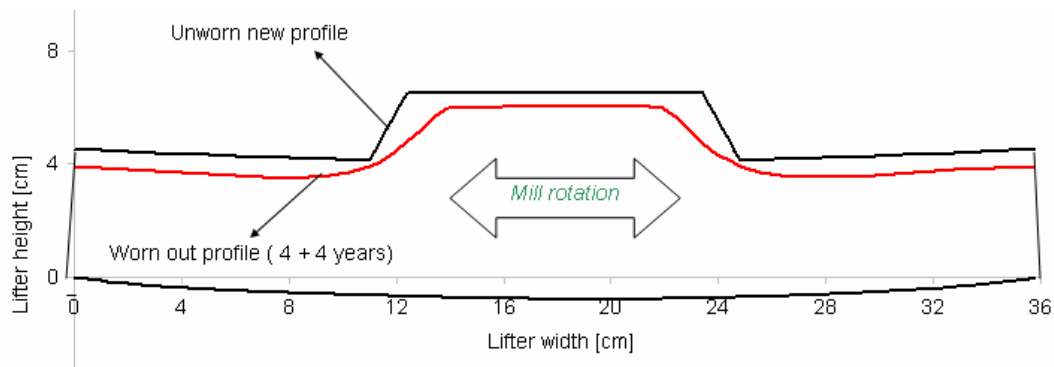
At ESKOM KENDAL power station, tumbling mills are equipped with lifters represented in Figure 7.2. The average measured profile of 12 worn lifters after 70 900 hours and their standard deviation is also represented in the same Figure. A profiling gage was used to measure worn profiles. Appendix H shows the location of measured worn lifters in the mill. No particular trend from the worn lifters close to the feeds or in the middle was noticed. It can be seen from Figure 7.2 that there is a dramatic change in the profile from the unworn to the worn out profile.



**Figure 7.2** Unworn and worn out lifter profile used at KENDAL power station

#### 7.2.4 Lifters used in tumbling mills at MATIMBA power station

Figure 7.3 represents a lifter in tumbling mills in use at ESKOM MATIMBA power station. It can be seen from Figure 7.3 that in comparison to lifters used at Lethabo and Kendal power stations characterised by waves, lifters used at Matimba power station are more aggressive. Once the unworn profile reaches a critical worn profile from one side, lifters are reversed in the mill to exploit the other side not affected previously by the wear. Each side of the lifter runs for approximately 4 years.



**Figure 7.3** Unworn and worn out lifter profile used at MATIMBA power station

### 7.3 Parameters used in the DEM simulation and wear model

Parameters reported in Table 7.2 were used in the DEM simulations to model the load behaviour and wear of lifters. The choice of these parameters was motivated by Couvas and Moys (2002), and Moys et al (2004) work comparing the power and load

behaviour measured and DEM simulated respectively at Matimba and Kendal power stations.

A full three-dimensional (3D) simulation with full range of ball size distribution is appropriate to simulate accurately the behaviour of these industrial tumbling mills. However, this approach takes several weeks to have the results of one complete revolution. To reduce this time, the 3D simulation was reduced to one ball slice simulation using only the top ball size.

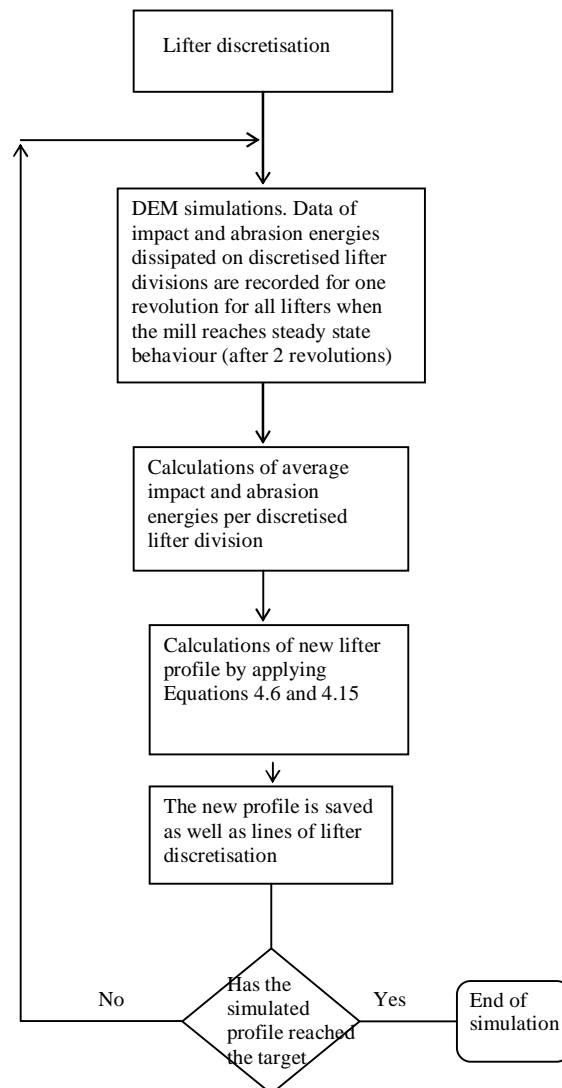
**Table 7.2** Parameters used in the DEM simulation to simulate the wear of lifters used at ESKOM Lethabo, Kendal and Matimba power stations

	Ball	Wall
Coefficient of friction	0.2	0.2
Coefficient of restitution	0.5	0.4
Normal stiffness (Nm <sup>-1</sup> )	400,000	400,000
Tangential stiffness (Nm <sup>-1</sup> )	300,000	300,000

Equations 4.6 and 4.15 (Chapter 4) were used to remove material on lifters. The weight factors given to impact and abrasion energies were back-calculated. The same values found were used for all lifters (Lethabo, Kendal and Matimba) since they have similar properties. It was found that the contribution of impact energy to the wear of lifters was more important than the contribution of abrasion energies. This observation agrees with preliminary results found by Radziszewski (2001) in his attempt to determine impact, abrasive and corrosive contributions to total media wear. The back-calculated weight factor given to impact energy was equal to 1 ( $a_{impact} = 1$ ) and the weight factor given to adhesion/abrasion energy equal to 0.1 ( $a_{ad-abr} = 0.1$ ).

#### 7.4 Procedure to model the wear of lifters

Once parameters in Equations 4.6 and 4.15 are determined, the following procedure (Figure 7.4) is followed to model the wear of industrial lifters.



**Figure 7.4** Procedure to model the wear of lifters

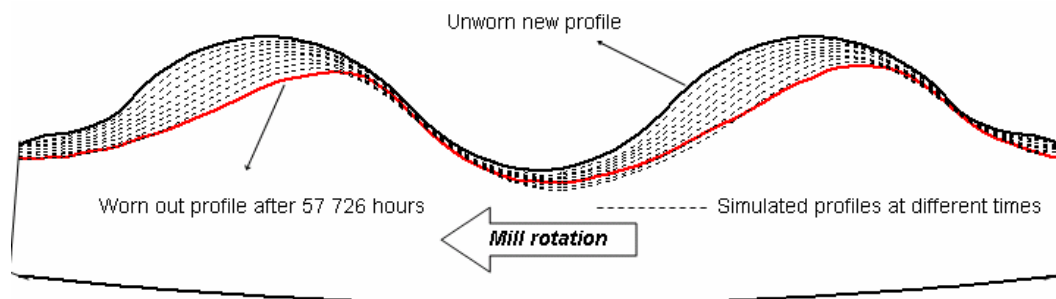
## 7.5 Modelling of the wear of tumbling mill lifters used at LETHABO power station

### 7.5.1 Introduction

Having only the unworn and the worn out lifter profiles without any intermediate stage, we used a constant wear rate and parameters in the wear model to predict the worn out profile from the unworn. By using a constant wear rate, we assume that ore, lifters and balls properties as well as the load charge were constant during the useful life of lifters.

### 7.5.2 Simulated profiles

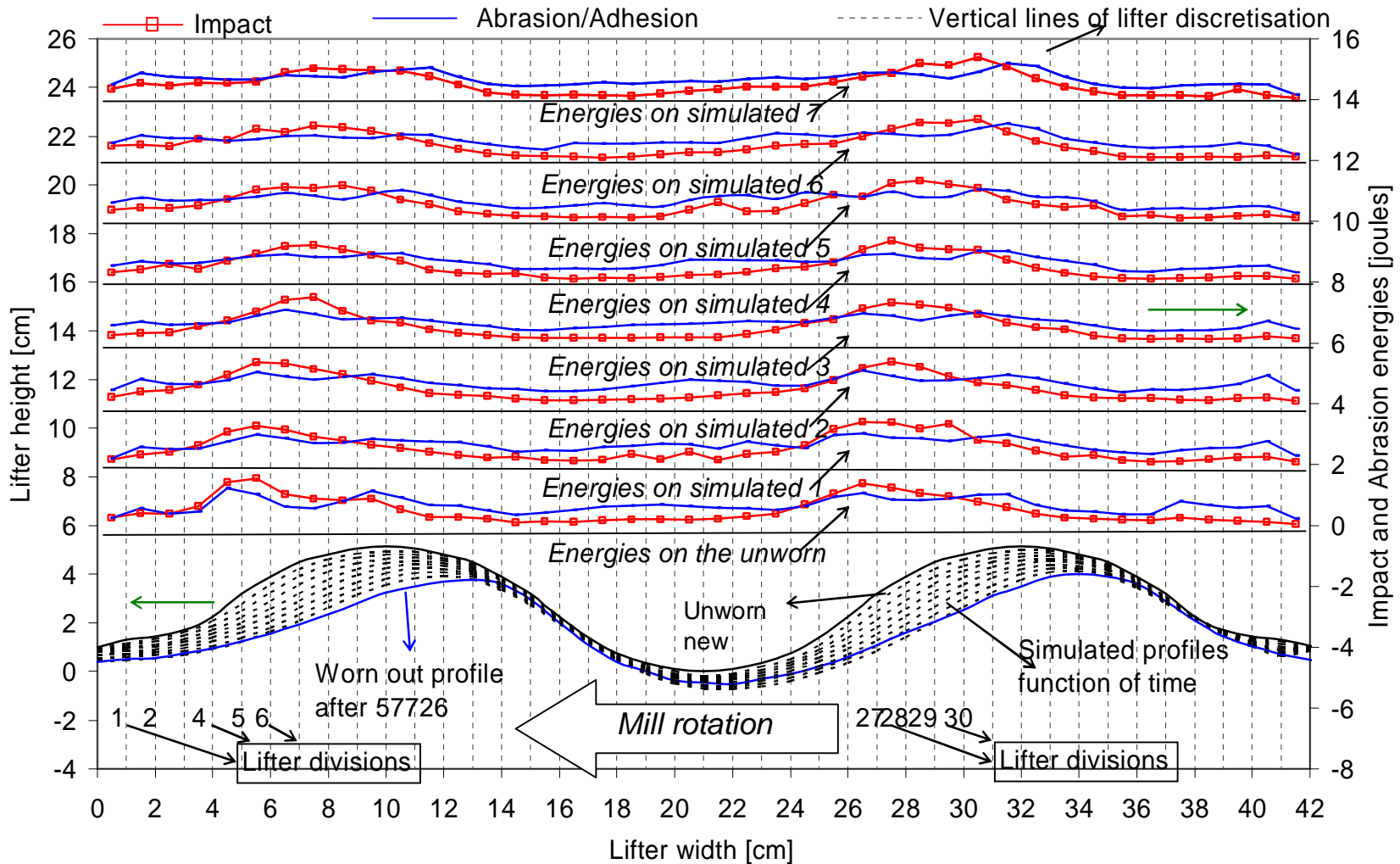
Figure 7.5 shows the DEM simulated profile results. The wear rate chosen allows reaching the worn out profile in 8 steps. The last simulated profile is in good agreement with the worn out profile measured after 57 726 hours. Appendix I provides the data at each step.



**Figure 7.5** DEM simulated evolving LETHABO double wave lifter profile

### 7.5.3 Impact and abrasion energies dissipated on discretised lifter divisions as a function of time

The lifter was vertically discretised in 42 equally spaced divisions.

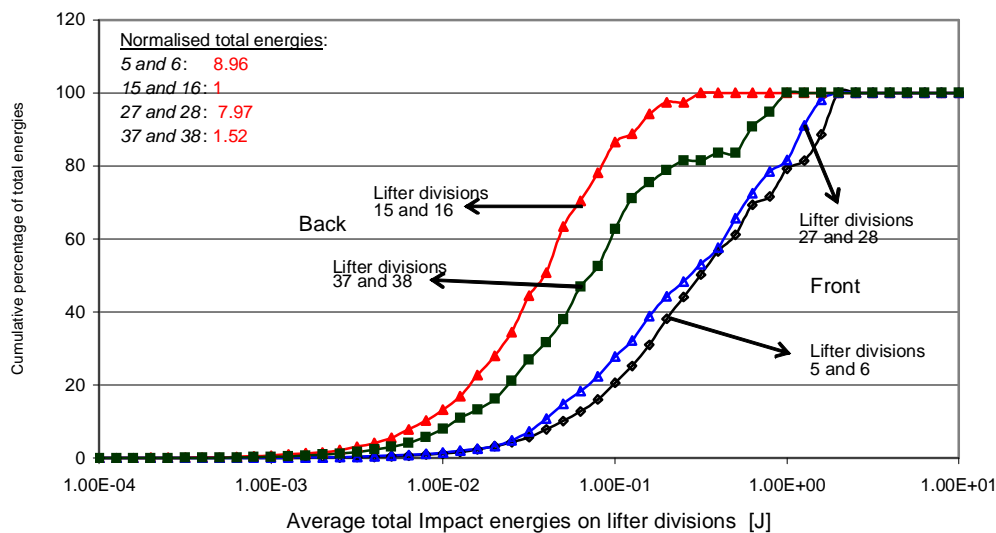


**Figure 7.6** Impact and abrasion energies dissipated on discretised lifter divisions of the double wave lifter used at Lethabo power station as a function of lifter wear

Impact and abrasion energies dissipated on the discretised lifter divisions as a function of time are represented by Figure 7.6. Lifter divisions 4 to 8 for the first lifter wave and 26 to 30 for the second lifter wave constitute the front of the unworn profile.

As the lifter profiles evolve, the front of the lifter changes. It can be seen from Figure 7.6 that impact energies are higher than the abrasion energies at the front of lifter profiles and the opposite at the back. These results are in agreement with the observation of the DEM simulated load behaviour in the mill where it can be seen that most of impacts occur at the front of lifters waves while at the back, balls are merely sliding.

A detailed comparison of impact energies dissipated on lifter discretisation surface at the frontal side of the lifter waves (5, 6 and 27, 28) and at the back (15, 16 and 37, 38) of the unworn lifter is shown by Figure 7.7. This figure shows the cumulative percentage of total energy as a function of impact energy. It can be seen from the graph that 80% of total impact energies dissipated at the front of the unworn lifter has a value of 1 Joule while the same variable for the back of the lifter is very roughly 0.1 Joules.

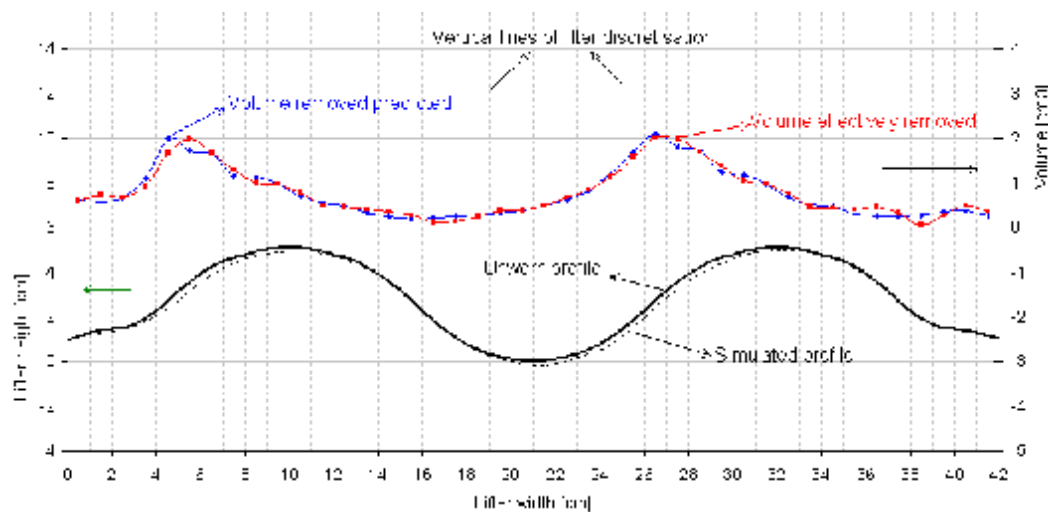


**Figure 7.7** Cumulative percentage of total energy as a function of impact energy on the discretised unworn lifter division at the front and back of lifter waves.

#### 7.5.4 Comparison between the volume removed predicted and effectively removed

The predicted volume removed on a discretised lifter division is given by equation 4.6. The volume effectively removed is slightly different from the predicted since the removal of material on lifters is operated via an objective function (Equation 4.15) in order to predict realistic profiles.

Figure 7.8 shows the difference between the volume removed predicted and the volume effectively removed on discretised lifter divisions of the unworn double wave lifter used at Lethabo power station. It can be seen from Figure 7.8 that there is a slight difference between the predicted and the effectively removed volume. Therefore, weight parameters used in the objective function were adequate since they do not violate rules motivated in Chapter 4 which stipulate that the lifter profile predicted must be a function of operating conditions in the mill and initial lifter profile. Appendix J shows the difference at each step.



**Figure 7.8** Volume removed predicted and effectively removed on discretised lifter divisions of the unworn double wave lifter used at Lethabo power station.

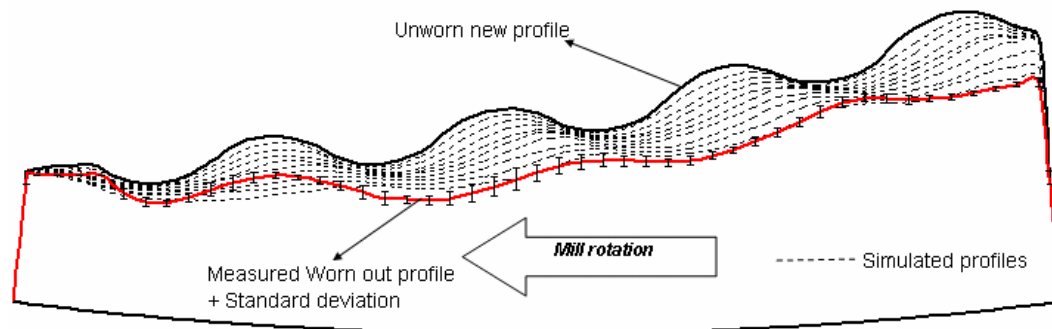


## 7.6 Modelling of the wear of tumbling mill lifters used at KENDAL power station

### 7.6.1 Simulated profiles

Only the unworn and the worn out lifter profiles without any intermediate stage were available. We therefore also used a constant wear rate and parameters in the wear model to predict the worn out profile from the unworn.

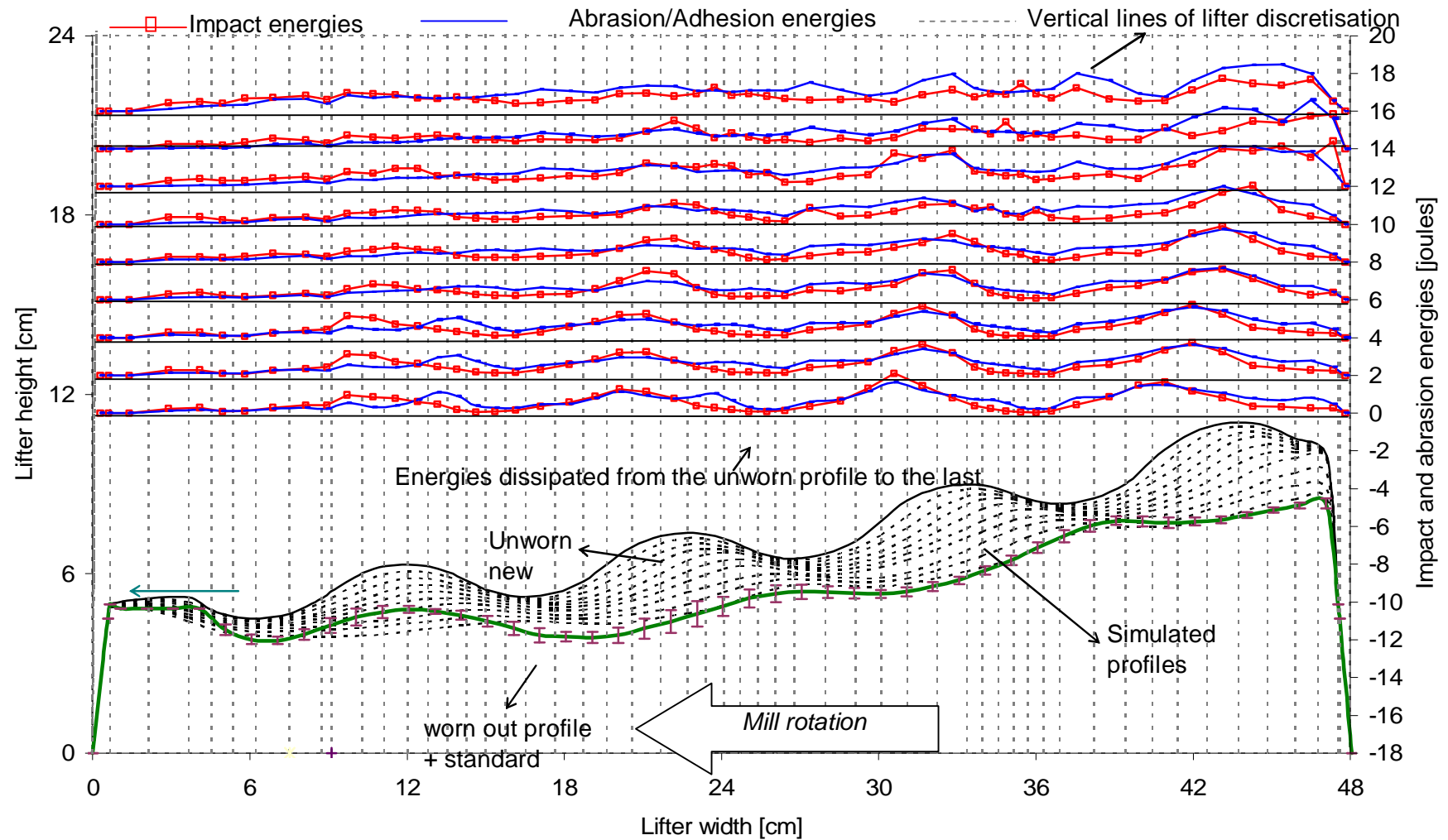
Figure 7.9 shows the DEM simulated results of the wear of the lifter used at Kendal power station. The wear rate chosen allows reaching the worn out profile in nine (9) steps. The last simulated profile is not in very good agreement with the worn out profile measured after 70900 hours at the first wave where our model predict a high wear. A good agreement is found beyond that interval. Appendix I provides the data at each step.



**Figure 7.9** DEM simulated evolving lifter profile used at KENDAL power station.

### 7.6.2 Impact and abrasion/adhesion energies as a function of time

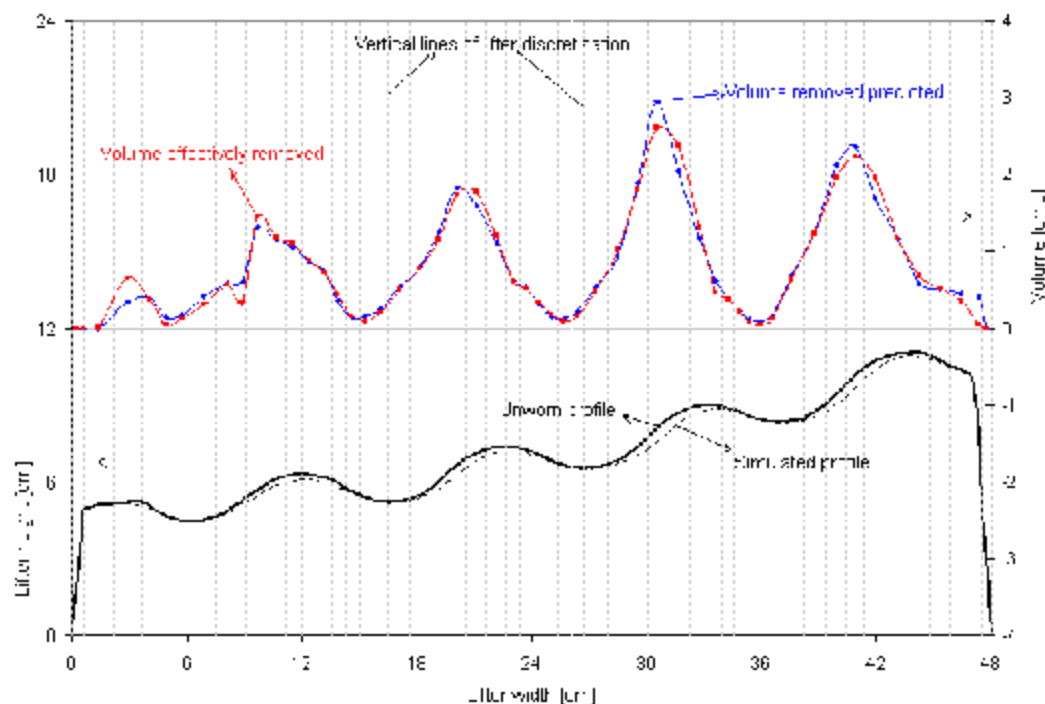
The lifter was discretised in 52 divisions. Impact and abrasion energies dissipated on discretised lifter divisions at each step are represented in Figure 7.10. It can be seen from Figure 7.10 that, like in the case of lifters used at Lethabo power station, impact energies are higher than abrasion energies on discretised lifter divisions at the front of lifter waves and the opposite at the back.



**Figure 7.10** Impact and abrasion energies dissipated on discretised lifter divisions of the lifter used at Kendal power station as a function of lifter wear

As lifters are wearing, the waves are disappearing and abrasion energies on discretised lifter divisions are increasing due to the sliding of the load charge.

Figure 7.11 shows the difference between the volume removed predicted and effectively removed on the discretised lifter division on the unworn profiles. It can also be seen from Figure 7.11 that the difference is not significant. Parameters in the objective function were therefore adequately chosen. Appendix J gives the comparison at each stage.



**Figure 7.11** Volume removed predicted and effectively removed on discretised lifter divisions of the unworn lifter used at Kendal power station

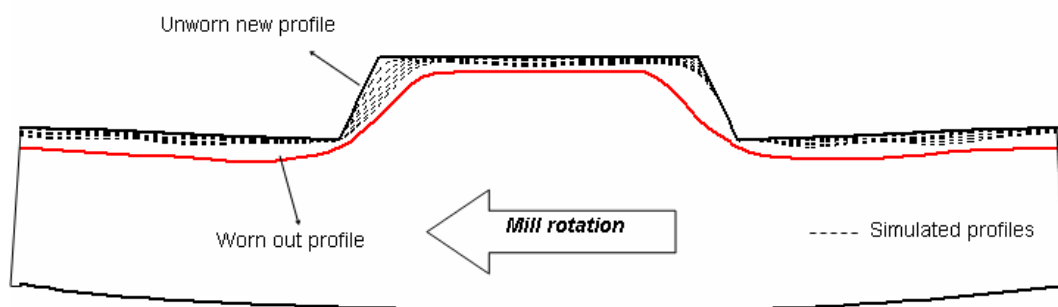
## 7.7 Modelling of the wear of tumbling mill lifters used at MATIMBA power station

### 7.7.1 Simulated profiles

Only the unworn and the worn out lifter profiles after 8 years without any intermediate stage were available. We used again a constant wear rate and parameters in the wear model to predict the worn out profile from the unworn.

Only the wear of one side of the lifter was simulated since the other side is not affected by the wear.

Figure 7.12 shows the DEM simulated results of the wear of lifter used at Matimba power station. The wear rate chosen allows reaching the worn out profile on one side in five (5) steps. It can be seen from Figure 7.12 that the wear is effected mainly on the frontal side of the lifter while the back of the lifter is less affected. This prediction is in agreement with observation at the plant. Once the lifters reach a critical profile from one side, lifters are reversed in the mill to exploit the other side. Appendix I provides the data at each step.

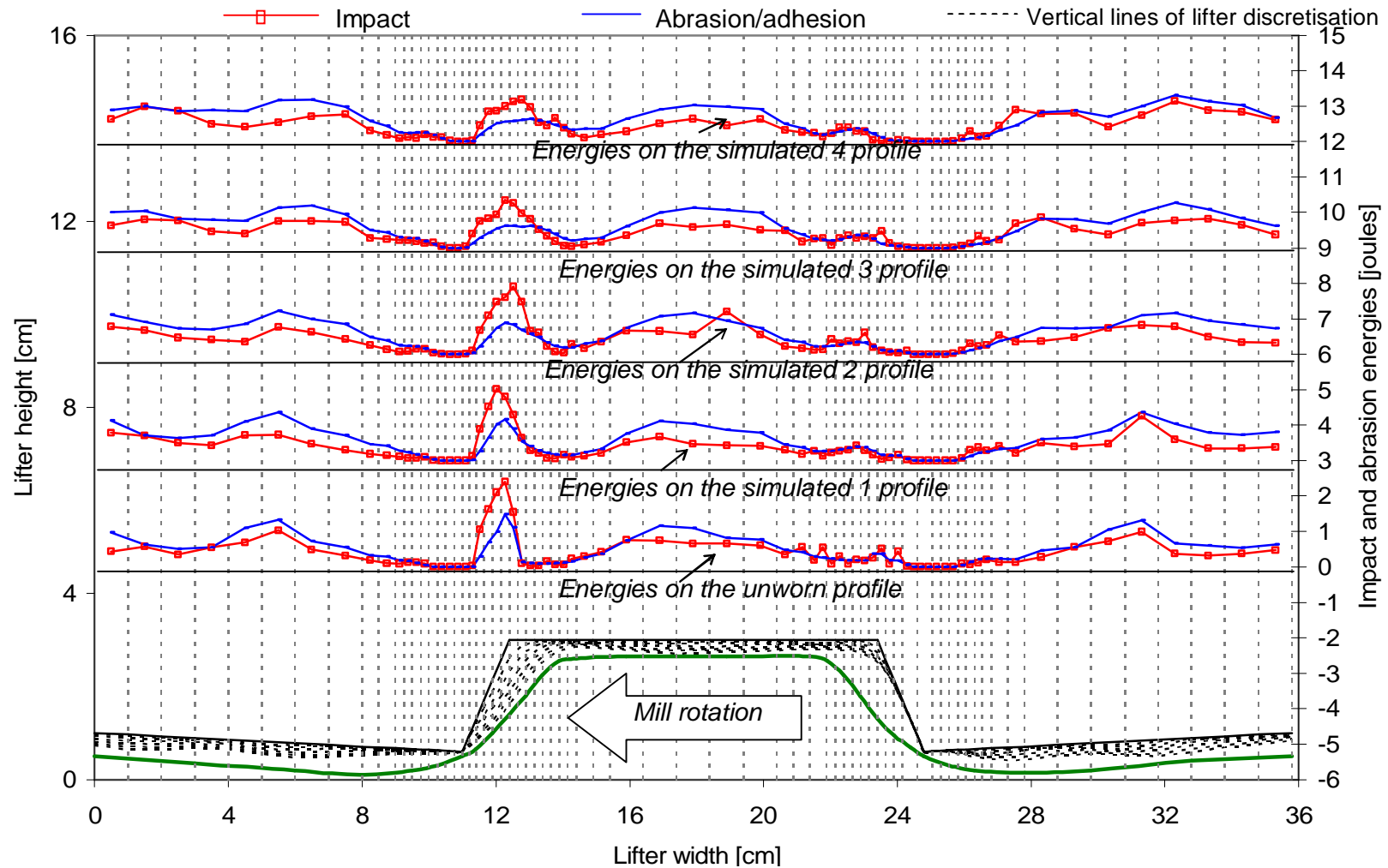


**Figure 7.12** DEM simulated evolving lifter profile used at Matimba power station

### 7.7.2 Impact and abrasion/adhesion energies as a function of time

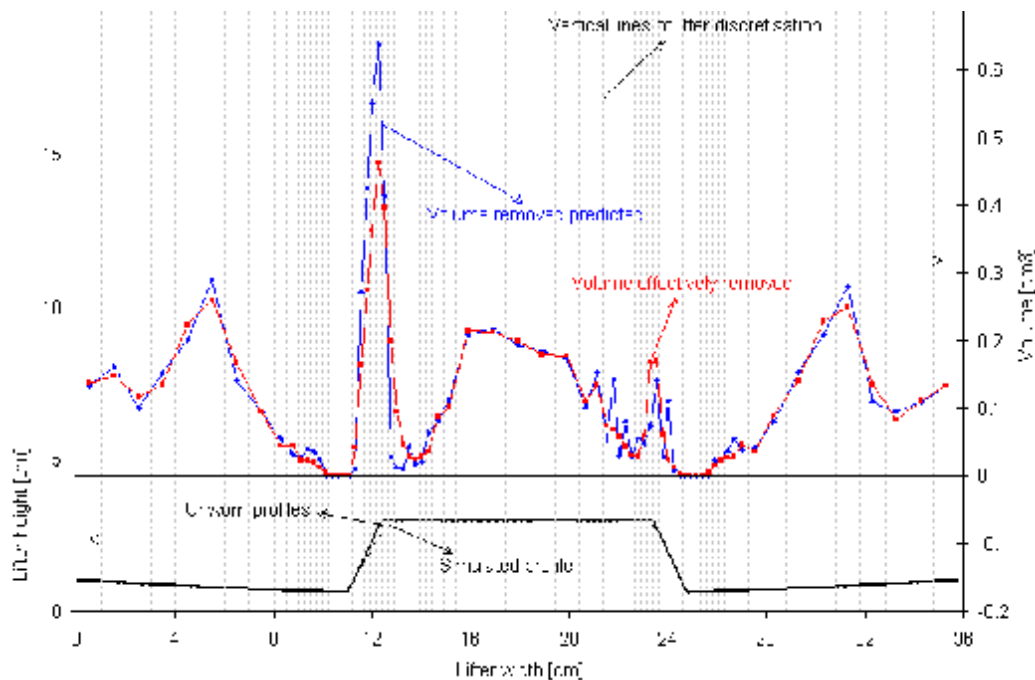
To simulate the wear, the lifter was discretised in 73 divisions. A non uniform discretisation was used. More lifter divisions were made on the frontal side of the lifter since most events and change in profile occurs at corners.

Figure 7.13 shows impact and abrasion energies dissipated on lifter discretised divisions at each step. It can be seen from Figure 7.13 that discretised lifter divisions which did not have any interaction with balls during the mill revolution have an impact and abrasion energy equal to zero. It can also be seen that while the frontal side of the lifter is affected by high energies events, the back is less affected.



**Figure 7.13** Impact and abrasion energies dissipated on discretised lifter divisions of the lifter used at Matimba power station as a function of lifter wear

Figure 7.14 shows the difference between the volume removed predicted and effectively removed on discretised lifter divisions of the unworn lifter used at Matimba power station. It can be seen From Figure 7.14 there is a difference between the volume removed predicted and effectively removed on lifter divisions close to the frontal corner of the lifter (Appendix J shows the difference at different steps). In that region, the volume removed predicted is higher than the volume effectively removed. Direct subtractions lead to unrealistic simulated profiles. The objective function via its parameter  $\alpha$  and  $\lambda$  ensure that simulated profiles are realistic. Beyond the corner region, the difference between the volumes removed predicted and effectively removed is not very significant which means that parameters were adequately chosen.

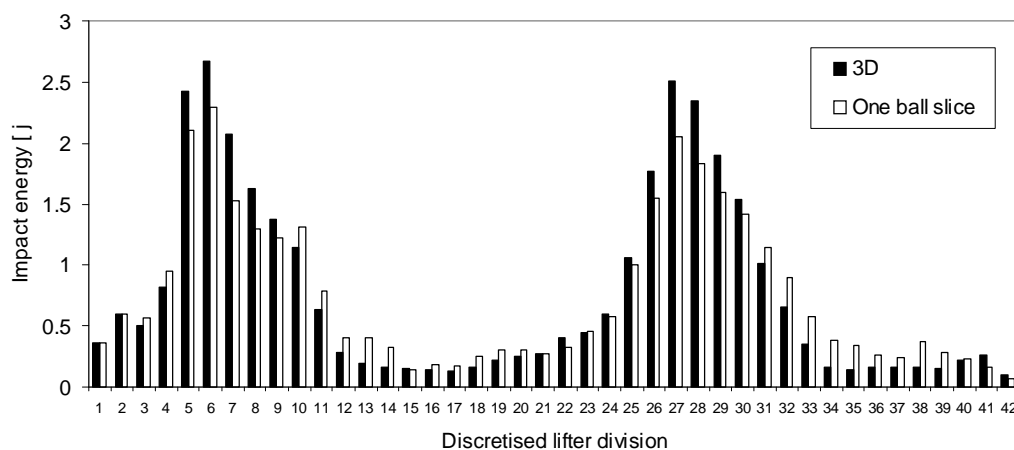


**Figure 7.14** Comparison between volume removed predicted and effectively removed on discretised lifter divisions of the unworn lifter used at Matimba power station

## 7.8 Discussions

### 7.8.1 Simulating wear of lifters using one ball slice length

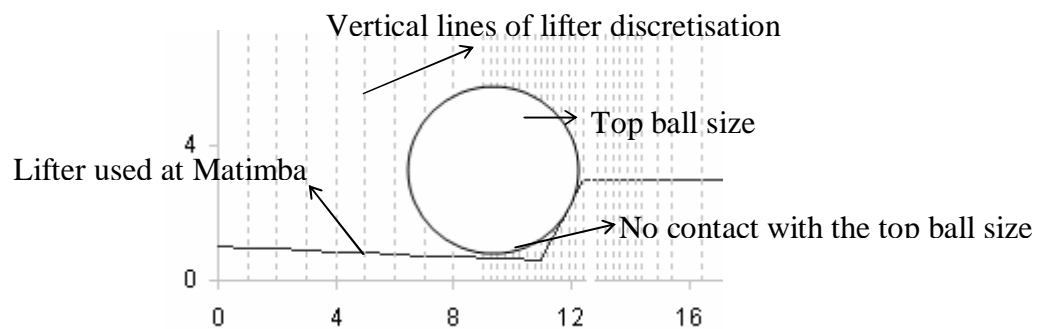
Three dimensional (3D) simulations using full ball size distribution provide better understanding of interactions occurring in tumbling mills. It is therefore expected that 3D simulations will provide better prediction than one ball slice length simulations. Actually, it is not practical to perform 3D simulations due to the time constraint. One 3D simulation was conducted using the unworn lifter equipped in tumbling mills at Lethabo power station. It took 32 days to perform a 3D simulation against 3 days for a one slice ball. The comparison between the normalised impact energy dissipated on discretised lifter division is shown in Figure 7.15. It can be seen from Figure 7.15 comparing the impact energies that the trends are similar but DEM 3D simulations predict high impact energies at the frontal side of the lifter in comparison to one slice simulations. The difference between 3D and one ball slice DEM simulation is not very dramatic. So it was assumed to be acceptable to use one ball slice simulation taking into account the time saved.



**Figure 7.15** 3D vs One ball slice normalised impact energies dissipated on discretised unworn lifter used at Lethabo power station

One the other hand, using only the top ball size to predict the impact and abrasion energies dissipated on lifter divisions cause problem for lifters having corners as

indicated in Figure 7.16. It can be seen from Figure 7.16 showing a top ball size (50mm) in contact with the Matimba lifter that some discretised lifter divisions are not in contact with the top ball size while they could have been with smaller ball size. It is therefore more accurate to use 3D simulations with full ball size range of media and particles especially for lifters having concave corners.



**Figure 7.16** Top ball size in contact with lifter used at Matimba power station

### 7.8.2 Determination of weight parameters ( $\alpha$ , $\lambda$ ) in the objective function

$\lambda$  and  $\alpha$  are respectively weight factors which decide the importance to give to the difference between neighbouring slopes of discretised simulated profiles and the difference of slope between the  $j^{\text{th}}$  and the  $(j+1)^{\text{th}}$  discretised simulated profiles.

#### Physical significance of parameters

Although lifters are discretised into small surfaces on which materials are removed according to impact and abrasion energies dissipated on them, lifters are continuous material. In reality, a high energy dissipated on one discretised lifter division will have also an impact on the neighbouring discretised lifter divisions. The weight parameter  $\lambda$  plays the role of making sure that an event on a discretised lifter division affects also its neighbouring discretised divisions. Consequently, lifters though discretised into small independent surfaces undergo wear process as one unit through the use of  $\lambda$ .

On the other hand, the wear of a tumbling mill lifter is a slow continuous process where materials are removed directly as opposed to our simulations where materials are removed after a revolution. Ideally, simulated profiles should have been calculated



each time step instead of waiting for a full revolution. Parameters  $\alpha$  and  $\lambda$  are introduced to take into account this difference.

#### Determination of parameters

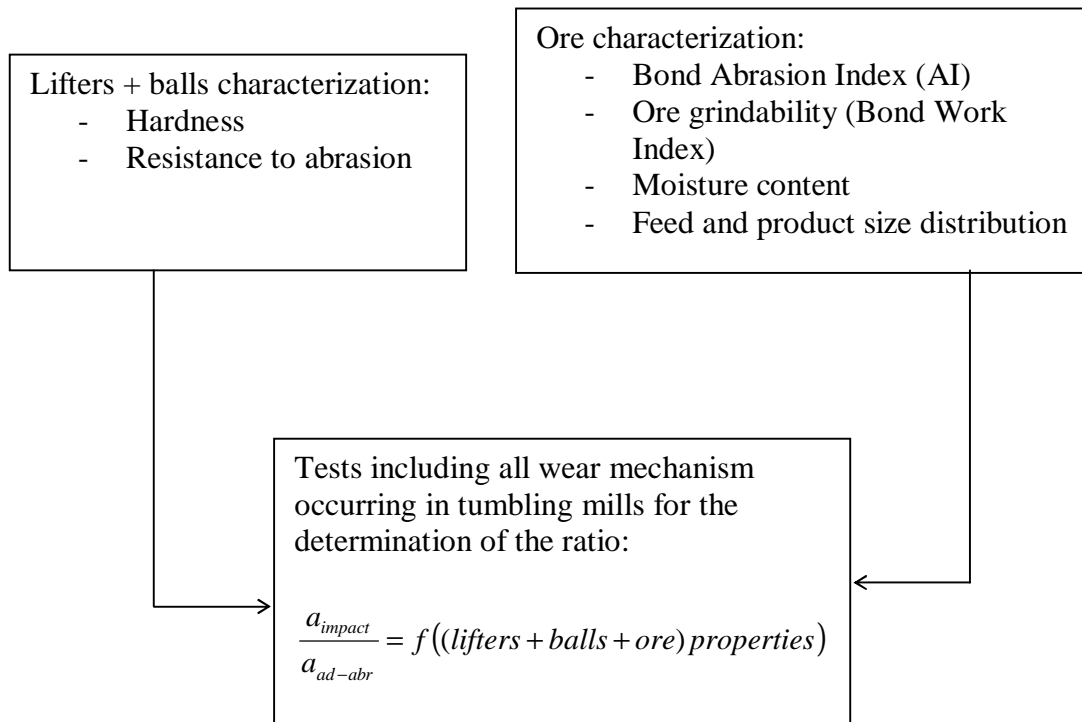
The values of parameters ( $\lambda$  and  $\alpha$ ) used in the objective function were chosen at the same time to produce realistic profiles and minimise the difference of volume removed predicted and effectively removed. It can be seen from Figures 7.5; 7.9 and 7.12 that the simulated profiles are realistic. To evaluate their ( $\lambda$  and  $\alpha$ ) contribution to the removal of material on lifters, Appendix J shows the difference between the volume removed predicted and effectively removed on discretised lifter divisions of lifter used at Lethabo, Kendal and Matimba power station. It can be seen from Appendix J that the differences are not very significant, parameters were therefore adequately chosen.

#### 7.8.3 Determination of weight parameters $a_{\text{impact}}$ and $a_{\text{abr/ad}}$

The weight factors given to impact ( $a_{\text{impact}}$ ) and abrasion ( $a_{\text{abr/ad}}$ ) energies in order to remove material on discretised lifter divisions depend on:

- Lifters and ball properties ( hardness, resistance to abrasion, sharpness)
- Ore being ground properties (Abrasion Index, size distribution, particles shape, moisture ..)

Although in our investigation they have been calculated recursively, experimental tests (Figure 7.17) including all wear mechanism (adhesive, abrasive and impact wear) with samples of lifters, balls and ore linking all above-mentioned parameters should be developed to calculate directly the ratio of  $a_{\text{impact}}$  and  $a_{\text{abr/ad}}$ . The development of such tests is beyond the scope of this thesis. Efforts are currently done by Radziszewski (2001) to isolate the contribution of each type of wear.



**Figure 7.17** Procedure to calculate the ratio ( $a_{impact} / a_{abr/ad}$ )

The test described in Figure 7.17 can involve a laboratory grinding mill operating continuously. A minimum diameter of 600 mm should be ideal to allow impact events to take place. The laboratory mill should have a variable speed drive, an accurate measurement of torque and equipped with removable lifters. To determine the ratio  $a_{impact}$  and  $a_{abr/ad}$ , a specimen of the material(s) studied having the same profile as other lifters are placed in the mill. A matrix of tests (minimum 2 tests since we have 2 parameters) can be conducted continuously by feeding ore for several hours. The matrix of tests involves changing at least one mill operating condition (speed or ball percentage filling) and ore type. The weight loss by the specimen lifter(s) can be determined for each test by the difference of weight before and after the test. DEM simulations are conducted in the same condition as tests to determine impact and abrasion energies involved in collisions. DEM parameters (coefficient of friction and coefficient of restitution) are derived to have the same power and load behaviour as predicted in experimental tests. The total impact and abrasion energies dissipated

in collisions for each test and each lifter is determined from DEM simulations. Since the mass or volume removed on discretised lifter division per lifter from each test is proportional to impact and abrasion energies dissipated on them (Equation 4.6 and 4.15), for each ore type, we can determine the ratio  $a_{\text{impact}}$  and  $a_{\text{abr/ad}}$ . The ratio obtained can be used in the prediction of lifter wear.

#### 7.8.4 Decoupling abrasion and impact energy in the prediction of wear

We assumed (Equation 4.6) that the total wear is the sum of the contribution of impactive and abrasive wear. Weight factors are given to impact and abrasion energies as a function of their contribution in the wear process.

The disadvantage of decoupling abrasion and impact energies in the wear process is the fact that synergy between these two processes which may exist is not considered. While in our case, the simple Equation 4.6 predicted successfully the wear of lifters, a more general equation can be envisaged.

#### 7.8.5 Detachment versus removal of particles in the wear process

In simulating the wear of lifters, we assumed that material removed from lifter surfaces disappear completely from the interface balls or particles and lifters. Consequently, these particles do not influence or play a role in the wear process. This assumption can be considered as valid in our study cases where the milling occurs in dry conditions and air is swept in these tumbling mills in order to remove fine particles. It has been demonstrated by many researchers (Fillot et al, 2007) that these particles detached play the role of a third body and consequently influence the wear process. These third bodies constitute a layer especially for adhesive particles and their influence depends on the rate at which they are removed from the contact.

## 7.9 Conclusions

In this chapter, our approach to modelling the wear of lifters was tested to predict the evolving lifter profiles used in industrial tumbling mills. The industrial tumbling mills chosen are equipped with different lifters and operate in dry conditions for the grinding of coal at ESKOM Lethabo, Kendal and Matimba power stations in South Africa. Only unworn (0 hour of service) and worn out lifter profiles without any intermediate stage were available. Simulations were therefore performed at constant wear rate to predict worn out profiles from unworn profiles. Discrete Element Method parameters of the simulation were derived from Moys et al (2002, 2004) work comparing the measured and DEM simulated load behaviour and power draw in these mills. Although we did not have intermediate measured profiles in order to verify the accuracy at different steps, our last DEM simulated profiles agree with worn out profiles for all the three case. Simulated profiles at each step for all lifters are realistic. Parameters used in the objective function are therefore adequate.

Our approach can therefore be used with confidence to simulate the wear of laboratory and industrial tumbling mill liners.

## Chapter 8

# DEM studies of the influence of lifter wear on the load behaviour of industrial dry tumbling mills

### **8.1 Introduction**

### **8.2 Variation of load behaviour in tumbling mills used at Lethabo power station**

#### 8.2.1 DEM simulated load behaviour

#### 8.2.2 Tangential velocities of balls as a function of lifters wear

### **8.3 Variation of load behaviour in tumbling mills used at Kendal power station**

#### 8.3.1 Introduction

#### 8.3.2 DEM simulated load behaviour

#### 8.3.3 Impact energy spectra

### **8.4 Variation of load behaviour in tumbling mills used at Matimba power station**

### **8.5 Applications**

#### 8.5.1 DEM contribution to the prediction of ball wear

#### 8.5.2 Design of lifter profiles

#### 8.5.3 Determination of lifter replacement time

#### 8.5.4 Determination of lifter replacement type

### **8.6 Conclusions**

## 8.1 Introduction

The ability to predict the wear of lifters using the Discrete Element Method (DEM) as demonstrated in Chapters 6 and 7 can only be of great interest or economic significance if it can help:

- to improve the understanding of the grinding process as a function of lifter wear,
- a lifter designer to produce or choose from a set of lifters an optimal initial profile which optimises mill performances over the entire lifter life,
- to evaluate lifters replacement time and type,
- to explore modifications which can be performed on mill operating conditions or lifters in order to extend useful life of lifters.

In this Chapter, the variation of load behaviour of industrial tumbling mills used at Lethabo, Kendal and Matimba power stations described in Chapter 7 is studied. Modifications in order to extend the useful life of these lifters are also explored.

To reduce the amount of simulations time, DEM simulations were performed using one ball slice (top ball size) instead of using 3D simulations with full size range of balls.

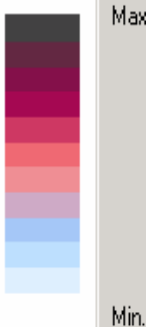
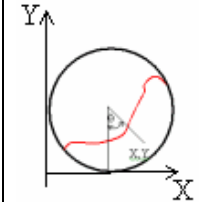
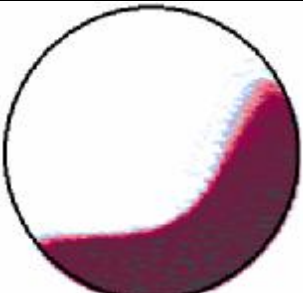
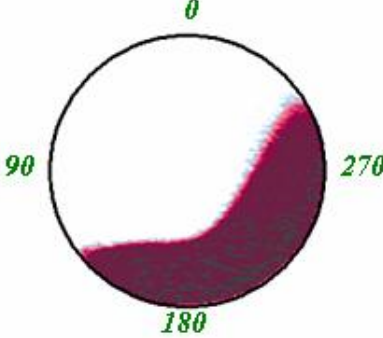


## 8.2 Variation of load behaviour in tumbling mills used at Lethabo power station

### 8.2.1 DEM simulated load behaviour

Tumbling mills used at ESKOM Lethabo power station are equipped with double wave lifters described in Chapter 7. Contour plot of DEM position density plot of load behaviour associated to the unworn, the third simulated, the fourth simulated and the worn out profile are represented in Table 8.1. The characteristics of the load behaviour are also represented in the same table.

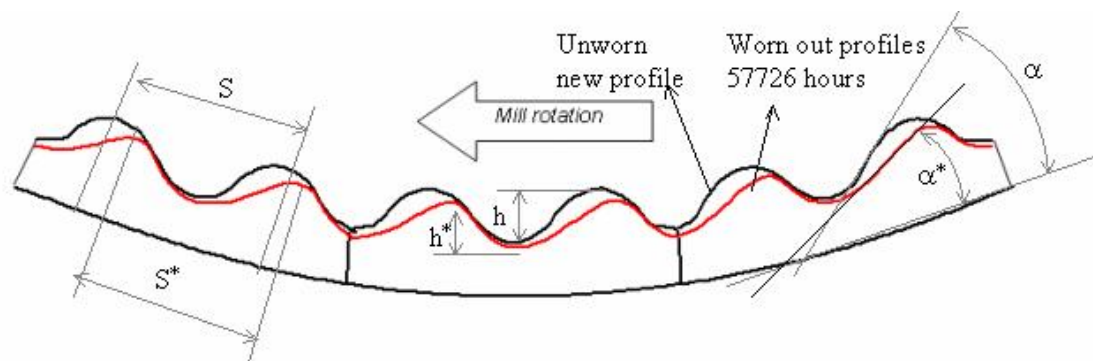
It can be seen from the contour plot of the position density plot in Table 8.1 that not much difference is observed on the load behaviour as lifters wear. The unworn lifter produces slightly more cataracting particles. The shoulder and toe position are also very similar as indicated in Table 8.1. Standard deviations of 3 and 5 degrees were found respectively at the shoulder and toe. The relative power draw and angle  $\theta$  are also very similar.

**Table 8.1** DEM Variation of the load behaviour as a function of lifters wear in tumbling mills used at Lethabo power station

Lifter profiles		0 degree=12 O'clock position, mill rotation = Anticlockwise			$X_o = \frac{\sum_{i=1}^n x_i}{n}$ $Y_o = \frac{\sum_{i=1}^n y_i}{n}$
		Shoulder (Degrees)	Toe (Degrees)	Angle $\theta$ (Degrees)	Relative power
Unworn new profile		303	128	34.68	1
Worn 3 <sup>rd</sup> simulated profile		300	129	34.46	0.994
Worn 4 <sup>th</sup> simulated profile		302	128	34.78	1
Worn out profile (8 <sup>th</sup> profile)		298	131	34.25	0.98

The DEM simulated results are validated by observation at the plant where it is observed that the throughput remains almost constant as lifters wear. In this case, lifters are replaced in the mill because they reach a critical thickness susceptible to breakage.

A close look on the double wave lifter used at Lethabo power station indicates that as lifters are evolving due to wear, the spacing ( $S$ ) remains almost constant while the height ( $h$ ) decreases as shown in Figure 8.1. Table 8.2 shows the variation of the lifter angle and the ratio  $S/h$  as a function of lifter age. The ratio of lifter spacing to height varies from 4.27 to 4.78. Bigg, A.C.T. and Raabe, H. (1996), studying the variation of the ratio  $S/h$  for SAG mills reported an optimal value around 4.5. The angle  $\alpha$  decreases while the ratio ( $S/h$ ) increases.



**Figure 8.1** Moving lifter waves as lifters wear in a mill used at Lethabo power station

**Table 8.2** Variation of lifter angle and ratio spacing: height as a function of lifter wear for the double wave lifter used at Lethabo power station

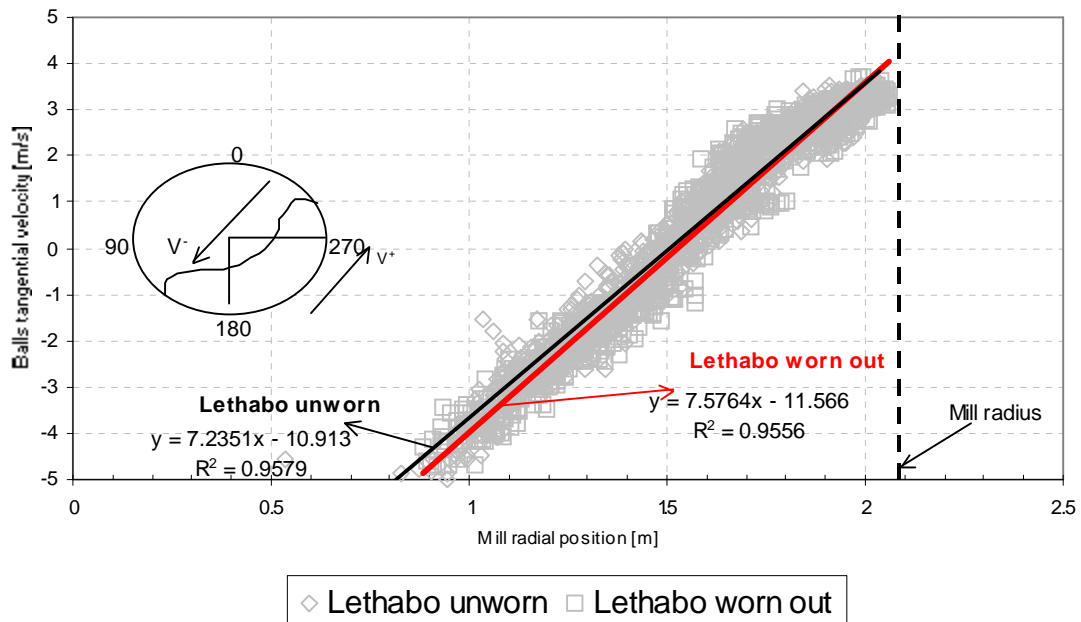
Lifter age [hours]	Lifter angle $\alpha$ [ Degrees]	Double wave liner		
		Spacing (S) [mm]	Height (h) [mm]	Ratio (S/h)
0 (unworn)	43.53	220	51.5	4.27
21647 (estimated)	37.06	220	49	4.49
28863 (estimated)	34.50	215	47.5	4.53
57726	25.98	215	45	4.78



### 8.2.2 Tangential velocities of balls as a function of lifter wear

This study was performed to compare the dynamic behaviour of balls as a function of lifters wear. Figure 8.2 shows the DEM simulated variation of tangential velocities of balls as a function of their respective radial position in the mill for the unworn and the worn out lifter profiles. The study was performed in the region between 180 and 270 degrees as indicated in the figure. The balls' tangential velocities are positive for ascending balls and negative for descending balls in the mill. It was found in both case that the relationship between the tangential velocity of balls and their radial position could be approximate with reasonable accuracy ( $R^2 > 0.95$ ) using a linear trend. Morrel (1993) in his study of the load behaviour in wet conditions found also that there was a linear trend between the tangential velocity of balls and their respective mill radial position.

It can be seen from Figure 8.2 that worn and unworn trends are very similar. The dynamic behaviour of balls is therefore very similar as lifters are wearing in the mill, which explain the constancy of mill throughput through lifters' useful life.



**Figure 8.2** Tangential velocities of balls as a function of their respective radial position at different lifter age in the mill used at Lethabo power station

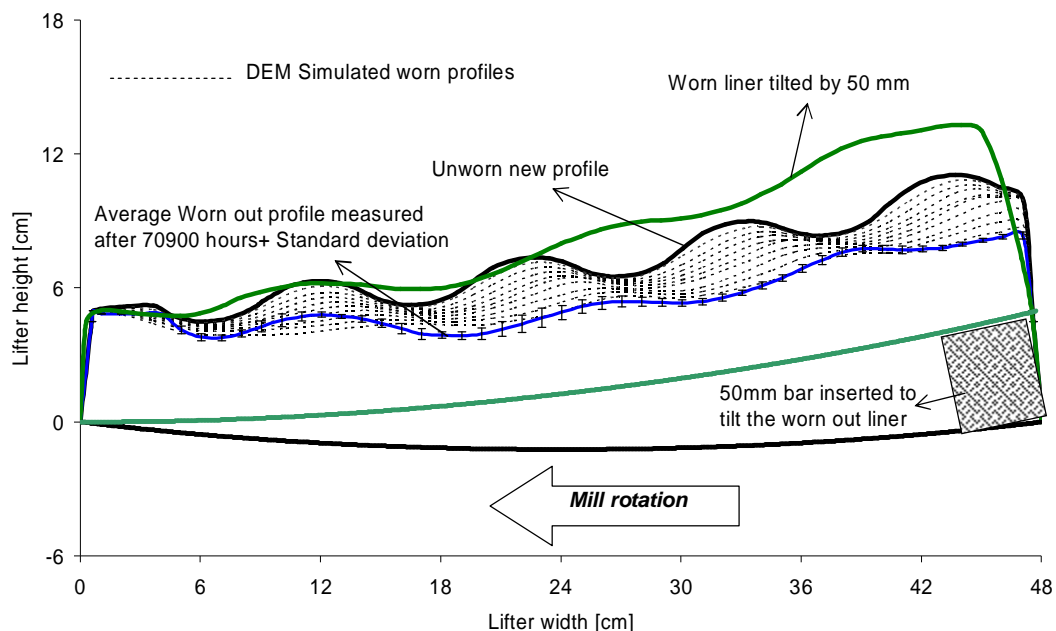
### 8.3 Variation of load behaviour in tumbling mills used at Kendal power station

#### 8.3.1 Introduction

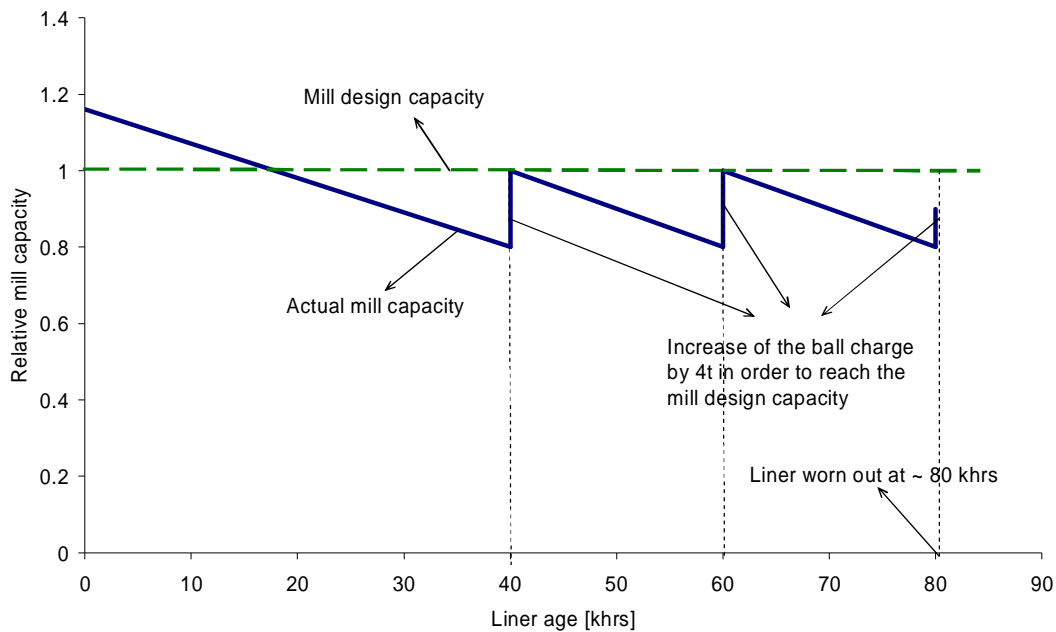
Tumbling mills used at Eskom Kendal power station are equipped with unworn lifters represented in Figure 8.3. DEM prediction of the wear of these lifters was discussed in the last Chapter. Results are also shown in the same figure where it can be seen that the last (9<sup>th</sup>) simulated profile is in good agreement with the measured profile after 70 900 hours. As lifters wear, it is observed at the plant that the mill throughput or capacity decreases as indicated in Figure 8.4. The ball charge is increased at 40, 60 and 80 khrs in order to reach the mill design capacity. Usually after 80 khrs, the mill cannot produce the minimum required capacity and lifters are replaced in the mill.

In order to extend the useful life of these lifters beyond 80 khrs and restore at the same time the mill throughput, modifications were performed at the plant on worn out lifter profiles. These modifications consist of inserting bars of 50mm height at the back of worn out lifters as indicated in Figure 8.3.

The unworn new lifter has a maximum height of 110mm and the worn out lifter a maximum height of 80mm. Tilting the worn out lifter by 50mm provides a new lifter with a maximum height of 130mm as indicated in Figure 8.3.



**Figure 8.3** Evolving lifter profile used at Kendal power station and modifications performed

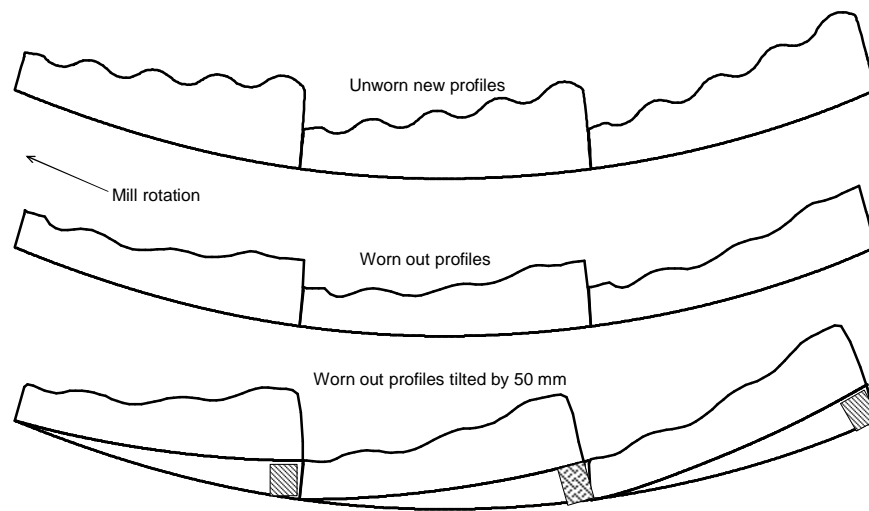


**Figure 8.4** Relative mill capacity as a function of lifter age

Tilting the worn out lifters by 30 mm instead of 50 mm would have been sufficient to provide a new lifter profile having the same height as the unworn new lifter. However, in order to fit consecutive lifters around the circumference of the mill shell, tilting the worn lifters by 30 mm was a high cost option since it requires cutting lifters in order to fit them. By tilting by 50 mm, there is no need to cut lifters since 50mm correspond to the height of the frontal side of the lifter. Lifters are therefore almost sitting on top of each other around the circumference of the mill shell as indicated by Figure 8.5.

It was observed at the plant that, after tilting the worn out lifters in the mill by 50 mm, the mill throughput was restored. However the ball wear rate was increased and the operation became prohibitively costly due to the increase in the running cost.

DEM simulations were conducted: i) in order to improve our understanding on the variation of the load behaviour as a function of lifter wear and lifter modifications, ii) to find the reason of the increase of the ball wear rate following the tilting of the worn out profiles and iii) to evaluate mill performances beyond modifications performed.



**Figure 8.5** Lifters in the mill used at Kendal power station

### 8.3.2 DEM simulated load behaviour

DEM simulated contour plot of the position density plot of the load behaviour corresponding to the unworn, the 4<sup>th</sup> simulated, the worn out and the 50 mm tilted lifter profiles are represented in Table 8.3. The characteristics of the load behaviour are also represented in the same table.

It can be seen from Table 8.3 that as lifters are wearing the shoulder position is decreasing in the mill. Since the mill is running at the same speed and filling, the diminution of the shoulder position can be explained by the sliding of the load charge. The shoulder position decreases from the unworn new profile at a position of 294 degrees to the worn out profile at a position of 284 degrees. The position of the centre of circulation (angle  $\theta$ ) decreases also as lifters wear, consequently, the power draw decreases also as lifters wear.

Once the worn out lifter is tilted by 50 mm, the load charge inside the mill is lifted. The shoulder position increases from 284 to 291 degrees. Standard deviations were 4 and 6 degrees respectively for the shoulder and toe.

**Table 8.3** DEM Variation of the load behaviour as a function of lifter wear in tumbling mills used at Kendal power station

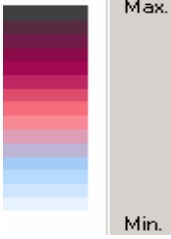
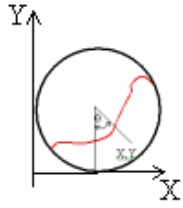

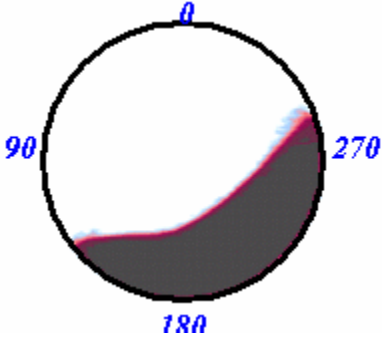
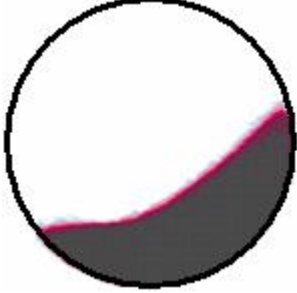
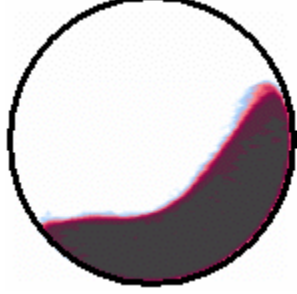
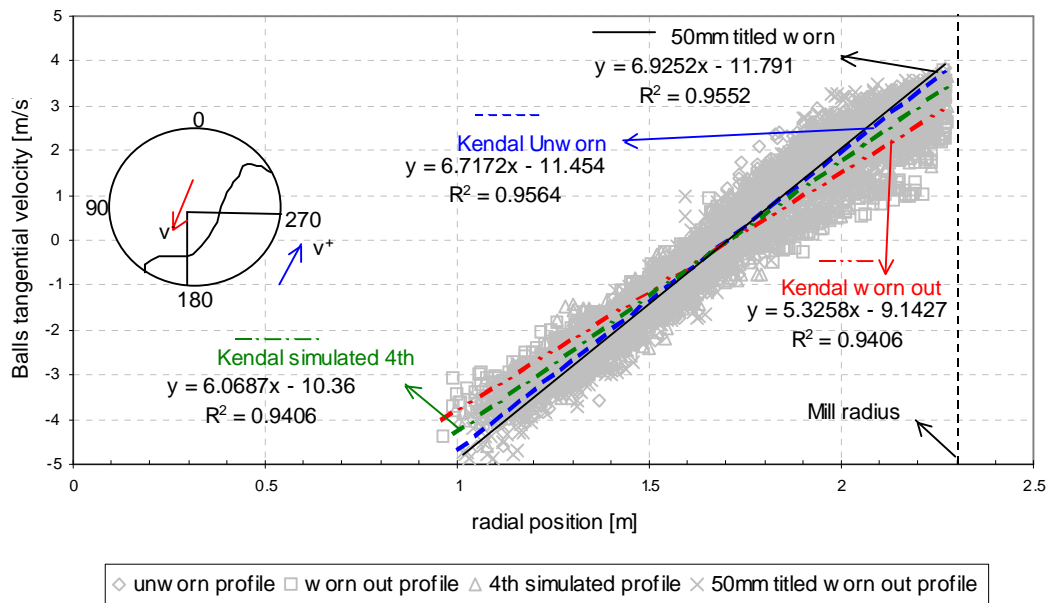
Lifter profiles		0 degree=12 O'clock position, mill rotation = Anticlockwise			$X_o = \frac{\sum_{i=1}^n x_i}{n}$ $Y_o = \frac{\sum_{i=1}^n y_i}{n}$
		Shoulder (Degrees)	Toe (Degrees)	Angle $\theta$ ( Degrees)	Relative power
Unworn new profile		294	123	31.51	1
Worn 4 <sup>th</sup> simulate d profile		290	127	29.17	0.963
Worn out profile		284	130	29.12	0.922
Worn out profile tilted by 50mm		291	126	32.01	1.033

Figure 8.6 shows the load tangential velocities of balls as a function of their respective mill radial position for the load behaviour associated to the unworn, the 4<sup>th</sup> simulated, the worn out and the 50mm tilted worn out profile. The balls tangential velocities are positive for ascending balls and negative for descending balls in the mill. It was also found in all cases that the relationship between the tangential velocities of balls and their respective radial position could be approximate with reasonable accuracy ( $R^2 > 0.94$ ) using a linear trend.

The transfer of energy from the mill lifters to the load charge is influenced by lifter profiles. It can be seen from Figure 8.6, that as lifters wear, the tangential velocity of balls decreases due to the sliding of the charge. Energy transmission from the mill shell to the mill charge decreases therefore as lifters wear. Tilting the worn out lifters eliminates the sliding effect as shown by Figure 8.6 where it can be seen that the tangential velocities of balls at the mill shell increase to a value slightly higher in comparison to the unworn.



**Figure 8.6** Tangential velocities of balls as a function of their respective radial position at different lifter age in the Kendal mill

Table 8.4 shows the relationship between tangential velocities of balls in the mill at different liner profile age. The first observation is that, equations of tangential velocity of balls as a function of their respective radial position at different liner age can be represented by the linear equation  $y = k(ax - b)$  with  $k$  a constant. The value of  $k$ , with  $k=1$  for the unworn liner, gives an indication of the transmission of energy from the mill shell to the mill charge.

**Table 8.4** Equations of tangential velocities of balls as a function of their respective radial position at different lifter age

Lifter profile	Equations of balls tangential velocities (y) as a function of their respective radial position (x)	Relation between tangential velocities of balls in the mill at different liner age
Unworn (0 hour of service)	$y_o = 6.7172x - 11.454$ $R^2 = 0.9564$	$y_o = y_o$
4 <sup>th</sup> simulated	$y_1 = 6.0687x - 10.36$ $R^2 = 0.9406$	$y_1 = 0.904y_o$
Worn out	$y_2 = 5.3258x - 9.1427$ $R^2 = 0.9406$	$y_2 = 0.795y_o$
Worn out tilted by 50mm	$y_3 = 6.9252x - 11.791$ $R^2 = 0.9552$	$y_3 = 1.03y_o$

### 8.3.3 Impact energy spectra

Tumbling mill impact energies dissipated in collisions between balls and between balls and lifters and their distribution are valuable information in estimating grinding efficiency. Tumbling mills are efficient when most impacts that occur in the mill are in an energy range that can break ore particles and they occur in regions where the probability of finding the ore is very high (Agrawala, S. et al, 1997).

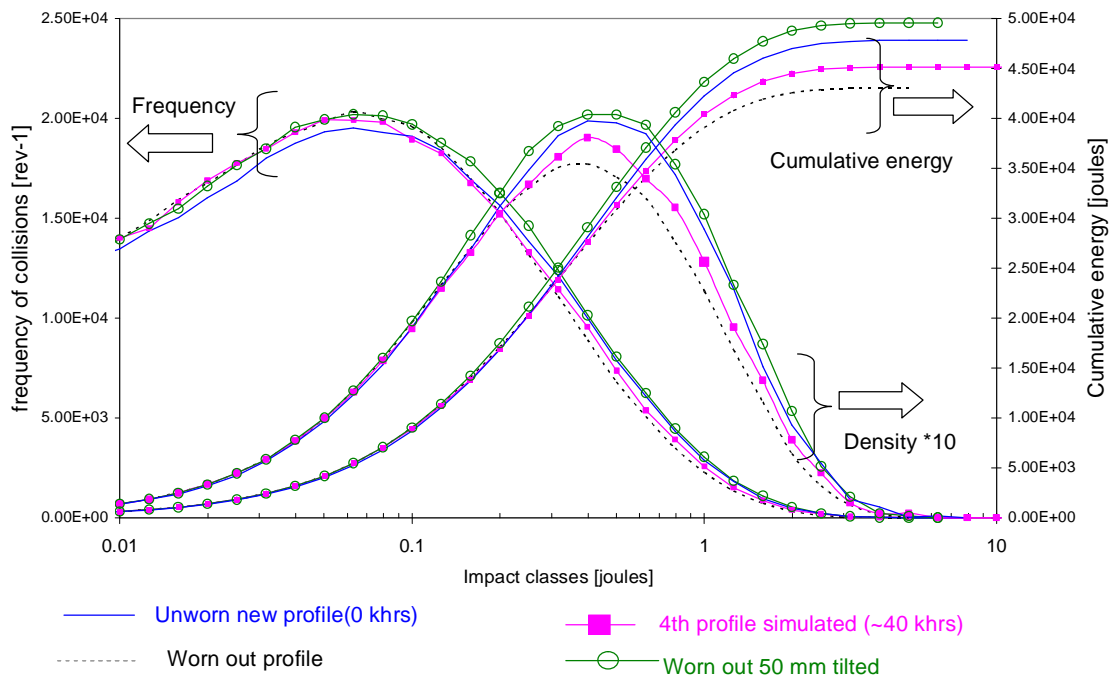
Very high impact energy should be avoided because not only energy is wasted in collisions but also they are more responsible of the wear of grinding media and lifters.

Figure 8.7 represents the impact energy spectra of the Kendal mill as a function of lifter wear and for the 50 mm tilted worn out profile. The frequency of collisions at an impact energy  $I_i$  is represented by  $f_i$ . The density of impact energy  $d_i$  is the product of the frequency of collisions and the impact energy intensity or  $d_i = f_i I_i$ . The

cumulative energy is defined as  $E_i = \sum_{i=1}^n f_i I_i$ .

It can be seen from Figure 8.7 that starting from the unworn lifter profile, as lifters wear, the total cumulative energy dissipated in collisions between balls and between balls and lifters decreases. There is therefore less total energy available in the mill as lifters wear. Densities of impact energy were also incorporated in Figure 8.7 in order to investigate in more detailed the variation of impact energy classes as a function of lifter wear and lifter modifications. The density of impact energies reveals that as lifters wear: i) there is a decrease in the frequency of high impact ( $> 0.25$  Joules) energy events. ii) there is an increase in low impact energy events. These observations justify the increase of the ball charge in the mill as lifters wear to reach the mill design capacity. Increasing the ball charge in the mill as lifters wear, increases the total energy available and allows reaching the mill design capacity. After 80khrs, due to sliding occurring in the mill, lifters reach a point where increasing the ball charge is not enough to reach the mill design capacity. Once worn out lifters are tilted by 50mm, the cumulative energy dissipated increases to a value higher than for the unworn profile. The density of impact energies shows that in comparison to the load behaviour associated to the unworn lifter there is an increase in higher impact energy events when the worn out liner is tilted by 50mm.





**Figure 8.7** Impact energy spectra as a function of lifters wear and modifications in the Kendal Mill

Table 8.5 represents the variation of the ball to ball and ball to liners total impact and frictional energy dissipated in collisions between balls and between balls and liners relative to the new liner. It can be seen that the total impact energy dissipated in the mill (ball to ball and ball to liners) decreases as liners wear but the frictional energy dissipated (ball to ball and ball to liners) increases. The cumulated total impact energy dissipated decreases due to a reduction in high impact energy events while the frictional energy dissipated in the mill increases mainly due to the slippage of the charge that is observed from DEM simulations in the mill as liners wear. The increase in high impact energy events when the liner is tilted and the increase in frictional energy dissipated justifies to some extent the increase of ball wear rate observed at the plant.

**Table 8.5** Variation of relative total cumulated impact and frictional energy dissipated by the ball charge as a function of lifter wear

Lifter profile used at Kendal	Relative impact energy dissipated		Relative frictional energy dissipated	
	Ball- Ball	Ball – Lifter	Ball – Ball	Ball – Lifter
Unworn	1	1	1	1
Simulated 4 <sup>th</sup> profile	0.966	0.941	1.010	1.011
Worn out profile	0.894	0.875	1.133	1.215
50 mm tilted worn out profile	1.040	1.031	1.143	1.247

The action of tilting the worn out lifters by 50 mm reduces the effective volume of the mill. Therefore, for the same mass of balls in the mill, when lifters are tilted, there is an increase in the mill percentage of filling (J). To reduce the ball wear rate, the ball charge was decrease to maintain the same percentage of filling.

To evaluate mill performances beyond 80 000 hours after tilting the worn out lifters, simulations were conducted to model the wear of tilted lifters and analyse their associated load behaviours. Appendix K shows the predicted lifter profiles beyond the 50 mm tilted worn out profile and the load behaviour associated. It is expected that the mill performance will not going to change dramatically till 140 000 hours. The lifter thickness may be the limiting factor to extend the lifter useful life since the DEM simulated variation of the load behaviour is not very significant beyond tilting the worn out lifter by 50mm as indicated in Appendix K.




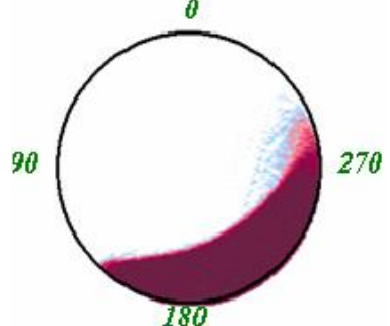


#### **8.4 Variation of load behaviour in tumbling mills used at Matimba power station**

DEM simulated contour plot of the position density plot of the load behaviour in tumbling mills used at Matimba power station are represented in Table 8.6. It can be seen from Table 8.6 that there is a remarkable change in terms of load behaviour as lifters wear. The amount of cataracting balls in the mill decreases as lifters wear. The shoulder angle decreases from 315 degrees for the unworn lifter to 298 for the worn out lifter. The toe angle is less affected by the wear of lifters. The angle  $\theta$  decreases also as lifters wear. Standard deviations were 3 and 6 degrees respectively for the shoulder and toe.

In comparison to the DEM simulated load behaviour of the Lethabo (Table 8.1) and Kendal (Table 8.3) tumbling mills, in this case, the amount of cataracting particles is higher due to the aggressiveness of the lifter used at Matimba power station (unworn lifter front angle Lethabo= 43.53 degrees, Kendal=39 degrees, Matimba= 60 degrees). The Matimba worn out lifter still produce cataracting balls in the mill in comparison to worn out lifter profiles used at Lethabo and Kendal but it is nevertheless replaced. This observation suggests that the transport of coal in these mills is different (See the difference in the design of these mills in Appendix G).

To explore ways of extending the useful life of lifters used at Matimba power station and restore the load behaviour at the same time, DEM simulations were conducted by increasing the mill speed when lifters are worn out. Technically this is equivalent to equip these mills with variable speed drive. It was found that the tangential velocity of balls at the mill shell decreases from the unworn profile to the worn out profile by 6.5%. The mill speed was increased by the same proportion from 15.5 to 16.51 rpm and the results are also presented in Table 8.6. It can be seen from Table 8.6 that the load behaviour is restored.

**Table 8.6** DEM Variation of the load behaviour as a function of lifter wear in tumbling mills used at Matimba power station

Lifter profiles		0 degree=12 O'clock position, mill rotation = Anticlockwise			$X_o = \frac{\sum_{i=1}^n x_i}{n}$ $Y_o = \frac{\sum_{i=1}^n y_i}{n}$
		Shoulder (Degrees)	Toe (Degrees)	Angle $\theta$ (Degrees)	Relative power
Unworn new profile		315	131	32.52	1
Worn 3 <sup>rd</sup> simulated profile		306	131	30.09	0.963
Worn out profile		298	132	29.73	0.950
Worn out profile Mill speed increased by 6.5%		310	135	31.07	1.020

## 8.5 Applications

### 8.5.1 DEM contribution to the prediction of ball wear

In dry milling, balls (as well as lifters) wear due to abrasion and impact energies dissipated in collisions between balls (particles) and between balls (particles) and lifters. Since the DEM can predict those energies as a function of operating conditions and for different ball sizes, it can therefore be used to predict the wear of balls. Study performed in this Chapter for the mill used at Kendal power station is an example. The impact energy spectra derived and the frictional energy dissipated in the mill for different ball sizes can be used to predict the wear of balls. Appendix L shows the DEM simulated results of impact and abrasion energies dissipated in a mill of 600 mm of diameter filled at 30% with different ball size ranging from 10 to 40 mm. The results found show the potential that has the DEM to predict more accurately the wear of balls than using Bond's empirical equations.

Based on tests from different ores and milling conditions, Radziszewski (2002) shows that, predictions of ball wear using the widely accepted Bond equation (See Appendix L) have an average error of 73% with a standard deviation of 192.5%. The difference observed can be explained by the fact that the main mechanism of ball charge wear in Bond's tests is abrasion. The augmentation in mill diameter worldwide makes the contribution of impact wear very significant. The DEM can therefore be used to predict more precisely the wear of balls since interactions are more accurately simulated.

### 8.5.2 Design of lifter profiles

The best lifter profile for a particular operation combines a good lifter life and a high throughput over the lifter useful life (Powell, 2004). Initially lifter profiles were designed on the basis of trial - error and experience of lifter manufacturer. If studying the mill load behaviour using the DEM helps to determine if a particular lifter profile is suitable, simulating the evolving lifter profile allows determining an initial lifter profile, which optimises the mill performance over the useful lifter life.

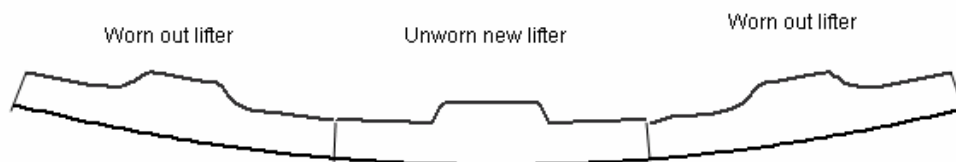
### 8.5.3 Determination of lifter replacement time

When the milling performance drop as tumbling mill lifters wear, the lifter replacement time is an economical point where the cost due to the lost of production caused by the wear of lifter is higher than the cost of relining (Meekel, 1996). The time of lifter replacement can also be associated to a particular load behaviour in the mill determine by the worn out profile. This particular load behaviour can be called “the critical mill load behaviour” as it does correspond to the limit of profitability. In simulating the evolving lifter profiles due to wear, we record the mill load behaviour for each simulated lifter profile. It is consequently possible to detect the load behaviour corresponding to the critical mill load behaviour and estimate the time required to reach the critical load behaviour.

### 8.5.4 Determination of lifter replacement type

Two types of lifter replacement are typically used in milling plants: the total lifter replacement and the pattern lifter replacement (Parks, J.L., 1996). The total replacement consists of replacing all lifters at once while the pattern replacement consists of lifters replacement in a sequence. Each method of replacement has its advantage and disadvantage. The ability to simulate evolving lifter profiles due to wear can be used to find the optimal type of lifter replacement.

Since lifters used at Matimba power station are losing less than 10% of their volume during their useful life, a pattern replacement can be explored as indicated by Figure 8.8.



**Figure 8.8** Lifter pattern replacement at Matimba power station

## 8.6 Conclusions

In this chapter, our approach of modelling the wear of lifters was applied to study the variation of the load behaviour of industrial tumbling mills as a function of their respective lifter wear. The industrial tumbling mills chosen and their respective evolving lifter profiles due to wear were described in Chapter 7.

DEM study of the variation of the load behaviour as a function of wear of lifters used at Lethabo power station reveals that not much change occurs in the load behaviour in terms of shoulder and toe position, tangential velocity of balls and power. This observation agrees with industrial data where it is noticed that the throughput remains almost constant as lifters wear. In this case, lifters are removed from the mill when they reach a critical thickness susceptible to breakage. A close look at double wave lifters used at Lethabo power station shows that waves are moving back in the mill. The spacing between consecutive waves remains almost constant. The profile is therefore almost conserving as lifters wear in this case.

DEM study of the variation of load behaviour as a function of lifter wear in tumbling mills used at Kendal power station shows that the load behaviour is deteriorating as lifters wear. Slippages occur within the charge as lifters wear and the shoulder position, power and tangential velocity of balls decreases for the same mill filling. To extend the useful life of lifters used at Kendal power station beyond 80000 hours and restore at the same time the mill throughput, worn out lifters were tilted by 50 mm. Following the modifications, the throughput was restored but the ball wear rate was increased significantly making the operation costly. Our DEM simulations of the load behaviour not only improve our understanding of the grinding process as a function of lifter wear but also show the reason for the increase in the ball wear rate following the tilting of lifters. Operating conditions are recommended to decrease the ball wear rate and performances beyond the change operated are predicted.

Study of the load behaviour in tumbling mills used at Matimba power station shows that as lifters are wearing the amount of cataracting balls in the mill and the shoulder position decreases. To extend the useful life of lifters used at Matimba power station, DEM simulations shows that increasing the mill speed can be considered as an option.

We showed that impact and abrasion energies dissipated in collision between balls and between balls and lifters can be explored to predict the wear of balls as a function of operating conditions.

We also proposed that studying the variation of load behaviour as a function of lifter wear can be applied to choose for a particular operation the best initial lifter profile, the optimum time and type of lifter replacement.



## Chapter 9

# Development of lifters wear model from the description of the load behaviour

### **9.1 Introduction**

### **9.2 Development of lifter wear model**

#### 9.2.1 Introduction

#### 9.2.2 Impactive wear

#### 9.2.3 Adhesive- abrasive wear

### **9.3 Derivation of semi-empirical equations predicting the wear of lifters**

#### 9.3.1 Introduction

#### 9.3.2 Impact energies

#### 9.3.3 Adhesion – abrasion energies

### **9.4 Conclusions**

## 9.1 Introduction

In order to simulate the wear of tumbling mill lifters it is important to predict the impact and abrasion energies dissipated on discretised lifter divisions. We showed in Chapters 6 and 7 that the DEM predict successfully these energies as a function of operating conditions in tumbling mills. This success makes the DEM as the first choice method to predict the wear of lifters.

Predictions of the wear of tumbling mill lifters using the Discrete Element Method as developed in the present thesis are time consuming due to the prodigious amount of calculations performed per second. An attempt is made in this Chapter to develop equations from the description of the load behaviour in order to predict the impact and abrasion energies dissipated on discretised lifter division. The turbulent nature of interaction between balls and lifters makes this study difficult. A simplistic approach is taken in this Chapter in order to derive semi-empirical equations predicting the wear of lifters.

It is important to describe accurately the mill load behaviour in order to derive a model predicting the wear of liners/lifters. For its simplicity and validation of power against laboratory and industrial data, we use the model derived by Morrel (1993) described in the literature review (Chapter 2). Although, Morrel's model was developed for wet milling, similarities can be established for dry milling.

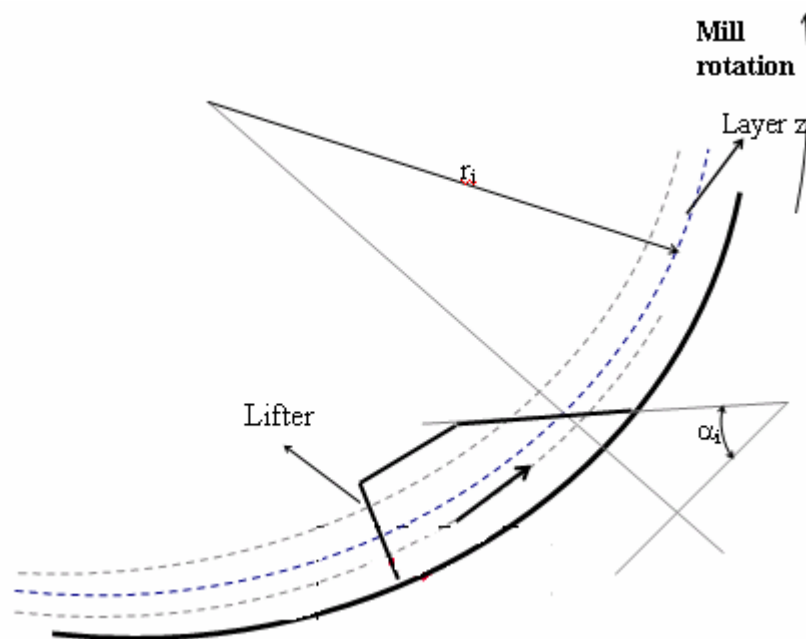
## 9.2 Development of wear lifter model

### 9.2.1 Introduction

In dry milling conditions, lifters wear due to adhesive-abrasive and impact energies dissipated on them by the load charge. Once those energies are determined on discretised lifter divisions, it is possible to predict the evolving lifter profiles. Impact and abrasion/adhesion energies derived will be used to predict the volume of material removed on discretised lifter division (Equation 4.6). To predict realistic simulated profiles, the removal of material on discretised lifter divisions will be operated via the objective function developed in Chapter 4 (Equation 4.15)

### 9.2.2 Impactive wear

We assume that the active load charge is moving in different layers as represented by Figure 9.1. On layer  $z$ , the discretised lifter division  $i$  is moving at the tangential speed  $v_i$  while the charge layer corresponding to the discretised lifter division  $i$  is moving at the tangential speed  $v_{z,i}$



**Figure 9.1:** Collision between a discretised lifter division  $i$  and a mill charge layer  $z$

The load charge in layer  $z$  at a radial position  $r_i$  is moving at a tangential velocity of  $v_{z,i}$  given by:

$$v_{z,i} = W_l r_i \quad (9.1)$$

On the layer  $z$ , the tangential velocity of lifter is given by:

$$v_i = wr_i \quad (9.2)$$

The collision between lifter and load charge in layer  $z$  will therefore occur at a speed  $v$  given by:

$$v = (w - w_i)r_i \quad (9.3)$$

Studies by different authors: Finnie (1960, 1972), Bitter (1963), Neilson, J.H. and Gilchrist, A. (1968), Tilly (1973) show that the volume of material removed due to collision between particles (balls) and material is proportional to  $v^2$ . At low velocities, collisions produced are purely elastic, consequently, no removal of particles occurs on the surface of material. There is therefore a minimum velocity or better a minimum energy (since energy is proportional to  $v^2$ ) required in order to remove materials on a surface.

Using the same approach, Bitter (1963) derived the following equation:

$$V = \frac{M}{2e}(v \sin a - k)^2 \quad (9.4)$$

where

$V$  is the volume of material removed

$M$  is the mass of particles impacting

$a$  is the impact angle

$v$  is the speed of particles

$k$  is the maximum particle velocity at which collision still is purely elastic

$e$  is the energy needed to remove a unit volume of material from the body by deformation wear (deformation wear factor)

Applying Bitter's equation to a discretised lifter division  $i$  belonging to a layer  $z$  as shown in Figure 9.1 give for a mill revolution:

$$V_{i,i} = \frac{f_{i,z} m_{i,z}}{2e} ((w - w_l) r_i \sin a_i - k)^2 \quad (9.5)$$

where

$f_{i,z}$  is the frequency of collisions between a mass  $m_{i,z}$  of mill charge (layer z) and the discretised lifter division i during a mill revolution (from the toe to the shoulder),  $\text{rev}^{-1}$

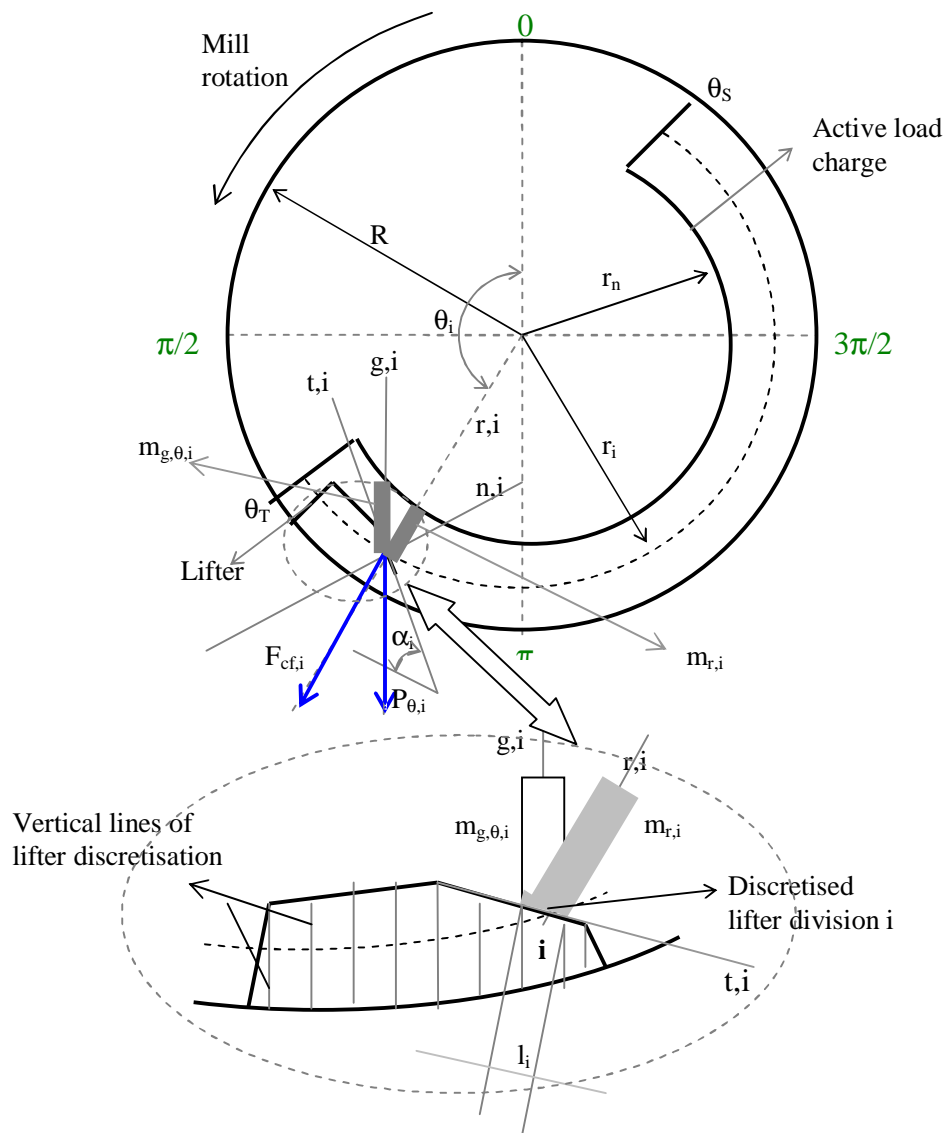
$m_{i,z}$  is the mass of the mill charge ( layer z) impacting a discretised lifter division i.  $m_{i,z}$  varies from the toe to the shoulder providing different impact energy intensity on a discretised lifter division i.

The frequency of collisions is a function of:

- Lifter height
- Mill speed and charge speed
- Mill filling (Shoulder and toe position)
- Lifter angle (front and back of lifters)
- Space between two consecutive lifters
- Ball and media size distribution

### 9.2.3 Adhesive – Abrasive wear

Lifters wear by abrasion/adhesion as a result of the relative motion between the mill charge and mill lifters.



**Figure 9.2** Description of load behaviour and centrifugal and gravitational forces exerted on a discretised lifter division  $i$  at the mill position  $\theta_i$  (the size of the lifter relative to the mill has been exaggerated to increase legibility)

Gravitational and centrifugal forces are exerted by the mill charge on lifters during mill revolutions. Figure 9.2 illustrates the gravitational and centrifugal forces exerted on a discretised lifter division  $i$  on one lifter at the mill position  $\theta_i$ .

Since it was found that impact energies on discretised lifter divisions play a key role in the wear of lifters described in Chapter 7, more emphasis was directed towards the derivation of a semi-empirical model from wear due to impact. Development of abrasive wear equation from the gravitational and centrifugal forces is reported in Appendix M.

### 9.3 Derivation of semi-empirical equations predicting the wear of lifters

#### 9.3.1 Introduction

The developed equations of volume removed on a discretised lifter division  $i$  due to impact and abrasion (See Appendix M) energies dissipated on them show that the volume removed in the wear process is a function of the discretised lifter division length  $l_i$ , angle  $\alpha_i$ , radial position  $r_i$  or height, the angular velocity of the load charge  $w_i$  and the percentage of mill filling (shoulder and toe position).

Studies of the variation of the load behaviour in industrial tumbling mills (Chapter 8) shows that as lifters wear the angular velocity of the load charge varies for tumbling mills used at Kendal and Matimba power stations. It was found that the load behaviour in tumbling mills used at Lethabo power station is very similar as lifters wear. We will therefore use only the data from Lethabo power station since  $w_i$  is constant.

The first step was to verify that DEM data of impact and abrasion/adhesion energies dissipated on different discretised lifter divisions from the lifter profile used at Lethabo power station can be fitted to developed models.

The double wave lifter used at Lethabo power station was discretised in 42 equally spaced lifter divisions. The prediction of the completely worn profile was achieved in 8 steps. Therefore 294 (42 x 7) data of DEM impact and abrasion/adhesion energies were generated.

### 9.3.2 Impact energies

In the case of lifters used at Lethabo power station,  $w_i$  can be considered as constant in Equation 9.5.

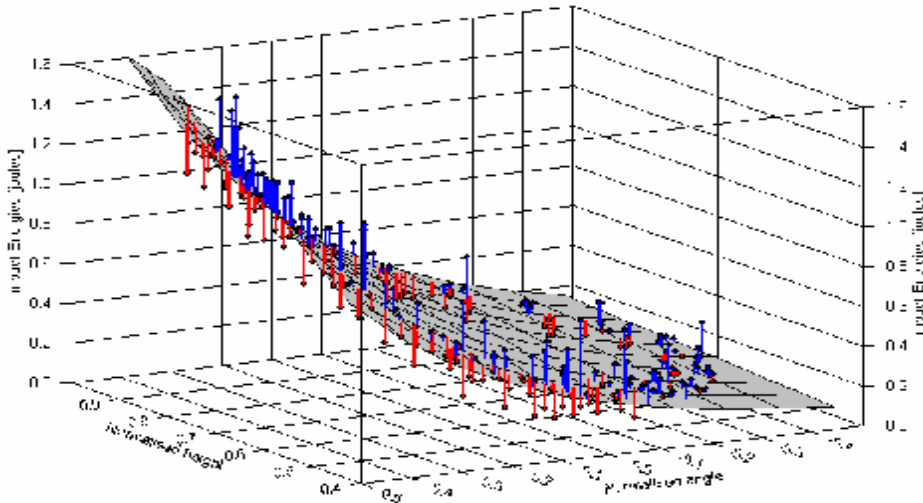
The volume removed on a discretised lifter division  $i$  being proportional to the impact energy dissipated on it, all 294 impact energies on different discretised lifter divisions and their corresponding angle and radial position derived from DEM simulations were fitted to the following model:

$$E_i = k_2 (r_i \sin a_i - k_1)^2 \quad (9.6)$$

The discretised lifter division length was taken as a constant since we used an equally spaced lifter discretisation.

Figure 9.3 represents the correlation between the impact energy and the discretised lifter divisions angles and heights. Negative angle refers to angle greater than 90 degrees. Table 9.1 gives the detailed results of the correlation. A good correlation has been found between these data.



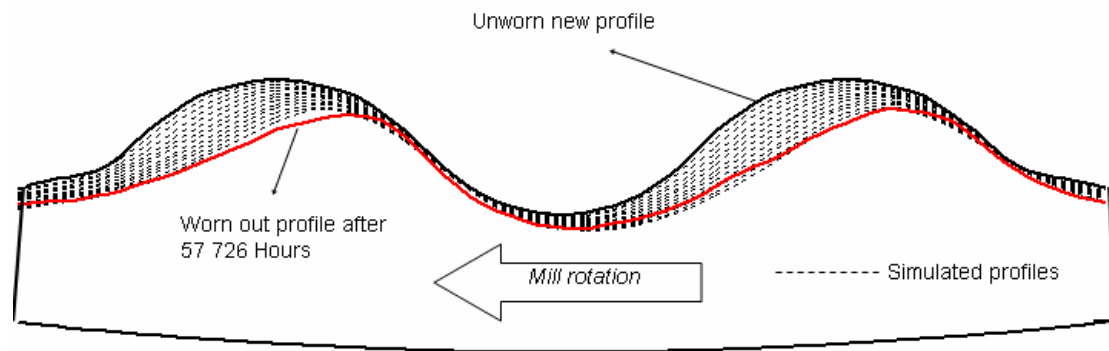


**Figure 9.3** Impact energies as a function of Lethabo double wave discretised lifter divisions angle and height

**Table 9.1** Correlation results of impact energy as a function of discretised lifter divisions height and angle for the double wave lifter used at Lethabo power station

Number of observation	292	292	292
Empirical Model Equation:	$Y = a((X_1 \sin(bX_2 + c) - d)^2$	$Y = aX_1^b * (c)^{X_2}$	$Y = aX_1^b * \exp(cX_2)$
$a$	21.480	0.573	0.573
$b$	-0.304	1.082	1.082
$c$	0.088	14.464	2.672
$d$	0.079	-	-
Coefficient of correlation	$R^2 = 0.89$	$R^2 = 0.934$	$R^2 = 0.934$
$Y$	Impact Energy		
$X_1 = \frac{h_i}{h_{\max}}$	Normalised height		
$X_2 = \frac{a_i}{90}$	Normalised angle		

Since the impact energy is the main parameters in the contribution to lifter wear in the Lethabo case study in Chapter 7 ( $a_{impact} = 1$ ,  $a_{ad-abr} = 0.1$ ), it is possible to use the empirical equation to predict the wear of this particular lifter. Figure 9.4 shows the results obtained using the proposed empirical model.



**Figure 9.4** Simulation of the wear of the double wave lifter used at Lethabo power station using an empirical model

The comparison between the simulated profiles using our DEM approach and the profiles derived from the empirical model shows a better prediction using the DEM. The empirical model offers the advantage of simulating the wear of this lifter in a fraction of time that is required by the DEM. This takes a few hours while two weeks are required to evolve the lifter using the DEM

### 9.3.3 Adhesion – abrasion energies

Equations derived in Appendix M predicting the volume removed on a discretised lifter division  $i$  due to abrasion-adhesion show that many parameters are involved in the solution. An attempt of fitting the DEM simulated data to simple empirical relationship was not successful. The best fit provides a correlation coefficient  $R^2$  of 0.65.

## 9.4 Conclusions

An attempt was made in this Chapter to develop equations of impact and abrasion/adhesion energies dissipated on discretised lifter divisions in order to predict the wear of lifters without using the Discrete Element Method. Morrel's description of load behaviour was used for its simplicity and validation of power against laboratory and industrial data.

It was found that equations of impact and abrasion/adhesion energies derived are related to mill operating conditions (speed, filling), load charge conditions (angular velocity, bulk density) and discretised lifter divisions length, angle and radial position. It has been demonstrated in Chapter 8 that as lifters wear, there is a variation of angular velocity of the load charge. The variation of angular velocity of load charge as a function of lifter wear implies that energies dissipated in collisions between lifters and load charge vary as lifters wear. Since it is difficult to predict the variation of angular velocity of load charge as a function of lifters wear, it is difficult to predict the wear of lifters from developed equations.

In the special case of lifters used at Lethabo power station, it was found that the load behaviour is very similar as lifters wear. In this particular case, the angular velocity of the load charge is almost constant as a function of time. It was found in this case that DEM predicted impact energies on discretised lifter divisions as a function of lifter wear fit well the impact energy equation derived from the description of load behaviour. Since the impact energy was the major contributing factor to the wear of lifters, it was possible to predict the wear of lifter using the equation derived.

Development conducted in this Chapter provide at the same time a foundation to develop equations predicting the wear of lifters from the description of the load behaviour and highlight the limitation of such models. In fact, none of the model available in the literature, describing the load behaviour is able to predict accurately the load behaviour as affected by lifter profiles except the Discrete Element Method.

The DEM is therefore the adequate tool to model the wear of lifters. Only in special case where the angular velocity of the charge is almost constant as lifters wear, developed equations or semi-empirical equations can predict successfully the wear of lifters.

## Nomenclature

$R$  is the mill radius, m

$r_i$  is the distance from the mill center to the discretised lifter division  $i$ , m

$r_n$  is the inner radius of the active load charge, m

$L$  is the effective mill length, m

$l_i$  is the length of the discretised lifter division  $i$ , m

$\alpha$  is an impact angle, rad

$\alpha_i$  is the angle of the discretised lifter division  $i$ , rad

$\alpha_i^*$  is the angle of the discretised lifter division  $i$  located at the back of the lifter, rad

$\theta_S$  is the mill shoulder angle, rad

$\theta_T$  is the mill toe angle, rad

$\theta_i$  is the mill position angle of the discretised lifter division  $i$ , rad

$\rho_b$  is the bulk density of the active charge,  $\text{kgm}^{-3}$

$V$  is the volume of material removed on a surface,  $\text{m}^3$

$V_i$  is the volume of material removed on the discretised lifter division  $i$ ,  $\text{m}^3$

$V_{c,i}$  is the volume of material removed on the discretised lifter division  $i$  due to centrifugal forces exerted on it,  $\text{m}^3$

$V_{p,i}$  is the volume of material removed on the discretised lifter division  $i$  due to the weight of the load,  $\text{m}^3$

$V_{q,i}$  is the volume of material removed on the discretised lifter division  $i$  at the mill angle  $\theta$ ,  $\text{m}^3$

$n,i$  is the normal direction to the discretised lifter division  $i$ , -

$t,i$  is the tangential direction to the discretised lifter division  $i$ , -

$g,i$  is the gravitational direction to the discretised lifter division  $i$ , -

$r,i$  is the radial direction to the discretised lifter division  $i$ , -

$S_i$  is the sliding distance on the discretised lifter division  $i$ , m

$W$  is the wear rate

$N$  is the mill speed,  $\text{rev min}^{-1}$

$\omega$  is the angular velocity of the mill,  $\text{rad s}^{-1}$

$\omega_i$  is the angular velocity of the mill charge,  $\text{rad s}^{-1}$

$H$  is the hardness of the lifter

$K$  is the coefficient of wear, -

$k$  is the maximum particle velocity at which collision between lifter and particles in the mill charge is purely elastic,  $\text{ms}^{-1}$

$k_i$  are constant, -

$F_{cf,i}$  is the centrifugal force exerted on a discretised lifter division  $i$ , N

$F_{n,cf,i}$  is the component of  $F_{cf,i}$  exerted in the normal direction to the discretised lifter division, N

$v_i$  is the tangential speed of the discretised lifter division  $i$ ,  $\text{m s}^{-1}$

$v_{t,i}$  is the component of  $v_i$  in the tangential direction to  $i$ ,  $\text{m s}^{-1}$

$v_{n,i}$  is the component of  $v_i$  in the normal direction to  $i$ ,  $\text{m s}^{-1}$

$v_{z,i}$  is the tangential speed of the charge layer  $z$  belonging to the discretised lifter division  $i$ ,  $\text{m s}^{-1}$

$v_{n,z,i}$  is the component of  $v_{z,i}$  in the normal direction to  $i$ ,  $\text{m s}^{-1}$

$v_{t,z,i}$  is the component of  $v_{z,i}$  in the tangential direction to  $I$ ,  $\text{m s}^{-1}$

$m_{r,i}$  is the mass of the active charge exerted on the discretised lifter division  $i$  in the radial direction, Kg

$m_{g,i}$  is the mass of the active charge exerted on the discretised lifter division  $i$  in the gravitational direction, Kg

$m_{g,\theta,i}$  is the mass of the active charge exerted on the discretised lifter division  $i$  in the gravitational direction at the mill angle  $\theta_i$ , Kg

$g$  is the acceleration due to gravity,  $\text{m s}^{-2}$

$P_{q,i}$  is the weight exerted on a discretised liner division  $i$  at the mill angle  $\theta$ , N

$E_{i,z}$  is the impact energy dissipated on a discretised lifter division  $i$  belonging to a layer  $z$ , J

$(x_i, y_i)$  are the coordinates of the discretised lifter division  $i$

$J$  is the percentage of mill filling, -

$b$  is the proportion of  $J$  which constitutes the active charge, -

$q$  is the probability of abrasion events during the mill revolution,  $q$  is a function of  $\theta_i$  and  $\alpha_i$

$r_{c,mr}$  is the distance from the mill center to the center of mass of  $m_{r,i}$

# Chapter 10

## Conclusions and recommendations

### **10.1 Introduction**

### **10.2 DEM modelling of forces exerted by mill charge lifters**

### **10.3 DEM modelling of evolving lifter profiles due to wear in dry milling**

### **10.4 Recommendations**

## 10.1 Introduction

The Discrete Element Method applied to tumbling mills has been extensively used in order to improve our understanding of the milling process. This method shows great potential since it can be used not only to design milling equipment but also to optimize milling performances by providing details such as energies involved in collisions and transport of material in tumbling mills. To achieve this objective, a more rigorous validation of the Discrete Element Method, such as the predictions of forces involve in collisions between balls, particles and lifters, is required in order to produce realistic outputs.

Lifter profiles play a key role in the performance of tumbling mills since they influence tumbling mill load behaviour. Due to the wear occurring in the milling environment, lifter profiles change during their useful life. Mill performance will correspondingly vary. There is therefore a need to predict the evolving lifter profiles due to wear and quantify the change in mill performance in order: i) to choose an optimal initial lifter design for a particular operation, ii) to determine the optimum time and type of lifter replacement, iii) to explore modifications which can be performed on lifters or operating conditions in order to extend lifters useful life.

Two objectives were pursued in this thesis. Firstly, to assess the ability of the Discrete Element Method applied to tumbling mills to model the normal and tangential forces exerted by the mill charge on lifters as affected by mills operating conditions. Secondly, to assess the ability of the Discrete Element Method to predict the evolving mill lifter profiles due to wear.

The results of our investigations and recommendations for further researches are summarized in the followings paragraphs.

## **10.2 DEM Modelling of forces exerted by mill charge on lifters**

To assess the ability of the Discrete Element Method to model the normal and tangential forces exerted by the mill charge on lifters, experimental measured data available have been compared to DEM simulated predictions in the same conditions. The experimental raw data provided by Van Nierop et al (2000) were measured in a laboratory two – dimensional mill designed in order to record the normal and tangential forces exerted by the mill charge on an instrumented lifter bar. The experimental mill had a diameter of 0.55m and a length of 0.023m. It was equipped with 12 square lifters (22 x 22 mm). The measured forces at 60, 50 and 30% of critical speed when the mill was filled at 20% have been compared to the DEM simulated forces in the same conditions. Parameters in the DEM simulations were chosen in order to have the same load behaviour and power draw.

A good agreement has been found between the measured and the DEM simulated forces in terms of positions of shoulder and toe at all mill speed studied. A good agreement was also found in terms of amplitude of forces at 30% of critical speed while rough similarities were observed in terms of amplitude of forces at 50 and 60% of critical speed due to the inherent nature of noise and random collisions occurring in tumbling mills at higher speed.

## **10.3 DEM Modelling of evolving lifter profiles due to wear in dry milling**

From the review of published work related to the prediction of evolving lifter profiles due to wear, we show the need to develop a new approach taking into account all types of wear occurring in mill environments and predicting realistic simulated profiles.

We developed a mathematical wear model removing material on lifters which takes into account the impact and abrasion or adhesion wear occurring in dry milling conditions. Our wear equation assumes that the total volume removed on a surface is the sum of the contribution of all types of wear. To take into account the difference of ore properties, material (lifters and balls) resistance to different types of wear which is



a function of material properties, we implemented in our model weight factors given to different types of wear. To implement the wear equation in the DEM code, we show the necessity to discretise lifter profiles into small surfaces. Depending on lifter design, we developed the vertical or the radial lifter discretisation. In order to produce realistic simulated profiles our wear model is implemented in the DEM code using an objective function having four components. The first component minimises the difference of volume removed predicted by our wear mathematical model and the volume effectively removed. The second component ensures that the simulated profile is smooth. The third component prevents a dramatic change for the simulated profile. The fourth component maintains the ordinates of the worn simulated profiles lower than the ordinate of the initial profiles.

Our new approach developed has been tested against published laboratory data of evolving lifter profiles due to wear. The laboratory tests were conducted by Valderrama et al (1996) studying the effect of cascading and cataracting ball motion on the wear of lifters. Their results at 75 % of critical speed in the presence and in the absence of a deflector preventing cataracting balls to hit lifters directly were compared to our DEM predictions in the same conditions. A good agreement has been found between the measured and the simulated profiles.

To ensure that our approach developed has the ability to accurately predict the evolving lifter profiles of in all cases, our model was also tested to predict the wear of three (3) different lifters used in industrial tumbling mill operating in dry conditions. The industrial tumbling mills chosen are used at ESKOM Lethabo, Kendal and Matimba power stations for the grinding of coal. In all three cases, only the unworn and the worn out lifter profiles without any intermediate stage were available. A constant wear rate was therefore used to predict the worn out profiles from the unworn profiles.

A good agreement has been found between our last simulated profile and the worn out measured profile in all three cases.

A study of the variation of the load behaviour as a function of lifters wear was also performed on these tumbling mills. The study was performed not only to improve the understanding of the grinding process as a function of lifter wear and quantify the change in milling performances but also to explore modifications on lifters and operating conditions in order to extend lifters useful life. This study was successful since predicted trends correspond to observations at plants.

The contribution of DEM to predict the ball charge wear was also explored in this thesis. Since the DEM can predict per ball size impact and abrasion energies dissipated in collisions between balls and between balls and lifters, it can therefore be used to predict the wear of balls.

An attempt was also made in this thesis to predict the wear of lifters without using the Discrete Element Method. Equations developed were derived from the load behaviour described by Morrel (1993). This attempt highlights the complexity and difficulties of such study. A success which needs more validation has been achieved in predicting impact energies dissipated on discretised lifter divisions of the lifter used at Lethabo power station.

#### **10.4 Recommendations**

We have shown that the DEM can accurately predict the normal and tangential forces exerted by the mill charge on lifters as affected by the mill speed and the mill charge composition at lower speed. Our tests have been performed at a maximum mill speed of 60% of critical speed. We recommend this study to be extended at higher speed. The sampling rate and the number of revolutions recorded during experimental measurement should be increased in order to increase the accuracy of prediction.

We have assessed the ability of the DEM to simulate the evolving mill lifter profiles due to wear. We believe that there will be more validation of our approach.

The simple linear spring, dashpot and slider contact model was used to predict the load behaviour, forces and wear of lifters. Other contact models taking into account material properties such as the Hertz model can be explored to improve the accuracy of prediction.

In order to predict the simulated evolving lifter profiles due to wear in a reasonable time, our simulations were performed using one ball slice instead of full 3 dimensional simulations. Since the ability of the DEM to predict the wear of lifters has been proven, we recommend the use of 3D simulations which have the potential to improve the accuracy of simulated results.

The mathematical wear model used in our thesis assumes that the total wear is the sum of contribution of each type of wear. Weight factors are given to impact and abrasion energies to take into account ore and material properties. In our investigation, weight factors were back calculated. We recommend the development of tests, such as tests conducted by Radziszewski (2001) studying the contribution of each type of wear to the total wear, to calculate them directly.

Although our wear mathematical model is valid for dry conditions, it can probably be used in wet conditions by incorporating a contribution due to corrosive wear.

## Appendices

**Appendix A:** Measurements of lifter profiles

**Appendix B:** Modelling of liner wear

**Appendix C:** Calculation of volume effectively removed in 3D lifter discretisation

**Appendix D:** Two dimensional mill

**Appendix E:** Comparison between measured and DEM simulated forces

**Appendix F:** Matlab program minimizing the objective function

**Appendix G:** ESKOM tumbling mills design

**Appendix H:** Measured lifters worn out profiles in tumbling mills used at Kendal power station

**Appendix I:** DEM simulated worn profiles of lifters used in tumbling mills at Lethabo, Kendal and Matimba power stations

**Appendix J:** Comparison between volume removed predicted and effectively removed

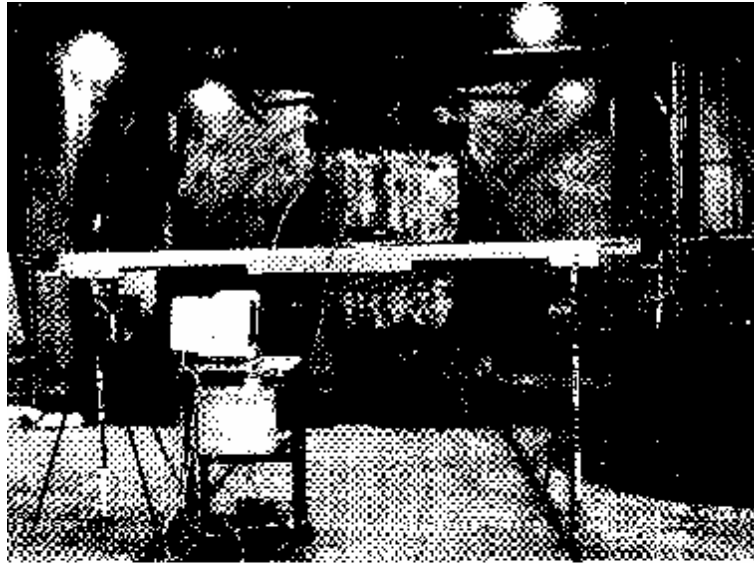
**Appendix K:** DEM simulated worn profiles beyond tilting the worn lifter by 50 mm in tumbling mills at ESKOM Kendal power station

**Appendix L:** DEM contribution to the prediction of ball wear

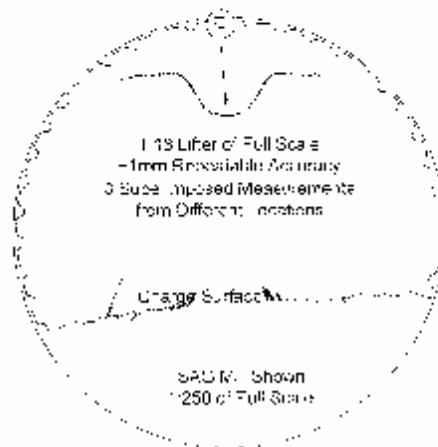
**Appendix M:** Development of abrasive mathematical wear model in dry tumbling mills

## APPENDIX A: Measurement of lifter profiles

### 1 Measurement of lifter profiles using a laser scanner



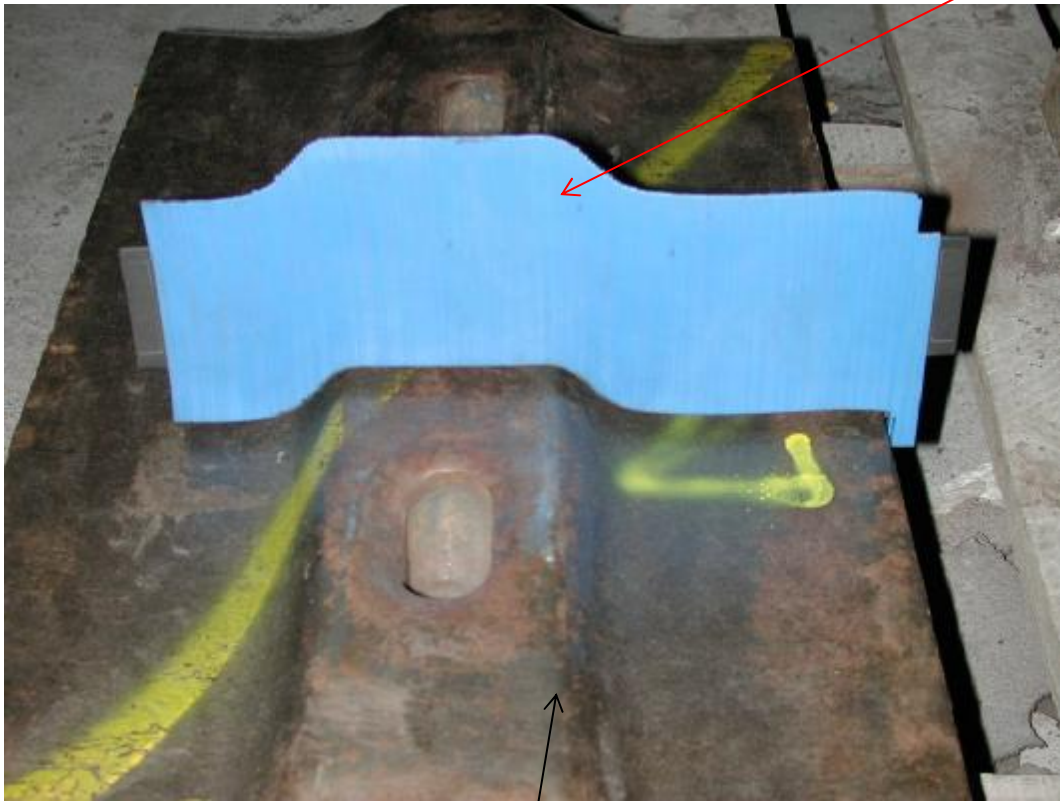
*Mill Laser Scanner fully assembled – 4 meter bar length*



**Figure A.1** Measurement of lifters profiles in a Semiautogenous mill using a laser scanner developed by Conveyor Dynamics International and Svedala (after Nordell and Potapov, 2001)

**2 Measurement of lifter profiles using a profiling gauge**

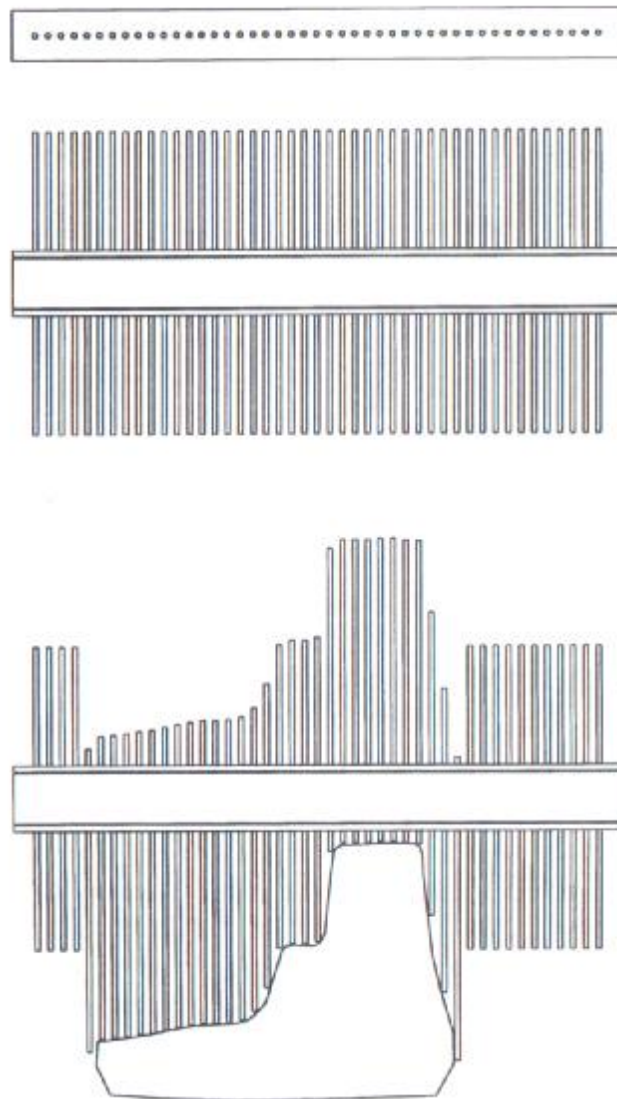
Profiling gauge



Lifter outside a mill

**Figure A.2** Measurement of lifter profile using a profiling gauge

### 3 Measurement of lifter profile using a pin profiling gauge



**Figure A.3.** Pin profiling gauge after Meekel et al (1996)

## Appendix B

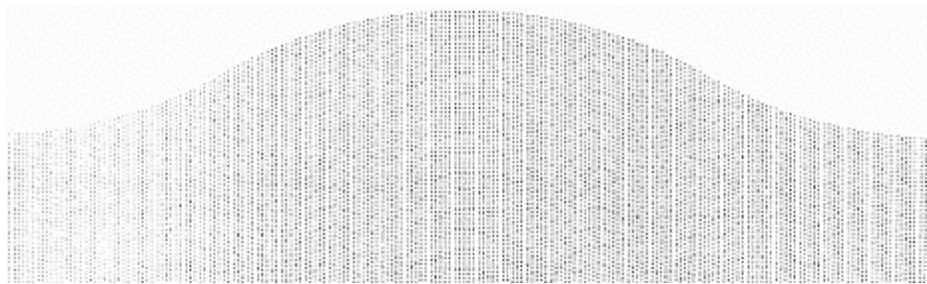
### Modelling of liner wear

#### 1 Radziszewski and Tarasiewicz (1993)

##### 1.1 liner discretisation

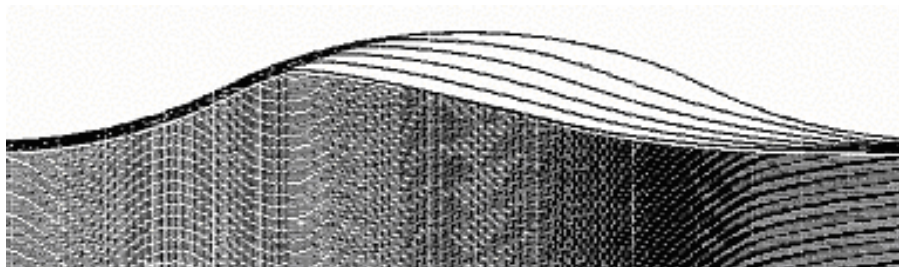
To discretise a lifter these authors divided the liner profile into small elements  $e_i$  having a height  $\Delta y$  and a width  $\Delta x$  and a depth of unity. Those elements are removed from the initial surface each time step as a function of interaction with the mill charge. The element mass is:

$$m_i = r\Delta x\Delta y \quad (\text{B1})$$



**Figure B.1** Wave lifter profile discretisation after Radziszewski and Tarasiewicz (1993)

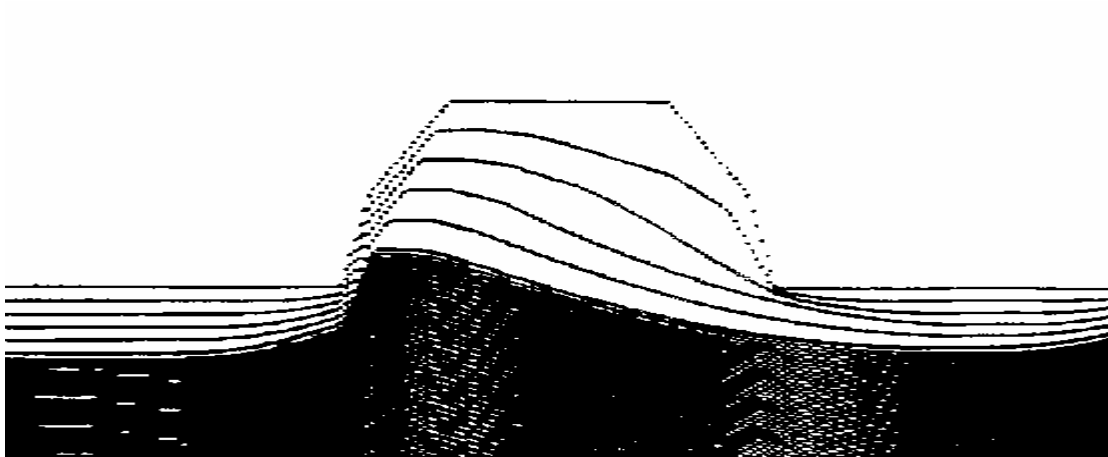
##### 1.2 Wave liner simulated profiles



**Figure B.2** Simulated wave liner profiles after Radziszewski and Tarasiewicz (1993)

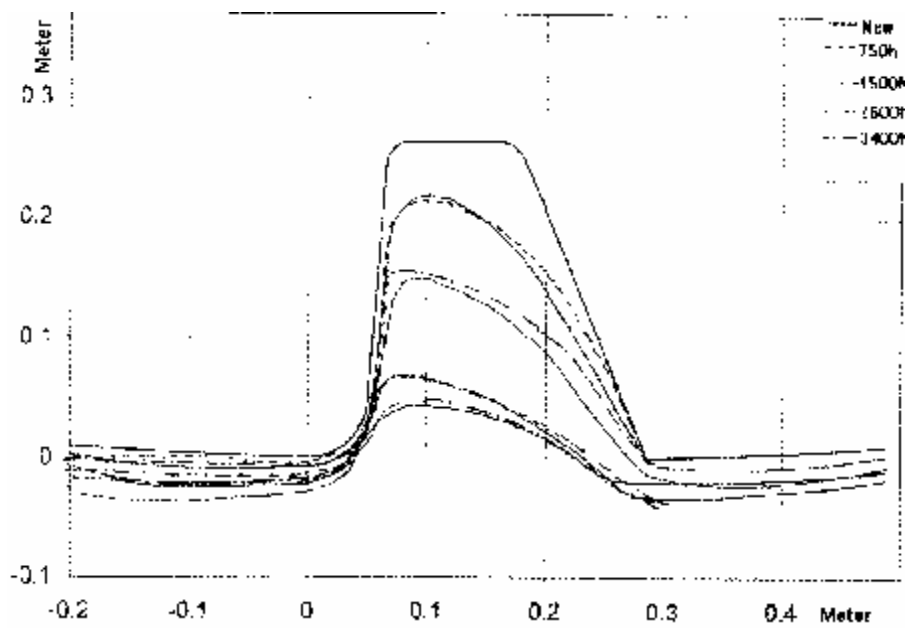


### 1.3 Bevelled liner simulated profiles



**Figure B.3** Simulated bevelled lifter profiles after Radziszewski and Tarasiewicz (1993)

### 2 Qiu et al (2001)



**Figure B.4** Comparison between experimental and simulated profiles after Qiu et al (2001)

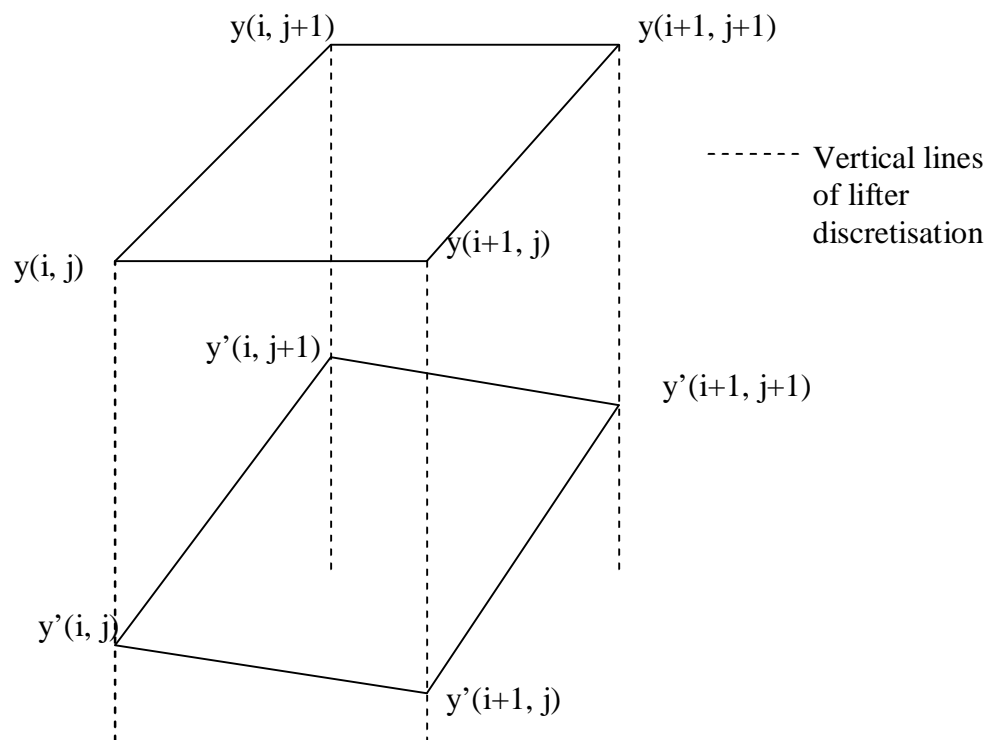
## Appendix C:

### Calculation of volume effectively removed in 3D lifter discretisation

#### 1. Introduction

The first component of the objective function in Equation 4.18, minimises the difference between the volume removed predicted  $V(i, j)$  and effectively removed  $V'(i, j)$ . Using the 3 D discretisation, the solid effectively removed does not have a regular shape and required therefore a subdivision into regular solid shapes.

#### 2. Subdivision of an element of volume into 6 tetrahedron



**Figure C 1:** 3D Discretised volume element

Figure C.1 shows a discretised volume element of a 3D discretisation of lifter. The following points are initial points :  $y(i, j)$  ;  $y(i+1, j)$  ;  $y(i, j+1)$  ;  $y(i+1, j+1)$  and the

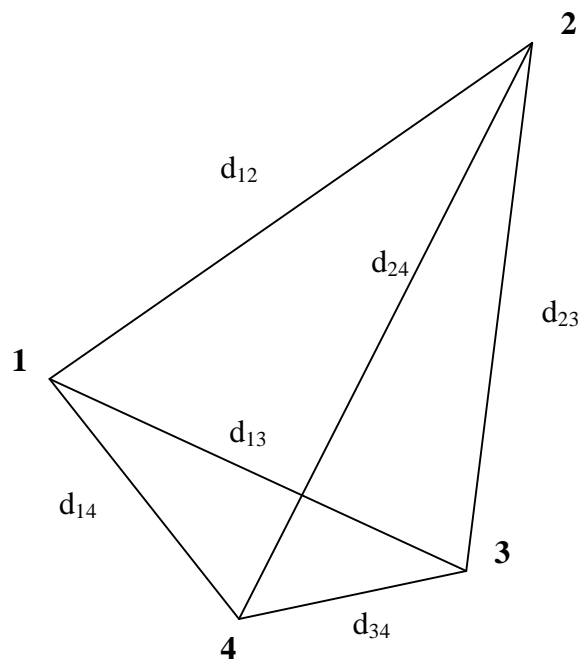
following points are their respective predicted points belonging to the same lines of lifter discretisation:  $y'(i, j)$  ;  $y'(i+1, j)$  ;  $y'(i, j+1)$  ;  $y'(i+1, j+1)$

The volume of this discretised volume element can be divided into the following 6 tetrahedron sharing the diagonal  $y(i, j+1)$  to  $y'(i+1, j)$  :

- $y(i, j+1)$  ;  $y'(i+1, j)$  ;  $y'(i+1, j+1)$  ;  $y'(i, j+1)$
- $y(i, j+1)$  ;  $y'(i+1, j)$  ;  $y'(i, j)$  ;  $y'(i, j+1)$
- $y(i, j+1)$  ;  $y'(i+1, j)$  ;  $y(i, j)$  ;  $y(i+1, j)$
- $y(i, j+1)$  ;  $y'(i+1, j)$  ;  $y(i+1, j)$  ;  $y(i+1, j+1)$
- $y(i, j+1)$  ;  $y'(i+1, j)$  ;  $y(i+1, j+1)$  ;  $y'(i+1, j+1)$
- $y(i, j+1)$  ;  $y'(i+1, j)$  ;  $y(i, j)$  ;  $y'(i, j)$

### 3. Volume calculations

Figure C.2 represents a tetrahedron



**Figure C.2** Representation of a tetrahedron

The volume of a tetrahedron from its edge length is given by:

$$Volume = \sqrt{\det \begin{bmatrix} 0 & d_{12}^2 & d_{14}^2 & d_{13}^2 & 1 \\ d_{12}^2 & 0 & d_{23}^2 & d_{24}^2 & 1 \\ d_{14}^2 & d_{23}^2 & 0 & d_{34}^2 & 1 \\ d_{13}^2 & d_{24}^2 & d_{34}^2 & 0 & 1 \\ 1 & 1 & 1 & 1 & 0 \end{bmatrix}} / 288$$

The volume of a single 3D discretised volume element (Figure C.1) can therefore be calculated as the sum of the 6 different tetrahedra comprise in that volume.

## Appendix D: Two - dimensional mill

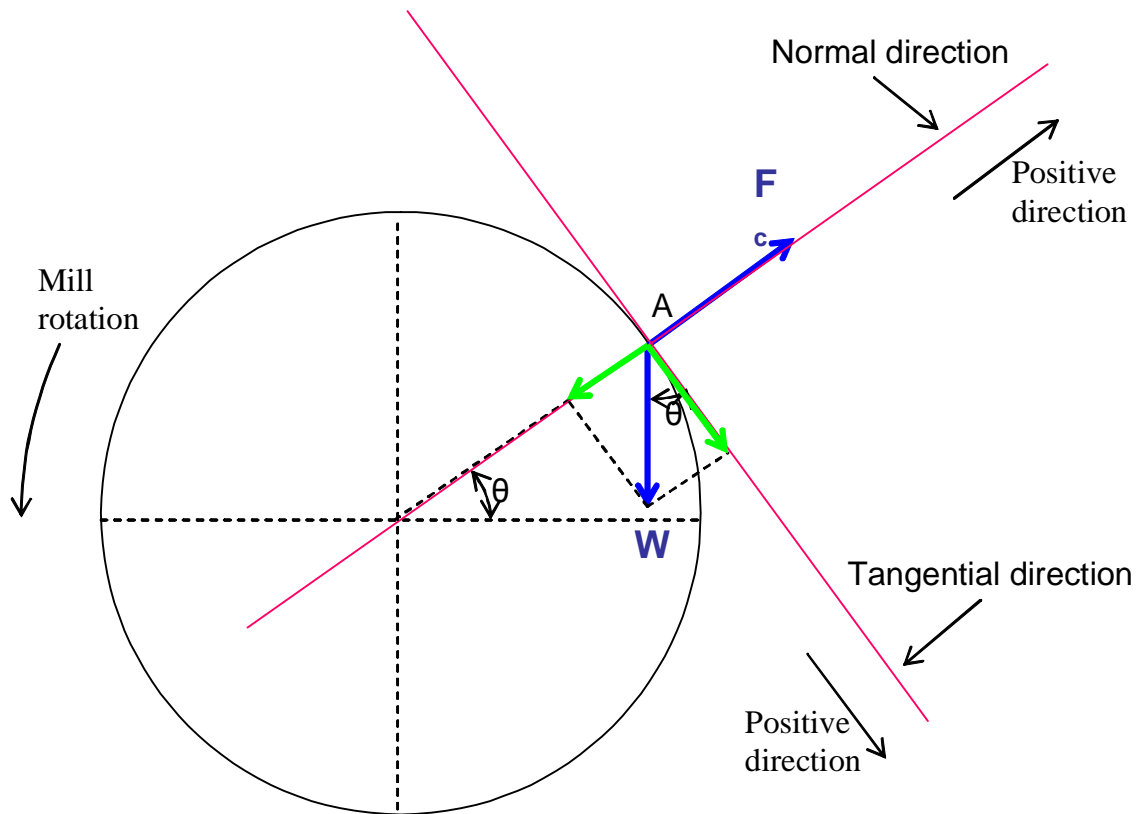
### 1. Photo of two- dimensional mill



**Figure D.1:** Two – dimensional mill

### 2. Tangential and normal forces at zero load

The forces exerted on the instrumented lifter in a position A represented by Figure D.2 when the mill is running without any load at  $N$  revolutions per minute are:



**Figure D.2** Normal and tangential forces exerted on the instrumented lifter at zero load

- The centrifugal forces  $F_c$  which can be calculated by:

$$F_c = m * \left( \frac{2\pi N}{60} \right)^2 * R \quad (\text{D.1})$$

- The weight of the lifter given by:

$$W = m * g \quad (\text{D.2})$$

Where

$m$  is the weight of the instrumented lifter

$N$  is the number of revolution per minute

$R$  is the mill radius

$g$  is the acceleration due to gravity

The resultant forces exerted in:

- The tangential direction is given by:

$$F_t = m * g * \cos q \quad (D.3)$$

- The normal direction is given by:

$$F_n = m * \left( \frac{2pN}{60} \right)^2 * R - (m * g * \sin q) \quad (D.4)$$

Equation (D.3) and (D.4) show that at zero-load the tangential force exerted on the instrumented lifter is only function of the mass of the lifter and the position  $q$  while the normal force is function of the mass of the lifter, the position  $q$  and also function of the mill speed.

## Appendix E:

### Comparison between measured and DEM simulated forces

A paired t-Test was performed to compare the measured  $X_i$  and DEM simulated  $Y_i$  forces at 30% of critical speed. The data are paired at each mill rotation angle  $q_i$  and the comparison was performed using the data between the toe and the shoulder.

$n$  is the number of data collected between the toe and shoulder

$\bar{X}$  and  $\bar{Y}$  are respectively the average measured and DEM simulated forces between the toe and the shoulder

$$\bar{X} = \sum_{i=1}^n \frac{X_i}{n} \quad ; \quad \bar{Y} = \sum_{i=1}^n \frac{Y_i}{n}$$

$n - 1$  is the degrees of freedom (DF)

then,

$$\hat{X}_i = (X_i - \bar{X})$$

$$\hat{Y}_i = (Y_i - \bar{Y})$$

and,

$$t = (\bar{X} - \bar{Y}) \sqrt{\frac{n(n-1)}{\sum_{i=1}^n (\hat{X}_i - \hat{Y}_i)^2}}$$



**Table E.1** Statistical comparison between measured and DEM simulated tangential forces at 30% of critical speed

t-Test		
Paired Comparison for tangential data		
	Measured	DEM Simulated
Mean	2.95783484	2.702778677
S.E.M.	0.09918982127	0.0815921822
S.D.	1.766024559	1.452707503
Variance	3.118842744	2.11035909
Sum	937.8336442	856.7808407
N	317	317
Sum(x <sup>2</sup> )	3758.919767	2982.56246
Sum(x) <sup>2</sup> /N	2773.36546	2315.688987
Correction Factor	5078.743444	
Df	316	
Expected Difference	0	
Variance of Difference	0.9362726888	
t(cal)	4.693148268	*** (P<=0.001) Two-sided
P(t<=t(cal)) Two-sided	4.01335E-006	
t(0.05) Two-sided	1.9674995	
Lower Conf. Limit of Difference	0.1038389686	
Upper Conf. Limit of Difference	0.4062733566	

**Table E.2** Statistical comparison between measured and DEM simulated normal forces at 30% of critical speed

t-Test		
Paired Comparison for normal forces		
	Measured	DEM simulated
Mean	1.508540727	1.264571071
S.E.M.	0.0725041162	0.06298164015
S.D.	1.286820408	1.117813224
Variance	1.655906763	1.249506404
Sum	475.1903291	398.3398873
N	315	315
Sum(x <sup>2</sup> )	1236.798688	896.0741085
Sum(x) <sup>2</sup> /N	716.8439648	503.7290977
Correction Factor	1211.198475	
Df	314	
Expected Difference	0	
Variance of Difference	0.8653175567	
t(cal)	4.654824746	*** (P<=0.001) Two-sided
P(t<=t(cal)) Two-sided	4.7902564E-006	
t(0.05) Two-sided	1.9675477	
Lower Conf. Limit of	0.09813096881	
Upper Conf. Limit of	0.3898083447	

## Appendix F:

### Matlab program minimizing the objective function

```

% This program minimises the objective function (Equation 4.15, vertical
discretisation) by using fminsearch function.
function F=objectives(X)
% The length of the mill, the wear rate, weight factors given to impact and abrasion,
% impact and abrasion energies dissipated on lifter divisions, weight factors in the
% objective function, discretised lifter divisions needs to be specified of read from an
% Excel spreadsheet in order to perform the minimisation.
L=input('L(mm)scalar') % L is the length of the mill in mm
W=input('Wscalar') % W is the wear rate
alpha=input('alphascalar') % alpha is the weight factor given to the difference of
slope between the jth and the (j+1)th profiles
beta=input('betascalar') % beta is the weight factor given to penalise any tendency for
y' to increase with time, a value of 5000 is usually used
lambda=input('lanbdascalar') % lambda is the weight factor given the difference of
neighbouring slope to have a smooth profile.
abrasion=input('a-abrasionscalar') % abrasion is the weight factor given to abrasion energy
impact=input('a-frictionscalar') % impact is the weight factor given to impact energy
Eimpact=input('E-frictionvector') % Eimpact is the matrix giving the average impact
energy on discretised lifter divisions
Eabrasion=input('E-abrasionvector') % Eabrasion is the matrix giving the average
abrasion energy on discretised lifter divisions
Y=input('Yvector') % Y are the coordinate (x,y) of the unworn profile
[m,n]=size(Y); % m=rows n=columns
% VOLUME V CALCULATED
Ta=W.*((impact.*Eimpact)+(abrasion.*Eabrasion));
T=Ta;
T(m,1)=0;
for j=1:m
    V(j,j)=T(j,1);
end
% A VOLUME PREDICTED-VOLUME CALCULATED
for j=1:m-1
Ea(j,1)=((((Y(j)-X(j))+(Y(j+1)-X(j+1))))));
end
for j=1:m-1
    Eb(j,1)=(H(j+1,1)-H(j,1));
end
Ec=Ea.*Eb;
E=Ec;
E(m,1)=0;
Aa=((L/2).*E)-T;
for j=1:m
    Ab(j,j)=Aa(j,1);
end

```

```

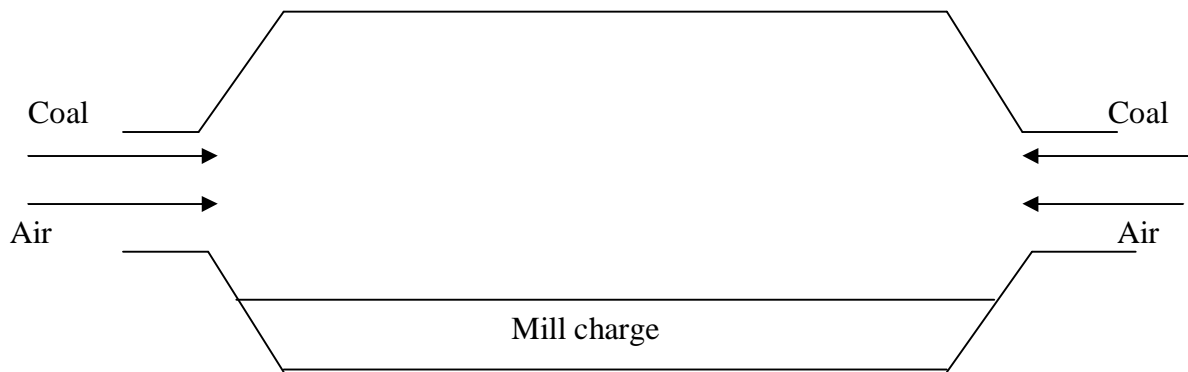
for j=1:m
Ac(j,j)=(Ab(j,j))^2;
end
A= trace (Ac);
% B SMOOTH LINE
for j=1:m-2
  Bb(j,1)=(((X(j+2)-X(j+1))/(H(j+2,1)-H(j+1,1))));
end
for j=1:m-2
  Bd(j,1)=((X(j+1)-X(j))/(H(j+1,1)-H(j,1)));
end
Be=Bb-Bd;
Ba=Be;
Ba(m-1,1)=0;
Bc=Ba;
Bc(m,1)=0;
for j=1:m
  Bf(j,j)=Bc(j,1);
end
for j=1:m
  Bg(j,j)=(Bf(j,j))^2;
end
B=(lambda)*trace (Bg);
% C NO LARGE CHANGES WITH TIME
for j=1:m-1
  Cb(j,1)=(((Y(j+1,1)-Y(j,1))/(H(j+1,1)-H(j,1))));
end
for j=1:m-1
  Cd(j,1)=((X(j+1)-X(j))/(H(j+1,1)-H(j,1)));
end
Ce=Cb-Cd;
Ca=Ce;
Ca(m,1)=0;
for j=1:m
  Cf(j,j)=Ca(j,1);
end
for j=1:m
  Cg(j,j)=(Cf(j,j))^2;
end
C=(alpha)*trace (Cg);
% D NO NEGATIVE WEAR
for j=1:m
  Da(j,1)=exp((beta*(X(j)-Y(j))));
end
for j=1:m
  Db(j,j)=Da(j,1);
end
for j=1:m
  Dc(j,j)=(Db(j,j))^2;
end
D=trace (Dc);
% MINIMISATION
F=A+B+C+D;

```

```
%[X,FVAL,EXITFLAG,OUTPUT]=fminsearch(@objectives,[coordinates of initial  
profile])
```

## Appendix G: ESKOM tumbling mill design

Tumbling mills used at Eskom for the grinding of coal are air swept mills fed from both side of the mill with coal and air as indicated in Figure G.1.

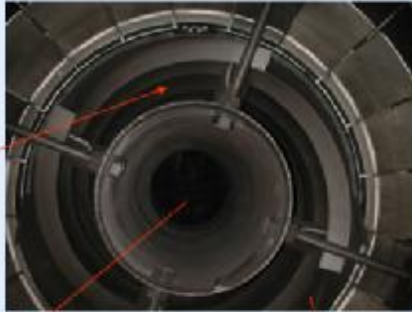


**Figure G.1** Air swept tumbling mill used at Eskom for the grinding of coal

Figure G.2 shows in detail the mill feed and removal design. The coal ground in the mill called pulverised fuel is removed in the air stream. The pulverised fuel passed through a cyclone where the overflow feed the boiler while the underflow is recycled to the mill. A screw conveyor is used at Matimba power station as indicated in Figure G.2 while a division wall is used at Lethabo and Kendal power stations. The difference between these designs justifies the difference observed in terms of load behaviour at Matimba, on one hand and Lethabo and Kendal on the other hand.

## Mill design: Coal Feed +Removal system

Screw conveyor used at Matimba power station

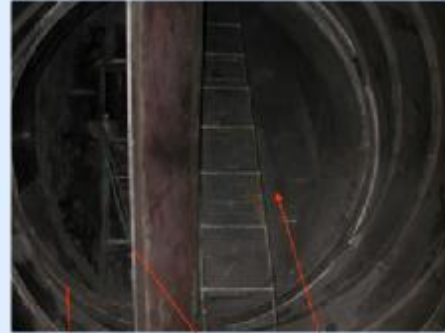


Air out  
+ PF

Primary hot air feed  
into the mill drum

Raw coal and  
Classifier rejects

Division wall used at Lethabo  
and Kendal power stations



Air out  
+ PF

Raw coal,  
Classifier rejects  
+Primary hot air

Division wall

**Figure G.2** Mill feed and removal design

## Appendix H:

### Measured worn out lifter profiles in tumbling mills used at Kendal power station

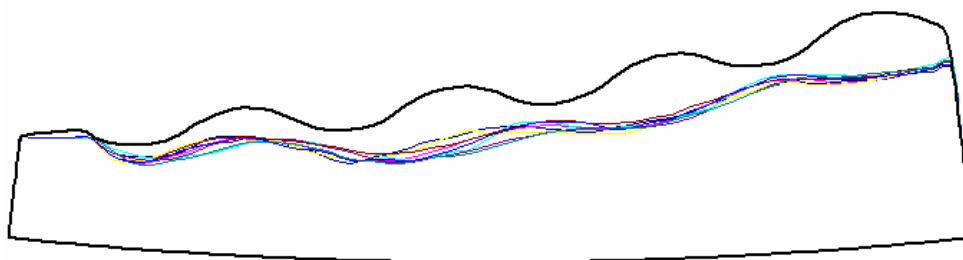
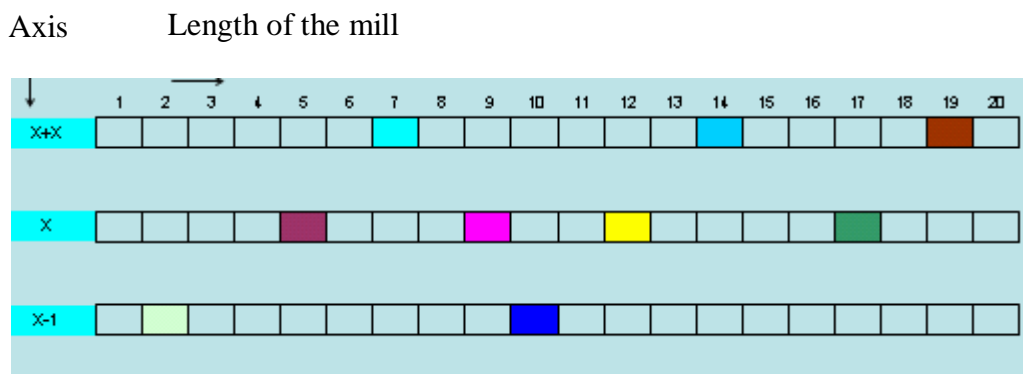
#### 1. Introduction

Lifters were measured inside tumbling mills at Kendal power station using a profiling gage. Measurements were performed randomly in the mill through the mill length and axis to investigate whether there is a non uniform wear as a function of mill length. The mill is fitted with 30 lifters around the circumference of the mill shell and 20 lifters along the mill length. Lifters were used for 70900 hours.

#### 2. Results

Table H.1 shows the location of measured lifter profiles inside the mill. Figure H.1 shows the measured data and the unworn lifter profile.

**Table H.1** Location of measured lifter profiles inside a mill used at Kendal power station



**Figure H.1** Measured worn out lifter profiles used at Kendal power station





## Appendix I

### Data of simulated profiles of lifters used at Eskom Lethabo, Kendal and Matimba power station

**Table I.1** Data of simulated profiles of lifters used in tumbling mills at Lethabo power station (the unworn lifter is used as reference and measurement are in cm)

	Simulated profiles									
	Unworn	worn out	1	2	3	4	5	6	7	8
0	1	0.4	0.9956	0.9911	0.9686	0.9206	0.8089	0.6864	0.5431	0.4451
1	1.3	0.5	1.1674	1.0889	1.0037	0.9334	0.8342	0.7206	0.5928	0.4728
2	1.45	0.55	1.3434	1.2365	1.1176	1.0271	0.9045	0.8007	0.6770	0.5427
3	1.7	0.75	1.6035	1.4789	1.3412	1.2247	1.0952	0.9738	0.8253	0.6883
4	2.25	0.95	2.0616	1.8789	1.6964	1.5457	1.4022	1.2364	1.0569	0.9159
5	3.2	1.25	2.7690	2.4887	2.2162	2.0059	1.8037	1.5849	1.3770	1.2333
6	3.9	1.55	3.5659	3.2351	2.8871	2.5740	2.3076	2.0460	1.8092	1.6267
7	4.5	1.95	4.2179	3.9186	3.5737	3.1893	2.8867	2.6053	2.3388	2.1002
8	4.8	2.35	4.6141	4.3927	4.1091	3.7719	3.4681	3.1735	2.8903	2.6336
9	5.05	2.8	4.8355	4.6642	4.4502	4.2157	3.9476	3.6655	3.4036	3.1474
10	5.15	3.25	4.9488	4.7959	4.6360	4.4625	4.2596	4.0349	3.8081	3.5601
11	5.05	3.5	4.9334	4.7991	4.6814	4.5405	4.3998	4.2320	4.0524	3.8288
12	4.8	3.7	4.7509	4.6497	4.5584	4.4499	4.3467	4.2238	4.0909	3.9184
13	4.5	3.75	4.4031	4.3195	4.2358	4.1504	4.0630	3.9760	3.8829	3.7740
14	3.9	3.6	3.8622	3.7793	3.7061	3.6345	3.5512	3.4875	3.4239	3.3590
15	3.2	2.95	3.1185	3.0433	2.9883	2.9283	2.8601	2.8078	2.7591	2.7124
16	2.25	2	2.2287	2.1905	2.1547	2.1057	2.0637	2.0198	1.9794	1.9391
17	1.4	1.1	1.3771	1.3540	1.3287	1.2901	1.2610	1.2298	1.1988	1.1607
18	0.75	0.4	0.7165	0.6670	0.6365	0.5967	0.5666	0.5394	0.5077	0.4678
19	0.35	0	0.2832	0.1954	0.1398	0.0883	0.0489	0.0089	-0.0444	-0.0935
20	0.1	-0.35	0.0074	-0.1021	-0.1669	-0.2235	-0.2794	-0.3598	-0.4288	-0.4920
21	0	-0.45	-0.1749	-0.2306	-0.2964	-0.3527	-0.4250	-0.5569	-0.6223	-0.7040
22	0.1	-0.5	-0.0976	-0.1622	-0.2528	-0.3240	-0.4126	-0.5444	-0.6314	-0.7359
23	0.35	-0.3	0.1982	0.0528	-0.0562	-0.1600	-0.2677	-0.3712	-0.4982	-0.6137
24	0.75	-0.1	0.5011	0.3850	0.2720	0.1321	0.0103	-0.1151	-0.2553	-0.3703
25	1.4	0.2	1.0676	0.8851	0.7403	0.5639	0.4139	0.2287	0.0898	-0.0441
26	2.25	0.6	1.9335	1.6059	1.3682	1.1322	0.9150	0.7005	0.5257	0.3553
27	3.2	1.1	2.8301	2.4594	2.1235	1.8195	1.5272	1.2760	1.0484	0.8427
28	3.9	1.6	3.6156	3.2645	2.9127	2.5774	2.2597	1.9396	1.6615	1.4062
29	4.5	2.05	4.2086	3.8864	3.6109	3.2917	2.9919	2.6504	2.3291	2.0279
30	4.8	2.55	4.6050	4.3456	4.1451	3.8729	3.5974	3.2998	2.9709	2.6509
31	5.05	3.1	4.8680	4.6735	4.5041	4.2979	4.0678	3.8398	3.5469	3.2398
32	5.15	3.5	4.9995	4.8471	4.7081	4.5562	4.3947	4.2260	4.0036	3.7572
33	5.05	3.9	4.9635	4.8626	4.7588	4.6352	4.5334	4.3935	4.2438	4.0812
34	4.8	4	4.7662	4.6945	4.6250	4.5274	4.4559	4.3244	4.2288	4.1315
35	4.5	3.9	4.4126	4.3396	4.2725	4.2010	4.1411	4.0370	3.9660	3.9014
36	3.9	3.6	3.8444	3.7755	3.6974	3.6415	3.5945	3.5287	3.4760	3.4264
37	3.2	2.9	3.0677	3.0204	2.9684	2.9282	2.8957	2.8587	2.8268	2.7899
38	2.25	2.1	2.2459	2.2413	2.2371	2.2119	2.1882	2.1715	2.1500	2.1196
39	1.7	1.45	1.6818	1.6559	1.6446	1.6294	1.6012	1.5810	1.5610	1.5134
40	1.45	1.05	1.3953	1.3224	1.2701	1.2286	1.1807	1.1337	1.0943	1.0326
41	1.3	0.7	1.2382	1.1332	1.0349	0.9472	0.8602	0.7733	0.6956	0.6414
42.2	1	0.45	0.9956	0.9911	0.9686	0.9206	0.9163	0.9124	0.9080	0.9039



**Table I.3** Data of simulated profiles of lifters used in tumbling mills at Eskom Matimba power station (the unworn lifter is used as reference and measurement are in cm)

	Simulated profiles						
	unworn	1	2	3	4	5	6
0	1	0.981	0.931	0.868	0.819	0.774	0.741
1	0.964	0.930	0.890	0.836	0.776	0.708	0.638
2	0.927	0.903	0.868	0.829	0.765	0.698	0.637
3	0.891	0.870	0.850	0.815	0.772	0.725	0.673
4	0.855	0.823	0.791	0.763	0.729	0.690	0.650
5	0.818	0.763	0.718	0.666	0.616	0.580	0.544
6	0.782	0.736	0.700	0.647	0.583	0.529	0.477
7	0.745	0.727	0.705	0.663	0.599	0.536	0.489
8	0.709	0.691	0.673	0.648	0.606	0.562	0.524
8.5	0.691	0.674	0.653	0.633	0.599	0.569	0.536
9	0.673	0.655	0.636	0.623	0.589	0.573	0.540
9.25	0.664	0.645	0.628	0.620	0.586	0.572	0.540
9.5	0.655	0.637	0.628	0.618	0.586	0.571	0.542
9.75	0.645	0.633	0.625	0.617	0.589	0.574	0.544
10	0.636	0.630	0.625	0.616	0.595	0.582	0.549
10.25	0.627	0.627	0.620	0.615	0.602	0.590	0.552
10.5	0.618	0.618	0.618	0.618	0.609	0.598	0.555
10.75	0.609	0.609	0.609	0.609	0.609	0.609	0.564
11	0.6	0.6	0.6	0.6	0.6	0.6	0.6
11.2	0.943	0.943	0.943	0.918	0.758	0.704	0.704
11.4	1.286	1.205	1.126	1.075	0.930	0.848	0.820
11.65	1.714	1.539	1.384	1.283	1.148	1.051	0.978
11.9	2.143	1.892	1.674	1.519	1.379	1.263	1.158
12.15	2.571	2.259	1.987	1.784	1.626	1.496	1.367
12.4	3	2.595	2.302	2.063	1.889	1.744	1.603
12.65	3	2.790	2.558	2.326	2.154	2.000	1.859
12.9	3	2.900	2.745	2.557	2.399	2.248	2.111
13.15	3	2.953	2.865	2.732	2.602	2.467	2.334
13.4	3	2.975	2.926	2.845	2.751	2.640	2.520
13.65	3	2.981	2.951	2.910	2.848	2.759	2.664
13.9	3	2.980	2.960	2.937	2.902	2.832	2.765
14.15	3	2.975	2.958	2.940	2.922	2.873	2.828
14.4	3	2.970	2.953	2.934	2.922	2.887	2.856
14.9	3	2.962	2.945	2.912	2.897	2.876	2.850
15.4	3	2.959	2.936	2.889	2.867	2.844	2.815
16.4	3	2.958	2.921	2.868	2.820	2.785	2.752
17.4	3	2.960	2.925	2.883	2.824	2.769	2.710
18.4	3	2.963	2.938	2.852	2.805	2.769	2.726
19.4	3	2.968	2.944	2.886	2.840	2.790	2.748
20.4	3	2.964	2.936	2.910	2.858	2.818	2.775
20.9	3	2.952	2.923	2.903	2.863	2.828	2.789
21.4	3	2.943	2.911	2.895	2.860	2.833	2.796
21.65	3	2.943	2.910	2.890	2.857	2.830	2.796
21.9	3	2.950	2.914	2.887	2.857	2.827	2.796
22.15	3	2.961	2.922	2.889	2.859	2.825	2.794
22.4	3	2.973	2.933	2.895	2.860	2.822	2.787
22.65	3	2.981	2.937	2.895	2.851	2.811	2.772
22.9	3	2.975	2.922	2.870	2.817	2.777	2.735
23.15	3	2.933	2.861	2.798	2.734	2.698	2.656
23.4	3	2.805	2.712	2.652	2.582	2.553	2.517
23.65	2.571	2.502	2.446	2.410	2.351	2.332	2.302
23.9	2.143	2.117	2.096	2.078	2.044	2.028	2.012
24.15	1.714	1.703	1.696	1.690	1.677	1.667	1.662
24.4	1.286	1.280	1.275	1.275	1.275	1.275	1.275
24.6	0.943	0.943	0.943	0.943	0.943	0.943	0.943
24.8	0.6	0.6	0.6	0.6	0.6	0.6	0.6
25.05	0.609	0.609	0.609	0.609	0.609	0.609	0.609
25.3	0.618	0.618	0.618	0.618	0.618	0.618	0.618
25.55	0.627	0.627	0.627	0.616	0.606	0.596	0.590
25.8	0.636	0.629	0.613	0.601	0.587	0.574	0.559
26.05	0.645	0.631	0.601	0.580	0.563	0.548	0.526
26.3	0.655	0.635	0.591	0.565	0.542	0.522	0.492
26.55	0.664	0.641	0.592	0.559	0.530	0.505	0.464
26.8	0.673	0.651	0.605	0.563	0.529	0.492	0.442
27.3	0.691	0.676	0.640	0.592	0.536	0.474	0.418
27.8	0.709	0.697	0.668	0.632	0.558	0.490	0.427
28.8	0.745	0.723	0.698	0.669	0.621	0.560	0.509
29.8	0.782	0.749	0.733	0.675	0.643	0.602	0.557
30.8	0.818	0.762	0.709	0.650	0.603	0.559	0.517
31.8	0.855	0.813	0.752	0.692	0.634	0.556	0.502
32.8	0.891	0.879	0.859	0.807	0.734	0.659	0.590
33.8	0.927	0.907	0.889	0.862	0.804	0.739	0.693
34.8	0.964	0.941	0.918	0.887	0.856	0.804	0.763
35.8	1.000	0.971	0.948	0.940	0.911	0.877	0.836

## Appendix J

### Difference between the predicted volume removed and the volume effectively removed on discretised lifter divisions

#### 1. Introduction

Using a 2D discretisation of lifter, the predicted volume removed on a discretised lifter division  $i$  is given by Equation (4.6):

$$V_i = W(a_{ad-abr} * E_{ad-abr,i} + a_{impact} * E_{impact,i}) \quad (J.1)$$

The volume effectively removed (2D vertical discretisation of lifter, Figure 4.7) on that discretised lifter is given by:

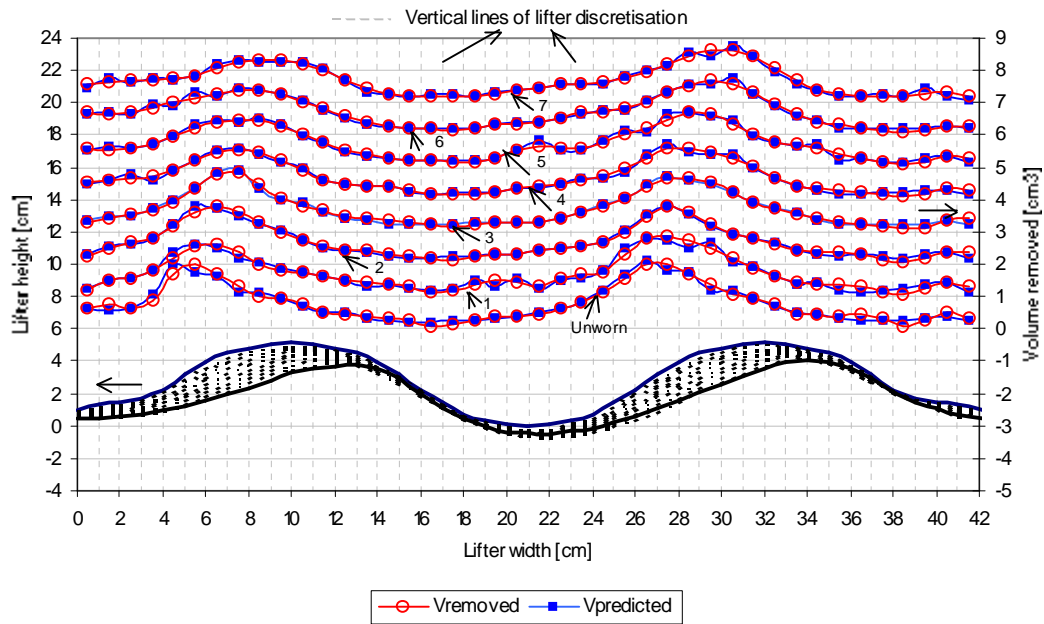
$$V'_i = \left( \frac{(y_i - y'_i) + (y_{i+1} - y'_{i+1})}{2} \right) \Delta x_i L \quad (J.2)$$

Since the removal of material on discretised lifter divisions is performed via an objective function (Equation 4.15), there is a difference between volumes removed predicted and effectively removed.

#### 2. Lifter used in tumbling mills at Lethabo power station

**Table J.1** Difference in percentage (%) between the total volume removed predicted and effectively removed at each step (double wave lifter used at Lethabo power station).

	% Difference
Unworn	0.81
Simulated 1	-0.08
Simulated 2	0.43
Simulated 3	0.13
Simulated 4	-0.13
Simulated 5	-0.01
Simulated 6	-0.08
Simulated 7	-0.11



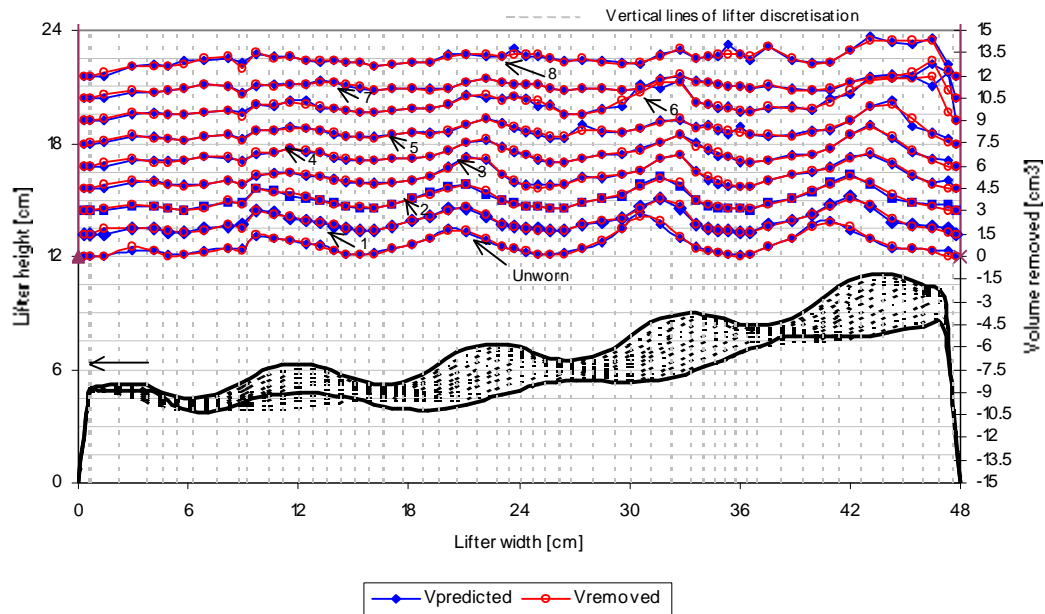
**Figure J.1** Difference of volume removed predicted and effectively removed at each step on different discretised lifter divisions (Lifter used at Lethabo power station)

Table J.1 gives the difference at each step while Figure J.1 shows the difference at each step on each discretised lifter division. The difference is not significant.

### 3. Lifter used in tumbling mills at Kendal power station

**Table J.2** Difference in % between the total volume removed predicted and effectively removed at each step (Lifter used at Kendal power station)

	% Difference
Unworn	1.8
Simulated 1	-0.06
Simulated 2	0.61
Simulated 3	2.32
Simulated 4	0.2
Simulated 5	0.09
Simulated 6	3.62
Simulated 7	2.35
Simulated 8	1.2



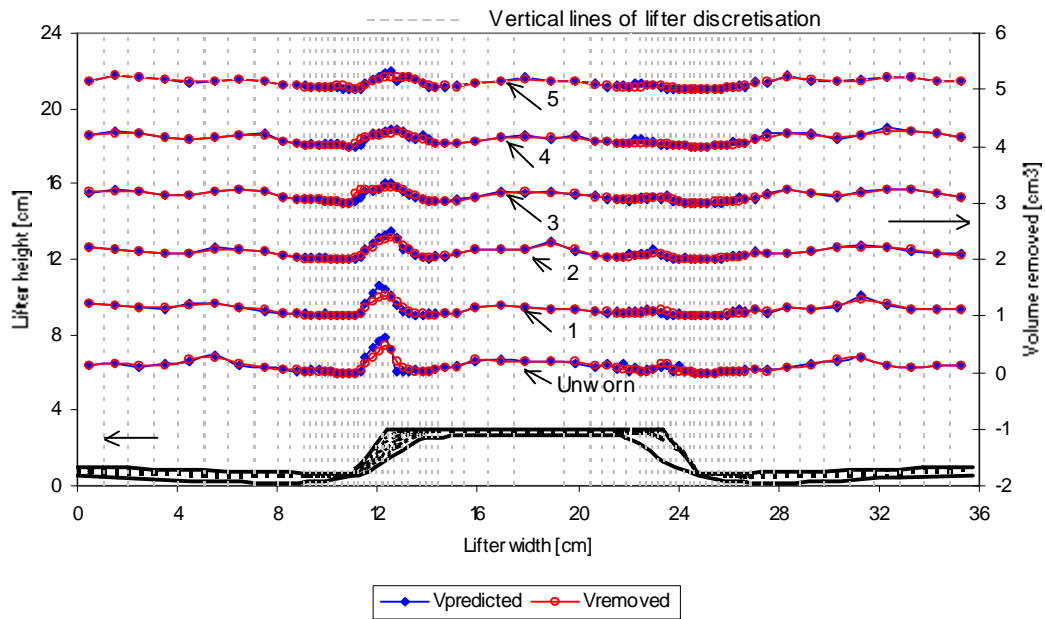
**Figure J.2** Difference of volume removed predicted and effectively removed at each step on different discretised lifter divisions (Lifter used at Kendal power station)

Table J.2 gives the difference at each step between the total volume removed predicted and effectively removed. Figure J.2 shows the difference at each step on each discretised lifter division for the lifter used at Kendal power station.

#### 4. Lifters used in tumbling mills at Matimba power station

**Table J.3** Difference in percentage (%) between the total volume removed predicted and effectively removed at each step (Lifter used at Matimba power station).

	% Difference
Unworn	5.6
Simulated 1	6.21
Simulated 2	8.21
Simulated 3	-3.69
Simulated 4	5.75
Simulated 5	1.61



**Figure J.3** Difference of volume removed predicted and effectively removed at each step on different discretised lifter divisions (Lifter used at Matimba power station)

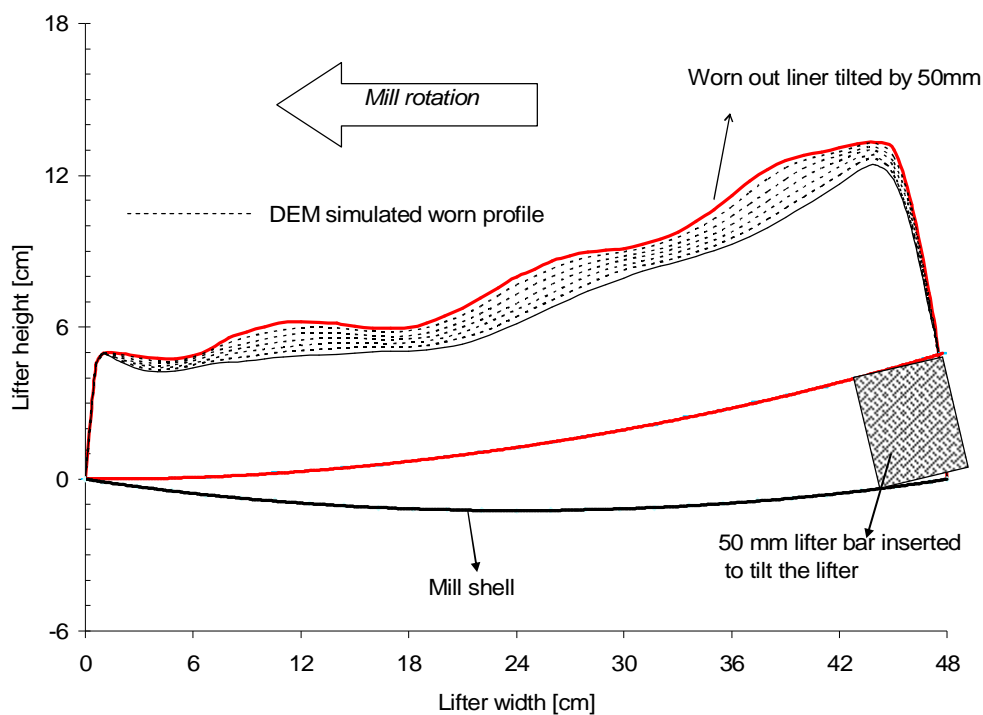
Table J.3 gives the difference at each step between the total volume removed predicted and effectively removed. Figure J.3 shows the difference at each step on each discretised lifter division.

## Appendix K: DEM simulated worn profiles beyond tilting the worn lifter by 50 mm in tumbling mills at ESKOM Kendal power station

### 1. Introduction

To evaluate the performance of tumbling mills used at Kendal power station beyond tilting the lifter by 50 mm, DEM simulations were conducted to firstly predict the lifter wear and secondly to compare the load behaviour.

### 2. Simulated lifter profile beyond tilting the lifter by 50 mm



**Figure K.1** DEM simulated worn profiles beyond tilting the worn lifter by 50 mm in tumbling mills at ESKOM Kendal power station

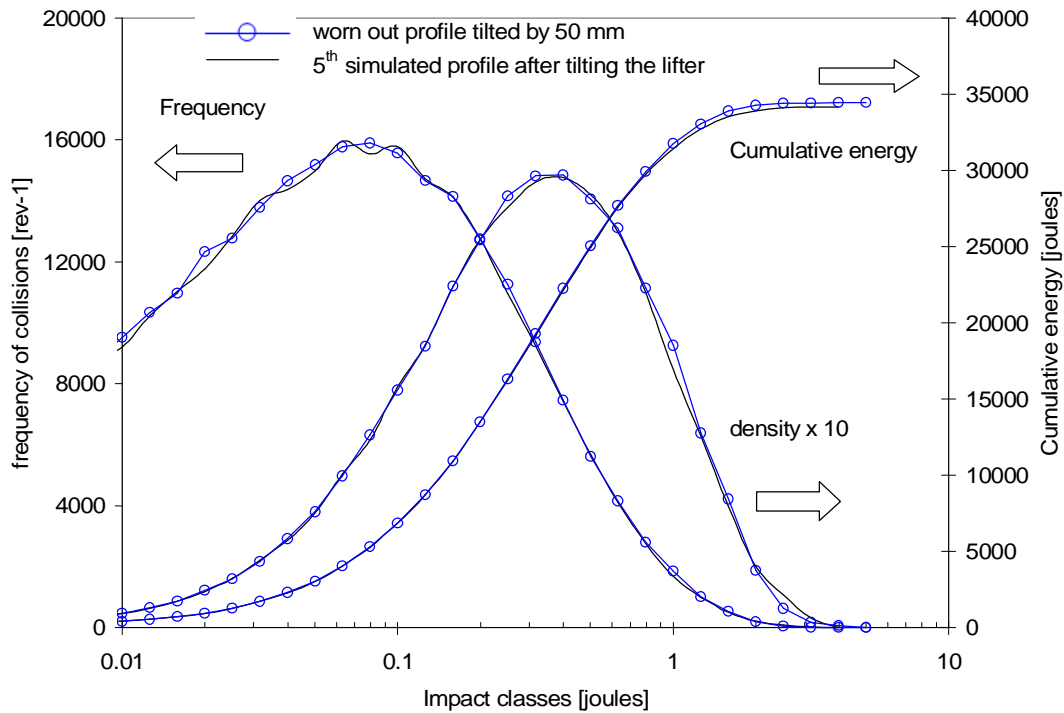
It can be seen from Figure K.1 that the profile does not change dramatically. The thickness of the lifter between 18 and 24 cm decreases considerably.



### 3. Comparison of DEM impact energy spectra

Figure K.2 shows the comparison between the impact energy spectra of the worn out lifter tilted by 50 mm (~ 80 000 hours) and the 5<sup>th</sup> simulated lifter which correspond to approximately 130 000 hours. The percentage filling used was 15.5 %.

It can be seen from Figure K.2 that the impact energy spectra are similar.



**Figure K.2** Comparison of impact energy spectra beyond tilting the worn lifter used at Kendal power station by 50 mm

### 4. Conclusion

Simulations to predict the wear of lifter and load behaviour beyond tilting lifters by 50 mm in tumbling mills at Kendal power station were conducted. The simulated profiles and load behaviour show that the thickness of the lifter will be the limiting factor since the load behaviour are similar beyond tilting the lifters.

# Appendix L:

## DEM contribution to the prediction of ball wear

### 1. Reasons of predicting the wear of balls

The wear of balls in tumbling mills is a substantial fraction of the total running cost in mineral processing plants using balls as grinding media. Improving our understanding of the wear of balls and deriving mathematical equation predicting the wear of balls is therefore of great economic significance. The prediction of the wear of balls will contribute also to:

- determine the optimum equilibrium ball mixture in tumbling mills.
- chose the optimum make-up balls size which gives a correct equilibrium ball mix producing an optimum throughput as a function of operating conditions.
- maintain the correct ball charge in tumbling mills.

### 2. Ball wear prediction

Bond (1964) developed, from laboratory experiments and available plant data, the following equations which relate the ball charge mass lost per kilowatt-hour of mill energy consumed:

$$\frac{\text{Wear}}{\text{energy}} = 0.159(A_i - 0.015)^{0.33} \quad [\text{Kg/kWh}] \quad (\text{L.1})$$

For dry milling, Bond derived the following equation:

$$\frac{\text{kg}}{\text{kWh}} = 0.023A_i^{0.5} \quad (\text{L.2})$$

where  $A_i$  is the Bond abrasion index.

Austin et al(1984) developed the following formula to predict the wear of balls of different diameter.

$$f(r) = k r_b 4 p r^{2+\Delta} \quad (\text{L.3})$$

where

$r$  is the ball radius

$\rho_b$  is the ball density

and  $\Delta$  is a parameter

$\Delta = 0$  : the wear is proportional to the surfaces of balls

$\Delta = 1$  : the wear is proportional to the balls

Based on tests from different ores and milling conditions, Radziszewski (2002) shows that predictions using Bond equation have an average error of 73% with a standard deviation of 192.5%. The difference observed can be explained by the fact that the main mechanism of ball charge wear in Bond's tests is abrasion. At the time Bond equations were derived, tumbling mills diameter were not high to produce high impact energy events in these mills.

Balls wear due to not only abrasion but also impact and corrosion occurring in milling environment. In dry milling environment, abrasion and impact are the main mechanism of the ball charge wear.

Since the DEM can predict the ball charge energy dissipated in impact and abrasion, it can therefore be used to predict the wear of the mill ball charge.

Using the same approach as in the prediction of the wear of lifters, we can assume that the volume lost by a ball  $b$  of size  $i$  is given by the following equation:

$$V_{b,i} = W \left( a_{\text{impact}} E_{\text{impact},i} + a_{\text{ad-fr}} E_{\text{ad-abr},i} \right) \quad (\text{L.4})$$

where

$V_{b,i}$  is the volume lost by a ball  $b$  of size  $i$

$W$  is the wear rate

$E_{\text{impact},i}$  is the impact energy dissipated by the ball  $b$  of size  $i$

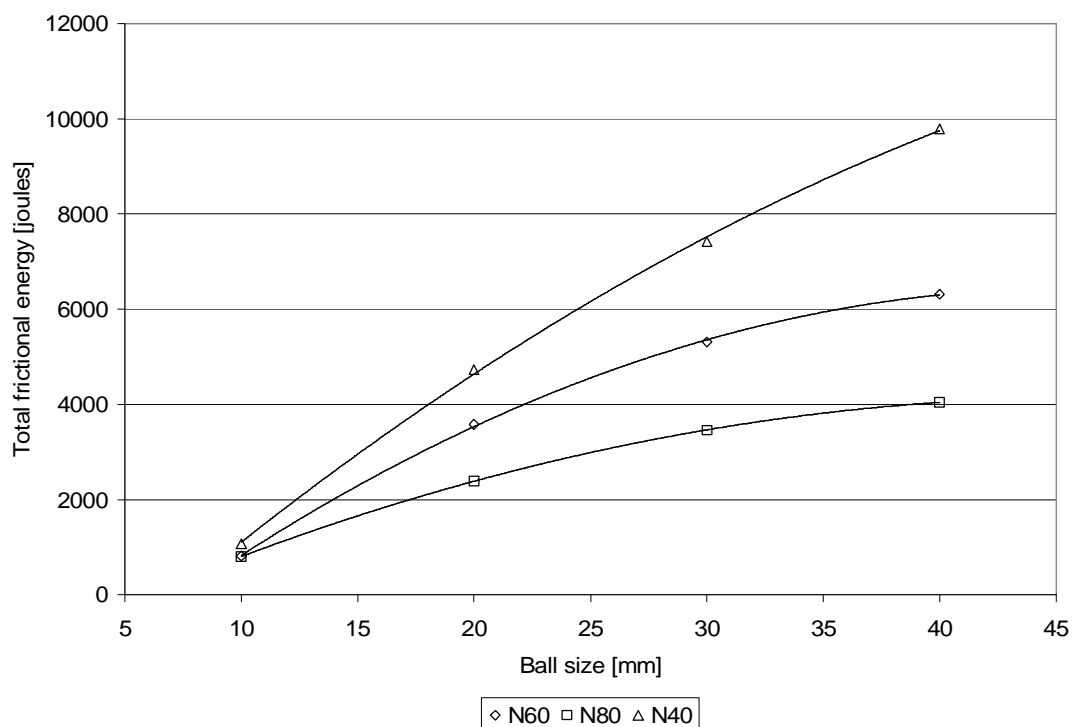
$E_{\text{ad-abr},i}$  is the frictional energy dissipated by the ball  $i$

$a_{\text{impact}}$  and  $a_{\text{ad-abr}}$  are weight factor given to impact or abrasion energies dissipated.

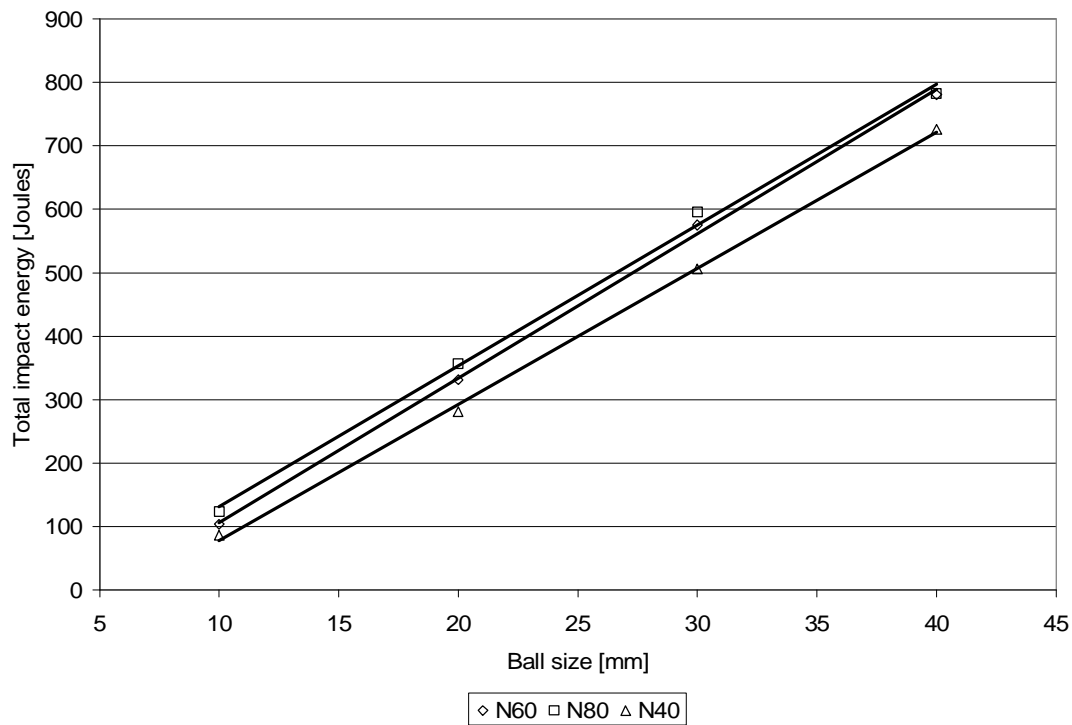
### 3. DEM contribution to the prediction of ball wear

Results obtained in investigating the increase of ball wear rate in tumbling mills at Kendal power station (Chapter 8) after tilting the worn out lifter by 50 mm indicate that the DEM can be used to predict the wear of lifters since predicted results are in agreement with observation at the plant.

Further DEM simulations were conducted in a mill of 600 mm of diameter and a length of 485 mm. The mill was filled at 30% with 4 ball size: 40, 30, 20 and 10 mm. Equal number of balls was used in all simulations. Three mill speed were used: 40 , 60 and 80 % of critical speed. The variation of total impact and abrasion/frictional energies dissipated in collisions between balls and between balls and lifters are represented in Figures L.1 and L.2.



**Figure L.1** Total frictional energy dissipated as a function of ball size at different mill speed in a mill of 600 mm of diameter filled at 30%

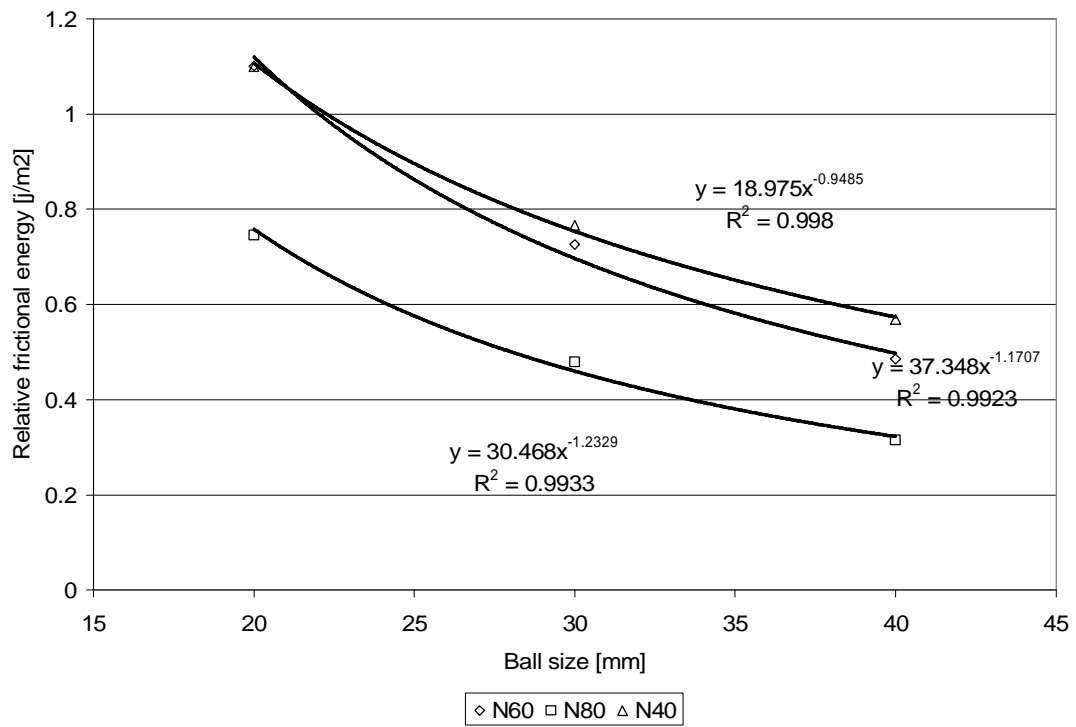


**Figure L.2** Total impact energy dissipated as a function of ball size at different mill speed in a mill of 600 mm of diameter filled at 30%

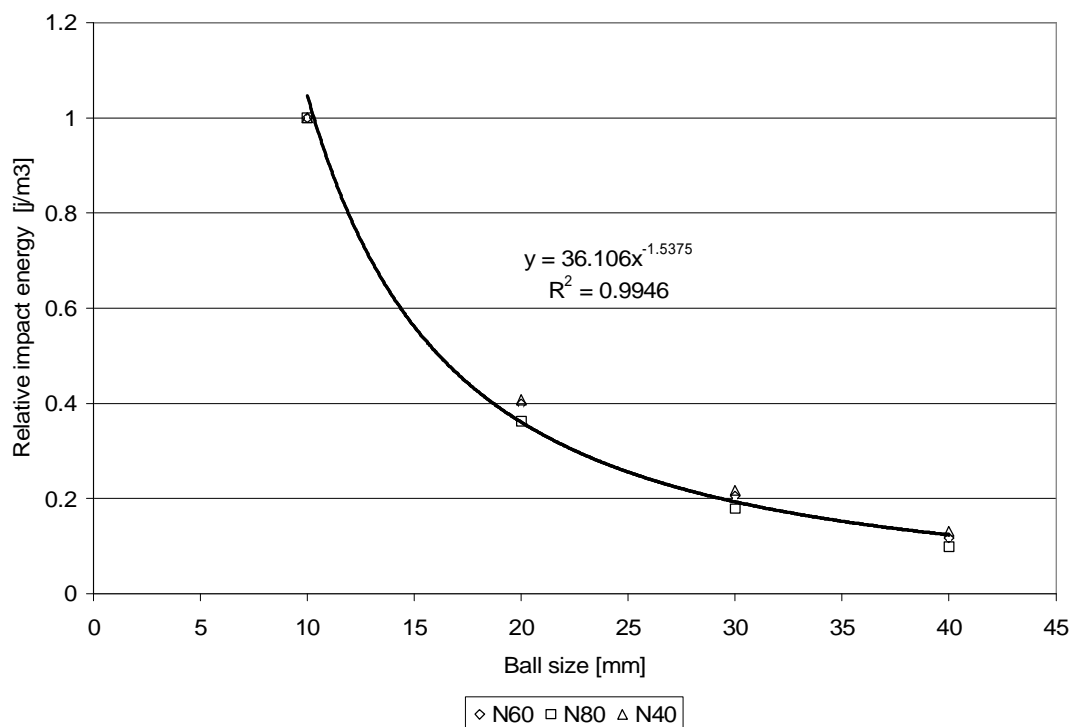
It can be seen from Figure L.1 that the frictional energy is higher at low speed. This is due to the cascading motion of balls which create much friction at low speed. Increasing the mill speed decreases the total frictional energy dissipated in the mill. At each speed, the total frictional energy dissipated in the mill increases as the ball size increases due to a higher surface exposed per ball. Figure L.1 shows also that the total frictional energy dissipated for balls of 10mm is similar at different speed.

It can be seen from Figure L.2 that the total impact energy dissipated in the mill increases by increasing the mill speed. This is due to high impact energy events occurring as the mill speed increases. At each speed, the total impact energy dissipated increases with increasing the ball size due to a higher volume (or mass) per ball.

To eliminate the effect of surface and volume in respectively the frictional and impact energies dissipated in the mill, relative energies were used.



**Figure L.3** Relative frictional energy per unit of ball surface



**Figure L.4** Relative impact energy per unit of ball volume

Figure L.3 shows the relative frictional energy per unit of ball surface. Different equations linking the frictional energy dissipated and the ball size can be derived as a function of mill speed.

Figure L.4 shows the relative impact energy per unit of ball volume. It can be seen that a single equation can fit all the data at different speed.

The impact energy at different speed is therefore proportional to:

$$E_{impact} \cong kd^{1.4625}$$

with d the ball diameter

#### **4. Conclusion**

DEM simulations conducted show a great potential in the prediction of ball wear as a function of tumbling mills operating conditions. The same general equation used to predict the wear of lifters can be used to predict the wear of balls. Parameter delta in the Austin et al (1984) equation (Equation L.3) can be derived since the total impact and frictional (abrasion) energy dissipated in the mill can be determined per ball size in DEM simulations.

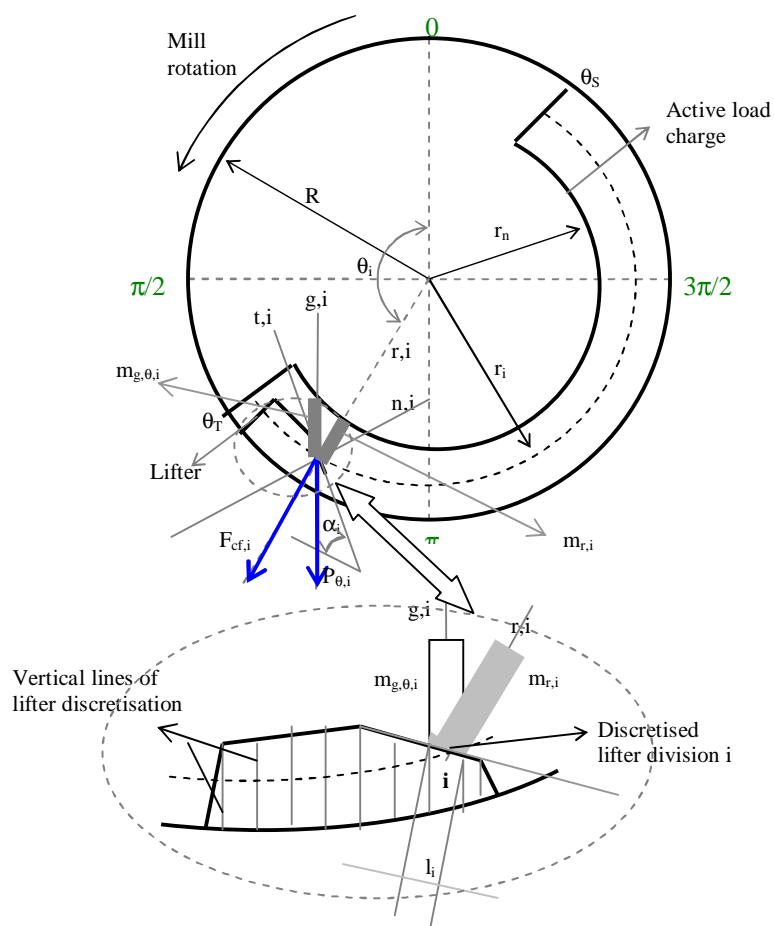
Experimental results are required to validate the approach presented.

## Appendix M:

# Development of abrasive wear model in dry tumbling mills

### 1 Introduction

Lifters wear by abrasion/adhesion as a result of the relative motion between the mill charge and mill lifters.



**Figure M.1** Description of load behaviour and centrifugal and gravitational forces exerted on a discretised lifter division  $i$  at the mill position  $\theta_i$  (the size of the lifter relative to the mill has been exaggerated to increase legibility)



Gravitational and centrifugal forces are exerted by the mill charge on lifters during mill revolutions. Figure M.1 illustrates the gravitational and centrifugal forces exerted on a discretised lifter division  $i$  on one lifter at the mill position  $\theta_i$ .

## 2. Centrifugal forces

Centrifugal forces are always exerted in the radial direction  $r,i$ .

The centrifugal force exerted on a discretised lifter division  $i$  at the mill position  $\theta_i$  as illustrated by Figure M.1 is expressed by:

$$F_{cf,q_i,i} = m_{r,i} \omega_l^2 r_{c,mr} \quad (\text{M.1})$$

It can be demonstrated that:

$$r_{c,mr} = \frac{r_i + r_n}{2} \quad (\text{M.2})$$

The mass  $m_{r,i}$  of the active charge exerted on the discretised lifter division  $i$  in the radial direction is given by:

$$m_{r,i} = Ll_i (r_i - r_n) r_{b,r,q_i} \cos \alpha_i \quad (\text{M.3})$$

We assume that the bulk density of the charge in the radial and gravitational direction at any mill position  $\theta_i$  is the same. Therefore  $r_{b,r,q_i} = r_b$

Using Morrel's description of load behaviour, as shown by equations M.1 to M.3, the centrifugal force is not a function of the mill position angle  $q_i$ . For a particular discretised lifter division, it has therefore a constant value from the toe to the shoulder.

From simple geometry (Morrel, 1993), it can be demonstrated that:

$$r_n = R \left( 1 - \frac{2pbJ}{q_s - q_T} \right)^{0.5} \quad (\text{M.4})$$

The centrifugal force exerted on the discretised lifter division  $i$  in the normal direction  $(n,i)$  to  $i$  is given by:

$$F_{n,cf,i} = F_{cf,i} \cos a_i \quad (\text{M.5})$$

Archard's abrasion equation applied to the discretised lifter division  $i$  due to the centrifugal forces for a mill rotation of  $dq_i$  is given by:

$$dV_{c,i} = \frac{KF_{n,cf,i} dS_i}{H} \quad (\text{M.6})$$

The sliding distance can be approximate by:

$$dS_i \cong q_i r_i dq_i \quad (\text{M.7})$$

with  $q_i$  the probability of abrasion events to occur on a discretised lifter division  $i$  during a mill rotation  $dq_i$ .  $q_i$  is a function of mill charge composition, lifter profile discretised lifter angle and height.

$$\text{Considering that } W = \frac{K}{H} \quad (\text{M.8})$$

The volume removed during one revolution due to centrifugal forces on the discretised lifter division  $i$  is given by:

$$V_{c,i} = \int_{q_r}^{q_s} \left( \frac{W}{2} q_i L l_i r_i \left( r_i^2 - R^2 \left( 1 - \frac{2pbJ}{q_s - q_T} \right) \right) r_b w_l^2 \cos^2 a_i \right) dq_i \quad (\text{M.9})$$

$$V_{c,i} = \frac{W}{2} L q_i l_i r_i \left( r_i^2 - R^2 \left( 1 - \frac{2pbJ}{q_s - q_T} \right) \right) (q_s - q_T) r_b w_i^2 \cos^2 a_i \quad (\text{M.10})$$

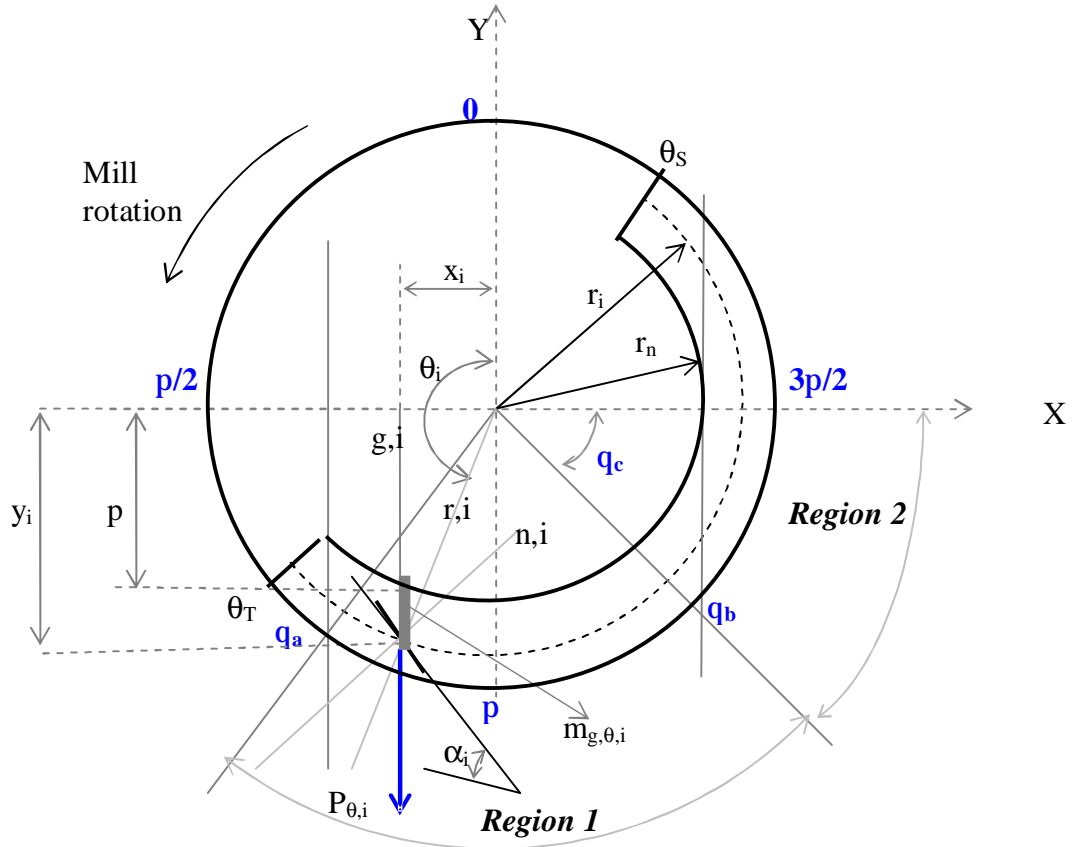
It can be seen from Equation M.10 that the volume removed on a discretised lifter division  $i$  due to centrifugal forces is influenced by mill dimensions (Diameter, length), mill operating conditions (mill filling, mill speed, shoulder and toe position), charge composition and lifter design (discretised lifter division angle and radial position in the mill or height).

### 3. Gravitational forces

The weight or gravitational force is always exerted in the gravitational direction (g,i). As illustrated by Figure M.2, the weight exerted on a discretised lifter division  $i$  at the mill position  $\theta_i$  is given by:

$$P_{q,i} = g * m_{g,q,i} \quad (\text{M.11})$$

It can be seen from Figure M.2 that the weight exerted on the discretised lifter division  $i$  is a function of the mill position angle  $q_i$  since  $m_{g,q,i}$  varies as a function of  $q_i$ .



**Figure M.2** Gravitational force exerted on a discretised lifter division  $i$  at the mill position  $\theta_i$

Based on observation of load behaviour in a laboratory ball mill, the mill was divided into 3 regions in order to derive gravitational forces. The first region start from  $\theta_a$  to  $\theta_b$ . The second region from  $\theta_b$  to  $3\pi/2$  and the last region from  $3\pi/2$  to  $\theta_s$ . We assume that in the first region ( $q_a \langle q_i \langle q_b$ ), the weight is exerted at the front ( $a_i \leq 90$ ) and at the back ( $a_i > 90$ ) of lifters. In the second region ( $q_b \langle q_i \langle \frac{3p}{2}$ ), the weight is exerted only at the front of the lifter or :

$$q_i = 0 \quad \text{for } q_b \langle q_i \langle \frac{3p}{2} \quad \text{when } a_i > 90$$

We assume that the gravitational force in the last region ( $\frac{3p}{2} \langle q_i \langle q_s$ ) is not very significant. In the present investigation we have developed equations for regions 1 and 2.

### 3.1 First region ( $q_a \langle q_i \langle q_b$ )

As illustrated by Figure M.2, at the mill position  $\theta_i$  (in the first region), the mass of the charge exerted on the discretised lifter division  $i$  in the gravitational direction  $g,i$  is expressed by:

$$m_{g,q,i} = Ll_i r_b (y_i - p) \cos(\mathbf{p} + \mathbf{a}_i - \mathbf{q}_i) \quad (\text{M.12})$$

The coordinates  $(x_i, y_i)$  of the centre of the discretised lifter division  $i$  are given by:

$$x_i = r_i \cos\left(\mathbf{q}_i - \frac{\mathbf{p}}{2}\right) \quad (\text{M.13})$$

$$y_i = r_i \sin\left(\mathbf{q}_i - \frac{\mathbf{p}}{2}\right) \quad (\text{M.14})$$

It can be demonstrated that:

$$x_i^2 + p^2 = r_n^2 \quad (\text{M.15})$$

Thus,

$$p = \left( r_n^2 - r_i^2 \cos^2\left(\mathbf{q}_i - \frac{\mathbf{p}}{2}\right) \right)^{\frac{1}{2}} \quad (\text{M.16})$$

Applying Equations (M.14) and (M.16) in (M.12) gives,

$$m_{g,q,i} = r_b Ll_i \left( r_i \sin\left(\mathbf{q}_i - \frac{\mathbf{p}}{2}\right) - \left( r_n^2 - r_i^2 \cos^2\left(\mathbf{q}_i - \frac{\mathbf{p}}{2}\right) \right)^{\frac{1}{2}} \right) \cos(\mathbf{p} + \mathbf{a}_i - \mathbf{q}_i) \quad (\text{M.17})$$

At the mill position angle  $\mathbf{q}_i = \mathbf{p}$ , the mass of the active charge acting on a discretised lifter division  $i$  due to centrifugal forces and due to weight are the same. Hence,

$$m_{r,i} = m_{g,q,i} \text{ when } \mathbf{q}_i = \mathbf{p} .$$

The weight exerted on the discretised lifter division  $i$  in the normal direction to  $i$  is given by:

$$P_{n,q,i} = P_{q,i} * \cos(a_i + p - q_i) \quad (\text{M.18})$$

Applying Archard's abrasion law on a discretised lifter division  $i$  due to the weight for a mill rotation of  $d\theta_i$  gives:

$$dV_{p,q,i} = WP_{n,q,i} dS_i \quad (\text{M.19})$$

Using equations (M.7), (M.11), (M.17), (M.18) in equation (M.19) we have:

$$dV_{p,q,i} = Wr_b g L l_i r_i \left( \cos^2(a_i + p - q_i) \left( r_i \sin(q_i - \frac{p}{2}) - \left( R^2 \left( 1 - \frac{2pbJ}{q_s - q_T} \right) - r_i^2 \sin^2 q_i \right)^{\frac{1}{2}} \right) \right) dq_i \quad (\text{M.20})$$

The volume removed on a discretised lifter division  $i$  due to gravitational forces in the first region for one revolution is given by:

$$V_{p,i} = Wr_b g L l_i r_i \int_{q_a}^{q_b} dq_i \cos^2(a_i + p - q_i) \left( r_i \sin(q_i - \frac{p}{2}) - \left( R^2 \left( 1 - \frac{2pbJ}{q_s - q_T} \right) - r_i^2 \sin^2 q_i \right)^{\frac{1}{2}} \right) dq_i \quad (\text{M.21})$$

–  $\theta_a$  calculations

The abscissas of the point A with reference to the inner circle of the active charge and the mill circle respectively are given by:

$$X_A = r_n \cos(q_T - \frac{p}{2}) \quad (\text{M.22})$$

and,

$$X_A = R \cos(q_a - \frac{p}{2}) \quad (\text{M.23})$$

From equations (M.22) and (M.23) we have:

$$q_a = \frac{p}{2} + \arccos\left(\frac{r_n}{R} \cos\left(q_T - \frac{p}{2}\right)\right) \quad (\text{M.24})$$

or,

$$q_a = \frac{p}{2} + \arccos\left(\left(1 - \frac{2pbJ}{q_s - q_T}\right)^{0.5} \cos\left(q_T - \frac{p}{2}\right)\right) \quad (\text{M.25})$$

–  $\theta_b$  Calculations

$$\tan q_c = \frac{\sqrt{R^2 - r_n^2}}{r_n} \quad (\text{M.26})$$

$$q_c = \arctan\left(\frac{2pbJ}{(q_s - q_T)^{0.5}(q_s - q_T - 2pbJ)^{0.5}}\right) \quad (\text{M.27})$$

$$q_b = \frac{3p}{2} - q_c \quad (\text{M.28})$$

$$q_b = \frac{3p}{2} - \arctan\left(\frac{2pbJ}{(q_s - q_T)^{0.5}(q_s - q_T - 2pbJ)^{0.5}}\right) \quad (\text{M.29})$$

### 3.2 Second region ( $q_b < q_i < \frac{3p}{2}$ )

In the second region, based on load behaviour observation and DEM simulations, we assume that the weight on discretised lifter division is exerted only at the front of lifters.

From Figure M.2, it can be demonstrated that:

$$x_i^2 + y_i^2 = r_i^2 \quad (\text{M.30})$$

and,

$$\tan q_i = \frac{y_i}{x_i} \quad (\text{M.31})$$

From (M.30) and (M.31) we have:

$$x_i = \frac{r_i}{\sqrt{1 + \tan^2 q_i}} \quad (\text{M.32})$$

and,

$$y_i = \frac{r_i \tan q_i}{\sqrt{1 + \tan^2 q_i}} \quad (\text{M.33})$$

In the second region, the mass of load charge exerted in the gravitational direction on a discretised lifter division  $i$  is given by:

$$m_{g,q,i} = 2r_b L l_i r_i \frac{\tan q_i}{\sqrt{1 + \tan^2 q_i}} \cos(p + a_i - q_i) \quad (\text{M.34})$$

or,

$$m_{g,q,i} = 2r_b L l_i r_i \sin q_i \cos(p + a_i - q_i) \quad (\text{M.35})$$

At the mill position  $\theta_i = \theta_c$ ,  $m_{g,\theta,i}$  in the first and second region are equal

Applying (M.35), (M.7), (M.18) in (M.19), we have:

$$dV_{p,q,i} = W r_b g q_i L l_i r_i^2 \sin q_i \cos^2(a_i + p - q_i) dq_i \quad (\text{M.36})$$

Applying this equation to the second region  $\theta_c < \theta < \frac{3p}{2}$  gives:



$$V_{p,q,i} = WR_b g L l_i r_i^2 \int_{q_c}^{3p/2} q_i \sin q_i \cos^2(a_i + p - q_i) dq_i \quad (\text{M.37})$$

### 3.3 Total adhesive-abrasive wear

The total wear on a discretised lifter division  $i$  for one revolution due to abrasion-adhesion is the sum of the contribution of wear due to centrifugal (Equation M.10) and gravitational forces (Equation M.21 and M.37).

$$V_{ad-abr,i} = (V_{c,i} + V_{p,i}) \quad (\text{M.38})$$

## 4. Conclusions

Developed equations indicate that many parameters are required to predict the volume of material removed on a discretised lifter division due to abrasion. Since in our investigations on wear of lifters used at Eskom power stations, it was found that impact energies play a major role, this study was not pursued further. The developments presented give a foundation for future work.

## Nomenclature

$R$  is the mill radius, m

$r_i$  is the distance from the mill center to the discretised lifter division  $i$ , m

$r_n$  is the inner radius of the active load charge, m

$L$  is the effective mill length, m

$l_i$  is the length of the discretised lifter division  $i$ , m

$\alpha$  is an impact angle, rad

$\alpha_i$  is the angle of the discretised lifter division  $i$ , rad

$\alpha_i^*$  is the angle of the discretised lifter division  $i$  located at the back of the lifter, rad

$\theta_S$  is the mill shoulder angle, rad

$\theta_T$  is the mill toe angle, rad

$\theta_i$  is the mill position angle of the discretised lifter division  $i$ , rad

$\rho_b$  is the bulk density of the active charge,  $\text{kgm}^{-3}$

$V$  is the volume of material removed on a surface,  $\text{m}^3$

$V_i$  is the volume of material removed on the discretised lifter division  $i$ ,  $\text{m}^3$

$V_{c,i}$  is the volume of material removed on the discretised lifter division  $i$  due to centrifugal forces exerted on it,  $\text{m}^3$

$V_{p,i}$  is the volume of material removed on the discretised lifter division  $i$  due to the weight of the load,  $\text{m}^3$

$V_{q,i}$  is the volume of material removed on the discretised lifter division  $i$  at the mill angle  $\theta$ ,  $\text{m}^3$

$n,i$  is the normal direction to the discretised lifter division  $i$ , -

$t,i$  is the tangential direction to the discretised lifter division  $i$ , -

$g,i$  is the gravitational direction to the discretised lifter division  $i$ , -

$r,i$  is the radial direction to the discretised lifter division  $i$ , -

$S_i$  is the sliding distance on the discretised lifter division  $i$ , m

$W$  is the wear rate

$N$  is the mill speed,  $\text{rev min}^{-1}$

$\omega$  is the angular velocity of the mill,  $\text{rad s}^{-1}$

$\omega_i$  is the angular velocity of the mill charge,  $\text{rad s}^{-1}$

$H$  is the hardness of the lifter

$K$  is the coefficient of wear, -

$k$  is the maximum particle velocity at which collision between lifter and particles in the mill charge is purely elastic,  $\text{ms}^{-1}$

$k_i$  are constant, -

$F_{cf,i}$  is the centrifugal force exerted on a discretised lifter division  $i$ , N

$F_{n,cf,i}$  is the component of  $F_{cf,i}$  exerted in the normal direction to the discretised lifter division, N

$v_i$  is the tangential speed of the discretised lifter division  $i$ ,  $m s^{-1}$

$v_{t,i}$  is the component of  $v_i$  in the tangential direction to  $i$ ,  $m s^{-1}$

$v_{n,i}$  is the component of  $v_i$  in the normal direction to  $i$ ,  $m s^{-1}$

$v_{z,i}$  is the tangential speed of the charge layer  $z$  belonging to the discretised lifter division  $i$ ,  $m s^{-1}$

$v_{n,z,i}$  is the component of  $v_{z,i}$  in the normal direction to  $i$ ,  $m s^{-1}$

$v_{t,z,i}$  is the component of  $v_{z,i}$  in the tangential direction to  $I$ ,  $m s^{-1}$

$m_{r,i}$  is the mass of the active charge exerted on the discretised lifter division  $i$  in the radial direction, Kg

$m_{g,i}$  is the mass of the active charge exerted on the discretised lifter division  $i$  in the gravitational direction, Kg

$m_{g,\theta,i}$  is the mass of the active charge exerted on the discretised lifter division  $i$  in the gravitational direction at the mill angle  $\theta_i$ , Kg

$g$  is the acceleration due to gravity,  $m s^{-2}$

$P_{q,i}$  is the weight exerted on a discretised liner division  $i$  at the mill angle  $\theta$ , N

$E_{i,z}$  is the impact energy dissipated on a discretised lifter division  $i$  belonging to a layer  $z$ , J

$(x_i, y_i)$  are the coordinates of the discretised lifter division  $i$

$J$  is the percentage of mill filling, -

$b$  is the proportion of  $J$  which constitutes the active charge, -

$q$  is the probability of abrasion events during the mill revolution,  $q$  is a function of  $\theta_i$  and  $\alpha_i$

$r_{c,mr}$  is the distance from the mill center to the center of mass of  $m_{r,i}$

## References

Agrawala, S., Rajamani, R.K., Songfack, P. and Mishra, B.K., 1997, Mechanics of media motion in tumbling mills with 3D Discrete Element Method, *Minerals Engineering*, Vol.10, No.2, pp. 215 – 227.

Archard, J.F. (1953), *Journal of Applied Physics*, 24, 981-988.

Austin, L.G. and Klimpel, R.R. (1985), Ball wear and ball size distribution in tumbling ball mills, *Powder Technology*, 41, 279-286

Banisa, S., Hadizadeh, M. (2006), 3-D liner wear profile measurement and analysis in industrial SAG mills, article in press in the *Minerals Engineering* journal.

Bigg, A.C.T. and Raabe, H. (1996), Studies of lifter height and spacing: Past and Present, *International Autogenous and Semiautogenous Grinding Technology*, Vol 3, 999 – 1005.

Bitter, J.G.A. (1963), A study of erosion phenomena, Part I and II, *Wear*, 6, 5, 169

Bond, F.C. (1961), Crushing and grinding calculations, *British Chemical Engineering*, August, Vol. 6, No 8, 543-548

Bond, F.C. (1964), Metal wear in crushing and grinding, *Chemical Engineering Progress*, Vol. 60, No 2, 90-93

Chandramohan, R. and Powell, M.S. (2006), A structured approach to modelling SAG mill liner wear – Monitoring wear, *International AG and SAG Grinding Technology*, Vol 3, 133-148

Cleary, P.W. (1998), Predicting charge motion, power draw, segregation and wear in ball mills using discrete element methods. *Minerals Engineering*, Vol.11, No11, pp 1061-1080.

Cleary, P.W., Morrison, R., Morrell, S. (2001), DEM validation for a scale model SAG Mill, *International AG and SAG Grinding Technology*, Vol. 4, 191 – 206

Cleary, P.W. (2001), Charge behaviour and power consumption in ball mills: sensitivity to mill operating conditions, liner geometry and charge composition, *International Journal of Mineral Processing*, 63, 79 – 114

Cundall, P. A. and Strack, O.D.L. (1979), A discrete numerical model for granular assemblies, *Geotechnique*, 29, No1, 47-65

Datta, A., Mishra, B.K., Rajamani, R.K, (1999), Analysis of power draw in ball mill by discrete element method. *Canadian Metallurgical Quarterly*, 38 (16), 130 – 138.

Davis, E.W., (1919), Fine crushing in ball-mills, *Trans. AIME*, Vol. LXI, 250-295

Dong, H. and Moys, M.H. (2001), A technique to measure velocities of a ball moving in a tumbling mill and its applications, *Minerals Engineering*, Vol.14, No 8, 841 - 850

Dong, H. and Moys, M.H. (2003), Measurement of impact behaviour between balls and walls in grinding mills, *Minerals Engineering*, 16, 543 – 550

Engel, P. A. (1978), *Impact wear of materials*, Elsevier Scientific Publishing Company

Fillot, N., Iordanoff, I. and Berthier, Y. (2007), Wear modelling and the third body concept, *Wear*, Vol. 262, 7-8, 949-957

Finnie, I. (1960), Erosion of surfaces by solid particles, *Wear*, 3, 87-103

Finnie, I. (1972), Some observations on the erosion of ductile metals, *Wear*, 19, 81-90

Fricke, R.W. and Allen, C. (1993), Repetitive impact wear of steels, *Wear*, 162-164, 837-847

Gangopadhyay, A.K. and Moore, J.J. (1987), Effect of impact on the grinding media and mill liner in a large semiautogenous mill, *Wear*, 114, 249-260

Glover, G. and de Beer, J.C.K. (1997), The application of the discrete element method to the optimisation of mill liner systems. Proceedings of the XX IMPC-Aachen, 21-26 September.

Harris, C.C., Schnock, E.M. and Arbiter, N., (1985), Grinding mill power consumption, Mineral Processing Technology Review, Vol. 1, 297-345

Hogg, R., and Fuerstenau, D.W., (1972), Power relationships for tumbling mills. Society of Mining Engineers, AIME Trans. Vol. 252, 418-423

Hutchings, I.M. (1992), Tribology, Friction and wear of engineering materials, London

Johnson, K.L. (1985), Contact mechanics, Cambridge university press

Kapur, P.C., Ranjan, S. and, Fuerstenau, D.W., (1992), A cascade-cataract charge flow model for power draft of tumbling mills. International Journal of Mineral Processing, 36, 9-29

Kauzlarich, J.J. and Williams, J.A. (2001), Archard wear and component geometry, Proceedings of the Institution of Mechanical Engineers, Journal of Engineering Tribology, Vol. 215, Part J, 387-403

Kelly, E.G. and Spottiswood, D.J. (1982), Introduction to mineral processing, John Wiley & Sons

Kreyszig, E. (1983), Advanced engineering mathematics, fifth edition, John Wiley & Sons

Meekel, W., Adams, A., Clark, J., Mitchell, J. (1996), Primary mill liner development at Highland Valley Copper, Int. AG and SAG Grinding Technology, Vol. 3 of 3, 913-932.

Meng, H.C. and Ludema, K.C. (1995), Wear models and predictive equations: their form and content, Wear, 181 – 183, 443-457

Mishra, B.K. (1991), Study of media mechanics in tumbling mills by the discrete element method, University of Utah, Ph.D. Thesis.

Mishra, B.K. and Rajamani, R.K. (1992), *Applied Mathematical Modelling*, 16, 598.

Mishra, B.K. and Rajamani, R.K. (1993), Numerical simulation of charge motion in ball mills – Lifter bar effect, *Minerals and Metallurgical Processing*, May, 85 – 90.

Mishra, B.K. and Murty, C.V.R. (2001), On the determination of contact parameters for the realistic DEM simulations of ball mills. *Powder Technology* 115, 290 - 297

Mishra, B.K. (2003), A review of computer simulation of tumbling mills by the discrete element method: Part I – Contact mechanics. *Int. J. Miner. Process.* 71, 73 - 93

Mishra, B.K. (2003), A review of computer simulation of tumbling mills by the discrete element method: Part II – Practical applications. *Int. J. Miner. Process.* 71, 95 - 112

Morrel, S. (1993), The prediction of power draw in wet tumbling mills, Julius Kruttschnitt Mineral Research Centre, Department of Mining and Metallurgical Engineering, University of Queensland, Ph.D. thesis.

Moys, M.H. (1993), A model of mill power as affected by the mill speed, load volume, and liner design, *Journal of South African Institute of Mining and Metallurgy*, Vol. 93, No6, 135-141

Moys, M.H. and Skorupa, J. (1993), Measurements of the radial and tangential forces exerted by the load on a liner in a ball mill, as a function of load volume and mill speed, *Int. J. Miner. Process.* 37, 239 – 256.

Moys, M.H., Van Nierop, M.A., Van Tonder, J.C., Glover, G., (2000), Validation of the discrete element method (DEM) by comparing predicted load behaviour of a grinding mill with measured data. *Proc. XXI IMPC, Rome, 23-28 July*, pp. C3-39-C3-44



Moys, M.H., Van Nierop, M. A., Glover, G., Hinde, A. L. (2001), A discrete element method investigation of the charge motion and power draw of an experimental two-dimensional mill. *Int. J. Miner. Process.* 61, 77-92.

Moys, M.H., Dong, H., Bwalya, M., Monama, G. (2004), Internal Private communications.

Neilson, J.H. and Gilchrist, A. (1968), Erosion by a stream of solid particles, *wear*, 111

Nordell, L.K., Potapov, A. and Herbst, J.A. (2001), Comminution simulation using discrete element method (DEM) approach – From single particle breakage to full-scale SAG mill operation. , *International AG and SAG Grinding Technology*, Vol 4, 235 – 251.

Parks, J.L. (1996), Liner designs, materials and maintenance practices for large primary mills – Past, Present and Future, *International AG and SAG Grinding Technology*, Vol 3, 881 – 903

Powell, M., (2004), Selection and ongoing optimisation of mill shell and discharge liners and discharge grates, 6<sup>th</sup> Annual Crushing and Grinding in Mining Summit, Midrand, 10-11 February.

Qiu, X., Potapov, A., Song, M., Nordell, L. (2001), Prediction of wear of mill lifters using discrete element method. *Int. AG and SAG Grinding Technology*, vol. IV, 260-271

Rabinowicz, E (1965), *Friction and wear of materials*, John Wiley, New York.

Radziszewski, P. (1993), Simulation of ball charge and liner wear. *Wear*, 169, 77-85

Radziszewski, P. and Tarasiewicz, S. (1993), Modelling and simulation of ball mill wear, *Wear*, 160, 309-316

Radziszewski, P. (1997), Predictive model for ball mill wear, *Canadian Metallurgical Quarterly*, Vol. 36, No 2, 87-93

Radziszewski, P. (2001), Determining impact, abrasive and corrosive contributions to total media wear, *Int. AG and SAG Grinding Technology*, Vol. IV, 252-259

Radziszewski, P. (2002), Exploring total media wear, *Minerals Engineering* 15, 1073 – 1087

Radziszewski, P., Martins, S., Li, W., Picard, B., Quan, Y.Y., Caron, S., (2006), Investigating the feasibility of liner wear sensor development, *Int. AG and SAG Grinding Technology*, Vol III, 149- 159

Rose, H.E. and Evans, D.E. (1956), The dynamics of the ball mill, Part I, Power requirements based on the ball and shell system. *Proc. Inst. Mech. Engineers*, 773-783

Rose, H.E. and Evans, D.E. (1956), The dynamics of the ball mill, Part II, The influence of the powder charge on power requirements. *Proc. Inst. Mech. Engineers*, 784-792

Sligar, J. (1996), Component of wear in vertical spindle mills grinding coal, *Int. J. Miner. Process*, 44-45, 569-581

Shimizu, K., Noguchi, T., Seitoh, H., Okada, M. and Matsubara, Y. (2001), FEM analysis of erosive wear, *Wear*, 250, 779-784

Sorokin, G. M., Grigor'ev, S.P. and Golova, A.G., Nature of impact wear of steel, *Strength of Materials*, Vol 23, 4, 463-467

Tilly, G.P. (1973), A two stage mechanism of ductile erosion, *Wear*, 23, 87

Uuemois, H., Kangur, H., and Veerus, I. (1996), Wear in high-speed impact mills, *Int. J. Miner. Process*. 44-45, 301-313

Valderrama, W., Magne, L., Moyano, G., Santander, C., Pontt, J. (1996), The role of cascading and cataracting in mill linear wear. *Int. AG and SAG Grinding Technology*, vol. III

Van Nierop, M.A., Glover, G., Hinde, A.L., Moys, M.H. (2001), A discrete element method investigation of the charge motion and power draw of an experimental two-dimensional mill, *Int. J. Miner. Process*, 61, 77- 92

Vermeulen, L.A. and Howat, D.D. (1986), Abrasive and impactive wear of grinding balls in rotary mills, *Journal of South African Institute of Mining and Metallurgy*, Vol 86, 4, 113-124

Wellinger, K. and Breckel, H. (1969), *Wear*, 13, 257-281

White, H.A. (1905), The theory of tube mill, *The Journal of the Chemical, Metallurgical and Mining Society of South Africa*, May, 290-305

Williams, J.A. (1999), Wear modelling: analytical, computational and mapping: a continuum mechanics approach, *Wear*, 225-229, 1-17

Wills, B.A. (1992), *Mineral processing technology, an introduction to the practical aspects of ore treatment and mineral recovery*, fifth edition, Pergamon Press